FINITE DIFFERENCE ANALYSES OF ELASTIC AND ELASTO-PLASTIC PROBLEMS

by

David K. Brown

Submitted to

The University of Glasgow

for the degree of

Doctor of Philosophy

July 1972

Acknowledgments

The writer is grateful for the facilities made available by the University of Glasgow and in particular to Professor J.D. Robson in whose department the work was carried out. The writer's thanks are also due to Dr. James Orr whose help and unflagging optimism have been a great inspiration and whose influence will not be forgotten. The writer also wishes to express his gratitude to Dr. A.C. Mackenzie for his enthusiasm and his many helpful suggestions.

In addition the writer is indebted to the following people:

- Professor D.C. Gillies and subsequently Dr. G.K.S. Browning and the staff of the University's KDF9 computer.
- Dr. J.H. Ludley and his staff of the UNIVAC 1108 computer at East Kilbride
- Mrs. J. Sweeney (née Taggart) who punched numerous computer programs with admirable speed and accuracy.
- Miss H. Leslie whose skill in typing the thesis is evident.

Notation

a	— breadth of minimum section
a,b	— strain increment functions (sphere)
a,b,c	— constants in evaluation of biharmonic difference equation
a,b,c	— strain functions, coefficients of general partial differential equation
a, etc.	— constant coefficients
d	— displacement function
e	— non-dimensional strain, error
f,g	— displacement functions, any function, f also constant
h	— grid coordinate, size parameter
i	— subscript
j	— grid coordinate
k	— grid coordinate, yield stress in pure shear, size parameter, subscript of number of iterations
l	— length
m	— work-hardening index
n	— creep index, geometric series index, normal, grid radial coordinate
p	— plastic strain defined as $\frac{d\bar{\varepsilon}^p}{(1+\nu)}$, internal pressure (sphere), reference stress (Neuber)
p_y	— surface stress intensity
p_1, p_2 etc.	— points on characteristic line
q	— accelerator in S.C.R. method
r	— radius, radial coordinate, subscript
r_o	— inner radius, reference radius

r_i — inner radius (sphere)

t — time

u — any variable, displacement

v — displacement

x,y,z — cartesian coordinates, stress ratios

A,B,C — non-dimensionalized strain functions

$\mathbf{A},\mathbf{B},\mathbf{C},\mathbf{W},\mathbf{U}$ — matrices

AS etc. — non-dimensionalized stress

C,C_1,C_2 — constants

D,F,G — non-dimensionalized displacement functions

E — modulus of elasticity

E' — plastic modulus

E_ξ etc. — non-dimensionalized strain (sphere)

$\dot{E}_\vartheta$ etc. — non-dimensionalized strain increment (sphere)

F — stress function

G — shear modulus of elasticity

H — grid size parameter

I,J,K,L — grid coordinates and subscripts

$K_{\varepsilon_\vartheta},K_{\sigma_\vartheta},K_{\bar{\sigma}}$ — stress and strain concentration factors

K — viscous damping factor, constant

KE — outer circumferential boundary

LE — outer radial boundary

M — applied moment

P — non-dimensionalized plastic strain

P_1 etc. — functions of plastic strain

Q — work-hardening index, characteristic determinant

R — radius, non-dimensional radius

RHSX — right hand size of any equation used in solution of any variable X

RC1, RB1, RF1, RCC1 etc. — constant coefficients of gradient and curvature formulae

S_ϑ etc. — non-dimensionalized stress (sphere and creep); S'_ϑ etc. are stress increments in creep

$\dot{S}_\vartheta$ etc. — non-dimensionalized stress increment (sphere); stress rate (creep)

SYD — effective stress and end of previous load stage

T — radial grid size parameter, non-dimensionalised time

U — any variable

V2 etc. — constant coefficients of Poisson's Ratio

X,Y,Z — non-dimensionalized stress ratios

X — any variable

XH — gradient $\frac{\partial X}{\partial \vartheta}$ of any variable X

XN — gradient $R\frac{\partial X}{\partial R}$ of any variable X

X2H — curvature $\frac{\partial^2 X}{\partial \vartheta^2}$ of any variable X

X2N — curvature $R^2\frac{\partial^2 X}{\partial R^2}$ of any variable X

XNH — curvature $R\frac{\partial^2 X}{\partial \vartheta \partial R}$ of any variable X

α, β — constant coefficients, strain functions (sphere), curvilinear slip line coordinate system

$\gamma_{r\vartheta}$ — shear strain

δ, Δ — increments

ε — normal strain

$\bar{\varepsilon}^p, d\bar{\varepsilon}^p$ — effective plastic strain and its increment

$\varepsilon_x, d\varepsilon_x$ etc. — component total and incremental strains

ε_x^e etc. — component elastic strains

ε_x^p etc. — total plastic component strain up to but not including the current increment

$d\varepsilon_x^p$ etc. — current plastic component strain

ε' — modified strain (Mendelson)

$\bar{\varepsilon}$ — effective total strain

ε_{et} — modified total strain

$\varepsilon_{\theta c}$ etc. — total creep strain components

ε_o — reference strain

ε_b — reference bending strain

η — angle

θ — angle, circumferential coordinate, subscript

$\lambda, d\lambda$ — constant in flow rule, constant coefficient, angle

μ — constant coefficient

ν — Poisson's ratio

π — pi, 3.1415926536

σ — normal stress, mean stress (slip line analysis)

$\sigma_x, d\sigma_x$ etc. — total and incremental total stresses

σ_o — reference stress

σ_b — reference bending stress

σ_m — mean stress

σ_Y — yield stress

$\bar{\sigma}$ — effective stress

τ — shear stress, root of characteristic equation

ϕ — Airy stress function, angle between x and α axes (slip line analysis)

ϕ_e, ϕ_p	– elastic and plastic stress functions (Mendelson)
ψ	– Airy stress function, angle
$\psi', \psi`$	– gradients of stress function
$\psi'', \psi'', \psi\hat{}$	– curvatures of stress function
Σ	– sum
∂	– partial differential operator
$\nabla, \nabla^2, \nabla^4$	– del or nabla, partial differential operators
$\mathbb{R}$	– a region
$\partial\mathbb{R}$	– a boundary
$\dot{}$	– rate of change of variable with time (creep)

List of Contents

CHAPTER 1

INTRODUCTION

CHAPTER 1

INTRODUCTION

A research group in our Department has been studying fracture of metals and has been concentrating on high yield--strength steels. Various aspects have been examined such as the effects of discontinuities, inclusions and second phase particles, and the growth of voids. My role as a member of this group has been to study the continuum aspects and has been chiefly concerned with the early stages of fracture — the so--called void--nucleation stage. It is thought that especially in higher strength steels, the amount of plastic strain in this stage would be limited to perhaps 4--5% at the root of a notch so that a small geometry change theory would be permissible. Slip line solutions give some insight into the general problem and a brief account is given, for comparative purposes, of such a solution for one of our test specimens.

The main part of the thesis describes the attempts and final choice of method of solution of two dimensional stress problems. In our fracture research a keyhole notched bar was finally selected as a bend test specimen; this choice had advantages both theoretically and experimentally.

The task of solving the elastic and plane strain elasto--plastic stress and strain fields under a keyhole notch had thus to be tackled. The elastic solution was attempted in several ways as detailed in chapter 3, using the Airy Stress function with, initially, finite boundaries although finally the solution was for a region close to the keyhole and modelled to its shape with cylindrical coordinates.

Finite differences were employed with a graded net because it was felt that by so doing the sharp changes in variable gradients and curvatures could best be determined.

The solution using the Airy stress function involves the biharmonic equation and fourth order differences which are troublesome when dealing with boundaries. Thus it was at this stage that Professor I.N. Sneddon[21] suggested the use of a set of first order partial differential equations; this method of solution had not been tried previously and a thorough investigation into the method of using them had to be instigated. It is known that on the one hand the rigid plastic slip line equations are hyperbolic while on the other hand the elasticity equations are elliptical. Careful consideration was given in Chapters 5 and 6 to the initial-value and boundary-value approaches to the solution of the equations. Since the geometry of the fields is similar, the better known solution of the hole in uniaxial tension was used in the evaluation.

The method having been proved feasible, the elasto-plastic solution was attempted and details of this and the results are given in Chapters 7 and 8.

In order to verify some results the limiting slip line solution of the keyhole notch was obtained and this is given in Chapter 10. Further verification of certain features of the results is obtained from the elasto-plastic solution of the thick sphere under internal pressure, details of which are given in Chapter 9.

Having been satisfied with the validity of the method, the governing equations were re-formulated to solve the creep problem with very similar equations to the elasto-plastic problem; results for the hole in tension are given as an example in Chapter 11.

CHAPTER 2

THE DEVELOPMENT OF ELASTO-PLASTIC SOLUTIONS

CHAPTER 2

THE DEVELOPMENT OF ELASTO-PLASTIC SOLUTIONS

2.1 Introduction

In the complete solution to elasto-plastic problems, the equations of equilibrium and strain/displacement and the stress-strain relations must be simultaneously satisfied. There are thus fifteen unknowns; in cartesian coordinates these are

$$\sigma_x, \sigma_y, \sigma_z, \tau_{xy}, \tau_{yz}, \tau_{zx}, \varepsilon_x, \varepsilon_y, \varepsilon_z, \gamma_{xy}, \gamma_{yz}, \gamma_{zx}, u, v, w.$$

The fifteen equations involving these unknowns comprise 3 equilibrium equations, 6 strain/displacement equations and 6 stress-strain relations. In the non-linear elasto-plastic problem the stress-strain curve is also required to link stress and strain.

The thought of attempting a solution using these 15 equations in this form poses a daunting challenge, which has not yet been taken up. The development of elasto-plastic solutions has been dependent on the degree of simplification which could be applied to the 15 equations as well as on the availability of computing machinery in the case of numerical solutions.

The complexity of three-dimensional problems is reduced by working with plane stress and plane strain conditions. These give the two limits in plane elasto-plastic problems. The problems most often and most usefully tackled are those of plane strain since several methods exist to determine plane stress conditions experimentally.

There are several methods of solving the plane constitutive equations:-

1. Reduce to one dimension - this requires both symmetry of loading and symmetry of field geometry.
2. Reduce to the biharmonic equation.
3. Reduce to two simultaneous second order partial differential equations in the two component displacements u and v.
4. Re-arrange the equations to work with five first order simultaneous partial differential equations in two displacements and three stresses or reduce to four first order simultaneous partial differential equations in three stresses and a displacement function or reduce to three first/second order simultaneous partial differential equations in the stresses or the strains.

Each of these methods have their difficulties and some of these are as follows:- (the numbers correspond to the methods above)

1. This very special type of symmetrical problem is usually solved by multiple integration but this can, with the least complexity, become impossible analytically and has to be done numerically.
2. The solution of the biharmonic requires a difference equation applied to a grid of points over a field. The five-point spread (in both coordinate directions) of the difference operator makes the tackling of boundaries difficult and detremental to accuracy. In addition, solving a problem with fourth order differences and then taking curvatures of the stress function, to determine stress, must suffer the penalties of numerical approximation.

3. Using displacement prescribed boundaries is tricky, since it is very difficult to determine the final displacement components on a boundary after yielding has occurred. Consequently the boundary conditions are derived functions from the known stress and strain boundary conditions. Also the interaction of the two variables in simultaneous governing equations is extremely difficult to assess.

4. In comparison to (2), working with lesser order difference equations has the advantage of greater numerical accuracy as well as easier handling of boundaries. However, against that there is the difficulty of handling simultaneously a number of variables which are interacting with each other.

A review of the development of each of these above methods is now presented in sections 2.2 to 2.5.

2.2 One Dimensional Problems

In 1956 Bland[1]† tackled the problem of the thick tube in plane strain. He employed the easier Tresca yield criterion with its associated flow rule. He used materials with work-hardening and, for linear work-hardening, produced his solution in closed form.

In 1965 Tuba[2] solved another basic axisymmetric problem of the thick sphere under various loading with various work-hardening indices, and the Mises yield criterion; solution was achieved by an iterative technique. However in his book[3] Mendelson shows how

---

† detailed references are found in the 'List of References' after Chapter 12.

this problem with internal or external pressure loadings and linear work-hardening can be solved in closed form. This result was also shown independently by Orr[4] in a slightly different way.

2.3 Plane Elasto-plastic Stress function Problems

The first real attempt at solving plane elasto-plastic problems was made in 1950 by Allen and Southwell[5]. They put forward solutions for edge-notched bars (figs. 2.1 and 2.2) in tension, under both plane stress and plane strain conditions. The material was assumed elastic perfectly plastic.

These solutions were a further application of the relaxation technique developed by Southwell and originally pioneered by Professor A. Thom. The problem was formulated in terms of the Airy stress function ψ, which had to satisfy the boundaries as well as the governing equations of the elastic and plastic regimes.

In the elastic zone the normal biharmonic equation governs the stress function

$$\nabla^4 \psi = 0. \qquad (2.1)$$

However the governing equation in the plastic zone is based on the yield criterion expressed in terms of the stress function. In plane stress

$$\sigma_Y^2 = \bar{\sigma}^2 = \text{const} = \sigma_x^2 - \sigma_x\sigma_y + \sigma_y^2 + 3\tau_{xy}^2 \qquad (2.2)$$

in plane strain

$$\sigma_Y^2 = \bar{\sigma}^2 = \text{const} = \tfrac{3}{4}(\sigma_x - \sigma_y)^2 + 3\tau_{xy}^2 \qquad (2.3)$$

where σ_Y is the yield stress in simple tension. For plane strain it was assumed in the plastic zone that Poisson's ratio $\nu = \frac{1}{2}$ for the elastic as well as the plastic components of the strains. This enabled the third

stress component σ_z to be defined as

$$\sigma_z = \frac{1}{2}(\sigma_x + \sigma_y) \qquad (2.4)$$

thus giving an easier yield criterion.

The method of solution proceeded as follows. The elastic stress function field was initially solved over the whole field, the field having been covered by a regular grid, and the differential equation being expressed in finite differences. It must be added in here that all solutions were done on hand calculating machines, – a truly monumental task when dealing with up to 120 internal mesh points. Final convergence to a solution may possibly be doubtful due to the very slow movement even in an accelerated method.

The elastic field was then incremented and a check made for all points having an effective stress greater than σ_Y. This then defined an elastic/plastic boundary and two distinct regions, in which the appropriate governing equations were applied. However, continuity of all stresses over the boundary requires that the stress function and its first and second derivatives normal to the boundary must also be continuous over the boundary. Consequently constant readjustment was required at the boundary.

Computation of strains in the plastic region involves a tortuous procedure. The ratio $\Delta\lambda = \bar{\varepsilon}^p/\bar{\sigma}$ was found at each point. A hyperbolic (initial value) process was used to proceed from the boundary into the plastic zone along orthogonal lines, and, making use of the compatibility of total strains and the values of $\Delta\lambda$, the plastic strain could be found at points on the intersection of these lines.

Although the above solution has many assumptions, it did lay the way open for further advances, by highlighting difficulties.

The solution for edge slits (fig. 2.3) is given in a paper by Jacobs[6] also in 1950. This paper is identical in method to that of Allen and Southwell. Allen and Southwell[5] and Jacobs[6] implicitly assume that as load increases, the stress in the regions which are already plastic remains constant. There is in general no reason why this should be physically valid, but it might be taken as a reasonable approximation.

In 1963 a check was made by Griffin and Varga[7] on Allen and Southwell's semi-circular edge notch elastic solution using a computer, a successive over-relaxation process and a variable grid with half again as many points. Fair agreement was reached. The important aspect of this paper is the variable grid which was able to concentrate a greater number of point in the high stress region while leaving the comparatively 'dead' region with a coarse grid.

As late as 1962, however, Spencer[8] was still solving plane elasto-plastic problems by hand using a stress-function approach with an elastic perfectly plastic material and an assumption that $\nu = \frac{1}{2}$. He tackled the problem of working in plastic zones in a radically different way from Allen and Southwell[5] and Jacobs[6]. In the latter two papers, the plastic zone governing equation was (2.3) –

$$\sigma_Y^2 = \bar{\sigma}^2 = \text{const} = \frac{3}{4}(\sigma_x - \sigma_y)^2 + 3\tau_{xy}^2$$

OR using the stress function

$$\left(\frac{\partial^2\psi}{\partial x^2} - \frac{\partial^2\psi}{\partial y^2}\right)^2 + 4\left(\frac{\partial^2\psi}{\partial x \partial y}\right)^2 = \text{constant.} \qquad (2.5)$$

Spencer states . 'As this equation is both hyperbolic and non-linear, it is not well adapted to a relaxation treatment, and it is desirable to try to use the hyperbolic properties of the plasticity equations to simplify the numerical treatment'.

Using the idea of characteristics or slip lines developed by Hill[9], he defined two possible stress functions ψ_1^p and ψ_2^p which satisfy boundary conditions as well as the above equation, different expressions existing, depending on proximity to any particular boundary. Thus by manipulating ψ^e in the elastic field with ψ_1^p and ψ_2^p in the plastic zone to give continuity of stress function and its first and second derivatives over the elastic/plastic boundary, a solution is given in which 'every point in the plastic region is joined to the boundary by two slip lines, lying entirely within the plastic region! With this latter condition met, the problem is statically determined and the solution unique.

Spencer then proceeded to solve the problem of a square (finite) plate with a concentric hole in simple tension.

The above solutions, despite the enormous amount of effort put into them, however, have several drawbacks. 1. The material properties assumed were elastic perfectly plastic with the assumption of Poisson's ratio = $\frac{1}{2}$ in the plastic region. 2. The methods of solution were laborious and many parts of them were not easily adaptable to the computer, which in the 1950's was making such great strides forward. 3. The determination of plastic strains as an integral part of the solution procedure was not countemplated — thus making the solutions of Allen and Southwell[5] and Jacobs[6] not unique.

It was in the light of the above, that in 1959 Mendelson and Manson[10] developed their new approach to elasto-plastic solutions. This approach enabled (a) work-hardening materials to be considered, (b) computers to be employed and (c) a comprehensive method of solution to be used.

In contrast to previous researchers Mendelson and Manson decided to deal with elastic and plastic regions together and to work with one stress function (say $\emptyset$)

valid in both elastic and plastic regions. Defined in the usual way by,

$$\sigma_x = \frac{\partial^2 \phi}{\partial y^2} \qquad \sigma_y = \frac{\partial^2 \phi}{\partial x^2} \qquad \tau_{xy} = -\frac{\partial^2 \phi}{\partial x \partial y}, \quad (2.6)$$

the biharmonic governing equation, as used by Mendelson for a plane strain incremental procedure, is given by

$$\nabla^4 \phi = -(g+dg) = \frac{\partial^4 \phi}{\partial x^2} + 2\frac{\partial^4 \phi}{\partial x^2 \partial y^2} + \frac{\partial^4 \phi}{\partial y^4} \quad (2.7)$$

where

$$g \equiv \frac{E}{1-\nu^2}\left(\frac{\partial^2 \varepsilon_x^{\,p}}{\partial y^2} + \frac{\partial^2 \varepsilon_y^{\,p}}{\partial x^2} - \frac{\partial^2 \gamma_{xy}^{\,p}}{\partial x \partial y}\right) - \frac{\nu E}{1-\nu^2}\nabla^2(\varepsilon_x^{\,p} + \varepsilon_y^{\,p})$$

$$dg \equiv \frac{E}{1-\nu^2}\left(\frac{\partial^2 (d\varepsilon_x^{\,p})}{\partial y^2} + \frac{\partial^2 (d\varepsilon_y^{\,p})}{\partial x^2} - \frac{\partial^2 (d\gamma_{xy}^{\,p})}{\partial x \partial y}\right) - \frac{\nu E}{1-\nu^2}\nabla^2(d\varepsilon_x^{\,p} + d\varepsilon_y^{\,p})$$

and $\varepsilon_i^{\,p}$ = the sum of the component plastic strain increment up to but not including the current load stage

$d\varepsilon_i^{\,p}$ = the current component plastic strain increment.

In the elastic region all the plastic strains are zero and equation (2.7) reverts back to $\nabla^4 \phi = 0$ as equation (2.1). An iterative technique can be used to solve the elasto-plastic problem using the above equation. The technique requires the use of the Levy Mises equations which are given below in plane strain form for convenience:-

The component plastic strain increments are given by -

$$\left.\begin{aligned} d\varepsilon_x^{\,p} &= \frac{d\bar{\varepsilon}^p}{\bar{\sigma}}\left(\sigma_x - \tfrac{1}{2}(\sigma_y + \sigma_z)\right) \\ d\varepsilon_y^{\,p} &= \frac{d\bar{\varepsilon}^p}{\bar{\sigma}}\left(\sigma_y - \tfrac{1}{2}(\sigma_x + \sigma_z)\right) \\ d\gamma_{xy}^{\,p} &= \frac{d\bar{\varepsilon}^p}{\bar{\sigma}} \cdot 3\tau_{xy} \end{aligned}\right\} \quad (2.8)$$

where the effective stress,

$$\bar{\sigma} = \sqrt{\tfrac{1}{2}\left[(\sigma_x-\sigma_y)^2 + (\sigma_y-\sigma_z)^2 + (\sigma_z-\sigma_x)^2\right] + 3\tau_{xy}^2} \qquad (2.9)$$

and the effective plastic strain increment,

$$d\bar{\varepsilon}^p = \sqrt{\tfrac{4}{3}(d\varepsilon_x^p + d\varepsilon_y^2 - d\varepsilon_x^p . d\varepsilon_y^p) + \tfrac{1}{3}(d\gamma_{xy}^p)^2} \qquad (2.10)$$

since $d\varepsilon_z^p = -(d\varepsilon_x^p + d\varepsilon_y^p)$

A summary of the procedure for the first load stage in an incremental process (ε_x^p† etc. being zero) would be as follows:-

(a_1) Guess/estimate $d\varepsilon_x^p$ etc. everywhere in the field.

(b_1) Evaluate the finite difference form of 'dg' in equation (2.7) ('g' being zero) at each mesh point on a grid covering the field.

(c_1) Solve difference form of equation (2.7) to satisfy boundary conditions.

(d_1) Compute stresses from stress function ϕ using equations (2.6) and so determine $\bar{\sigma}$ from (2.9).

(e_1) Where $\bar{\sigma} > \sigma_Y$, use the stress-strain curve to evaluate $d\bar{\varepsilon}^p$.

(f_1) Find $d\varepsilon_x^p$ etc. from Levy Mises equations (2.8).

(g_1) Return to (b_1) and iterate until convergence.

The difficulty in the above procedure lay in finding $d\bar{\varepsilon}^p$ from $\bar{\sigma}$ where there was low work-hardening, since a small change in $\bar{\sigma}$ would mean a large change in $d\bar{\varepsilon}^p$. There was also the inconvenience in working in both

---

† ε_x^p etc. refer to the sum of the component plastic strain increments up to but not including the current load stage.

stresses and strains. Mendelson and Manson[10] thus developed an 'all strain' version of the Levy Mises equations for deformation theory (i.e. only one plastic strain increment) as follows:-

The two basic 'physical' equations of elasticity and plasticity relate the strain response of a material to stress loading in terms of dilation and distortion.

In plasticity these are -

Constant Volume Condition - $d\varepsilon_x^p + d\varepsilon_y^p + d\varepsilon_z^p = 0$.

Flow Rule - $$\frac{2(d\varepsilon_x^p - d\varepsilon_y^p)}{\sigma_x - \sigma_y} = \frac{2(d\varepsilon_y^p - d\varepsilon_z^p)}{\sigma_y - \sigma_z} = \frac{2(d\varepsilon_z^p - d\varepsilon_x^p)}{\sigma_z - \sigma_x} = \frac{\gamma_{xy}^p}{\tau_{xy}} = \frac{\gamma_{yz}^p}{\tau_{yz}} = \frac{\gamma_{zx}^p}{\tau_{zx}} = d\lambda.$$

In elasticity these are -

Elastic dilation - $$\varepsilon_x^e + \varepsilon_y^e + \varepsilon_z^e = \frac{1}{K}(\sigma_x + \sigma_y + \sigma_z).$$

Flow Rule - $$\frac{2(\varepsilon_x^e - \varepsilon_y^e)}{\sigma_x - \sigma_y} = \frac{2(\varepsilon_y^e - \varepsilon_z^e)}{\sigma_y - \sigma_z} = \frac{2(\varepsilon_z^e - \varepsilon_x^e)}{\sigma_z - \sigma_x} = \frac{\gamma_{xy}^e}{\tau_{xy}} = \frac{\gamma_{yz}^e}{\tau_{yz}} = \frac{\gamma_{zx}^e}{\tau_{zx}} = \frac{1}{G} = \frac{2(1+\nu)}{E}$$

where G and K are elastic shear and bulk moduli.

Mendelson and Manson now note that

$$\varepsilon^e = \varepsilon - d\varepsilon^p,$$

Therefore from the elastic flow rule

$$\varepsilon_x^e - \varepsilon_y^e = \frac{1+\nu}{E}(\sigma_x - \sigma_y).$$

But $$d\varepsilon_x^p - d\varepsilon_y^p = \frac{d\lambda}{2}(\sigma_x - \sigma_y)$$

therefore $$\frac{1+\nu}{E}\cdot\frac{d\varepsilon_x^p - d\varepsilon_y^p}{\frac{d\lambda}{2}} = \varepsilon_x - \varepsilon_y - (d\varepsilon_x^p - d\varepsilon_y^p)$$

OR $$\frac{d\varepsilon_x^p - d\varepsilon_y^p}{\varepsilon_x - \varepsilon_y} = \frac{d\lambda}{d\lambda + \frac{2(1+\nu)}{E}}$$

$$= \frac{d\varepsilon_y^p - d\varepsilon_z^p}{\varepsilon_y - \varepsilon_z} = \frac{d\varepsilon_z^p - d\varepsilon_x^p}{\varepsilon_z - \varepsilon_x}$$

$$= \sqrt{\frac{1.5}{1.5}}\,\frac{d\gamma_{xy}^p}{\gamma_{xy}} = \sqrt{\frac{1.5}{1.5}}\,\frac{d\gamma_{yz}^p}{\gamma_{yz}} = \sqrt{\frac{1.5}{1.5}}\,\frac{d\gamma_{zx}^p}{\gamma_{zx}} .$$

Remembering $$\frac{a}{b} = \frac{c}{d} = \frac{e}{f} = \frac{\sqrt{a^2+c^2+e^2}}{\sqrt{b^2+d^2+f^2}}$$

gives

$$\frac{d\varepsilon_x^p - d\varepsilon_y^p}{\varepsilon_x - \varepsilon_y} = \frac{\sqrt{(d\varepsilon_x^p - d\varepsilon_y^p)^2 + (d\varepsilon_y^p - d\varepsilon_z^p)^2 + (d\varepsilon_z^p - d\varepsilon_x^p)^2 + \cdots \; \dfrac{1.5\left[(d\gamma_{xy}^p)^2 + (d\gamma_{yz}^p)^2 + (d\gamma_{zx}^p)^2\right]}{1.5\left[\gamma_{xy}^2 + \gamma_{yz}^2 + \gamma_{zx}^2\right]}}}{\sqrt{(\varepsilon_x - \varepsilon_y)^2 + (\varepsilon_y - \varepsilon_z)^2 + (\varepsilon_z - \varepsilon_x)^2 + \cdots}} .$$

Now

$$d\bar{\varepsilon}^p = \frac{\sqrt{2}}{3}\sqrt{(d\varepsilon_x^p - d\varepsilon_y^p)^2 + (d\varepsilon_y^p - d\varepsilon_z^p)^2 + (d\varepsilon_z^p - d\varepsilon_x^p)^2 + 1.5\left[(d\gamma_{xy}^p)^2 + (d\gamma_{yz}^p)^2 + (d\gamma_{zx}^p)^2\right]} .$$

Therefore multiply top and bottom by $\frac{\sqrt{2}}{3}$ and define the quantity 'modified total strain' by the mathematical expression

$$\varepsilon_{et} = \frac{\sqrt{2}}{3}\sqrt{(\varepsilon_x - \varepsilon_y)^2 + (\varepsilon_y - \varepsilon_z)^2 + (\varepsilon_z - \varepsilon_x)^2 + 1.5\left[\gamma_{xy}^2 + \gamma_{yz}^2 + \gamma_{zx}^2\right]} . \qquad (2.11)$$

This gives

$$d\varepsilon_x^p - d\varepsilon_y^p = \frac{d\bar{\varepsilon}^p}{\varepsilon_{et}}(\varepsilon_x - \varepsilon_y) \quad \text{etc.}$$

and

$$\frac{d\bar{\varepsilon}^p}{\varepsilon_{et}} = \frac{d\lambda}{\left(d\lambda + \frac{2(1+\nu)}{E}\right)} .$$

Using the condition of constant volume plastic flow gives the plastic strain total strain equations of Mendelson and Manson –

$$\left.\begin{aligned} d\varepsilon_x^p &= \frac{d\bar{\varepsilon}^p}{3\varepsilon_{et}}(2\varepsilon_x - \varepsilon_y - \varepsilon_z) \\ d\varepsilon_y^p &= \frac{d\bar{\varepsilon}^p}{3\varepsilon_{et}}(2\varepsilon_y - \varepsilon_z - \varepsilon_x) \\ d\varepsilon_z^p &= \frac{d\bar{\varepsilon}^p}{3\varepsilon_{et}}(2\varepsilon_z - \varepsilon_x - \varepsilon_y) \\ d\gamma_{xy}^p &= \frac{d\bar{\varepsilon}^p}{\varepsilon_{et}}\gamma_{xy} \\ d\gamma_{yz}^p &= \frac{d\bar{\varepsilon}^p}{\varepsilon_{et}}\gamma_{yz} \\ d\gamma_{zx}^p &= \frac{d\bar{\varepsilon}^p}{\varepsilon_{et}}\gamma_{zx} \end{aligned}\right\} \qquad (2.12)$$

However $d\bar{\varepsilon}^p$ and ε_{et} must be linked through the stress–strain curve.

From the usual plastic flow rule

$$d\lambda = \frac{3d\bar{\varepsilon}^p}{\bar{\sigma}}$$

and so by substitution into

$$\frac{d\bar{\varepsilon}^p}{\varepsilon_{et}} = \frac{d\lambda}{d\lambda + \frac{2(1+\nu)}{E}}$$

gives

$$\varepsilon_{et} = \frac{2}{3}\left(\frac{1+\nu}{E}\right)\bar{\sigma} + d\bar{\varepsilon}^p. \qquad (2.13)$$

Thus from any stress–strain curve, ε_{et} can be calculated using equation (2.13) from the extracted values of $\bar{\sigma}$ and $d\bar{\varepsilon}^p$, and then plotted against $d\bar{\varepsilon}^p$. Thus a new strain–strain curve can be used.

With these above considerations, an alternative iteration procedure with strain governing equations and the deformation theory was evolved by Mendelson and Manson.

(a_2) Estimate $d\varepsilon_x^p$ etc. everywhere on the field.

(b_2) Solve the governing equations in terms of total strains ε_x etc.

(c_2) Calculate ε_{et} from (2.11).

(d_2) From (2.13), find new $d\bar{\varepsilon}^p$.

(e_2) Evaluate new $d\varepsilon_x^p$ etc. from (2.12) and so loop back to (b_2) and iterate to convergence.

In their first attempts to utilise this procedure Mendelson and Manson tackled four, basically one dimensional thermal stress problems using the deformation theory of plasticity. In these problems, the equations reduced to expressions for the total strains in terms of integrals of thermal and plastic strains. In the discussion they note two possible extensions to their method.

1. The incremental theory can be applied, but no details are given.

2. Although the examples in their paper had their governing equations expressed in strains, a slightly modified method could be employed, where the governing equations were in terms of the stresses.

Their second development is possible since once a stress state is fully defined then all the elastic strain components can be determined. The modified procedure for the deformation theory is as follows†—

(a_3) Estimate $d\varepsilon_x^p$ etc. everywhere in the field.

(b_3) Solve the governing equations in terms of stresses.

---

† Note: this method is essentially that used in section 7.3 on the Stress Oriented Approach to the Elasto-plastic Problem although employing the incremental theory.

(c_3) Compute the elastic strains from the stresses viz $\varepsilon_x^e = \frac{1}{E}(\sigma_x - \nu(\sigma_y + \sigma_z))$ etc.

(d_3) Evaluate the total strains, by adding to the elastic strains the estimated plastic strain or the plastic strain from the previous iteration viz $\varepsilon_x = \varepsilon_x^e + d\varepsilon_x^p$ etc.

(e_3) Calculate the effective total strain from (2.11).

(f_3) From (2.13) find $d\bar{\varepsilon}^p$.

(g_3) Using (2.12) calculate $d\varepsilon_x^p$ etc. and so loop back to (b_3) and iterate to convergence.

It is this paper in 1959 that paved the way in the 1960's for more elasto-plastic solutions.

In 1962, the elasto-plastic thermal stress plate problem, of great interest to N.A.S.A. at that time, was more thoroughly tackled by Mendelson and Spero[11] employing techniques as shown above. The problem is still one dimensional, under plane stress conditions and employing the deformation theory; it is of interest that in the written discussion to that paper E.A. Davis of Westinghouse Laboratories was beginning to show interest in this method.

Subsequently in 1963, Davis[12] produced his paper on the elasto-plastic solution of a uniformly loaded plate with a hole - once again a one dimensional problem due to the symmetry of loading and geometry and once again plane stress. Davis reduced his governing equations to integral equations in strains. However, he used the incremental theory of plasticity to reach his final load. He employed basically the Mendelson Manson technique at each increment of load, but he defined a 'modified total' strain as

$$\varepsilon' = \varepsilon - \varepsilon^p = \varepsilon^e + d\varepsilon^p. \qquad (2.14)$$

This modified total strain was used in the evaluation of

the effective total strain. Thus equation (2.11) becomes

$$\varepsilon_{et} = \frac{\sqrt{2}}{3}\sqrt{(\varepsilon_x'-\varepsilon_y')^2 + (\varepsilon_y'-\varepsilon_z')^2 + (\varepsilon_z'-\varepsilon_x')^2 + 1.5\left[(\gamma_{xy}')^2 + (\gamma_{yz}')^2 + (\gamma_{zx}')^2\right]} \quad (2.15)$$

Some controversy arose, however, regarding the application of the Mendelson Manson technique to the incremental theory. Davis had to consider two new difficulties.

1. The summation of strains after n load stages.
2. The evaluation after at least one stage of $d\bar{\varepsilon}^p$ from ε_{et}.

1. Davis concluded that

$$\bar{\varepsilon}_n^{\,p} = \frac{\sqrt{2}}{3}\left[(\sum_1^n d\varepsilon_x^{\,p} - \sum_1^n d\varepsilon_y^{\,p})^2 \text{ ..etc. } \right]^{\frac{1}{2}}$$

but Mendelson corrected this to

$$\bar{\varepsilon}_n^{\,p} = \sum_1^n d\bar{\varepsilon}^p.$$

2. Davis evolved an iterative technique to determine $d\bar{\varepsilon}^p$ from ε_{et}. In the written discussion, Mendelson developed a quicker method by a Taylor Series expansion for the stress-strain curve (fig. 2.4), past yield

viz $$\bar{\sigma}_n = \bar{\sigma}_{n-1} + \left(\frac{d\bar{\sigma}}{d\bar{\varepsilon}^p}\right)_{n-1} . d\bar{\varepsilon}^p . \ldots$$

With linear strain hardening no more terms are needed in the expansion. With (2.13) this gives

$$d\bar{\varepsilon}^p = \frac{\varepsilon_{et} - \frac{2}{3}\frac{(1+\nu)}{E} . \bar{\sigma}_{n-1}}{1 + \frac{2}{3}\frac{(1+\nu)}{E} . \left(\frac{d\bar{\sigma}}{d\bar{\varepsilon}^p}\right)_{n-1}} \quad (2.16)$$

where $\bar{\sigma}_{n-1} = \bar{\sigma}$ at the end of the (n-1)th load stage

and $\left(\frac{d\bar{\sigma}}{d\bar{\varepsilon}^p}\right)_{n-1}$ = the slope of the uniaxial tensile curve

replotted as 'true' stress vs. 'true' plastic strain.

This exercise spurred Mendelson on to formalise the incremental approach and this was done in 1964 by Roberts and Mendelson[13] in a N.A.S.A. Technical Report. In this paper, the incremental method is now applied to the two dimensional thermal plane stress problem of a thin plate of work-hardening material using a biharmonic ∇^4 as the governing equation. The difficulty in using the biharmonic stress function equation, lies in the extraction of the information from the solution. The stresses come from the stress function through equations (2.6) and so essentially the governing equation is in stresses, with all the attendant difficulties as discussed. However, the solution proceeds using steps (a_1) to (g_1) for a material with a 0.1 modulus of work-hardening. The differential governing equation is put into difference form and the field is covered with a grid giving 400 internal points for solution. The difficulty relating grid size to load increment is mentioned due to the need to supply a fine enough grid to register increase in plastic zone size with each load stage.

The 400 simultaneous linear algebraic equations (with constant RHS for each iteration of each load stage) are solved by a matrix inversion, details of which are given in appendix (A) of the paper. In appendix (B) is formalised the incremental theory form of the total strain plastic strain equations as related to the plane stress problem. In his book Mendelson[3] gives a fuller account of the equations and procedures for both plane stress and plane strain.

This paper is thus complementary to the earlier Mendelson Hanson paper[10] and again represents a major step forward in elasto-plastic solutions. In the early 1960's, I.S. Tuba had taken up interest in these methods and in the spring of 1964 was awarded his Ph.D. from the

University of Pittsburg for his thesis on 'Elastic/Plastic Strain Concentrations'. His contribution to the literature on this subject is considerable.

In 1965, Tuba started publishing his solutions to the one dimensional problems of the thick sphere[2] and the hole in the plate under uniform tension[14]. The latter problem is the same as that of Davis, although a one dimensional stress function governing equation is used. In 1965/66 his attention moved on to the plane stress and plane strain problems.

In his 1966 paper 'A Method of Elastic-Plastic Plane Stress and Strain Analysis'[15], he sets out his justification for using stress functions governing equations compared with the integral governing equations of the one dimensional problems –

'This leads to the problem of generalising the method for two dimensional plane problems. It seems that conversion to an integral equation in terms of total strain components is not practical, because the variables cannot be separated for any one of the components. Since two dimensional elasticity problems are usually solved in terms of a stress function, it is natural to consider some sort of stress function formulation for plane elasto-plastic problems'.

His approach is essentially that of Roberts and Mendelson and the problem he tackles is that of a finite thick plate (plane strain) with edge slits under tension (fig. 2.5) using the deformation theory. Due to it being a finite plate a special boundary stress function is evolved by integration. Apart from evolving the usual plane stress/plane strain form of the biharmonic in cartesian coordinates, he shows it also in terms of an arbitrary orthogonal plane coordinate system. Then follows the usual recasting of the differential governing equation into a difference equation.

Since the problem is symmetrical a quarter is considered and a 20 x 20 grid laid over it. The elastic stress function solution is found and from an extrapolated elastic field past yield, first estimates of the plastic strains are evaluated from the Mendelson Manson procedure. An iterative technique following Griffin and Varga[16] (Chebyschev semi-iterative) is used to solve the stress function. Matrix inversion is considered but rejected due to computational difficulties in handling such a large matrix. The material is assumed to have a bilinear stress-strain curve with m = 0.017 and 0.1. He notes the restriction of the solution -- 'Because of the finite difference representation, stress at the tips of the cracks is finite. As a result, it can be expected that the elasto-plastic solution will not be exact at the tip of the crack'. Despite these inaccuracies, however, the solution can be expected to give an indication of the shape and growth of the plastic zone.

In his book[3] (1968) Mendelson, himself, tackles the crack problem using the elasto-plastic biharmonic difference equation. There are, however, a few differences from Tuba's solution. The problem is that of the central crack in an infinite sheet under tension. Both plane stress and plane strain conditions are considered.

The elastic solution of Muskhelishvili gives the stress function values ϕ_e over the grid of the field indicated. A second stress function ϕ_p is introduced which is a 'stress function increment' such that $\phi = \phi_e + \phi_p$. The governing equation for ϕ_p is then

$$\nabla^4 \phi_p = g(x,y) - dg(x,y) \qquad (2.17)$$

with the appropriate boundary conditions.

This solution, in fact, approaches the exact solution, since the elastic stress function produces the stress and strain singularities at the crack tip.

Interesting plots of plastic zone shape are given for varying linear work-hardening for both plane stress and plane strain at different loads.

In 1965, Tuba[17] produced his solution to the problem of an infinite plate with hyperbolic edge notches in tension, bending and shear, all under plane stress conditions – fig. 2.7. The elastic solution which is used as a starting point is that of Neuber[18] – using an elliptical/hyperbolic coordinate system. The boundary AB, is chosen for the symmetrical quarter and the field covered with an elliptical hyperbolic grid, giving 200 points for solution. The distribution of grid points is very favourable since there is a high density of points at the notch root.

The biharmonic differential equation is given and it is then recast in difference form. Once again the extrapolated elastic solution gives a first estimate of the plastic strains using the Mendelson Manson procedure, and the deformation theory since although 'the incremental theory gives more realistic results', the deformation theory 'requires less work'. The stress function is thus settled in the field using an over-relaxation factor of 1.5, and satisfying fixed boundary conditions on AB, symmetrical relations on the ξ's and $\phi = \frac{\partial \phi}{\partial n} = 0$ on the notch surface. The material used had linear work-hardening of $m = 0.1$.

2.4 Approach by Solving Second Order Differential Equations of the Displacements

In 1967, Tuba produced his paper 'An Analytic Method for Elastic Plastic Solutions'[19], which, marks another important step forward. He breaks away from the traditional approach to plane problems of reducing to, and working in one variable (usually the stress function). Instead he returns to the basic equations and reduces these to two equations in the coordinate displacements u and v.

In cylindrical polar coordinates the resultant two second order simultaneous partial differential equations are – for plane stress.

$$\frac{\partial}{\partial r}\left[\frac{1}{r}\frac{\partial}{\partial r}(ru)\right] + \frac{\partial}{\partial \vartheta}\left[\frac{1-\nu}{2r^2}\frac{\partial u}{\partial \vartheta} - \frac{3-\nu}{2}\frac{v}{r^2} + \frac{1+\nu}{2r}\frac{\partial v}{\partial r}\right]$$
$$= \frac{\partial \varepsilon_r^{\,p}}{\partial r} + \frac{1-\nu}{r}\varepsilon_r^{\,p} + \nu\frac{\partial \varepsilon_\vartheta^{\,p}}{\partial r} - \frac{1-\nu}{r}\varepsilon_\vartheta^{\,p} + \frac{1-\nu}{2r}\frac{\partial \gamma_{r\vartheta}^{\,p}}{\partial \vartheta} \qquad (2.18)$$

and

$$\frac{1-\nu}{2}\frac{\partial}{\partial r}\left[\frac{1}{r}\frac{\partial}{\partial r}(rv)\right] + \frac{\partial}{\partial \vartheta}\left[\frac{3-\nu}{2}\frac{u}{r^2} + \frac{1+\nu}{2r}\frac{\partial u}{\partial r} + \frac{1}{r^2}\frac{\partial v}{\partial \vartheta}\right]$$
$$= \frac{\nu}{r}\frac{\partial \varepsilon_r^{\,p}}{\partial \vartheta} + \frac{1}{r}\frac{\partial \varepsilon_\vartheta^{\,p}}{\partial \vartheta} + \frac{1-\nu}{2}\frac{\partial \gamma_{r\vartheta}^{\,p}}{\partial r} + \frac{1-\nu}{r}\gamma_{r\vartheta}^{\,p} \qquad (2.19)$$

where $\varepsilon^p \equiv \varepsilon^p + d\varepsilon^p$ in previous notation.
These equations can be rewritten as

$$f_1(u) = f_2(v) + \text{plastic terms}$$
$$f_3(v) = f_4(u) + \text{plastic terms.}$$

The problem tackled as an illustration is that of the hole in the infinite plate under tension – a two dimensional plane stress problem using the deformation theory. He considers only a symmetrical quarter and covers the field with a graded net of concentric circles of varying radii and a set of equally spaced radial lines – fig. 2.8. The circle radii increase as

$$r_m = T^{m-1}a$$

where the constant $T = 1.082$ giving $r_{30} = 9.765a$, r_{30} is the arbitrarily chosen outer boundary.
He starts off with the analytical elastic solution of Timoshenko and Goodier[20] and finds his initial estimates of $d\bar{\varepsilon}^p$ etc. from the Mandelson Manson procedure.

The first of the two governing equations is then used to solve u over the field by a relaxation technique on the difference form of the equation, with the boundary

conditions as shown in fig. 2.8. Similarly the second equation is then used to solve v over the field using the re-estimated values of u and the boundary conditions. The first equation is then resolved and so on until convergence is achieved. The resultant displacements are thus continuous. The boundary gradients on the circumferential boundaries are complex functions of stress, displacement and plastic strain. This Neumann boundary condition is very difficult to maintain.

The paper gives no resultant values of displacement, but only the stresses, which are found by integration from the displacements. This evaluation of stresses from a solution is certainly to be commended over the previous double differentiation of a stress function.

Stress-strain curves for real materials are used to compare the results with other experimental researchers. All materials have the equivalent of work-hardening $m < 0.1$.

Regarding the elastic/plastic boundary he comments -

'For many real materials, elastic/plastic boundaries are very difficult to define because the transition is very smooth. On the other hand when an idealized material is assumed, with well defined yield-point, there are discontinuities in the derivatives of the stresses and plastic strains at the elastic/plastic interface. Fortunately this causes no more difficulty in the computation than a real boundary. Simply, when derivatives are evaluated the appropriate forward and backward difference equations are used'.

This latter statement is put forward without proof and further detail as to the action to take when the boundary does not cross through a grid point. Difficulty was found by the writer when doing this in the simple elasto-plastic solution of a thick sphere under internal pressure, using a difference governing equation.

In his conclusion, he states how the method can be used for three dimensional problems using three simultaneous partial differential equations of second order to solve for u, v, and w in a simultaneous iteration process. This he intends to pursue, although no paper has yet been published.

2.5 Approach by Solving First Order Differential Equations

Considering all the difficulties of the other approaches and the fact that no researcher had appeared to have tackled the elasto-plastic problem from the basic constitutive equations, Professor I.N. Sneddon[21] suggested this should be attempted.

The only reference to a similar method using a set of first order partial differential governing equations was found in Chapter 6 of Mitchell[22]. The problems, however, were in fluid mechanics and of a hyperbolic nature. It is with this background that this present work was undertaken -- to thoroughly investigate the feasibility of applying this method to elasto-plastic problems.

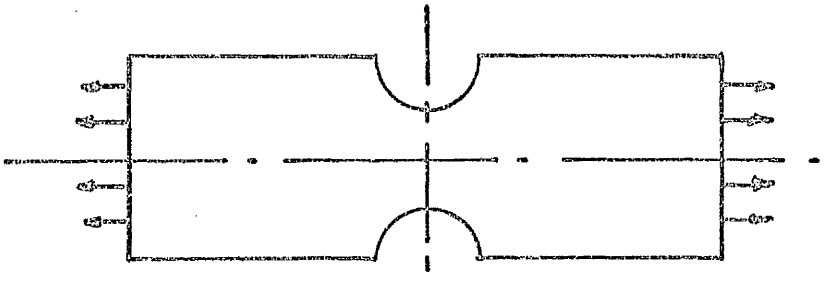

Fig 2.1

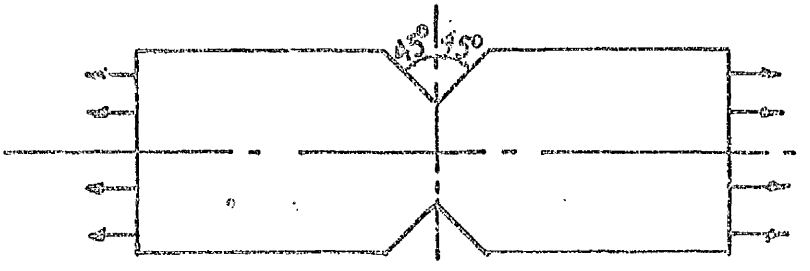

Fig 2.2

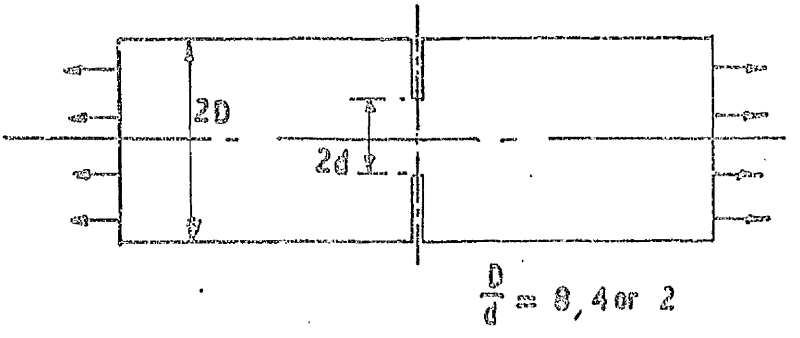

Fig 2.3

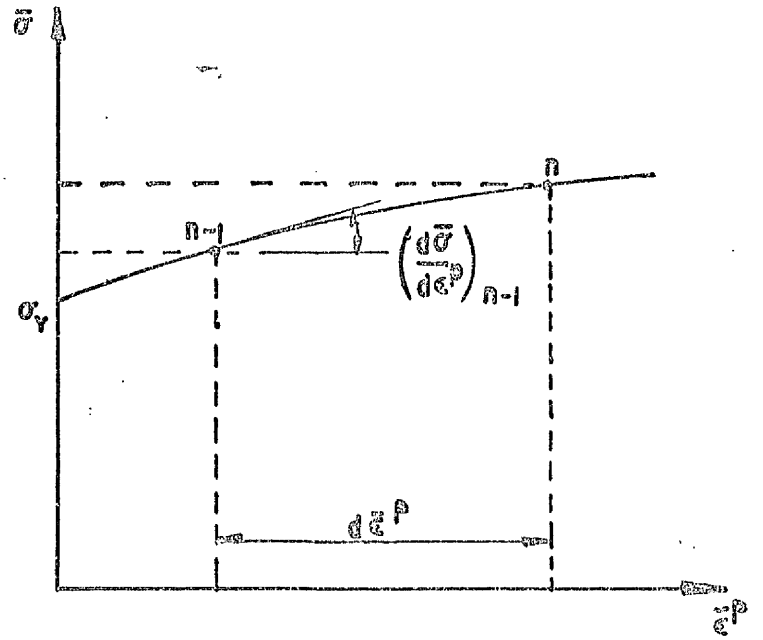
$\bar{\sigma}$
n
n-1
$\left(\frac{d\bar{\sigma}}{d\varepsilon^p}\right)_{n-1}$
σ_Y
$d\bar{\varepsilon}^p$
$\bar{\varepsilon}^p$

Fig 2.4

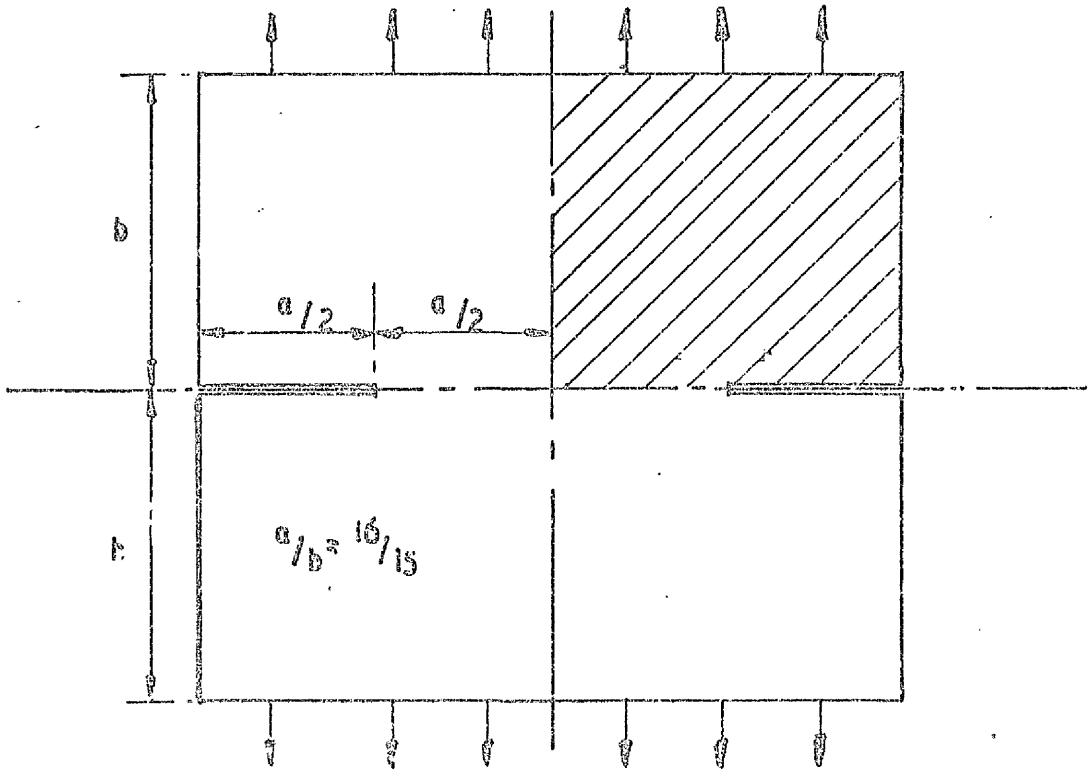
b
a/2
a/2
a/b = 16/15

Fig 2.5

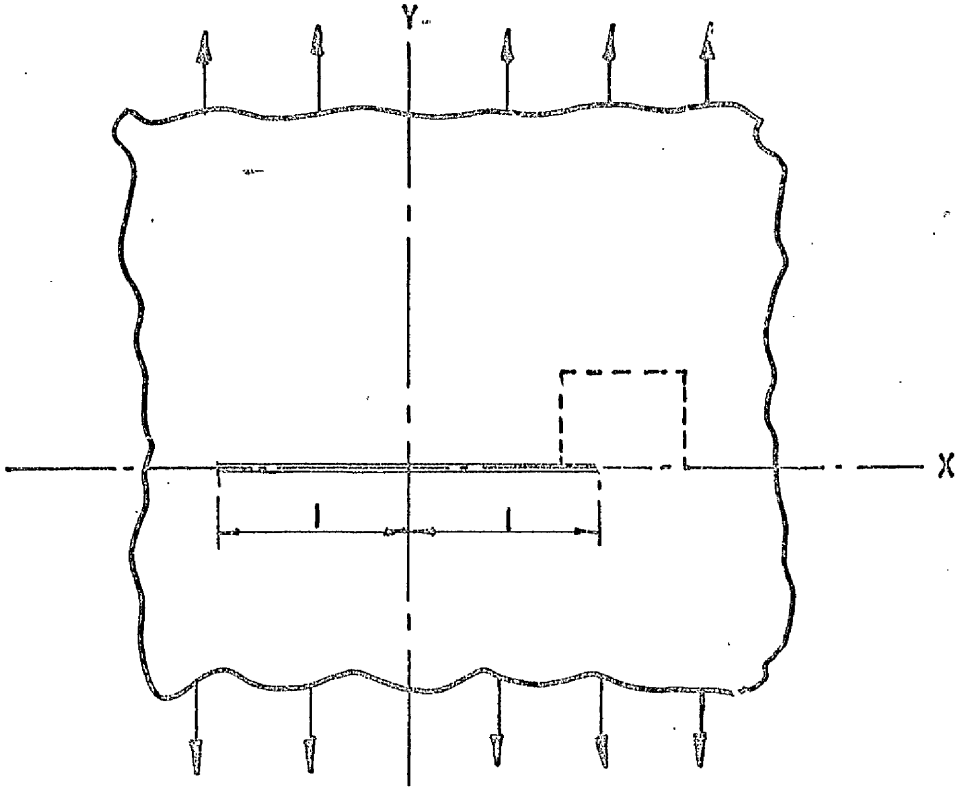

Fig 2.6

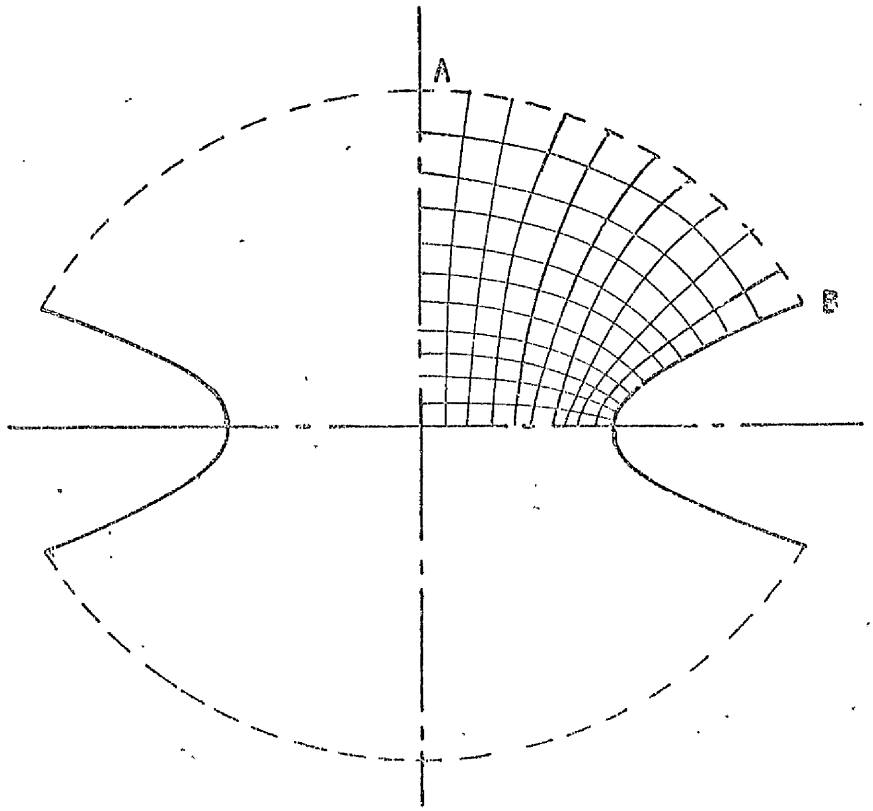

Fig 2.7

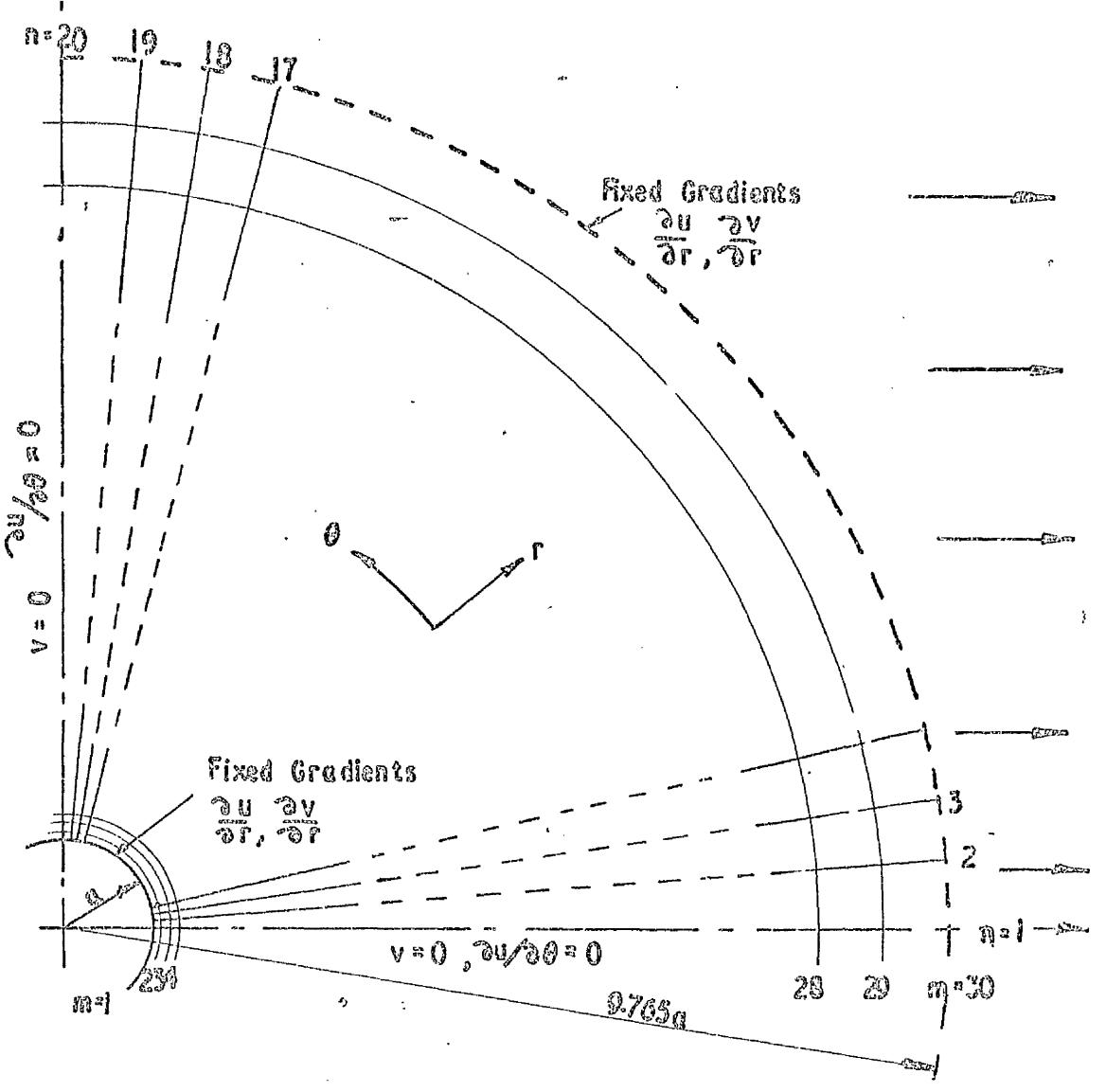
n=20
19
18
17
Fixed Gradients
∂u/∂r , ∂v/∂r
∂u/∂θ = 0
v = 0
θ
r
Fixed Gradients
∂u/∂r , ∂v/∂r
3
2
n=1
v = 0 , ∂u/∂θ = 0
m=1
23
28
29
n=30
0.765a

Fig 2.8

CHAPTER 3

ELASTIC SOLUTION OF KEYHOLE NOTCH

CHAPTER 3

ELASTIC SOLUTION OF KEYHOLE NOTCH

3.1 Introduction to Elastic Solution

This study is primarily interested in the states of stress and strain at a notch root, especially in the early stages of yielding where the area of plasticity is small. As a first step the elastic problem was solved by means of the Airy stress function which satisfies the biharmonic equation. It was thought that once this had been done, a new solution with plastic strain terms on the RHS of the equation could be solved. This was never done since a new method of elasto-plastic solution was devised. However, the elastic stress function solution provided the initial values of stresses for the elasto-plastic solution.

3.1.1 Early Attempts.

Two attempts were made to solve a stress function field for notched bars in tension and bending, using the actual specimen dimensions to give the geometry of the field.

(i) In the first attempt the notched bar was of dimensions shown in fig. 3.1. It was a single edge notched bar and so the first field was for a symmetrical half with boundary values of ψ and $\frac{\partial \psi}{\partial n}$ simulating the applied load system. A square grid of mesh points 27 x 27 covered the field A. It was hoped that following the solution of A, another field, B, of 27 x 27 mesh points but of half grid size, could be set up using values from the A field as boundaries and interpolated values as the first estimates of the stress function in this new field.

This process was to be continued into fields C and D with the grid size being halved each time. In this way, it was intended to find the solution at the notch root.

Two main disadvantages decided us to abandon this attempt

1. Convergence was too slow due to the size of field (and at this stage no accelerated procedure was contemplated).
2. The notch geometry required an increasing number of boundary interpolations to be carried out as the field grid sizes reduced.

(ii) The second attempt tried to rectify the disadvantages of the first. This time we considered a bar in tension with the geometry shown in fig. 3.2.

The bar was symmetrically notched and so a symmetrical quarter need only be considered. The first field had thus 12 x 8 mesh points. In addition, the slit geometry required no awkward interpolation on that boundary. Once again the main aim was to evaluate the stress field at the notch root, which had a small radius. It was proposed to progressively half the grid size and solve fields B, C, D and finally E, using the technique indicated in the description of the first attempt (i).

In contrast to (i) however a direct (matrix) method of solution was tried and difficulties encountered.

From these first attempts that it was decided (a) to work only in one field at the notch tip, (b) to model the geometry of that field to suit the mathematics, and (c) to look carefully at the number of mesh points used.

3.1.2 Final Selection of Notch Geometry.

From the experience gained from the first two attempts in paragraph 3.1.1 a new shape of notch was devised. This time, a keyhole shape was used, it having a root radius rather than a sharp crack with its intractable stress condition. The keyhole was chosen for several reasons.

1. The area could be covered with a net on which grid points could be defined by an r—θ coordinate system — fig. 3.3. The radii of the concentric circles were graded to give a greater coverage of points at the notch root

$$r = r_o T^{n-1}$$

(where T is a constant).

Using this cylindrical polar arrangement enabled a great simplification of boundaries since field equations could be expressed in polar form.

2. The manufacture of test specimens could be achieved more easily by simply drilling and honing the hole and then milling the slot. The honing was necessary to remove any pre-yielded surface layer.

3. A third advantage which was discovered later, was that when a strained specimen was sectioned, enlarged photographs could be easily scaled by measurement of AB (fig. 3.3). Good average values of notch surface strains could thus be found graphically. The actual dimensions of the test specimen used in the fracture research are given on fig. 3.4.

3.1.3 Search for Boundary Values

In selecting a stress condition for the outer (circular) boundary CD (fig. 3.3), we were influenced by a study of Neuber's solution of hyperbolic notches in an infinite plate under tensile, and bending conditions[18].

Both these give a similar pattern of stress at the notch root showing that the stressing condition at the outer boundary has very little affect there. What is more surprising is the similarity of the stress pattern for the sharp and radiused notches at a small distance from the root. Fig. 3.5 by Orr[23] illustrates this point.

For these reasons we chose, for the stress condition at the outer boundary, the fairly simple expressions for the sharp crack in the opening mode I. These could apply to both tension and bending. The important fact to remember is that although these solutions are for infinite plates, the accuracy is only acceptable in the vicinity of the notch or crack root. It may also be pointed out that Neuber produced solutions for single hyperbolic edge notched bars in bending and tension for the semi-infinite plate. These solutions were adapted from the symmetrical edge notch case. He states clearly however 'This method is only an approximation, since there are still certain small stresses present along the x-axis where now there should be a no-load boundary. This in fact is only a problem of the stress distribution in the immediate vicinity of the base of the notch, determined primarily by the flow of force through the narrowest section'- see fig. 3.6.

The values of the stress function ψ and its gradient $\frac{\partial \psi}{\partial n}$ are required on the outer boundary. This essentially fixes σ_r and $\tau_{r\vartheta}$ on that boundary. The inner boundary is stress free and has ψ and $\frac{\partial \psi}{\partial n}$ zero. The shape of the inner boundary can thus be altered slightly to give the keyhole shape CBAD (fig. 3.7) without altering the boundary conditions.

This certainly will slightly affect the field stress distribution since the outer boundary stresses (σ_r and $\tau_{r\vartheta}$) remain unchanged. This will be shown later.

Another benefit of using the sharp crack solution is that values of ψ and $\frac{\partial \psi}{\partial n}$ can be calculated right up

to C and D whereas, if a hyperbolic notch were used to match up root radii, the stress function values could only be given up to K and L. The values on arcs CK and DL would thus have to be adjusted.

The usual form of the crack stress equations is (reference to fig. 3.8)

$$\left.\begin{matrix}\sigma_x \\ \sigma_y\end{matrix}\right\} = \frac{C}{\sqrt{r}} \cos\frac{\vartheta}{2}\left(1 \mp \sin\frac{\vartheta}{2}\sin\frac{3\vartheta}{2}\right) \qquad (3.1)$$

$$\tau_{xy} = \frac{C}{\sqrt{r}} \cos\frac{\vartheta}{2}\sin\frac{\vartheta}{2}\cos\frac{3\vartheta}{2}\,. \qquad (3.3)$$

The constant C is usually given as $\sqrt{\frac{a}{2}}$ where 'a' is the half crack length. The physical situation is visualized in fig. 3.9 where the line KL would represent the upper surface of the notched bar and the broken circular line, the extent of the field solution. The values of σ_x, σ_y and τ_{xy} are plotted on the x and y axes.

Referring to fig. 3.10 the transformation relations from the X–Y to the r–ϑ coordinates are

$$\sigma_r = \frac{\sigma_x+\sigma_y}{2} + \frac{\sigma_x-\sigma_y}{2}\cos 2\vartheta + \tau_{xy}\sin 2\vartheta \qquad (3.4)$$

$$\sigma_\vartheta = \frac{\sigma_x+\sigma_y}{2} - \frac{\sigma_x-\sigma_y}{2}\cos 2\vartheta - \tau_{xy}\sin 2\vartheta \qquad (3.5)$$

$$\tau_{r\vartheta} = -\frac{\sigma_x-\sigma_y}{2}\sin 2\vartheta + \tau_{xy}\cos 2\vartheta. \qquad (3.6)$$

Adding (3.4) and (3.5) and substituting in (3.1) and (3.2) gives

$$\sigma_r+\sigma_\vartheta = \sigma_x+\sigma_y = 2Cr^{-\frac{1}{2}}\cos\frac{\vartheta}{2}. \qquad (3.7)$$

Similarly subtraction of (3.4) and (3.5) gives

$$\sigma_\vartheta-\sigma_r = (\sigma_y-\sigma_x)\cos 2\vartheta - 2\tau_{xy}\sin 2\vartheta$$
$$= -2Cr^{-1/2}\cos\frac{\vartheta}{2}\left(\sin\frac{\vartheta}{2}\right)^2 \qquad (3.8)$$

Adding (3.7) and (3.8) to eliminate σ_r gives

$$\sigma_\vartheta = Cr^{-\frac{1}{2}} \cos\tfrac{\vartheta}{2}\,(1 - \sin^2\tfrac{\vartheta}{2}).$$

But

$$\sigma_\vartheta = \frac{\partial^2\psi}{\partial r^2} = Cr^{-\frac{1}{2}} (\cos\tfrac{\vartheta}{2})^3$$

therefore $$\frac{\partial\psi}{\partial r} = \frac{Cr^{\frac{1}{2}}}{\frac{1}{2}} (\cos\tfrac{\vartheta}{2})^3 + C_1$$

and $$\psi = C.\frac{r^{\frac{3}{2}}}{\frac{3}{4}} (\cos\tfrac{\vartheta}{2})^3 + C_1 r + C_2.$$

Arbitrarily choosing the constants of integration $C_1 = C_2 = 0$ and letting $K = \frac{4C}{3}$ gives

$$\psi = K\, r^{\frac{3}{2}} (\cos\tfrac{\vartheta}{2})^3. \qquad (3.9)$$

The problem so formulated has no scale, since essentially it is a vicinity solution with no finite boundaries. For the determination of applied loads the solution must be matched up to our specimen geometry — fig. 3.4. For this reason a search was made of the literature for finite boundary solutions. This search it was hoped might have furnished a field elastic solution for an edge notched bar with finite boundaries. This proved not to be so.

Consequently it was decided to proceed in the following way. The moment can be calculated by integration from the σ_x (or σ_ϑ) distribution in the minimum section MN — see fig. 3.11. The solution obtained however can only be used out to two to three r_o radii and M is distant some 31 r_o radii distant. From fig. 3.11, it can be seen that Neuber predicts a concentration of 4.7 for σ_x at K; this does not mean that at K, $\sigma_x \equiv -1.0$ but at a first approximation it can be taken so.

This means that at first yielding the distribution of $\frac{\sigma_x}{\sigma_Y}$ starts at N with a value 1.1251 and is known out to 2 to 3 r_o radii and then ends up at M with a value $\frac{-1.1251}{4.7} = -0.239$. A stress distribution must be fitted in between these known values, while still maintaining the equilibrium condition that there is no net x-direction force through the minimum section. As a check on Neuber's concentration factor, a stress distribution was graphically 'smoothed' into the calculated stress field and adjusted to satisfy equilibrium; the resulting factor was approximately 4.9.

Such a distribution is shown in fig. 3.12. The moment so obtained is approximately 47 $r_o^2 \sigma_Y$ kNm/m thickness. Thus for Q1 Navy steel† and bar dimensions r_o = 1.4 mm and 36.6 mm thickness the moment $\doteq$ 2.1 kNm.

As a rough check consider a rectangular bar of section 43.1 mm x 36.6 mm; for Q1 Navy steel yielding will initiate at 7.9 kNm. If on one outer fibre there is a stress concentration of 4.7, then very roughly yielding will initiate at approximately $\frac{7.9}{4.7}$ = 1.7 kNm.

As a final check if the applied moment 2.1 kNm is plotted against the notch opening of 0.108 mm from paragraph 3.4.4 on an experimental graph there is reasonable agreement (see chapter 8).

---

† as used in our research program $\sigma_Y \doteq 630$ N/mm^2.

3.2 Numerical Formulation of the Problem

3.2.1 Selection of Actual Field Size

With the decision being taken on the analytical solution used, the field dimensions must be set and the boundary values of stress function ψ and its normal gradient $\frac{\partial \psi}{\partial n}$ must be evaluated. Due to the symmetry of the field only half need be considered.

The inner boundary BN, fig. 3.13, is designated $m = 2$ and has radius $r_o = 1.0$. The field extends out to $m = 18$ where

$$\text{outer radius} = T^{(18-2)} . r_o = 6.58325\ r_o .$$

(This outer radius is indicated on figs. 3.3 and 3.9).

The radial lines are designated $n = 1$ to 19 with $n = 3$ being the $\not{\text{C}}$ and $n = 19$ being the notch surface, CB.

The analytical form of the stress function from (3.9) is

$$\psi = K\, r^{\frac{3}{2}} \left(\cos \tfrac{\vartheta}{2}\right)^3 .$$

On the inner surface, CBN, as discussed previously, $\psi = \frac{\partial \psi}{\partial r} = \text{constant} = 0$ say, since

$$\sigma_r = \frac{1}{r}\frac{\partial \psi}{\partial r} + \frac{1}{r^2}\frac{\partial^2 \psi}{\partial \vartheta^2} = 0$$

and

$$\tau_{r\vartheta} = -\frac{\partial}{\partial r}\left(\frac{1}{r}\frac{\partial \psi}{\partial \vartheta}\right) = 0.$$

However, on the outer surface, the arbitrary choice of value of K will determine the value of ψ and $\frac{\partial \psi}{\partial r}$. Since

$$\frac{\partial \psi}{\partial r} = \frac{3}{2} K\, r^{\frac{1}{2}} \left(\cos \tfrac{\vartheta}{2}\right)^3 ,$$ it was decided to

make $K = \frac{1}{r_{m=18}^{\frac{1}{2}}} = \frac{1}{(6.58325)^{\frac{1}{2}}} = 0.38974$ so that

$$\left(\frac{\partial \psi}{\partial r}\right)_{m=18} = 1.5 \left(\cos \tfrac{\vartheta}{2}\right)^3 .$$

Thus $$\psi_{m=18} = \frac{1}{r_{m=18}^{\frac{1}{2}}} r_{m=18}^{\frac{3}{2}} (\cos\tfrac{\vartheta}{2})^3 = 6.58325(\cos\tfrac{\vartheta}{2})^3.$$

Varying ϑ for $n = 1$ to $n = 19$ will give the values of ψ and $\frac{\partial\psi}{\partial r}$ on the outer boundary.

3.2.2 Boundary Conditions

The field equation $\nabla^4\psi = 0$, must solve points for $n = 3$ to 18 and $m = 3$ to 17 inclusive. Using the finite difference form of $\nabla^4\psi$ for the solution of a value $\psi_{m,n}$ requires values up to $\psi_{m\pm2,n\pm2}$. This can be done near the boundaries as follows; consider each boundary in turn – fig. 3.13. (Formulae from Taylor series expansion radially and circumferentially).

1) Boundary EFC. Values ψ_a on $n = 3$ to 18 based at b, c and ψ_{18} and gradient $(\frac{\partial\psi}{\partial r})_{18}$ given by

$$\psi_a = 3.370665 \times (\cos((n-3).\tfrac{\pi}{32}))^3 + 0.595586 \times \psi_6 - 0.156748 \times \psi_c.$$

Points b, c etc. found from field equation.

2) Boundary CB. Values of ψ_d on $m = 4$ to 16 based on values of ψ at e, f and considering ψ and $\frac{\partial\psi}{\partial\vartheta}$ both zero on $n = 19$, given by the interpolation formula

$$\psi_d = 0.4929 \times \psi_e - \frac{\psi_f}{9}.$$

Special point g i.e. ($m = 3$, $n = 18$)

$$\psi_g = 0.418301\,\psi_h - 0.077319\,\psi_i.$$

Points e, f etc. found from field equation.

3) Boundary EN. In order that ψ_h might be found from the field equation the value at an external point j must be found on $m = 1$ for $n = 3$, 17. The formula is based

on values on inner boundary, k and ℓ. Thus the extrapolation formula is

$$\psi_j = 2.11675\,\psi_k - 0.292786\,\psi_\ell .$$

Points k, ℓ etc. can thus be found from the field equation.

4) Boundary NE. Symmetry of the stress function over the $\not\in$ dictates simply that

$$\psi_p = \psi_s \qquad \text{and} \qquad \psi_q = \psi_r .$$

Thus all points on the $\not\in$ (n = 3) from m = 3 to 16 can be evaluated from the field equation.

3.2.3 Evaluation of Coefficients of Finite Difference Expansion of Biharmonic Equation in Polar Coordinates

Refer to fig. 3.14.

Radii increase in geometric progression viz

$$\frac{r_{10}}{r_2} = \frac{r_2}{r_o} = \frac{r_o}{r_4} = \frac{r_4}{r_{12}} = (1+b) = \frac{1}{1-a} .$$

Radial lines at equal angles $\delta\vartheta = c$. Consider the truncated Taylor series expansion of ψ from point 0 to the points 1, 2, 3, 4.

$$\left.\begin{aligned}
\psi_1 &= \psi_o - c\psi_o' + \tfrac{1}{2}c^2\psi_o'' \\
\psi_2 &= \psi_o + br_o\psi_o' + \tfrac{1}{2}b^2r_o{}^2\psi_o'' \\
\psi_3 &= \psi_o + c\psi_o' + \tfrac{1}{2}c^2\psi_o'' \\
\psi_4 &= \psi_o - ar_o\psi_o' + \tfrac{1}{2}a^2r^2\psi_o''
\end{aligned}\right\} \qquad (3.10)$$

where $\psi_o' = \left(\frac{\partial\psi}{\partial\vartheta}\right)_o$

$\psi_o' = \left(\frac{\partial\psi}{\partial r}\right)_o$

and similarly for the curvatures.

The harmonic operator $\nabla^2 = (\frac{1}{r}\frac{\partial}{\partial r} + \frac{\partial^2}{\partial r^2} + \frac{1}{r^2}\frac{\partial^2}{\partial \vartheta^2})$, when discretized, is a function of ψ_0, ψ_1, ψ_2, ψ_3 and ψ_4. The coefficients of ψ_1, and ψ_3, say α, will be the same due to the constant angle, whereas the coefficients of ψ_2 and ψ_4 are different, say λ and μ.

Therefore multiply equations (3.10) by the appropriate constant and add

$$\alpha\psi_1 + \lambda\psi_2 + \alpha\psi_3 + \mu\psi_4 = \psi_0(2\alpha + \lambda + \mu) + r_0\psi_0'(\lambda b - \mu a) + c^2\alpha\psi_0'' + \tfrac{1}{2}r_0^2\psi_0''(\lambda b^2 + \mu a^2). \tag{3.11}$$

Multiplying the harmonic equation by another constant f and non-dimensionalizing it gives at 0

$$fr_0^2\nabla^2\psi_0 = fr_0^2(\frac{1}{r_0}\psi_0' + \psi_0'' + \frac{1}{r_0^2}\psi_0'') = fr_0\psi_0' + fr_0^2\psi_0'' + f\psi_0''.$$

Re-arranging (3.11) gives

$$\alpha\psi_1 + \lambda\psi_2 + \alpha\psi_3 + \mu\psi_4 - \psi_0(2\alpha + \lambda + \mu) = r_0\psi_0'(\lambda b - \mu a) + c^2\alpha\psi_0'' + \tfrac{1}{2}r_0^2\psi_0''(\lambda b^2 + \mu a^2)$$

and this is $\equiv fr_0^2\nabla^2\psi_0$.

Therefore equating terms gives

$$\lambda b - \mu a = f \tag{3.12}$$

$$\tfrac{1}{2}(\lambda b^2 + \mu a^2) = f \tag{3.13}$$

$$c^2\alpha = f. \tag{3.14}$$

Also $(1 + b) = \frac{1}{1-a}$ i.e. $b - a = ab.$ (3.15)

Four equations and seven unknowns allows an arbitrary choice of three variables. The geometry of the net is defined by a, b and c and so these are chosen.

Now

$$fr_o^2\nabla^2\psi_o = (\alpha\psi_1 + \lambda\psi_2 + \alpha\psi_3 + \mu\psi_4) - \psi_o(2\alpha + \mu + \lambda)$$

if $\psi_1 = \psi_2 = \psi_3 = \psi_4 = \psi_o$ then $\nabla^2\psi_o = 0$

therefore $\lambda + \mu = 2$

and coefficient of $\psi_o = 2(\alpha + 1)$.

To find $\nabla^4\psi_o$ use the identity $\nabla^4 = \nabla^2\nabla^2$ and get

$$fr_o^4\nabla^4\psi_o = (\alpha\nabla^2\psi_1 + \lambda\nabla^2\psi_2 + \alpha\nabla^2\psi_3 + \mu\nabla^2\psi_4) - \nabla^2\psi_o 2(\alpha + 1)$$

$$= \alpha\left[(\alpha\psi_9 + \lambda\psi_5 + \alpha\psi_o + \mu\psi_8) - \psi_1 2(\alpha + 1)\right]$$

$$+ \lambda\frac{r_o^2}{r_2^2}\left[(\alpha\psi_5 + \lambda\psi_{10} + \alpha\psi_6 + \mu\psi_o) - \psi_2 2(\alpha + 1)\right]$$

$$+ \alpha\left[(\alpha\psi_o + \lambda\psi_6 + \alpha\psi_{11} + \mu\psi_7) - \psi_3 2(\alpha + 1)\right]$$

$$+ \mu\frac{r_o^2}{r_4^2}\left[(\alpha\psi_8 + \lambda\psi_o + \alpha\psi_7 + \mu\psi_{12}) - \psi_4 2(\alpha + 1)\right]$$

$$- 2(\alpha + 1)\left[(\alpha\psi_1 + \lambda\psi_2 + \alpha\psi_3 + \mu\psi_4) - 2(\alpha + 1)\psi_o\right].$$

Giving

$$f^2r_o^4\nabla^4\psi_o = \psi_o(6\alpha^2 + 8\alpha + 4 + \lambda\mu\frac{r_o^2}{r_2^2} + \lambda\mu\frac{r_o^2}{r_4^2})$$

$$-(\psi_1 + \psi_3)4\alpha(\alpha + 1) - \psi_2 2\lambda(\alpha + 1)(1 + \frac{r_o^2}{r_2^2})$$

$$-\psi_4 2\mu(\alpha + 1)(1 + \frac{r_o^2}{r_4^2}) + (\psi_5 + \psi_6)\alpha\lambda(1 + \frac{r_o^2}{r_2^2})$$

$$+(\psi_7 + \psi_8)\alpha\mu(1 + \frac{r_o^2}{r_4^2}) + (\psi_9 + \psi_{11})\alpha^2$$

$$+ \psi_{10}\lambda^2\frac{r_o^2}{r_2^2} + \psi_{12}\mu^2\frac{r_o^2}{r_4^2}. \qquad (3.16)$$

Choice of constants

It was decided to make the angular division $\frac{\pi}{16}$ and the ratio of successive radii 1.125(= T) giving the dimensions of the a grid 'element' as shown in fig. 3.15. Thus

$$c = \frac{\pi}{16} = 0.19634954 \qquad \frac{r_o^2}{r_2^2} = \frac{r_o^2}{(Tr_o)^2} = \frac{1}{T^2}$$

$$b = (T-1) = 0.12500000$$

$$a = 1-\frac{1}{T} = 0.11111111 \qquad \frac{r_o^2}{r_4^2} = \frac{r_o^2}{(\frac{r_o}{T})^2} = T^2$$

therefore $$\mu = \frac{4b - 2b^2}{a^2 + 2a + 2b - b^2} = 0.99958860$$

$$\lambda = 1.00041140$$

$$f = 0.01398603$$

$$\alpha = 0.36277260.$$

Thus coefficient of ψ_o = 9.74755266

$$\frac{\text{coefficient of } \psi_1}{\text{coefficient of } \psi_o} = 0.2028718 = c_1 = c_3.$$

Similarly

$$c_2 = 0.5007483$$

$$c_4 = 0.6332385$$

$$c_5 = c_6 = -0.0666500$$

$$c_7 = c_8 = -0.0842845$$

$$c_9 = c_{11} = -0.0135012$$

$$c_{10} = -0.0811254$$

$$c_{12} = -0.1297336.$$

For the biharmonic equation for elastic conditions $\nabla^4\psi = 0$ in equation (3.16).

Thus re-arranging (3.16) gives ψ_o as a function of the other twelve points

$$\text{i.e.} \qquad \psi_o = \sum_{i=1}^{12} c_i \psi_i .$$

3.3 Choice of Numerical Method for the Solution of the Biharmonic Difference Equation

3.3.1 Choice of Method

The choice of method depends on several factor both numerical and physical. Essentially the solution of simultaneous linear algebraic equations can be achieved in two ways – direct methods and iterative methods. The direct method involves formulating the equations into a matrix equation $\mathbf{AU} = \mathbf{B}$ and solving by one of several methods to find $\mathbf{U} = \mathbf{A}^{-1}\mathbf{B}$. With the keyhole field there are 210 interior points to solve, each one having an equation of 13 coefficients and a RHS. Thus the matrix of coefficients $\mathbf{A}$ would be 210 x 210 over 44,000 elements of which over 41,000 are zero. Although nowadays computers could handle this storage problem it would not be easy. In addition should boundary conditions have to be varied the direct solution is not advised.

Forsyth and Wasow[24] comment 'iterative methods are preferred for solving large sparse systems $\mathbf{AU} = \mathbf{B}$ because they take full advantage of the numerous zeros in A, both in storage and operation. Moreover they tend to be self correcting in contrast to direct methods and hence minimize round-off error'.

Having made the decision to use an iterative method the problem now arises which one. One can use simultaneous or successive methods, explicitly or implicitly. By an explicit method is meant that the k^{th} approximation in the i^{th} component U_i^k can be determined by itself at its proper step of the algorithm, without the

necessity of simultaneously determining a group of other components U^k. Sometimes the formulae for explicit relaxation are recast such that they appear to define all the components of U^k at once (Method of Simultaneous Displacements), but for explicit methods this is only a notational convenience and not a computational necessity. In contrast are implicit formulae by which a group (usually block or rows and columns) of components of U^k are defined simultaneously in such an interrelated manner that it is necessary to solve a linear subsystem for the whole subset of components at once before a single one can be determined.

By a simultaneous method is meant one in which all the variables solved in the $(k-1)^{th}$ iteration U_i^{k-1}, are used in the k^{th} iteration, after which all values U_i^k are substituted simultaneously for U_i^{k-1}. Successive methods, however, update the values U_i^k successively as they are evaluated.

Obviously for maximum efficiency of solution, the method with the best rate of convergence must be found. An excellent comparison is found in Forsyth and Wasow[24]. A test problem is set and the rates of convergence are worked out for six methods.

The problem set is the solution of Laplace's Equation $F_u = \frac{\partial^2 u}{\partial x^2} + \frac{\partial^2 u}{\partial y^2} = 0$ in a square region of side π, divided into n^2 mesh squares with $nh = \pi$, fig. 3.16. There are $(n-1)^2$ interior points. The rates of convergence are valid for the solutions of Poisson's equation, with Dirichlet boundary conditions (U fixed on the boundary). The 5 point finite difference form of the equation is

$$\frac{1}{h^2}\left[U_{x+h,y} + U_{x,y+h} + U_{x-h,y} + U_{x,y-h} - 4U_{xy}\right] = 0.$$

Since the keyhole field has 14 x 15 interior points, a value of $n = 14$ is used for numerical comparison of each method.

Method	Approximate Rate of Convergence	Numerical values n = 14	
Simultaneous (Jacobi) Displacements by Points	$\frac{h^2}{2}$	0.025	Explicit
Successive (Gauss Seidel) Displacements by Points	h^2	0.050	
Optimum Successive (SOR) Overrelaxation by Points	$2h$	0.448	
Simultaneous Displacement Implicit by Lines	h^2	0.050	Implicit
Successive Displacement Implicit by Lines	$2h^2$	0.100	
Peaceman-Rachford (ADL) Alternating Direction Implicit	$\frac{-0.773}{\log_e \sin(\frac{h}{2})}$	0.353	

The Peaceman-Rachford Method is basically the implicit method of simultaneous displacements by lines with the essential difference that in alternate iterations vertical and horizontal lines are solved.

It was thus decided to use the explicit method of successive overrelaxation by points (SOR). In a paper in 1967, Otter, Cassell and Hobbs[25] consider another method -- Dynamic Relaxation. SOR is an accelerated method unlike the Jacobi and Gauss-Seidel methods. By use of an accelerator the rate of convergence can be enhanced, since

the difference of U values at two successive iterations is multiplied by a factor q

$$\text{i.e.} \quad U_i^k \text{ is corrected to } U_i^k + q(U_i^k - U_i^{k-1}).$$

Dynamic relaxation is an accelerated simultaneous method as shown below

	Simultaneous	Successive
Basic	Jacobi	Gauss Seidel
Accelerated	Dynamic Relaxation	SOR

Using Poisson's Equation each of these methods is represented by the following algorithms where $U^k_{x,y}$ is the k^{th} approximation of U at the point (x,y) and so on.

Jacobi: $$\delta U^{k+1}_{x,y} = \frac{1}{4}(U^k_{x+h,y}+U^k_{x,y+h}+U^k_{x-h,y}+U^k_{x,y-h})-U^k_{x,y}$$

Gauss-Seidel: $$\delta U^{k+1}_{x,y} = \frac{1}{4}(U^k_{x+h,y}+U^{k+1}_{x,y+h}+U^{k+1}_{x-h,y}+U^k_{x,y-h})-U^k_{x,y}$$

SOR: $$\delta U^{k+1}_{x,y} = \frac{\omega}{4}(U^k_{x+h,y}+U^{k+1}_{x,y+h}+U^{k+1}_{x-h,y}+U^k_{x,y-h}-4U^k_{x,y}),$$

In dynamic relaxation the equation is expressed as a damped wave equation to give

$$\delta U^{k+1}_{x,y} = \Big[(1-\tfrac{K}{2})\delta U^k_{x,y} + \tfrac{1}{2}(U^k_{x+h,y} + U^k_{x,y+h} + U^k_{x-h,y} + U^k_{x,y-h}) - 4U^k_{x,y}\Big] \Big/ (1+\tfrac{K}{2})$$

where K = viscous damping factor.

However the general conclusion indicates that SOR is more efficient than dynamic relaxation.

In addition to the above reasons, SOR is efficient in computer storage and is probably one of the easiest to program.

3.3.2 Determination of an Optimum Accelerating Factor

Having decided on the method to be used, the one remaining problem is the determination of an optimum accelerating factor q_{opt}.

Consider first a simplified model

Simplified Model for the Evaluation of Accelerators

Consider a square grid of side h — fig. 3.17. The finite difference form of the biharmonic is

$$h^4\nabla^4 F = 20F_o - 8\sum F_1 + 2\sum F_2 + \sum F_3 = 0$$

where F_i are the values of stress function F at points i.

Now in a non-converged field, if all the values of F_i are in error by e_i from the true values ψ then $F_i = \psi_i + e_i$ = true + error.

Thus in the next evaluation of the point 0, to give F_o' with error e_o'

$$F_o' = \psi_o + e_o' = (0.4\sum\psi_1 - 0.1\sum\psi_2 - 0.05\sum\psi_3) + (0.4\sum e_1 - 0.1\sum e_2 - 0.05\sum e_3).$$

But $$\psi_o - 0.4\sum\psi_1 - 0.1\sum\psi_2 - 0.05\sum\psi_3 = 0$$

and

$$0.4\sum e_1 - 0.1\sum e_2 - 0.05\sum e_3 = e_o - \frac{1}{20}h^4\nabla^4 e_o$$

therefore $$e_o' = e_o - \frac{1}{20}h^4\nabla^4 e_o = e_o - \Delta e_o$$

OR $$\delta e = -e_o' + e_o = \Delta e_o$$

where Δe_o = increment by which e_o is reduced in one evaluation of $F_o = \frac{h^4}{20}\nabla^4 e_o$

δe = actual value by which error is decreased.

With an accelerator q

$$F_o' = q\left[(0.4\sum F_1 - 0.1\sum F_2 - 0.05\sum F_3) - F_o\right] + F_o$$

and $e_o' = e_o - q\Delta e$ OR $\delta e = +q\Delta e_o$.

Now in a successively solved field, half the points in the evaluation of F_o will already have been re-evaluated and thus have a different error from the remainder. Consider the grid shown in fig. 3.18 where all points have an initial error of e_o. The points marked with a cross have been re-evaluated to give error e_o' and have reduced their error by δe

$$e_o' = e_o - \delta e.$$

The circled points still have error e_o

therefore
$$\begin{aligned} e_o' &= q\left[0.4(4e_o - 2\delta e) - 0.1\,(4e_o - 2\delta e)\right. \\ &\quad \left. -0.05(4e_o - 2\delta e)\right] - (q-1)e_o \\ &= q(e_o - \Delta e_o) - 0.5q\delta e - qe_o + e_o \end{aligned}$$

therefore
$$\delta e = + \frac{q\Delta e_o}{1 - 0.5q}.$$

This formula indicates the upper limit of q at 2 and when $q = 1$, $\delta e = 2\Delta e_o$ indicating twice the speed of convergence of successive over simultaneous solutions (e.g. Gauss-Seidel over Jacobi methods of iterative solution).

These ideas are certainly not new but the model gives a simple and clear picture of an accelerated successive iterative method. In the 1950's, Young[26] did much work in the search for optimum accelerators. One conclusion worthy of note is '... if q is slightly larger than q_{opt} then the increase in N (number of iterations to convergence) is relatively small but if q is smaller than q_{opt} then there is a much larger increase in N'. Many researchers have spent much time trying to analytically determine q_{opt} and in 1962, Carré[27] went to the extent of showing how successively better estimates of q_{opt} can be obtained during the course of a solution.

Forsyth and Wasow sum up the problem; 'q must be known in a relatively short computer time - certainly in less than the time it takes to solve the problem with

any reasonable guess of q_o. ---Three approaches to determining q_{opt} have occurred to the authors (1) one runs for a number of cycles with the method of successive displacements ($q = 1$) (2) one varies q over values near q_{opt} (3) one tries to approximate the least eigenvalue of a related problem with homogeneous boundary conditions. None of these methods has yet proved itself to be outstandingly successful and it may even be true that determining q_{opt} is as hard a problem as solving the original problem.

Having in mind all these facts, the problem of finding q_{opt} for the keyhole stress function field was solved practically by varying q from 1.3 to 1.8 and watching the effect on sample points. The results for the point $m = 10$, $n = 3$ are shown on the graph (fig. 3.19), from which it can be seen that q_{opt} lies around 1.7. Closer study indicated that q_{opt} lay between 1.69 and 1.70 depending on which part of the field was considered.

Concerning the number of iterations required, a simplified model was once again used.

Consider now a rectangular field $2a \times 2b$ covered by a square grid of side 'h', fig. 3.20, such that $a = mh$ and $b = nh$. If the error on this field is zero on the boundaries and maximum in the centre, suppose the error to be of the form

$$e = \frac{e_o}{4}\left(1 + \cos\frac{\pi x}{a}\right)\left(1 + \cos\frac{\pi y}{b}\right)$$

— see fig. 3.21

$$\nabla^4 e = \frac{\pi^4 e_o}{4}\left[\frac{1}{a^4}\cos\frac{\pi x}{a} + \frac{1}{b^4}\cos\frac{\pi y}{b} + \left(\frac{1}{a^2} + \frac{1}{b^2}\right)^2 \times \cos\frac{\pi x}{a}\cos\frac{\pi y}{b}\right].$$

If $m = 8$ and $n = 8$ i.e. a 16 x 16 mesh field of keyhole field.

$$\nabla^4 e_o = \frac{\pi^4 e_o}{4} \frac{5}{a^4}$$

therefore $$\Delta e_o = \frac{h^4}{20} \frac{\pi^4 e_o 5}{4a^4} = \frac{e_o}{670}$$

i.e. with no accelerator after 670 iterations the error would be zero.

This of course assumes that the error would decrease by the same amount e_o each time whereas in fact the actual decrease in error δe is less each time.

However it is interesting to note in passing that the keyhole field took between 600 and 700 iterations with an optimum accelerator of 1.7 to settle to within 5 significant digits.

To reduce the number of iterations to convergence an initial estimate was made of the field values viz

$$\psi = (0.392430 + 0.447491\ r^2 - 0.812390\ r - 0.027531\ r^3) \times (\cos((n - 3) \times \tfrac{\pi}{32}))^3.$$

However as can be seen from the graph (fig. 3.19), with a starting value of $\psi = 0$ for the point (10,3) and an accelerating factor of 1.7 (broken curve), the convergence is almost identical to that when an initial value of $\psi = 0.79$ (from the above formula) is used.

3.4 Results from Keyhole Elastic Solution

3.4.1 Non-dimensionalising of Stresses, Strains and Displacements

Due to the non-scalar formulation of the problem, the non-dimensionalising is done relative to the yield stress σ_Y. In other words it is assumed that the field is so stressed as to cause the effective stress at the notch root just to attain a yield value. At the notch root the radial and shear stresses are zero and for plane strain

the third strain $\varepsilon_z = 0$ thus

$$E\varepsilon_z = 0 = \sigma_z - \nu\sigma_\vartheta \Rightarrow \sigma_z = \nu\sigma_\vartheta .$$

Therefore effective stress

$$\bar{\sigma} = \sqrt{\sigma_\vartheta^2 + \sigma_z^2 - \sigma_\vartheta\sigma_z} = \sigma_\vartheta\sqrt{1 - \nu + \nu^2} .$$

Therefore at the notch root

$$\sigma_\vartheta = \frac{1}{\sqrt{1 - \nu + \nu^2}} . \quad \bar{\sigma} = 1.125\,\bar{\sigma} \text{ for } \nu = 0.3.$$

Therefore at yield $\frac{\sigma_\vartheta}{\sigma_Y} = 1.125$, $\frac{\bar{\sigma}}{\sigma_Y} = 1.000$ etc.

The strains are non-dimensionalized as follows

$$e_\vartheta = \frac{E\varepsilon_\vartheta}{\sigma_Y} , \qquad e_r = \frac{E\varepsilon_r}{\sigma_Y} , \qquad e_{r\vartheta} = \frac{E\gamma_{r\vartheta}}{\sigma_Y} .$$

The displacements u and r are non-dimensionalized and re-defined (for simplification in the strain displacement equations) as follows

$$D = \frac{Eu}{\sigma_Y r} \qquad G = \frac{Ev}{\sigma_Y r} .$$

3.4.2 Component Stress Distributions

From the settled stress function field the stresses were obtained using the difference form of the following equations and then non-dimensionalized

$$\sigma_r = \frac{1}{r}\frac{\partial\psi}{\partial r} + \frac{1}{r^2}\frac{\partial^2\psi}{\partial\vartheta^2}$$

$$\sigma_\vartheta = \frac{\partial^2\psi}{\partial r^2}$$

$$\tau_{r\vartheta} = -\frac{\partial}{\partial r}\left(\frac{1}{r}\frac{\partial\psi}{\partial\vartheta}\right).$$

The plot of stresses $\frac{\sigma_r}{\sigma_Y}$ and $\frac{\sigma_\vartheta}{\sigma_Y}$ along the $\measuredangle C_1C_2$ is shown in fig. 3.22. Also plotted on the same graph is the curve of $\frac{\sigma_r}{\sigma_Y}\left(= \frac{\sigma_\vartheta}{\sigma_Y}\right)$ given by the Westergaard crack solution -- equations (3.1) and (3.2). It can be seen how

the crack and $\frac{\sigma_r}{\sigma_Y}$ plots are converging. This is to be expected since the boundary stresses $\tau_{r\vartheta}$ and σ_r are fixed. On the other hand σ_ϑ drops down to nearly zero at the outer boundary. This must be due to the remodelling of the inner boundary. It must be remembered that we are dealing with 'vicinity' solutions and so as an approximation we can accept the solution up to say $\frac{r}{r_o} = 3$ where σ_r and σ_ϑ are approximately equal.

As a check on equilibrium, the surface stress intensities p_y along the line m = 17 (fig. 3.23) were graphically integrated and compared with the integrated value of p_y due to σ_ϑ along the $\mathcal{L}$ from $\frac{r}{r_o} = 1$ to 5.8517. Equilibrium was satisfied.

With the consideration that the solution is acceptable up to $\frac{r}{r_o} = 3$, various graphs have been plotted As a measure of ductility and for the use in the fracture studies, the ratio $\frac{\sigma_{mean}}{\bar{\sigma}}$ along the $\mathcal{L}$ is shown in fig. 3.24.

3.4.3 Component Strain Distributions

The strain distributions along the $\mathcal{L}$ and the notch surface are shown in figs. 3.25 and 3.26.

3.4.4 Evaluation of Notch Opening Displacement

In polar coordinates the following are the strain/displacement equations –

$$\varepsilon_\vartheta = \frac{u}{r} + \frac{\partial}{\partial \vartheta}\left(\frac{v}{r}\right)$$

$$\varepsilon_r = r\,\frac{\partial}{\partial r}\left(\frac{u}{r}\right) + \frac{u}{r}$$

$$\gamma_{r\vartheta} = \frac{\partial}{\partial \vartheta}\left(\frac{u}{r}\right) + r\,\frac{\partial}{\partial r}\left(\frac{v}{r}\right).$$

where u and v are the radial and circumferential displacements as shown in fig. 3.27.

Using the definitions of paragraph 3.4.1 gives

$$e_\vartheta = D + \frac{\partial G}{\partial \vartheta} = \frac{\sigma_\vartheta}{\sigma_Y}(1 - \nu^2) \text{ on } r = r_o \qquad (3.17)$$

$$e_r = r\frac{\partial D}{\partial r} + D = -\nu(1 + \nu)\frac{\sigma_\vartheta}{\sigma_Y} \text{ on } r = r_o \qquad (3.18)$$

$$e_{r\vartheta} = \frac{\partial D}{\partial \vartheta} + r\frac{\partial G}{\partial r} = 0 \text{ on } r = r_o. \qquad (3.19)$$

In chapter 4 a further variable F is introduced and this is also used here such that

$$F = \frac{\partial(rG)}{\partial r} = \frac{\partial}{\partial r}\left(\frac{Ev}{\sigma_Y}\right)$$

$$= r\frac{\partial G}{\partial r} + G. \qquad (3.20)$$

The gradients $\frac{\partial F}{\partial \vartheta}$ and $r\frac{\partial F}{\partial r}$ can now be expressed in terms of the strains —

$$\frac{\partial F}{\partial \vartheta} = R\frac{\partial e_\vartheta}{\partial r} + e_\vartheta - e_r \qquad (3.21)$$

$$r\frac{\partial F}{\partial r} = R\frac{\partial e_{r\vartheta}}{\partial r} + e_{r\vartheta} - \frac{\partial e_r}{\partial \vartheta}. \qquad (3.22)$$

These then are the equations required for giving the displacement. The purpose of finding displacements is to relate the solution to an experimentally measurable value. In the bend tests carried out by our fracture research group, the displacement was measured by using a gauge placed at points P_1 and P_2 on fig. 3.11. Consequently it was proposed to find this displacement by numerical integration of the strain/displacement equations around arc NB and up the notch side BF_1 (fig. 3.11). Consider the evaluation in two stages — ref. fig. 3.21 (e_r, e_ϑ are known throughout the field)

(1) Around arc NB.

On the notch surface there is no shear strain, therefore $e_{r\vartheta} = 0$.

(a) The circumferential gradient $\frac{\partial F}{\partial \vartheta}$ is found at all points using equation (3.21).

(b) From symmetry of F at point 2, $F_2 = 0$, and so by numerical integration

$$F_3 = \frac{\Pi}{2}\cdot\left(\left(\frac{\partial F}{\partial \vartheta}\right)_3 + \left(\frac{\partial F}{\partial \vartheta}\right)_2\right)$$

by trapezoidal rule.

By Simpson's rule

$$F_4 = F_{\rho=0} + \frac{H}{3}\left(\left(\frac{\partial F}{\partial \vartheta}\right)_2 + 4\left(\frac{\partial F}{\partial \vartheta}\right)_3 + \left(\frac{\partial F}{\partial \vartheta}\right)_4\right)$$

and similarly all values of F up to the point 18 can be found.

(c) Choosing $\left(\frac{\partial G}{\partial \vartheta}\right)_2$ as zero gives $D_2 = e_\vartheta$ from (3.17) and as a first approximation $G_3^2 = 0$.

(d) From (3.19) $\frac{\partial D}{\partial \vartheta} = -r\frac{\partial G}{\partial r}$

and from (3.20) $-r\frac{\partial G}{\partial r} = G - F$.

Therefore at point 3, $\left(\frac{\partial D}{\partial \vartheta}\right)_3 = G_3 - F_3$

$= -F_3$ (step c).

(e) By Simpson's Rule

$$D_3 = D_2 + \frac{H}{2}\left(\left(\frac{\partial D}{\partial \vartheta}\right)_2 + \left(\frac{\partial D}{\partial \vartheta}\right)_3\right)$$

$$= D_2 + \frac{H}{2}\left(\frac{\partial D}{\partial \vartheta}\right)_3$$

due to symmetry of D on the $\mathcal{L}$.

(f) From (3.17) $\left(\frac{\partial G}{\partial \vartheta}\right)_3 = e_{\vartheta_3} - D_3$.

(g) By simple integration $G_4 = G_2 + 2H\left(\frac{\partial G}{\partial \vartheta}\right)_3$.

(h) From equations (3.19) and (3.20) $\left(\frac{\partial D}{\partial \vartheta}\right)_4 = G_4 - F_4$.

(i) By numerical integration $D_4 = D_2 + \frac{H}{3}\left(\left(\frac{\partial D}{\partial \vartheta}\right)_2 + 4\left(\frac{\partial D}{\partial \vartheta}\right)_3 + \left(\frac{\partial D}{\partial \vartheta}\right)_4\right)$.

(j) Steps (f) to (i) are used in determining D and G at the point 4, in a similar fashion D and G can be found up to the point 18.

Since $G = \frac{Ev}{r\sigma_Y}$, substitution of values for E, σ_Y, r_o will give the symmetrical half notch opening at B.

(2) Up the notch side BP_1.

The value of v is known at the point B, and v is now required at the point P_1. The material along BP_1 is subject to very small stresses and can be considered 'dead', consequently remaining linear. As a check several values of displacement were evaluated as follows:—

($e_{r\vartheta}$ is still zero along BP_1)

(a) The radial gradient $r\frac{\partial F}{\partial r}$ is found from (3.22) viz

$$r\frac{\partial F}{\partial r} = -\frac{\partial e_r}{\partial \vartheta}.$$

(b) F is known at point 18, and so values of F can be found along BP_1 by a numerical integration of $r\frac{\partial F}{\partial r}$.

(c) From the definition of $F = \frac{E}{\sigma_Y}\frac{\partial v}{\partial r}$, it can be seen that a further graphical integration will give values of v along BP_1.

The values of displacement along BP_1 did indicate a linear distribution and so a linear extrapolation out to P_1 was carried out, which gave a value of 0.054 mm for the half opening. Thus for the full notch opening between P_1 and P_2 the displacement is $35.90\frac{\Sigma}{\sigma_Y}$ mm for a radius r_o = 1.4 mm. For Q1 Navy steel this gives an opening of 0.108 mm, at B the opening is 0.070 mm.

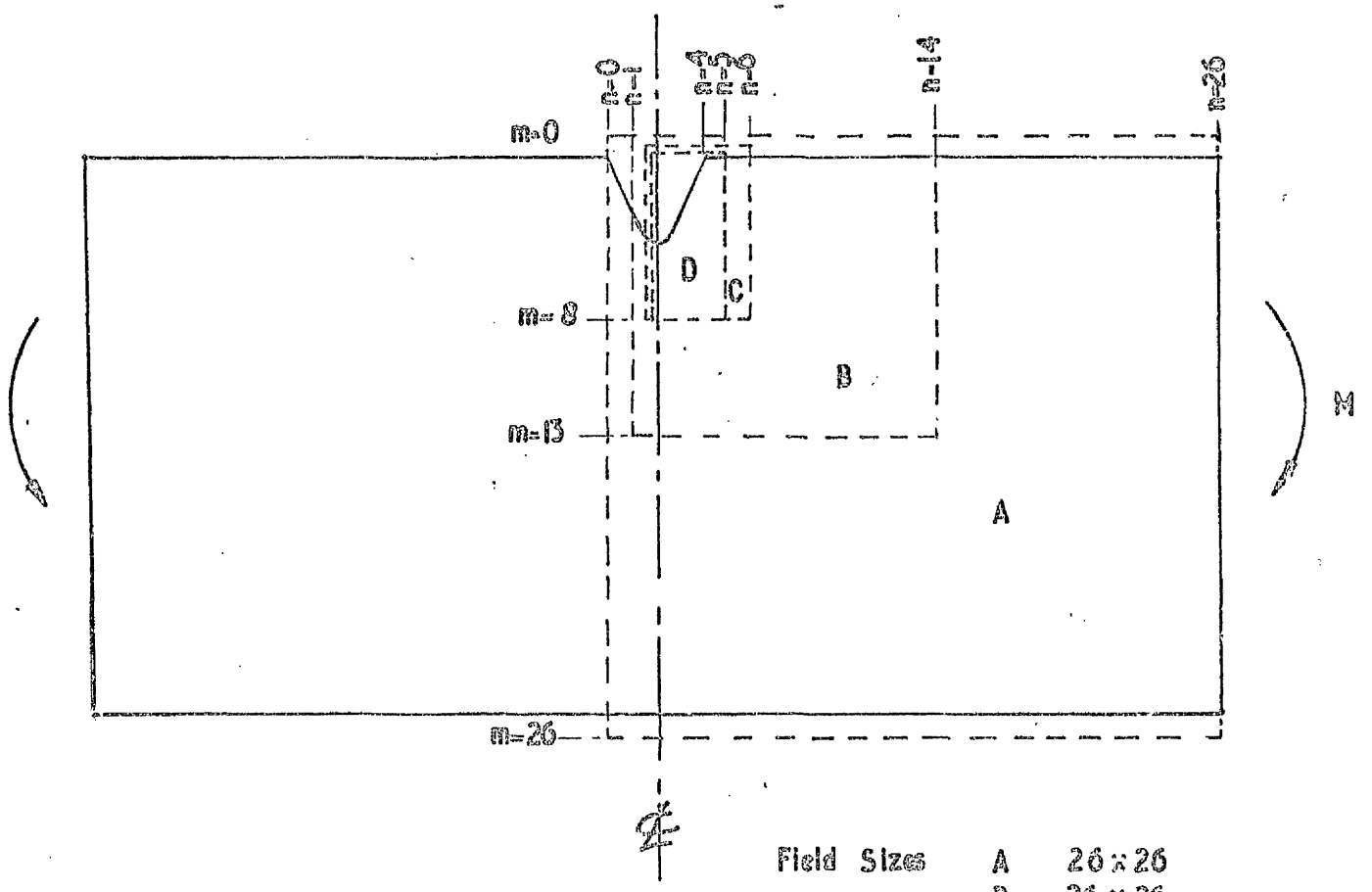

Field Sizes

A	26 x 26
B	26 x 26
C	30 x 18
D	44 x 26

Fig 3.1 First Attempt

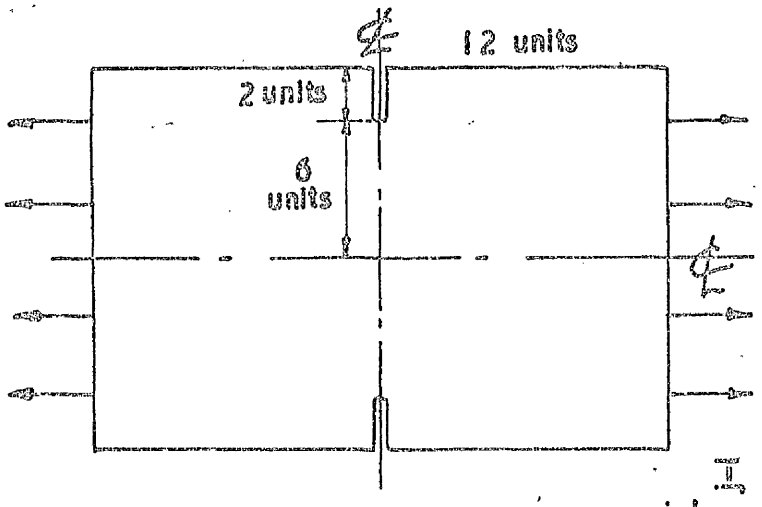

Fig 3.2 Second Attempt

(a) Overall Dimensions

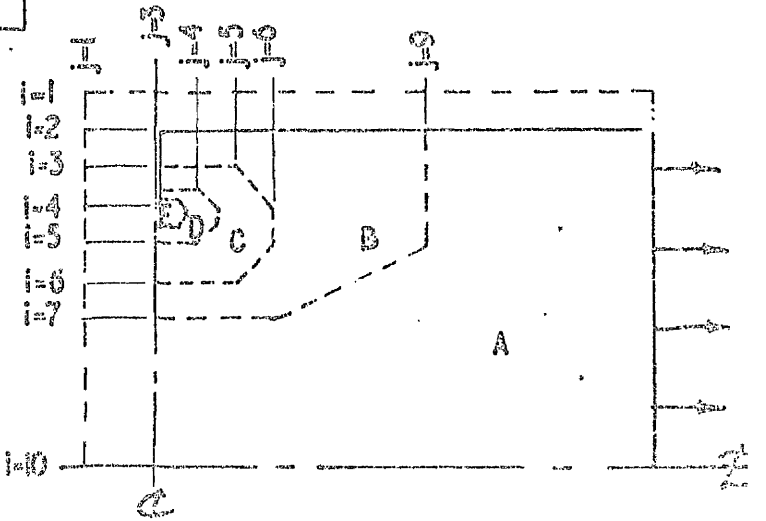

(b) Symmetrical Quarter

Field Sizes (approx)

A	12 x 8
B	12 x 10
C	12 x 12
D	12 x 12
E	12 x 12

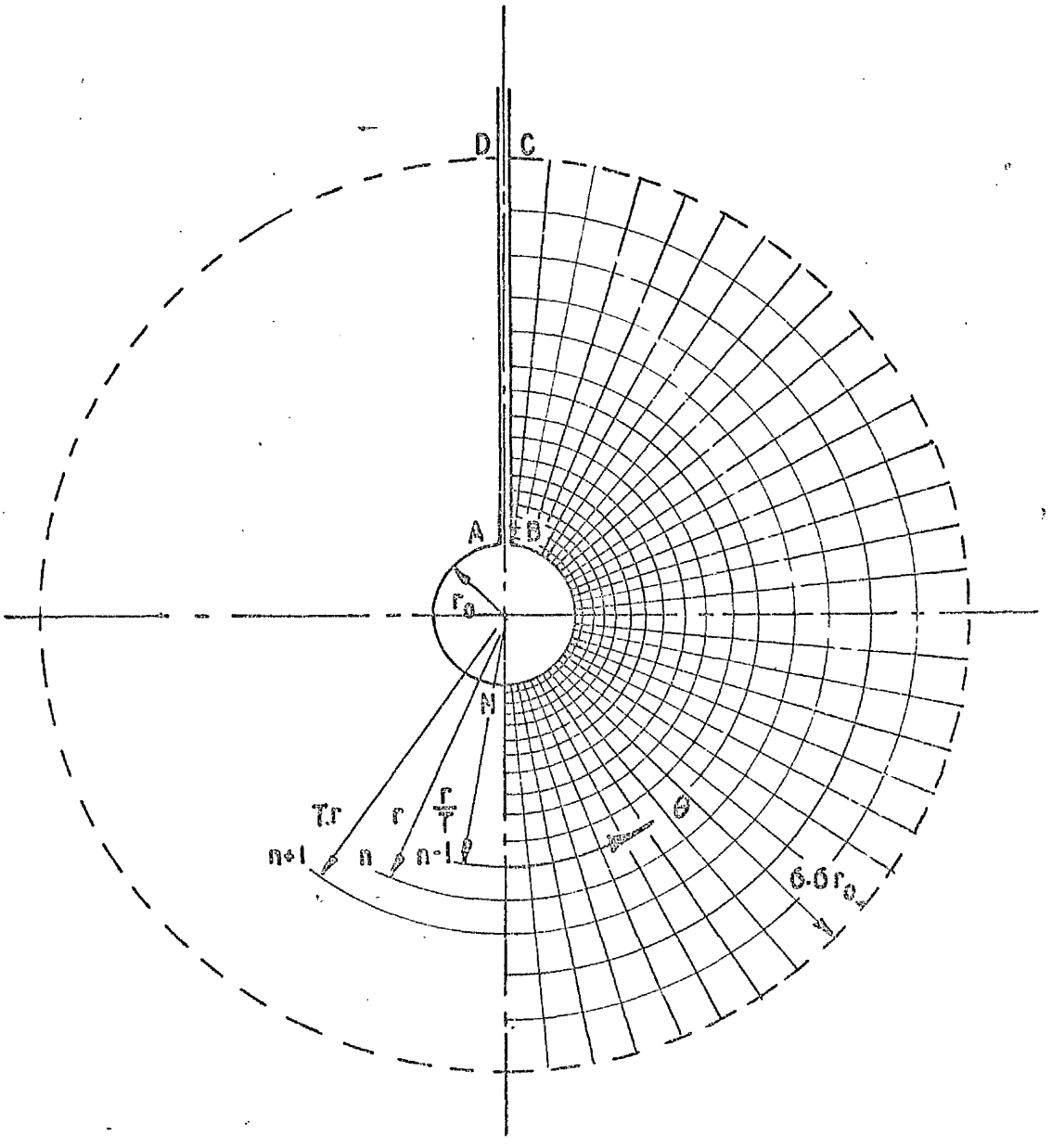

Fig 3.3

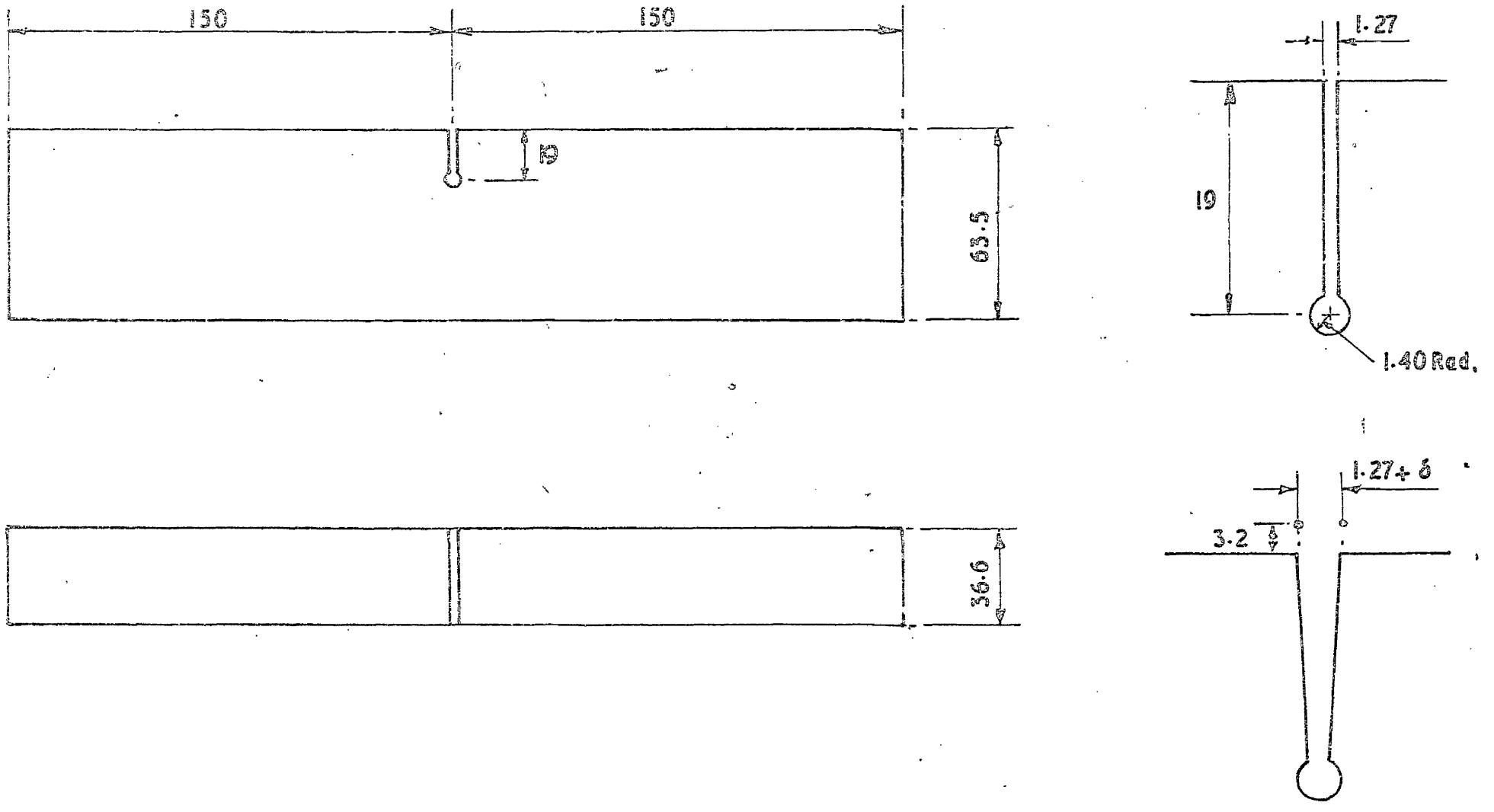

Fig 3.4 Notch Bend Specimens (ref (42))

(ALL DIMENSIONS IN mm.)

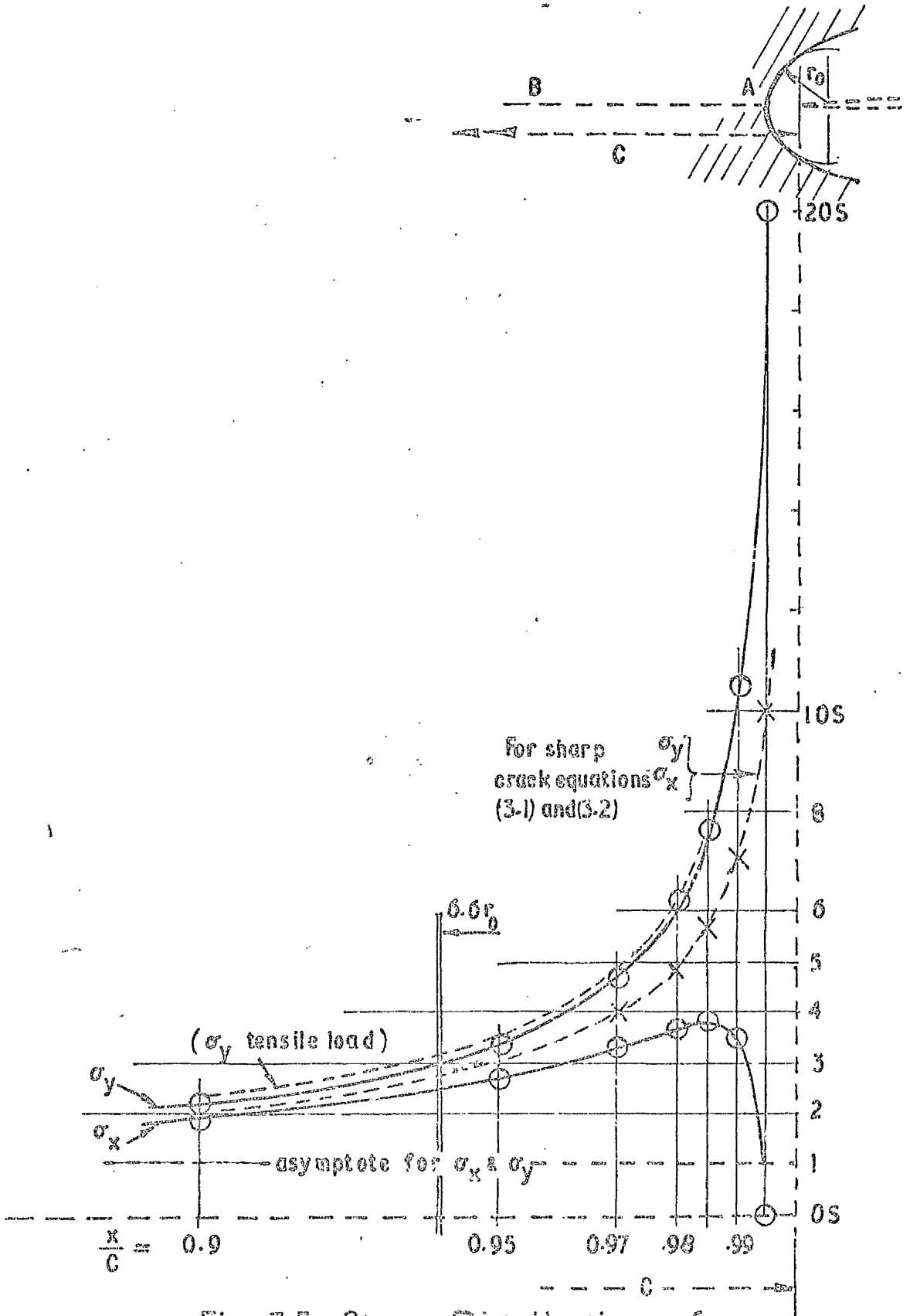

Fig 3.5 Stress Distributions for Hyperbolic Notches in Bending (ref (23))

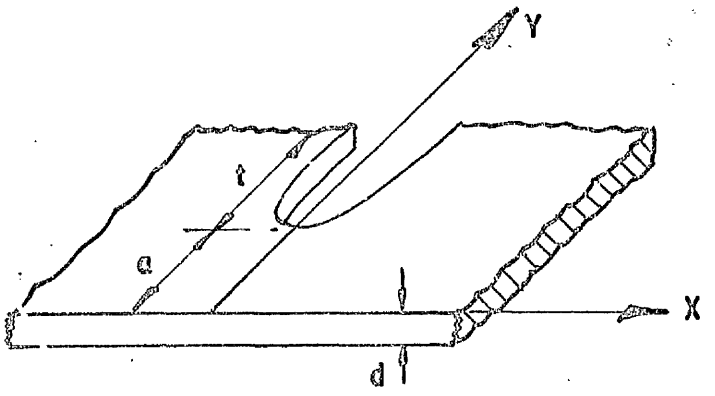

Fig 36
(ref. Neuber (18))

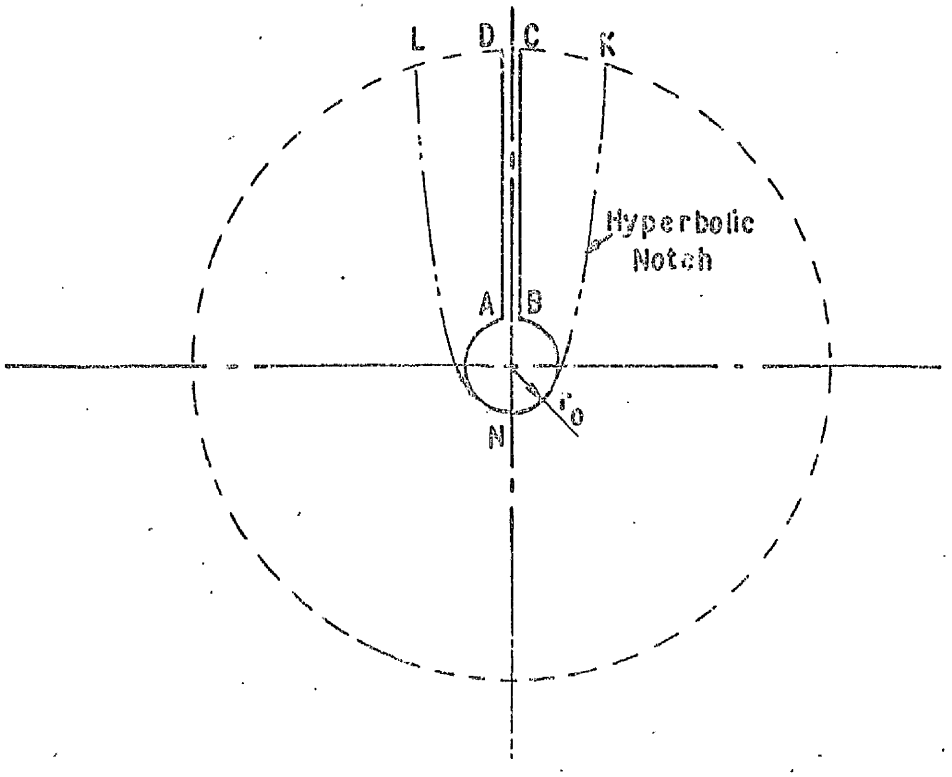

Fig 37

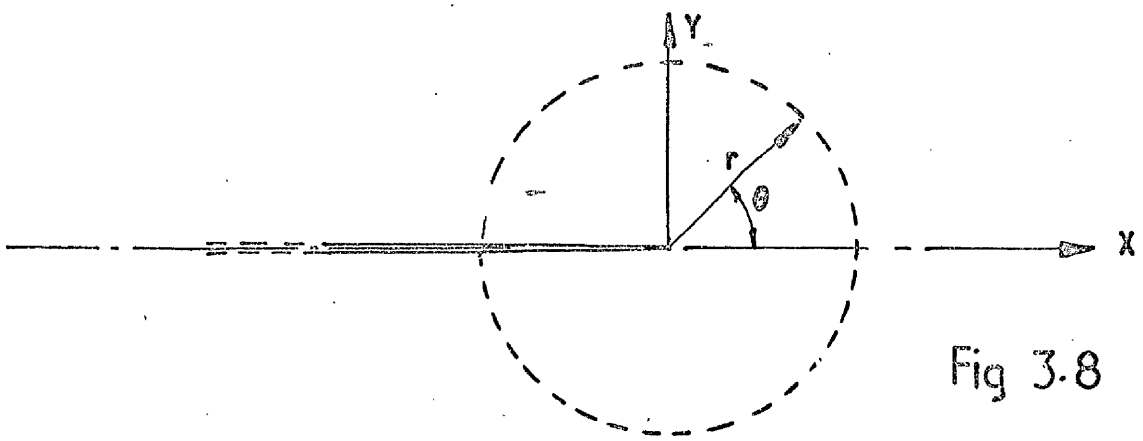

Fig 3.8

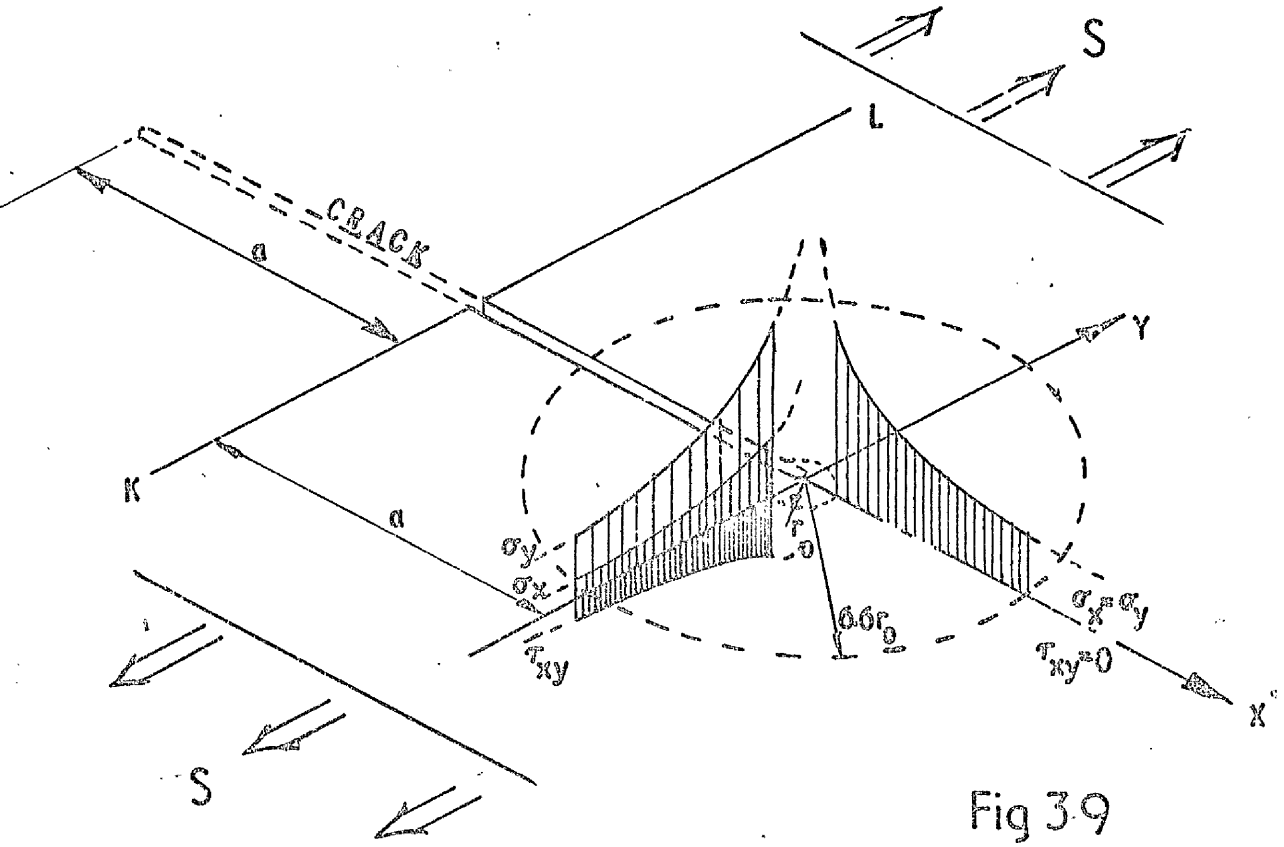

Fig 3.9

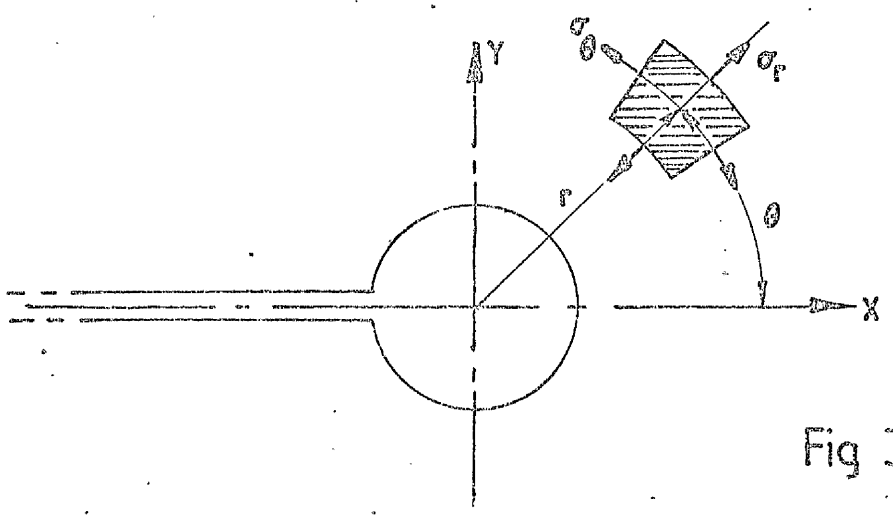

Fig 3.10

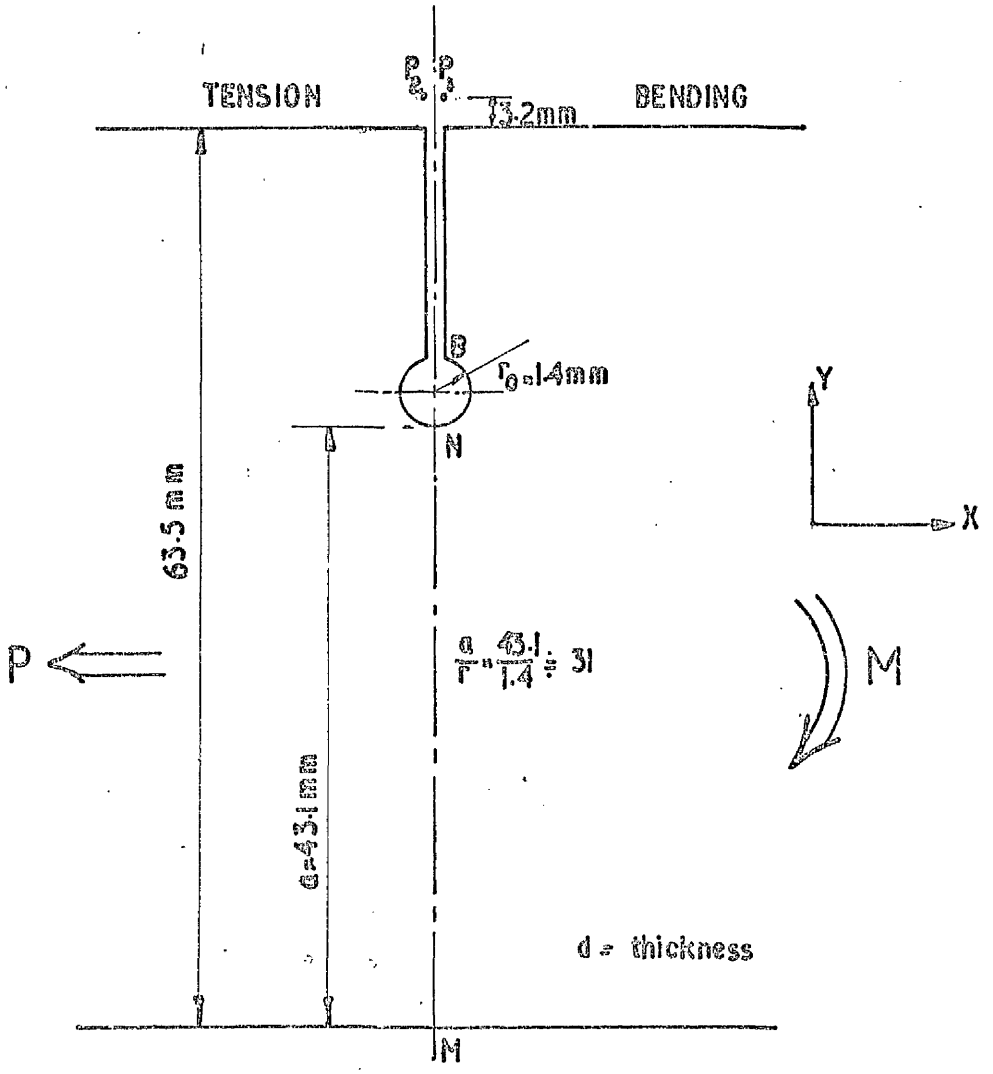

$$\left(\begin{matrix}\sigma_x = \\ \text{average} \\ \text{over MN}\end{matrix}\right) p=\frac{P}{a\,d}$$

$$\left(\begin{matrix}\text{nominal } \sigma_x = \\ \text{at N}\end{matrix}\right) p=\frac{6M}{a^2 d}$$

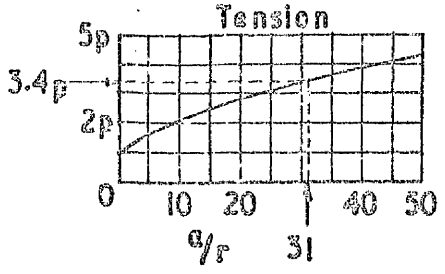

The maximum stress in a deep external notch on one side of a bar under tension

(ref Neuber(18))

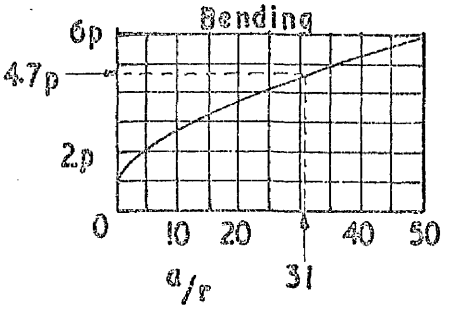

The maximum stress in deep external notches on one side of a bar under bending only

(ref Neuber(18))

Fig 3.11

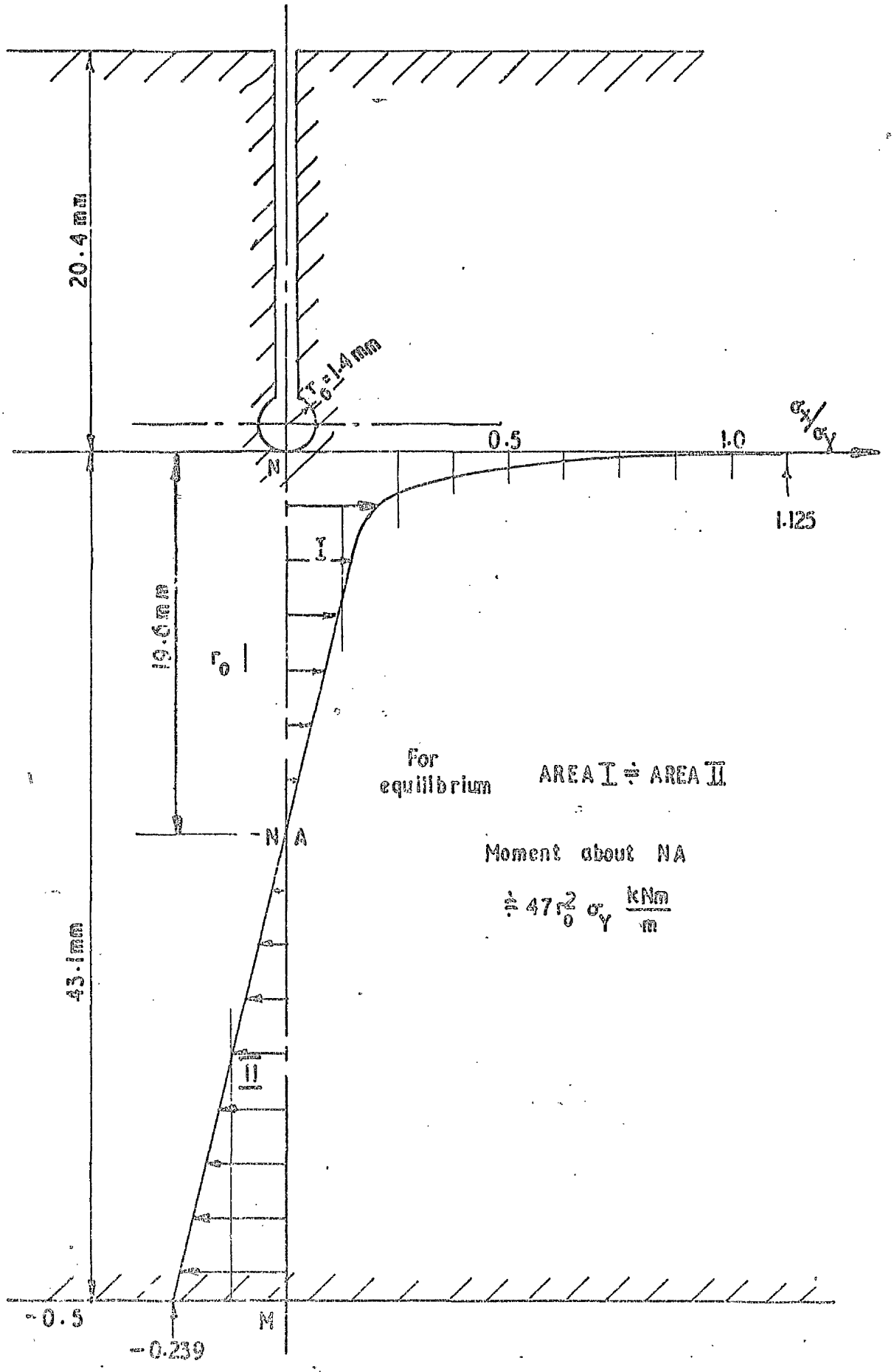
20.4 mm
$r_0 = 1.4$ mm
0.5
1.0
σ_x/σ_y
N
1.125
I
19.6 mm
r_0
For equilibrium AREA I ≒ AREA II
N A
Moment about NA
$\doteq 47 r_0^2 \sigma_y \frac{kNm}{m}$
43.1mm
II
-0.5
M
-0.239

Fig 3.12

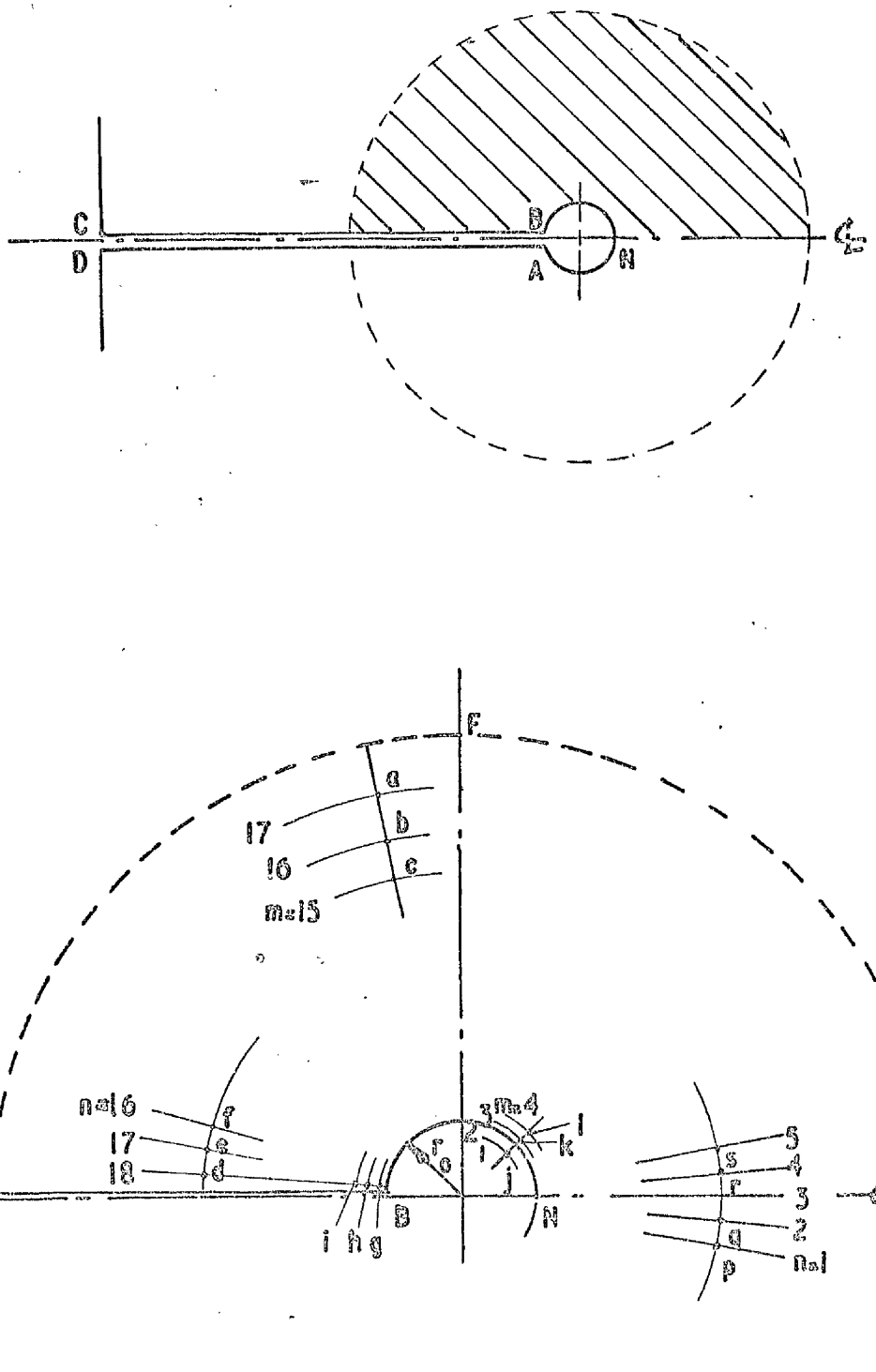

Fig 3.13

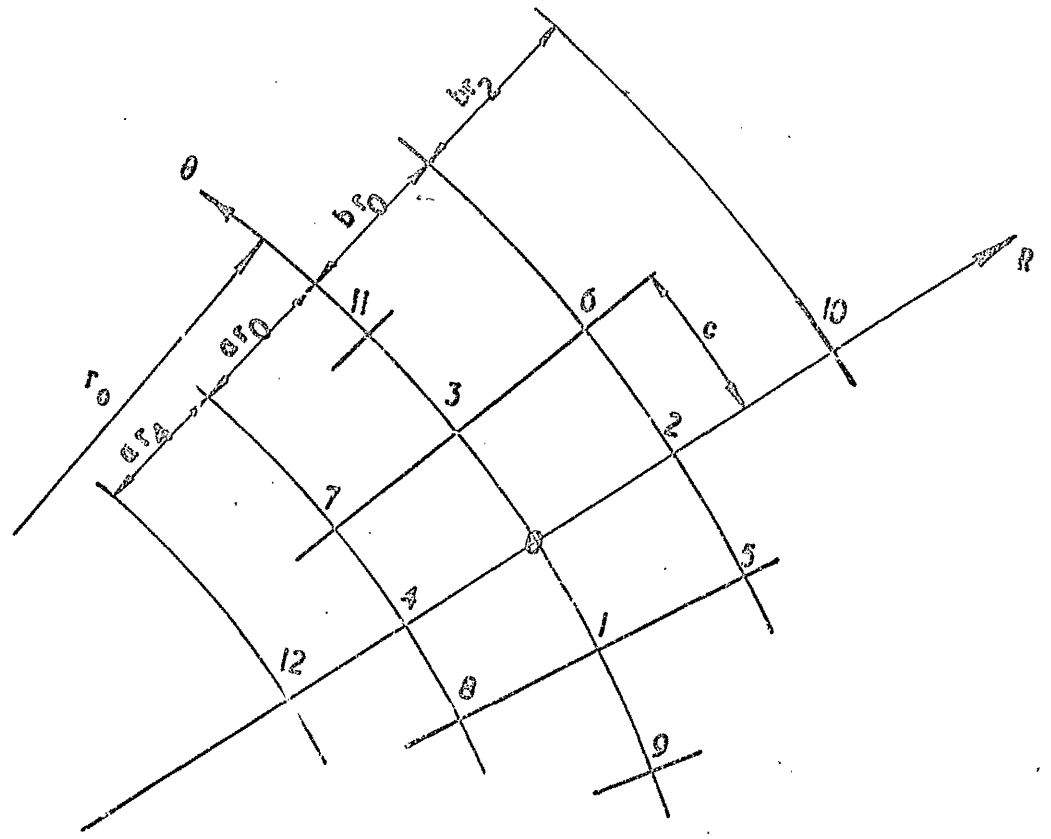

Fig 3.14

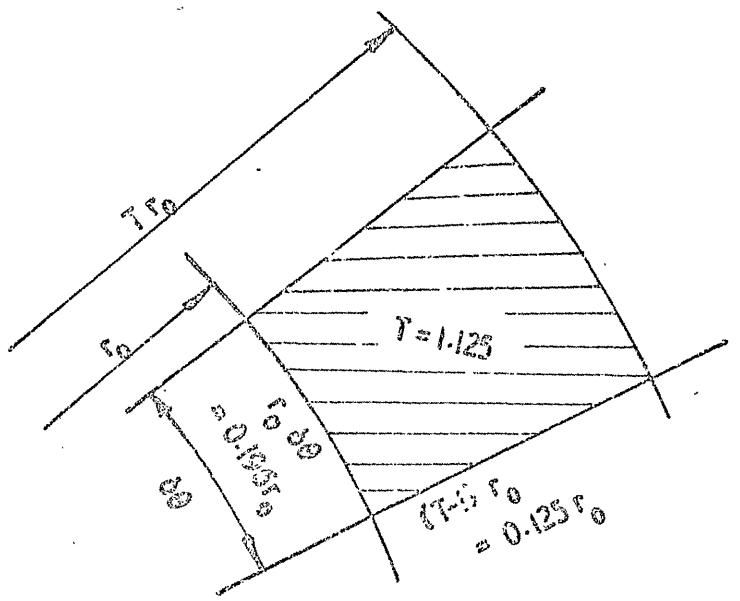

Fig 3.15

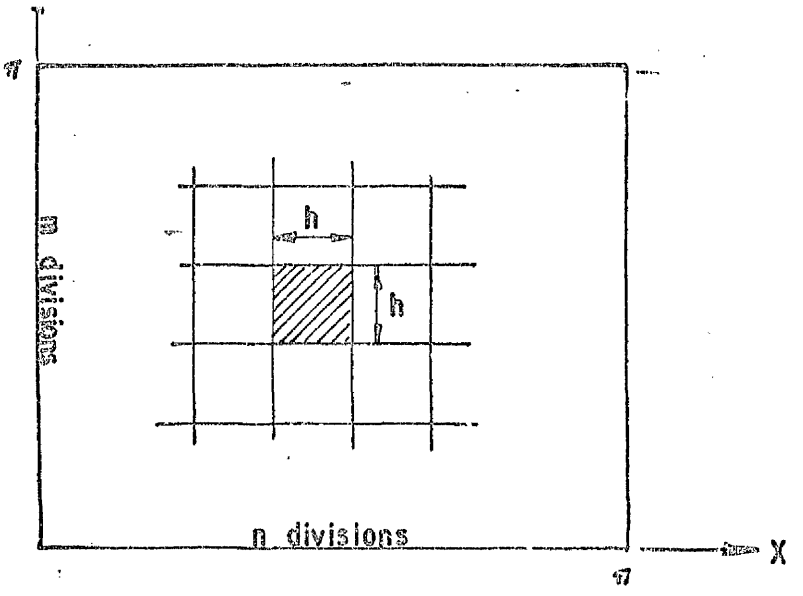

Fig 3.16

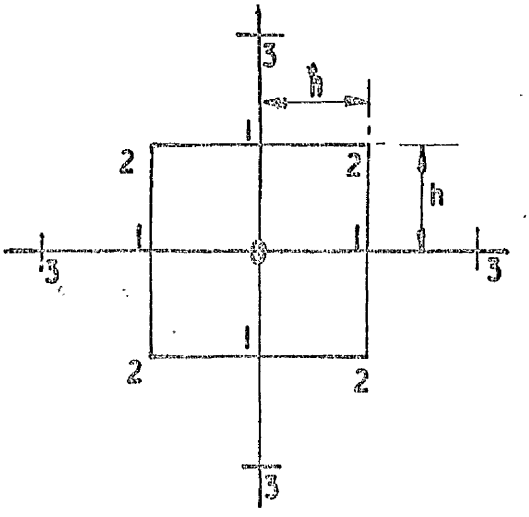

Fig 3.17

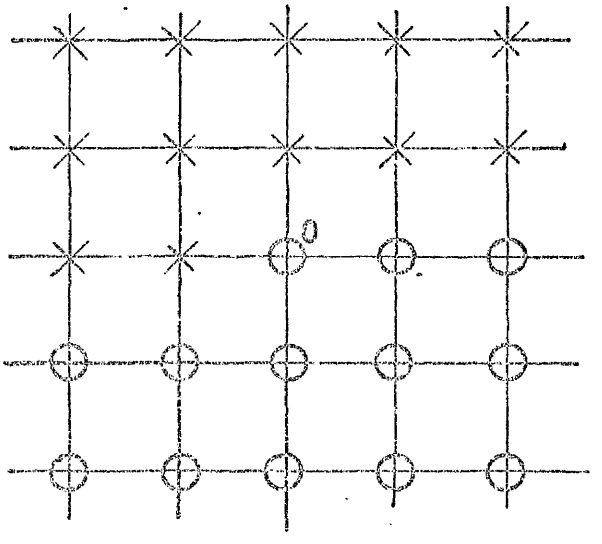

Fig 3.18

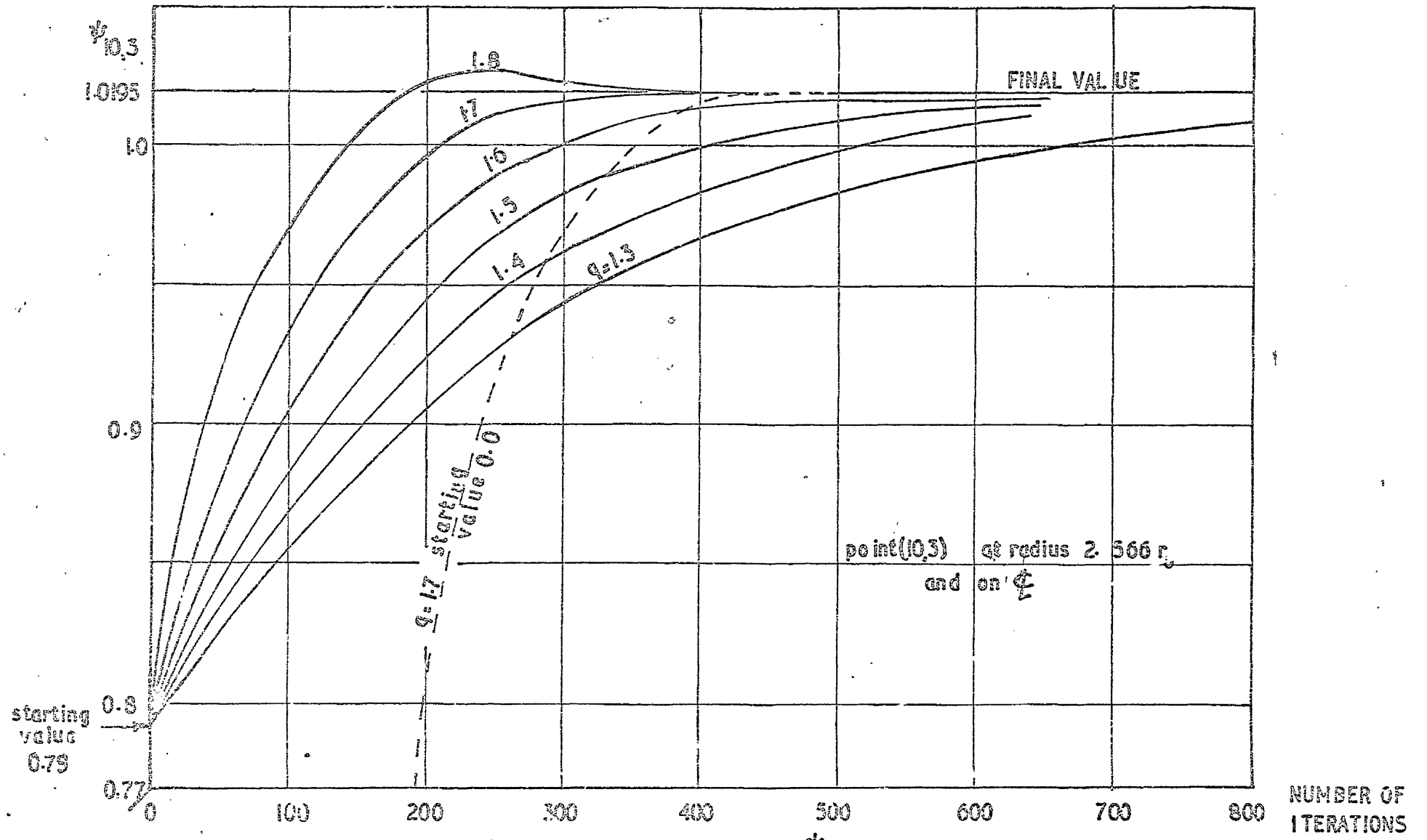

Fig 3.19 Variation of value of $\psi_{10,3}$ with number of iterations and accelerator q

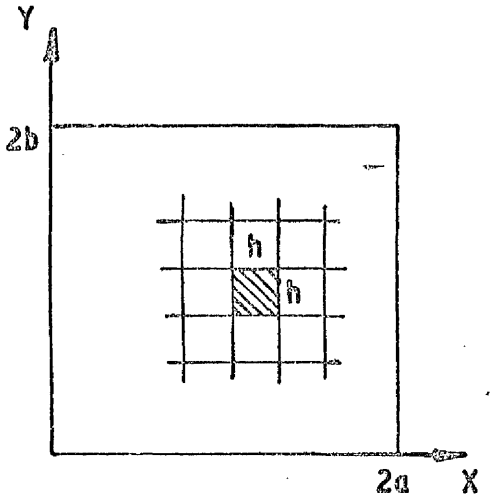

Fig 3.20

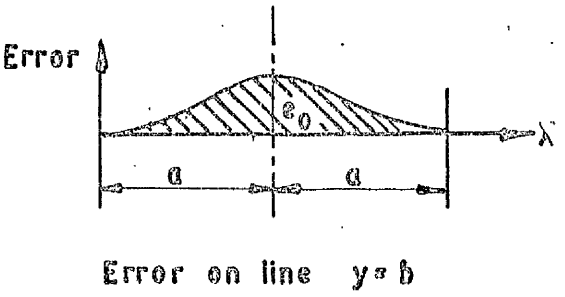

Fig 3.21

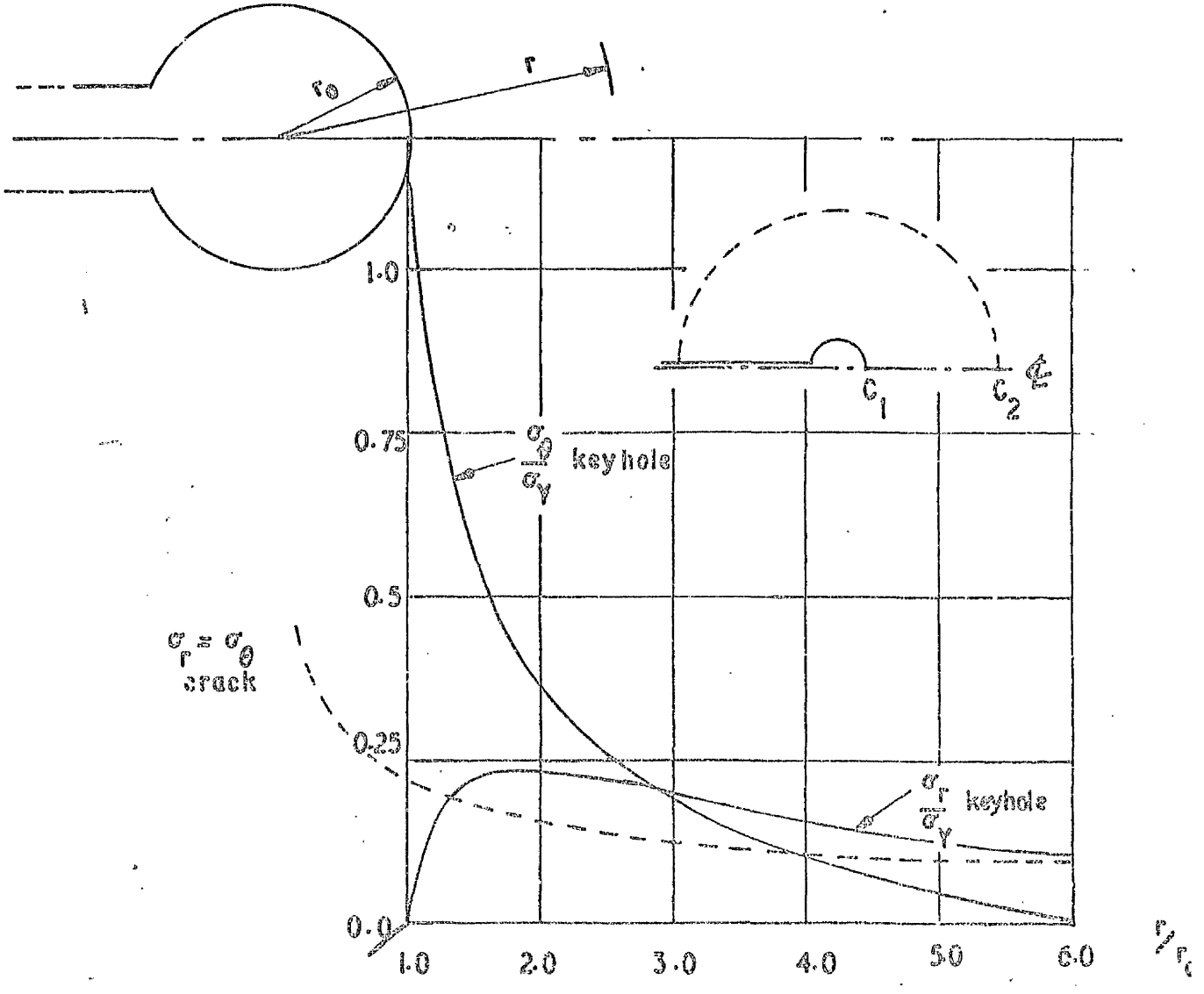

Fig 3.22 Plot of stresses across minimum section $c_1 c_2$

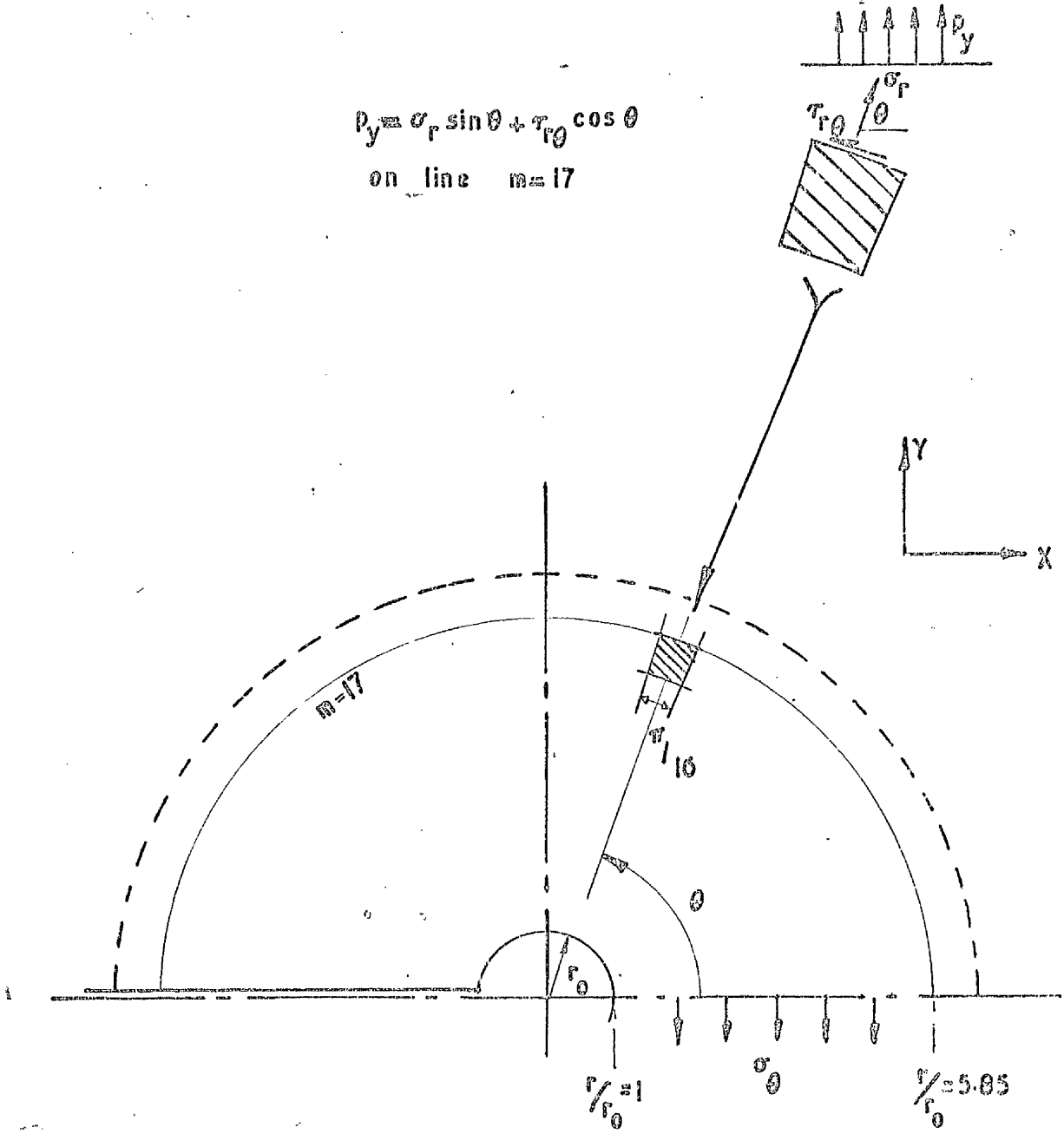
$p_y = \sigma_r \sin\theta + \tau_{r\theta} \cos\theta$
on line m = 17
p_y
σ_r
$\tau_{r\theta}$
θ
Y
X
m=17
$\pi/16$
θ
r_0
$r/r_0 = 1$
σ_θ
$r/r_0 = 5.85$

Fig 3.23

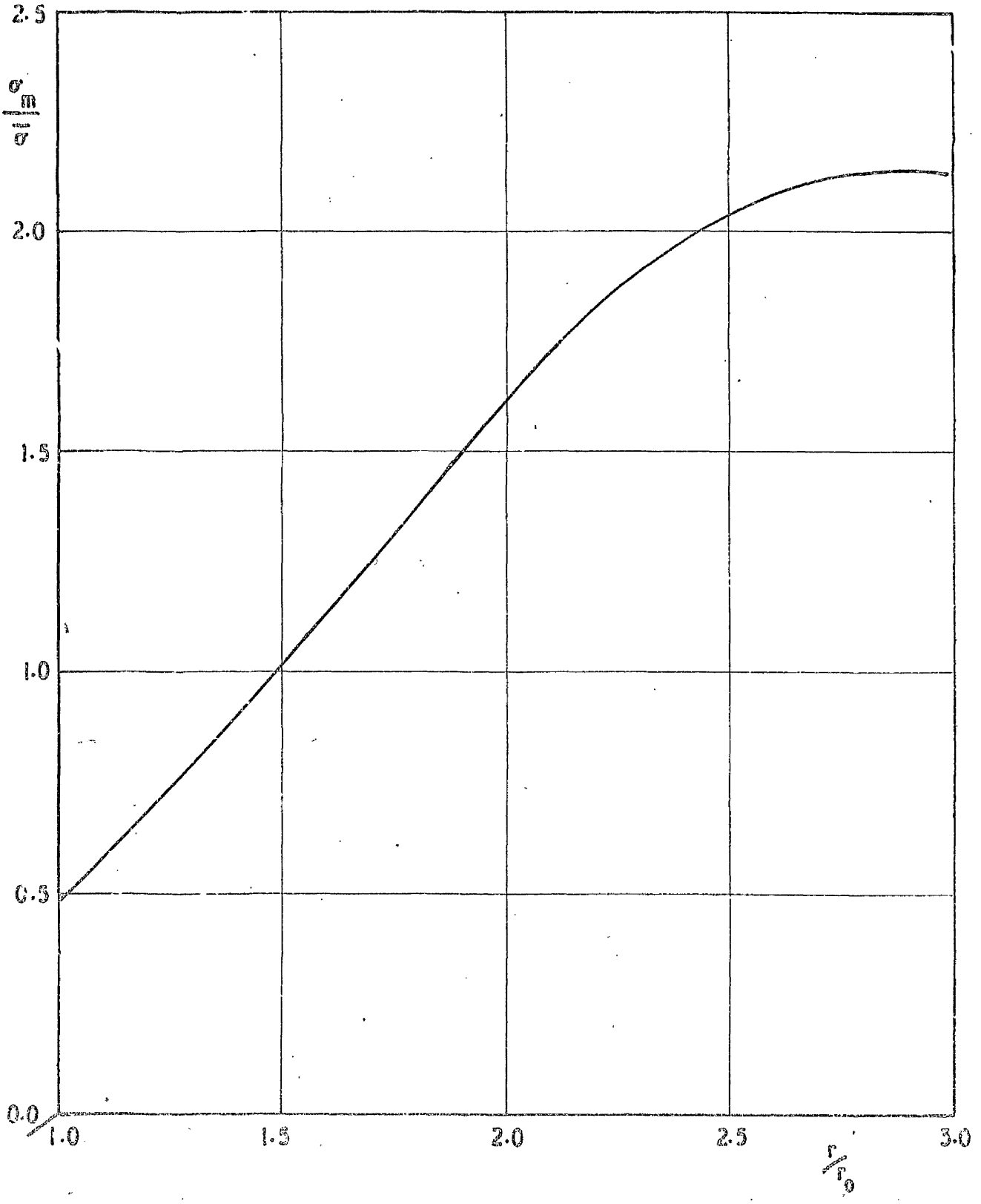

Fig 3.24 Mean to effective stress ratio along ℄

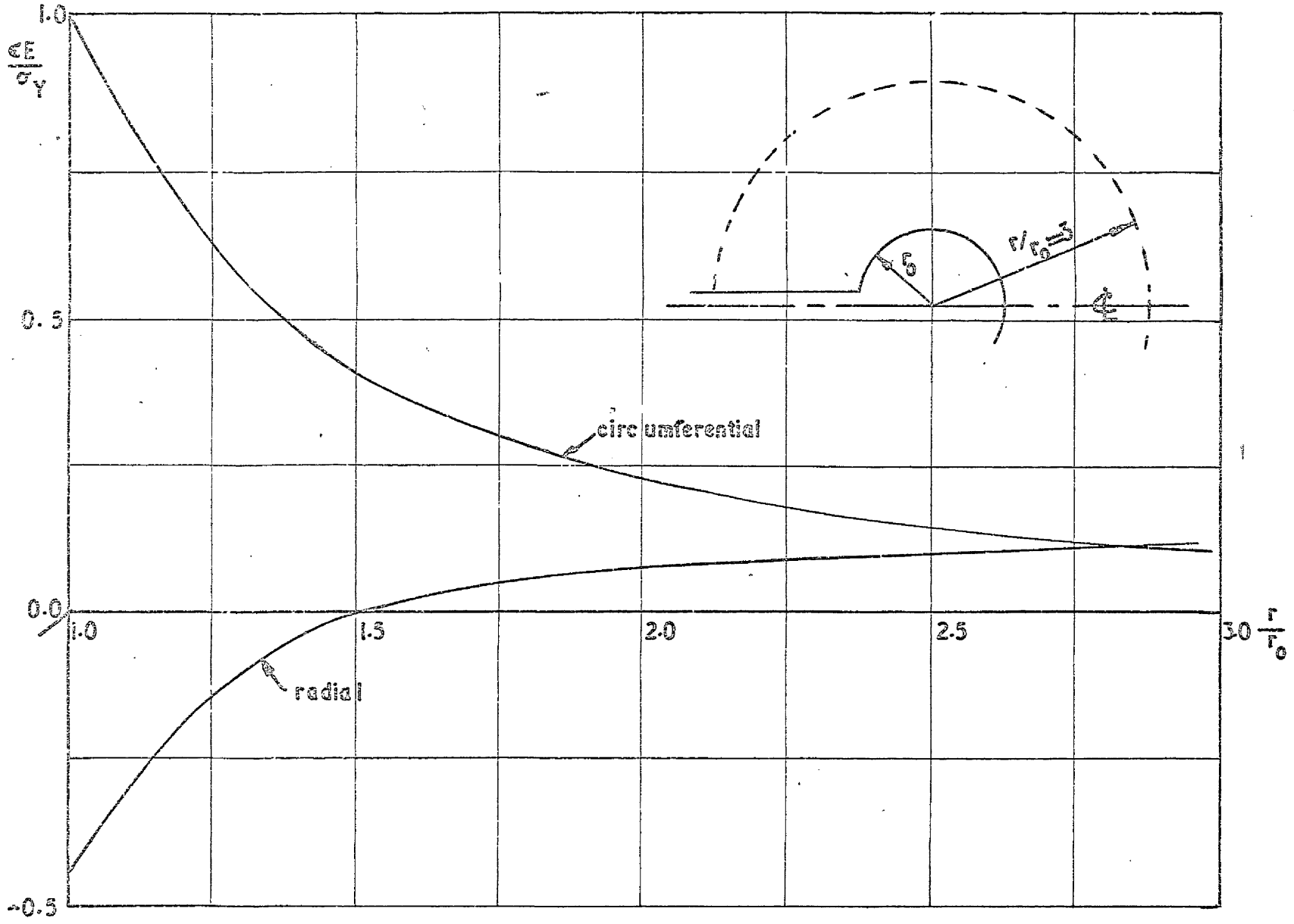

Fig 3·25 Distribution of strains $\frac{E\epsilon_r}{\sigma_Y}$ and $\frac{E\epsilon_\theta}{\sigma_Y}$ along ℄ under notch surface

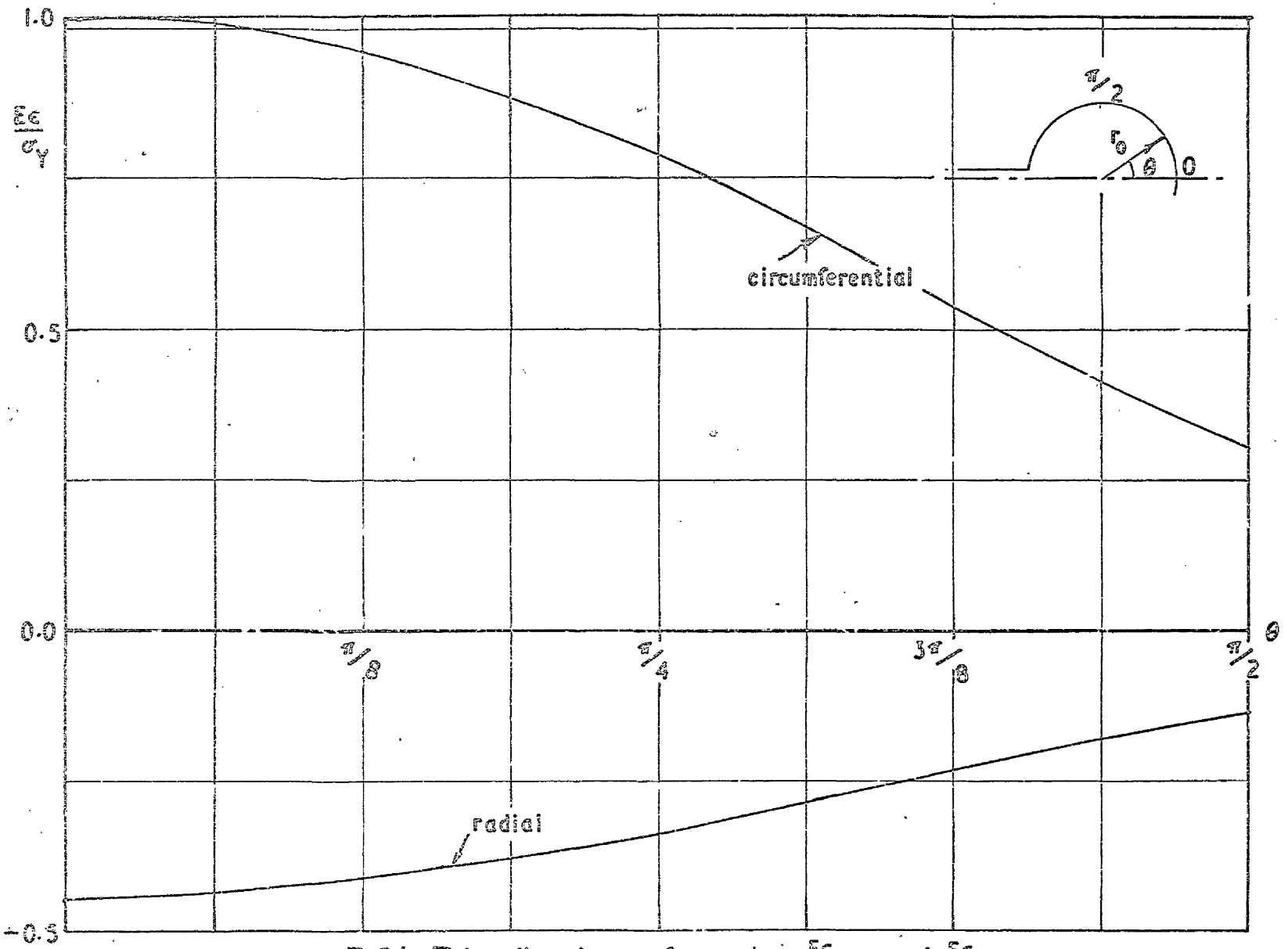

Fig 3.26 Distribution of strains $\frac{E\epsilon_r}{\sigma_Y}$ and $\frac{E\epsilon_\theta}{\sigma_Y}$ along notch surface

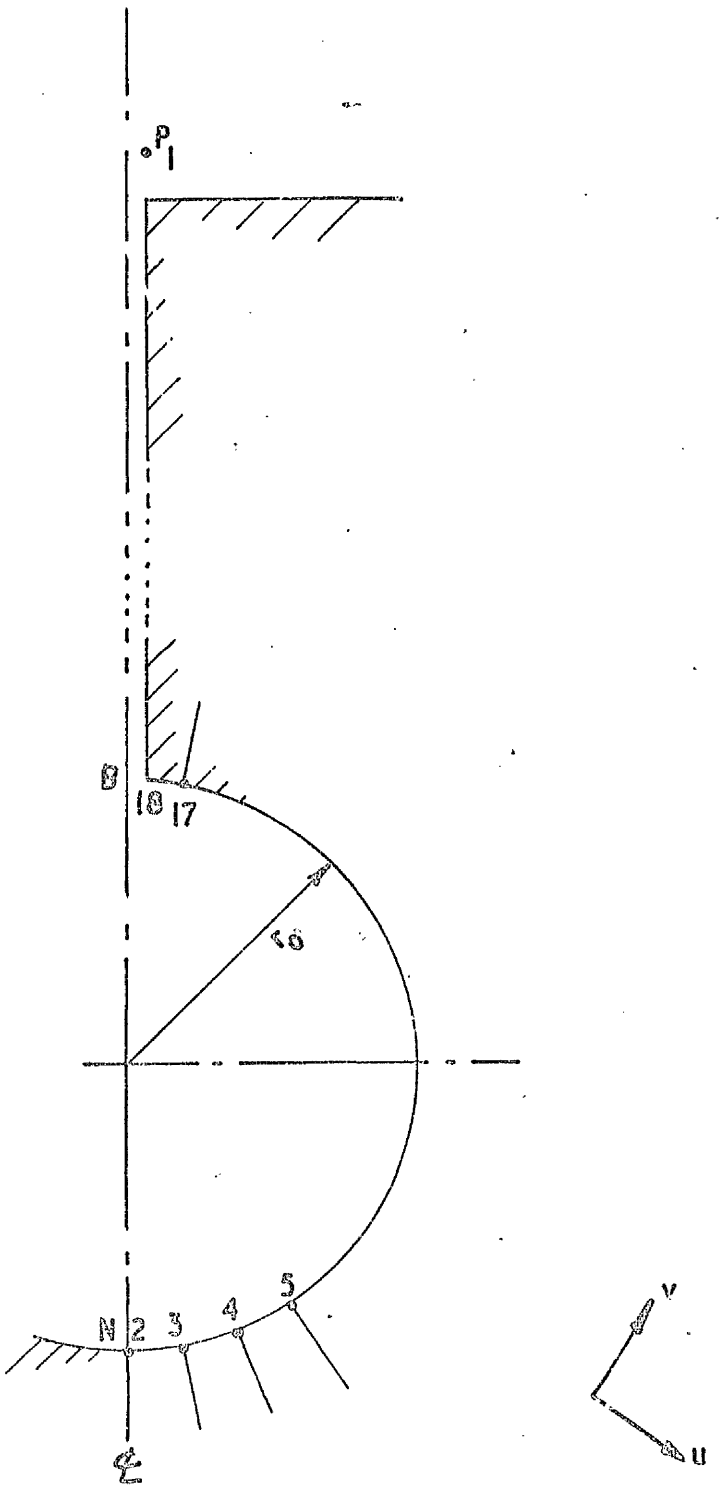

Fig 3.27

CHAPTER 4

FORMULATION AND CLASSIFICATION OF THE EQUATIONS OF ELASTICITY AND PLASTICITY

CHAPTER 4

FORMULATION AND CLASSIFICATION OF THE EQUATIONS OF ELASTICITY AND PLASTICITY

4.1 Introduction

For completeness the first part of this chapter deals with the more conventional approach to elasto-plastic formulation. For the convenience of the reader the equations are referred to the more familiar cartesian coordinates.

4.1.1 Basic Equations

In plasticity, several basic equations must be satisfied in any solution; these are repeated here, for plane strain conditions although they may be found in books like that by Mendelson[3],

(a) Equilibrium —

$$\frac{\partial \sigma_x}{\partial x} + \frac{\partial \tau_{yx}}{\partial y} = 0$$
$$\frac{\partial \tau_{xy}}{\partial x} + \frac{\partial \sigma_y}{\partial y} = 0. \qquad (4.1)$$

(b) Compatibility —

$$\frac{\partial^2 \varepsilon_x}{\partial y^2} + \frac{\partial^2 \varepsilon_y}{\partial x^2} = \frac{\partial^2 \gamma_{xy}}{\partial x \partial y}. \qquad (4.2)$$

(c) Stress-strain relations —

Total strains are made up of elastic strains which come directly from the stress and plastic strains. If there have been several, say i, loading increments then the plastic strain can be thought of being made up of the accumulated plastic strain increments, ε^p, (up to but not including the current increment)

plus the current increment $d\varepsilon^p$. Thus

$$\varepsilon^p = \sum_{k=1}^{i-1} d\varepsilon_k^p \quad \text{and} -$$

$$\left.\begin{aligned} \varepsilon_x &= \frac{1}{E}(\sigma_x - \nu(\sigma_y + \sigma_z)) + \varepsilon_x^p + d\varepsilon_x^p \\ \varepsilon_y &= \frac{1}{E}(\sigma_y - \nu(\sigma_x + \sigma_z)) + \varepsilon_y^p + d\varepsilon_y^p \\ \varepsilon_z = 0 &= \frac{1}{E}(\sigma_z - \nu(\sigma_x + \sigma_y)) + \varepsilon_z^p + d\varepsilon_z^p \\ \gamma_{xy} &= \frac{1}{G}\tau_{xy} + \gamma_{xy}^p + d\gamma_{xy}^p. \end{aligned}\right\} \qquad (4.3)$$

(d) Equations of plasticity

The following equations and formulae are formulated from the flow rule formed from the two basic 'physical' equations which relate the strain response of a material to stress loading in terms of dilation and distortion. The flow rule is the one associated with the von Mises yield condition discussed in section 4.2 below, and the equations are often referred to as the Levy Mises equations

$$\left.\begin{aligned} d\varepsilon_x^p &= \frac{d\bar{\varepsilon}^p}{2\bar{\sigma}}(2\sigma_x - \sigma_y - \sigma_z) \\ d\varepsilon_y^p &= \frac{d\bar{\varepsilon}^p}{2\bar{\sigma}}(2\sigma_y - \sigma_x - \sigma_z) \\ d\varepsilon_z^p &= \frac{d\bar{\varepsilon}^p}{d\bar{\sigma}}(2\sigma_z - \sigma_x - \sigma_y) \\ d\gamma_{xy}^p &= \frac{d\bar{\varepsilon}^p}{\bar{\sigma}} 3\tau_{xy} \end{aligned}\right\} \qquad (4.4)$$

where by definition $\bar{\sigma}$ and $d\bar{\varepsilon}^p$ are the effective stress and the effective plastic strain increment given by

$$\bar{\sigma} = \sqrt{\frac{1}{2}\left[(\sigma_x - \sigma_y)^2 + (\sigma_y - \sigma_z)^2 + (\sigma_z - \sigma_x)^2\right] + 3\tau_{xy}^2} \qquad (4.5)$$

$$\text{and } d\bar{\varepsilon}^p = \sqrt{\frac{2}{9}\left[(d\varepsilon_x^p - d\varepsilon_y^p)^2 + (d\varepsilon_y^p - d\varepsilon_z^p)^2 + (d\varepsilon_z^p - d\varepsilon_x^p)^2\right] + \frac{1}{3}(d\gamma_{xy}^p)^2} \qquad (4.6)$$

4.1.2 Classification of Equations

In elasticity the plane problems are often solved by introducing a stress function ϕ which is defined by —

$$\sigma_x = \frac{\partial^2\phi}{\partial y^2}, \quad \sigma_y = \frac{\partial^2\phi}{\partial x^2}, \quad \tau_{xy} = -\frac{\partial^2\phi}{\partial x \partial y}. \qquad (4.7)$$

When stresses are written, in the above form, into the stress/strain relations (4.3) and the resulting strains substituted into equation (4.2), the governing equations is of the well-known biharmonic form (for both plane stress and plane strain)

$$\nabla^4\phi = \nabla^2\nabla^2\phi = \nabla^2(\sigma_x + \sigma_y) = 0 \qquad (4.8)$$

where $$\nabla^2 \equiv a\frac{\partial^2\phi}{\partial x^2} + 2b\frac{\partial^2\phi}{\partial x \partial y} + c\frac{\partial^2\phi}{\partial y^2}$$

and $a = c = 1, \quad b = 0.$

In a bounded region $\mathbb{R}$ in the (x,y) plane with boundary $\partial\mathbb{R}$, the equation $\nabla^2\phi = 0$ is <u>elliptic</u> if

$$b^2 - ac < 0 \qquad \text{for all points } (x,y) \text{ in } \mathbb{R}.$$

Since in the ∇^2 operator $a = c = 1, \ b = 0,$ the test is proved, and, if $\nabla^2\phi = 0$ is elliptic, then so also is

$$\nabla^2\nabla^2\phi = 0 = \nabla^4\phi.$$

This classification of elliptic, means that the problem is of the boundary-value type requiring the governing equation (4.8) to be satisfied at all points (x,y) within boundary $\partial\mathbb{R}$ as well as with the specified boundary conditions on $\partial\mathbb{R}$.

When using a similar reduction of the constituative equations in a plastic zone, the resulting governing equation while still of the $\nabla^4\phi$ type has now a non-zero RHS. Equation (4.8) now becomes

$$\nabla^4\phi = -(g(x,y) + dg(x,y)) \qquad (4.9)$$

where

$$g(x,y) = E\left(\frac{\partial^2 \varepsilon_x^p}{\partial y^2} + \frac{\partial^2 \varepsilon_y^p}{\partial x^2} - \frac{\partial^2 \gamma_{xy}^p}{\partial x \partial y}\right)$$

$$\text{and} \quad dg(x,y) = E\left(\frac{\partial^2 (d\varepsilon_x^p)}{\partial y^2} + \frac{\partial^2 (d\varepsilon_y^p)^2}{\partial x^2} - \frac{\partial^2 (d\gamma_{xy}^p)}{\partial x \partial y}\right) \Bigg\} \text{ plane stress}$$

$$g(x,y) = \frac{E}{1-\nu^2}\left(\frac{\partial^2 \varepsilon_x^p}{\partial y^2} + \frac{\partial^2 \varepsilon_y^p}{\partial x^2} - \frac{\partial^2 \gamma_{xy}^p}{\partial x \partial y}\right) - \frac{\nu E}{1-\nu^2} \nabla^2 (\varepsilon_x^p + \varepsilon_y^p)$$

$$dg(x,y) = \frac{E}{1-\nu^2}\left(\frac{\partial^2 (d\varepsilon_x^p)}{\partial y^2} + \frac{\partial^2 (d\varepsilon_y^p)}{\partial x^2} - \frac{\partial^2 (d\gamma_{xy}^p)}{\partial x \partial y}\right) - \frac{\nu E}{1-\nu^2} \nabla^2 (d\varepsilon_x^p + d\varepsilon_y^p). \Bigg\} \text{ plane strain}$$

In any solution of equation (4.9) with a constant RHS, the elliptical approach is obviously the correct one, but the effect on the elliptical character of the equation by changing the RHS during convergence to a solution cannot be easily assessed.

It is however instructive to look at the approach taken in deriving the governing equations for the slip line fields. Once again the three dimensional problem is reduced to two dimensions with the assumption of plane strain ($\varepsilon_z = 0$). The material is assumed to be rigid-plastic, thus there are no elastic strains considered, i.e. $\varepsilon = \varepsilon^p$. Constant volume in plastic flow thus gives that

$$\varepsilon_x + \varepsilon_y + \cancel{\varepsilon_z}^{\,=0} = 0 \quad \text{i.e.} \quad \varepsilon_x = -\varepsilon_y.$$

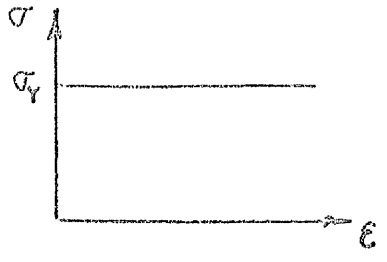

The integrated form of the Levy Mises equations (4.4) gives

$$\varepsilon_x = \frac{\bar{\varepsilon}}{\bar{\sigma}}\left(\sigma_x - \tfrac{1}{2}(\sigma_y + \sigma_z)\right)$$

$$\varepsilon_y = \frac{\bar{\varepsilon}}{\bar{\sigma}}\left(\sigma_y - \tfrac{1}{2}(\sigma_x + \sigma_z)\right)$$

$$\varepsilon_z = 0 = \frac{\bar{\varepsilon}}{\bar{\sigma}}\left(\sigma_z - \tfrac{1}{2}(\sigma_x + \sigma_y)\right) \Rightarrow \sigma_z = \tfrac{1}{2}(\sigma_x + \sigma_y).$$

$$\text{Also} \quad \varepsilon_x = -\varepsilon_y = \frac{3}{4}\frac{\bar{\varepsilon}}{\bar{\sigma}}(\sigma_x - \sigma_y)$$

$$\gamma_{xy} = 3\frac{\bar{\varepsilon}}{\bar{\sigma}}\tau_{xy}.$$

The stress or strain state is defined fully by σ_x, σ_y, τ_{xy}. However this state could be defined by an angle 2ϕ and the mean stress σ (shown graphically on Mohr's Circle) if the value of k (radius of Mohr's Circle) were known or constant. This leads to consideration of the von Mises yield condition, (see section 4.2 below) which states the yielding commences when the effective stress (4.5) reaches a critical value – say k

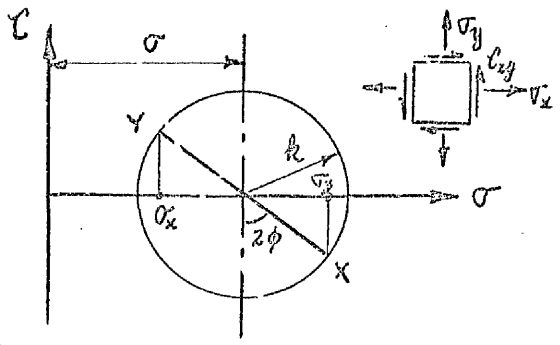

$$\bar{\sigma}^2 = \frac{3}{4}(\sigma_x - \sigma_y)^2 + 3\tau_{xy}^2$$

$$\text{OR} \quad \left(\frac{\sigma_x - \sigma_y}{2}\right)^2 + \tau_{xy}^2 = \frac{\bar{\sigma}^3}{3} = k^2 = (\text{Radius of Mohr's Circle})^2$$

k is also the yield stress in pure shear $\bar{\sigma} = \sqrt{3\tau_{xy}^2}$. Thus when the maximum shear stress reaches k, yielding starts and since there is no work-hardening, the yield stress is constant in the plastic zone. The stress/strain state can thus be defined by σ, 2ϕ and k. The coordinate axes are usually X,Y with the maximum shear axes being designated α,β. On the physical plane the XY axes remain fixed while the $\alpha\beta$ axes rotate and determine the gradients of the α,β slip lines, the angle ϕ being that between the positive directions of the α and X axes.

The new variables in the problem must now be substituted into the equilibrium equations. First the stresses must be expressed in terms of σ, k, 2ϕ. They are

$$\left.\begin{aligned} \sigma_x &= \sigma - k\sin 2\phi \\ \sigma_y &= \sigma + k\sin 2\phi \\ \tau_{xy} &= k\cos 2\phi \end{aligned}\right\} \quad \text{as can be seen from the geometry of Mohr's Circle.}$$

The two equilibrium equations in plane strain (4.1) become

$$\left.\begin{aligned} \frac{\partial \sigma}{\partial x} - 2k \cos 2\phi \frac{\partial \phi}{\partial x} - 2k \sin 2\phi \frac{\partial \phi}{\partial y} &= 0 \\ \text{and} \quad \frac{\partial \sigma}{\partial y} - 2k \sin 2\phi \frac{\partial \phi}{\partial x} + 2k \cos 2\phi \frac{\partial \phi}{\partial y} &= 0 \end{aligned}\right\} \qquad (4.10)$$

where $\sigma = \frac{1}{2}(\sigma_x + \sigma_y)$.

When the characteristics of these two simultaneous first order partial differential equations are found, they are real, indicating these equations of plasticity to be of a hyperbolic type. Similarly the displacement or velocity equations become

$$\left.\begin{aligned} \frac{\partial u}{\partial x} + \frac{\partial v}{\partial y} &= 0 \\ \text{and} \quad \frac{\partial u}{\partial y} + \frac{\partial v}{\partial x} &= -\left(\frac{\partial u}{\partial x} - \frac{\partial v}{\partial y}\right) \cot 2\phi \end{aligned}\right\} \qquad (4.11)$$

and the characteristics of these equations (4.11) are identical to those of (4.10). The process of determining the slip lines is then to use the stress equations (4.10), not caring too much about matching the equilibrium in the plastic zone to the stresses in the rigid zone over the boundary and also noting that there may be discontinuities. Since the characteristics of (4.10) and (4.11) are the same, the stress-determined slip line field is used for determination of displacements or velocities in the plastic zone. The initial starting information on the plastic-rigid boundary is found by consideration of the bodily movement of the rigid part. The displacements are thus compatible on the field provided. The solution is an upper bound, since compatibility is satisfied overall but not equilibrium. The important point to note is that both sets of equations (4.10) and (4.11) are hyperbolic. This means that one can proceed into the plastic zone from the rigid/plastic boundary, having enough initial information supplied on the boundary. The classification of hyperbolic means the problem is of the initial value type.

This uncertainty of the type of equation has not satisfactorily been resolved. It can be seen that on one hand the elasto-plastic solution for materials which are work-hardening, are probably of the elliptical type while

on the other hand, the rigid plastic solution for materials, which have zero work-hardening are probably of the hyperbolic type. These would appear to be the two limits of the problem. Professor McClintock[28] states, without proof, 'While the equations become elliptical with some strain-hardening, still the tendency for hyperbolic behaviour is present'.

Thus both initial-value and boundary-value approaches should be attempted.

4.2 Yielding

In any analysis in plasticity, a yielding condition must be selected. In the history of plasticity six or more criteria have been evolved - see Mendelson[3]. Nowadays, however, two predominate as being most in agreement with experiment.

(a) Tresca or Maximum Shear Theory:-

This theory assumes that yielding will occur when the maximum shear stress reaches the value of the maximum shear stress at yielding in a simple tension test. The maximum shear stress is equal to half the difference between the maximum and minimum principal stresses.

For simple tension $\sigma_2 = \sigma_3 = 0$ and maximum shear stress at yield $= \frac{1}{2}\sigma_Y$. Tresca then asserts that yielding will occur when one of the following is reached -

$$|\sigma_1 - \sigma_2| = \sigma_Y$$
$$|\sigma_2 - \sigma_3| = \sigma_Y$$
$$|\sigma_3 - \sigma_1| = \sigma_Y.$$

This theory, while in fair agreement with experiment, is more difficult to apply since the relative sizes and signs of the principal stresses must be found first. Another drawback is that the association flow rule of the Tresca criterion will not produce the Levy Mises Equations (1.4), but equations which differ depending on the maximum and minimum principal stresses. For example,

if σ_1 and σ_3 are the maximum and minimum principal stresses, then $|\sigma_3 - \sigma_1| = \sigma_Y$ and the associated flow rule would give

$$d\varepsilon_1^p = 3\frac{d\bar{\varepsilon}^p}{\bar{\sigma}}$$

$$d\varepsilon_2^p = 0$$

$$d\varepsilon_3^p = -3\frac{d\bar{\varepsilon}^p}{\bar{\sigma}} .$$

Sometimes the Tresca criteria is used with the von Mises flow rule. (Levy Mises Equations (4.4)). There is, however, no theoretical justification for this.

(b) The von Mises or Distortion Energy Theory:-

This theory assumes that yielding will occur when the distortion energy equals the distortion energy at yield in simple tension, giving -

$$\sigma_Y^2 = \frac{1}{2}\left[(\sigma_1 - \sigma_2)^2 + (\sigma_2 - \sigma_3)^2 + (\sigma_3 - \sigma_1)^2\right]$$

or under plane strain conditions (4.12)

$$\sigma_Y^2 = \frac{1}{2}\left[(\sigma_x - \sigma_y)^2 + (\sigma_y - \sigma_z)^2 + (\sigma_z - \sigma_x)^2\right] + 3\tau_{xy}^2 .$$

It is essentially empirical, but it is interesting to note that σ_Y is proportional to the root mean square of the three principal shear stresses. Statistically this would appear to be a better approach to yielding and generally this is borne out experimentally. It is usually easier to apply than Tresca, and its associated flow rule is of the same form despite variations in the magnitude of the principal stresses.

If, however, the principal stresses are known and their relative magnitudes easily determined, then Tresca is easier to apply. An example of this is to be found in the solution of the thick walled cylinder by Bland[1].

Overall, however, the von Mises criterion is generally preferred and is used in all the elasto-plastic solutions in this work.

4.3 Formulation of First Order Partial Differential Equations for the Complete Solution of Plane Strain Elasto-plastic Problems.

4.3.1 Introduction

Since the problems being solved use polar coordinates and since the first order equations are used for this solution a switch is made here in coordinate systems.

For plane strain conditions in polar coordinates, there are two equilibrium equations and three strain displacement equations -

$$\left.\begin{aligned} \frac{\partial \sigma_\vartheta}{\partial \vartheta} + r\frac{\partial \tau_{r\vartheta}}{\partial r} + 2\tau_{r\vartheta} &= 0 \\ \frac{\partial \tau_{r\vartheta}}{\partial \vartheta} + r\frac{\partial \sigma_r}{\partial r} + \sigma_r - \sigma_\vartheta &= 0 \end{aligned}\right\} \qquad (4.13)$$

$$\left.\begin{aligned} \varepsilon_\vartheta &= \frac{u}{r} + \frac{1}{r}\frac{\partial v}{\partial \vartheta} \\ \varepsilon_r &= \frac{\partial u}{\partial r} \\ \gamma_{r\vartheta} &= \frac{1}{r}\frac{\partial u}{\partial \vartheta} + \frac{\partial v}{\partial r} - \frac{v}{r}\,. \end{aligned}\right\} \qquad (4.14)$$

If the stresses are expressed in terms of strains there are then five equations for five unknowns ε_ϑ, ε_r, $\gamma_{r\vartheta}$, u and v. On the other hand if the strains are expressed in terms of stresses the five unknowns are σ_r, σ_ϑ, $\tau_{r\vartheta}$, u and v.

If u and v are eliminated from the last three there is formed an equation of compatibility of strains. Thus three equations could be formed in terms of three components of strain (ε_ϑ, ε_r, $\gamma_{r\vartheta}$), but the simplicity of the first order equations is lost with the use of the second order compatibility equation viz

$$\frac{\partial^2(r\gamma_{r\vartheta})}{\partial r\partial \vartheta} - r\frac{\partial^2(r\varepsilon_\vartheta)}{\partial r^2} - \frac{\partial^2 \varepsilon_r}{\partial \vartheta^2} + r\frac{\partial \varepsilon_r}{\partial r} = 0.$$

4.3.2 Elasto—plastic Stress Strain Relations — Plain Strain

The usual basis for elasto—plastic analysis is the incremental formulae giving strains in terms of stresses. The strain increment is made up of an elastic increment, which can be calculated directly from the stress increments, and a plastic increment which can be found as a proportion of the effective plastic strain increment $d\bar{\varepsilon}^p$ from the Levy Mises Equations (4.4). Thus

$$\left.\begin{aligned}
d\varepsilon_\vartheta &= \frac{1}{E}(d\sigma_\vartheta - \nu(d\sigma_r + d\sigma_z)) + d\bar{\varepsilon}^p\left(\frac{\sigma_\vartheta - \frac{1}{2}(\sigma_r + \sigma_z)}{\bar{\sigma}}\right) \\
&= d\varepsilon_\vartheta{}^e + d\varepsilon_\vartheta{}^p \\
d\varepsilon_r &= \frac{1}{E}(d\sigma_r - \nu(d\sigma_\vartheta + d\sigma_z)) + d\bar{\varepsilon}^p\left(\frac{\sigma_r - \frac{1}{2}(\sigma_\vartheta + \sigma_z)}{\bar{\sigma}}\right) \\
&= d\varepsilon_r{}^e + d\varepsilon_r{}^p \\
d\varepsilon_z = 0 &= \frac{1}{E}(d\sigma_z - \nu(d\sigma_\vartheta + d\sigma_r)) + d\bar{\varepsilon}^p\left(\frac{\sigma_z - \frac{1}{2}(\sigma_\vartheta + \sigma_r)}{\bar{\sigma}}\right) \\
&= d\varepsilon_z{}^e + d\varepsilon_z{}^p = d\varepsilon_z{}^e - (d\varepsilon_r{}^p + d\varepsilon_\vartheta{}^p) \\
d\gamma_{r\vartheta} &= \frac{d\tau_{r\vartheta}}{G} + d\bar{\varepsilon}^p\,\frac{3\tau_{r\vartheta}}{\bar{\sigma}}\,.
\end{aligned}\right\} \quad (4.15)$$

For constant volume plastic flow $d\varepsilon_r{}^p + d\varepsilon_\vartheta{}^p + d\varepsilon_z{}^p = 0$. If one is considering several increments it is easier from a computational point of view to consider the total strains ε as made up of all the previous and the current strain increments. The equations (4.15) can thus be rewritten —

$$\left.\begin{aligned}
\varepsilon_\vartheta &= \frac{1}{E}(\sigma_\vartheta - \nu(\sigma_r + \sigma_z)) + \varepsilon_\vartheta{}^p + d\varepsilon_\vartheta{}^p \\
\varepsilon_r &= \frac{1}{E}(\sigma_r - \nu(\sigma_\vartheta + \sigma_z)) + \varepsilon_r{}^p + d\varepsilon_r{}^p \\
\varepsilon_z = 0 &= \frac{1}{E}(\sigma_z - \nu(\sigma_\vartheta + \sigma_r)) + \varepsilon_z{}^p + d\varepsilon_z{}^p \\
\gamma_{r\vartheta} &= \frac{\tau_{r\vartheta}}{G} + \gamma_{r\vartheta}{}^p + d\gamma_{r\vartheta}{}^p.
\end{aligned}\right\} \quad (4.16)$$

The third stress σ_z can be eliminated from the first two equations using the third, and, multiplying through all equations by E, this gives —

$$\left.\begin{aligned}
E\varepsilon_\vartheta = (1-\nu^2)\sigma_\vartheta - \nu(1+\nu)\sigma_r + (1-\nu)E(\varepsilon_\vartheta{}^p + d\varepsilon_\vartheta{}^p) \\
- \nu E(\varepsilon_r{}^p + d\varepsilon_r{}^p)
\end{aligned}\right.$$

$$\left.\begin{aligned} E\varepsilon_r &= (1-\nu^2)\sigma_r - \nu(1+\nu)\sigma_\vartheta + (1-\nu)E(\varepsilon_r{}^p + d\varepsilon_r{}^p) \\ &\qquad - \nu E(\varepsilon_\vartheta{}^p + d\varepsilon_\vartheta{}^p) \\ E\gamma_{r\vartheta} &= 2(1+\nu)\tau_{r\vartheta} + E(\gamma_{r\vartheta}{}^p + d\gamma_{r\vartheta}{}^p). \end{aligned}\right\} \quad (4.17)$$

These equations can be simplified by the introduction of the variables a, b, c, p, x, y, z defined by –

$$\left.\begin{aligned} a &= \sigma_\vartheta + \frac{E}{1+\nu}(\varepsilon_\vartheta{}^p + d\varepsilon_\vartheta{}^p) \\ b &= \sigma_r + \frac{E}{1+\nu}(\varepsilon_r{}^p + d\varepsilon_r{}^p) \\ c &= \tau_{r\vartheta} + \frac{E}{2(1+\nu)}(\gamma_{r\vartheta}{}^p + d\gamma_{r\vartheta}{}^p) \end{aligned}\right\} \quad (4.18)$$

$$p = \frac{E d\bar{\varepsilon}^p}{1+\nu} \quad (4.19)$$

$$\left.\begin{aligned} x &= \frac{\sigma_\vartheta - \frac{1}{2}(\sigma_r + \sigma_z)}{\bar{\sigma}} \\ y &= \frac{\sigma_r - \frac{1}{2}(\sigma_\vartheta + \sigma_z)}{\bar{\sigma}} \\ z &= \frac{3\tau_{r\vartheta}}{\bar{\sigma}}. \end{aligned}\right\} \quad (4.20)$$

Consider for example, the circumferential strain; from the Levy Mises equations and using equations (4.19) and (4.20) for the i^{th} load increment $d\varepsilon_\vartheta{}^p = p_i x_i$ and, since during the previous $(i-1)$ load increments values of p and x vary

$$\varepsilon_\vartheta{}^p = \sum_{k=1}^{i-1} d\varepsilon_{\vartheta_k}{}^p = \sum_{k=1}^{i-1} p_k x_k.$$

Thus $\varepsilon_\vartheta{}^p + d\varepsilon_\vartheta{}^p = \sum_{k=1}^{i} p_k x_k$ and this will be denoted by $\sum px$.

Equations (4.18) can thus be written

$$\left.\begin{aligned} a &= \sigma_\vartheta + \sum px \\ b &= \sigma_r + \sum py \\ c &= \tau_{r\vartheta} + \sum pz \end{aligned}\right\} \quad (4.21)$$

(Note: $\sigma_z = \nu(a+b) + (1+\nu)(\sum px + \sum py)$).

In order to extract total strains from a, b and c,

equations (4.17) may be rewritten

$$\left.\begin{aligned} E\varepsilon_\vartheta &= (1-\nu^2)a - \nu(1+\nu)b \\ E\varepsilon_r &= (1-\nu^2)b - \nu(1+\nu)a \\ E\gamma_{r\vartheta} &= 2(1+\nu)c\ . \end{aligned}\right\} \qquad (4.22)$$

4.3.3 Non-dimensionalizing and Simplification of Variables

It is convenient to non-dimensionalize the symbols throughout by the factor $\frac{E}{\sigma_Y}$ (where σ_Y is the yield stress) and by re-defining the variables as follows

$$A = \frac{a}{\sigma_Y} \qquad B = \frac{b}{\sigma_Y} \qquad C = \frac{c}{\sigma_Y}$$

$$AS = \frac{\sigma_\vartheta}{\sigma_Y} \qquad BS = \frac{\sigma_r}{\sigma_Y} \qquad CS = \frac{\tau_{r\vartheta}}{\sigma_Y}$$

$$P = \frac{Ed\bar{\varepsilon}^p}{\sigma_Y(1+\nu)} \qquad X = \frac{\left[\frac{\sigma_\vartheta}{\sigma_Y} - \nu\left(\frac{\sigma_r}{\sigma_Y} + \frac{\sigma_z}{\sigma_Y}\right)\right]}{\frac{\bar{\sigma}}{\sigma_Y}}\ .$$

Similarly for Y and Z.

The radius becomes $R = \frac{r}{r_o}$ where r_o is the radius of the inner surface. Similarly the displacements are non-dimensionalized to

$$D = \frac{E}{\sigma_Y}\frac{u}{R} \qquad G = \frac{E}{\sigma_Y}\frac{v}{R}\ .$$

Derivatives are denoted as follows (e.g. for variable X)

$$\frac{\partial X}{\partial \vartheta} = XH \qquad R\frac{\partial X}{\partial R} = XN$$

$$\frac{\partial^2 X}{\partial \vartheta^2} = X2H \qquad R^2\frac{\partial^2 X}{\partial R^2} = X2N$$

$$R\frac{\partial^2 X}{\partial \vartheta \partial R} = XNH.$$

The constants in ν are denoted as follows —

$$V3 = 1-\nu^2 \qquad V4 = \nu(1+\nu) \qquad V5 = 2(1+\nu).$$

The equilibrium equations (4.13) thus become

$$\left.\begin{aligned} ASH + CSN + 2CS &= 0 \\ CSH + BSN + BS - AS &= 0. \end{aligned}\right\} \qquad (4.23)$$

The stress strain relations (4.21) become

$$\left.\begin{aligned} A &= AS + PX^{\dagger} \\ B &= BS + PY^{\dagger} \\ C &= CS + PZ^{\dagger} \end{aligned}\right\} \qquad (4.24)$$

and use of these in (4.23) enables these equations to be expressed in terms of strains A, B, C

viz.
$$\left.\begin{aligned} AH + CN + 2C &= PXH + PZN + 2PZ \\ CH + BN + B-A &= PZH + PYN + PY-PX. \end{aligned}\right\} \qquad (4.25)$$

The strain displacement equations (4.14) become with (4.22)

$$\left.\begin{aligned} \frac{E\varepsilon_{\theta}}{\sigma_Y} &= D + GH = V3A - V4B \\ \frac{E\varepsilon_{r}}{\sigma_Y} &= D + DN = V3B - V4A \\ \frac{E\gamma_{r\theta}}{\sigma_Y} &= DH + GN = V5C. \end{aligned}\right\} \qquad (4.26)$$

4.3.4 Elastic Conditions

Under elastic conditions plastic strains are zero. Thus from equations (4.24)

A = AS, B = BS and C = CS since P = 0.

Equations (4.25) and (4.26) can now be written in terms of A, B, C, D and G —

$$\left.\begin{aligned} AH + CN + 2C &= 0 \\ CH + BN + B - A &= 0 \\ D + GH &= V3A - V4B \\ D + DN &= V3B - V4A \\ DH + GN &= V5C \end{aligned}\right\} \qquad (4.27)$$

These are the elastic equation in five variables.

---

† Note: PX, PY, PZ are used here among total quatities A, AS, etc. They stand for the sum of all the PX, PY, PZ products over the total number of increments. Thus for i increments

$$PX \equiv \sum_{k=1}^{i} P_k \times X_k.$$

4.3.5 Reduction to Four Variables

The equations (4.27) can be reduced to four equations in four unknowns by introducing a function F and eliminating D and G, where

$$F = \frac{\partial(RG)}{\partial R}.$$

The resulting four equations in the variables A, B, C and F are as follows where the derivatives are written in the usual form for use in the classification in paragraph 4.3.6 below

$$\left.\begin{aligned} R\frac{\partial C}{\partial R} + \frac{\partial A}{\partial \vartheta} &= -2C \\ R\frac{\partial B}{\partial R} + \frac{\partial C}{\partial \vartheta} &= A - B \\ V3R\frac{\partial A}{\partial R} - V4R\frac{\partial B}{\partial R} - \frac{\partial F}{\partial \vartheta} &= B(V3 + V4) - A(V3 + V4) \\ V5R\frac{\partial C}{\partial R} - R\frac{\partial F}{\partial R} - V3\frac{\partial B}{\partial \vartheta} + V4\frac{\partial A}{\partial \vartheta} &= -V5C. \end{aligned}\right\} \quad (4.28)$$

4.3.6 Classification of Equations (4.28)

It is important to know into which category the set of first order equations is classified. The test depends on finding whether the characteristics of the equations are real or imaginary. Details of the test can be found in Courant and Hilbert Vol. II[29].

Equations (4.28) are re-arranged and written in matrix form.

$$R\begin{bmatrix} 0 & 0 & 1 & 0 \\ 0 & 0 & V5 & -1 \\ 0 & 1 & C & 0 \\ V3 & -V4 & 0 & 0 \end{bmatrix}\frac{\partial}{\partial R}\begin{bmatrix} A \\ B \\ C \\ F \end{bmatrix} + \begin{bmatrix} 1 & 0 & 0 & C \\ V4 & -V3 & 0 & C \\ 0 & 0 & 1 & C \\ C & C & 0 & -1 \end{bmatrix}\frac{\partial}{\partial \vartheta}\begin{bmatrix} A \\ B \\ C \\ F \end{bmatrix}$$

$$= \begin{bmatrix} -2C \\ -V5C \\ A - B \\ (V3 + V4)(B - A) \end{bmatrix}$$

OR $$\mathbb{A}\frac{\partial}{\partial R}(W) + \mathbb{B}\frac{\partial}{\partial \vartheta}(W) = \mathbb{C}. \quad (4.29)$$

Since $\mathbb{A}$ and $\mathbb{B}$ do not depend on A, B, C or F and since $\mathbb{C}$ depends only linearly on A, B, and C, the system is

considered linear (Courant and Hilbert p 424,5). Either $\mathcal{A}$ or $\mathcal{B}$ must be non-singular for the test to be carried out and in this case $\mathcal{B}$ is non-singular.

The characteristic determinant is $Q = |\mathcal{A} - \tau\mathcal{B}|$ where τ are the roots of the equation $Q = 0$. If this equation does not possess real roots τ, then all characteristic curves are free: continuation into a step of initial values is always possible and unique. The system is then called elliptic (Courant and Hilbert p 171).

Thus

$$|\mathcal{A} - \tau\mathcal{B}| = \begin{vmatrix} -\tau & 0 & R & 0 \\ -\tau V4 & \tau V3 & RV5 & -R \\ 0 & R & -\tau & 0 \\ RV3 & -RV4 & 0 & \tau \end{vmatrix} = 0$$

giving $\tau = iR, iR, iR, iR.$

The system is thus elliptic. It must be remembered that the above classification refers only to the elastic equations (4.28): a similar test with similar results was carried out on equations (4.27) for the five variable equations. No way can be found to test the elasto-plastic form of the equations.

4.3.7 Reduction to Three Variables

A further reduction to three equations in three variables can be effected by elimination of F in (4.28). Re-introducing the distinction between stresses (AS etc.) and strains (A etc.) and also the plastic terms with the definitions of equations (4.24), equations (4.28) are formulated as follows:—

Equilibrium:—
$$\begin{cases} CSN + ASH + 2CS = 0 & (4.30) \\ BSN + CSH + BS - AS = 0 & (4.31) \end{cases}$$

OR
$$\begin{cases} CN + AH + 2C = PZH + PXH + 2PZ & (4.32)\dagger \\ CH + BN + B - A = PZH + PYN + PY - PZ & (4.33)\dagger \end{cases}$$

---

† Remember $PY = \sum_{k=1}^{i} P_k Y_k$ etc.

Strain/Displacement:-

$$\begin{cases} V3AN - V4BN - FH = (V3 + V4)(B - A) & (4.34) \\ V5CN - FN - V3BH + V4AH = -V5C & (4.35) \end{cases}$$

Operating on equation (4.34) by $R\frac{\partial}{\partial R}$ and equation (4.35) by $\frac{\partial}{\partial \vartheta}$ gives, on re-arrangement,

$$FNH = V3A2N - (2V3 + V4)AN - V4B2N - (V3 + 2V4)BN$$

and $$FNH = V5CNH + V5CH - V3B2H + V4A2H.$$

Subtracting these to eliminate FNH gives -

$$V3A2N + (2V3 + V4)AN - V4A2H - V4B2N - (V3 + 2V4)BN + V3B2H - V5CNH - V5CH = 0 \qquad (4.36)$$

Equations (4.32) and (4.33) can be used to eliminate CNH and CH from (4.36) to give

$$A2N + A2H + AN + B2N + B2H + BN = \frac{1}{1-\nu}\left[-PXN + PX2H + 2PYN + PY2N + 2PZH + 2PZNH\right]$$

$$= \frac{1}{1-\nu} P_3 \text{ (say).} \qquad (4.37)$$

The left-hand side of (4.37) represents $\nabla^2(A + B)$.
It is interesting to note that the left-hand side of (4.36) can be found directly from the strain compatibility equation -

$$\frac{\partial^2(r\gamma_{r\vartheta})}{\partial r \partial \vartheta} - r\frac{\partial^2(r\varepsilon_\vartheta)}{\partial r^2} - \frac{\partial^2 \varepsilon_r}{\partial \vartheta^2} + r\frac{\partial \varepsilon_r}{\partial r} = 0, \qquad (4.38)$$

as follows:-
Using the definitions of equations (4.22) in (4.38) gives

$$2(1 + \nu)\frac{\partial^2(rc)}{\partial r \partial \vartheta} - r\frac{\partial^2}{\partial r^2}\left[(1 - \nu^2)ra - \nu(1 + \nu)rb\right] - \frac{\partial^2}{\partial \vartheta^2}\left[(1 - \nu^2)b - \nu(1 + \nu)a\right] + r\frac{\partial}{\partial r}\left[(1 - \nu^2)b - \nu(1 + \nu)a\right] = 0$$

or in the non-dimensional form

$$(1 - \nu^2)A2H + \left[2(1 - \nu^2) + \nu(1 + \nu)\right]AN - \nu(1 + \nu)A2H - \nu(1 + \nu)B2N - \left[2\nu(1 + \nu) + (1 - \nu^2)\right]BN + (1 - \nu^2)B2H - 2(1 + \nu)CNH - 2(1 + \nu)CH = 0$$

which is identical to the LHS of (4.36).

The three governing equations in the three strain functions A, B and C are thus

$$\boxed{\begin{aligned} &AH + CN + 2C = PZN + PXH + 2PZ \\ &CH + BN + B - A = PZH + PYN + PY - PX \\ &A2N + A2H + AN + B2N + B2H + BN = \frac{P_3}{(1-\nu)} \end{aligned}}. \qquad (4.39)$$

Equations (4.39) can however also be expressed in terms of the stresses AS, BS and CS.

In this case the equilibrium equations remain unchanged (4.30), (4.31) while equation (4.37) must now be rephrased using the relations (4.24). Thus

$$\begin{aligned} &AS2N + AS2H + ASN + BS2N + BS2H + BSN \\ &\quad = \frac{1}{1-\nu} P_3 - (PX2N + PX2H + PXN \\ &\qquad\qquad + PY2N + PY2H + PYN) \\ &\quad = \frac{1}{1-\nu} \left\{ \begin{aligned} &-(1-\nu)PX2N + \nu\, PX2H - (2-\nu)PXN \\ &+\nu\, PY2N - (1-\nu)PY2H + (1+\nu)PYN \\ &+ 2PZH + 2PZNH \end{aligned} \right\} \\ &\quad = \frac{1}{(1-\nu)} P_4 \quad \text{(say)}. \end{aligned}$$

The three governing equations in the three stresses AS, BS and CS are thus

$$\boxed{\begin{aligned} &ASH + CSN + 2CS = 0 \\ &CSH + BSN + BS - AS = 0 \\ &AS2N + AS2H + ASN + BS2N + BS2H + BSN = \frac{P_4}{(1-\nu)} \end{aligned}} \qquad (4.40)$$

The classification of equations (4.39) and (4.40) does not seem possible in that no test could be found due to the complication of having two first order and one second order equation and in addition having a variable P which relates stress and strain through a non-linear stress-strain curve.

CHAPTER 5

FIRST ATTEMPTS AT USING FIRST ORDER EQUATIONS FOR PLANE STRAIN PROBLEMS

CHAPTER 5

FIRST ATTEMPTS AT USING FIRST ORDER EQUATIONS FOR PLANE STRAIN PROBLEMS

5.1. Introduction

When it was decided to investigate the use of the five first order equations, few guidelines could be found in the literature. Consequently much effort went into methods which had in the long run to be scrapped. Since this was the first time these lower order equations have been used in stress and strain problems, thorough study was made into each attempt. Reported below is a brief summary of each study in the order in which it was undertaken. The reason for this summary is to give an indication to future researchers where not to start.

This, then is largely a chapter of failures, describing a fair amount of work on methods which one by one had to be discarded. Essentially there were four main approaches tackled:-

(a) Solution by elements - section 5.2.
(b) Solution by interlacing grids - section 5.3.
(c) Solution by extrapolation and correction - section 5.4.
(d) Solution by Lax-Wendroff method - section 5.5.

The reasons for failure of each method led to remedial action being taken in the formulation of the next. The conclusions reached on completion of each method are underlined.

The eventual aim of this work was to study elasto-plastic stress and strain fields at the root of a keyhole notch. However due to the fact that the results from the new methods would have to be checked, a known analytical elastic solution was used. The problem of

the hole in an infinite media under uniaxial tension was selected since identical grid coordinates could be utilized. The only difference is that in this case a symmetrical quarter need only be considered due to the two axes of symmetry — fig. 5.1.

Once the solution for the hole had been found, the program could be re-run (with only slight alteration of the boundary conditions) with the keyhole data from the stress function solution.

5.2 Solution by Elements in the Elastic Phase

5.2.1 Introduction

Initially the five equations were as follows;—

— rewriting equations (4.13) and (4.14) for convenience

$$\left.\begin{aligned} \frac{\partial \sigma_\vartheta}{\partial \vartheta} + r\frac{\partial \tau_{r\vartheta}}{\partial r} + 2\tau_{r\vartheta} &= 0 \\ r\frac{\partial \sigma_r}{\partial r} + \frac{\partial \tau_{r\vartheta}}{\partial \vartheta} + \sigma_r - \sigma_\vartheta &= 0 \end{aligned}\right\} \text{Equilibrium} \qquad (5.1)$$

$$\left.\begin{aligned} \varepsilon_\vartheta &= \frac{u}{r} + \frac{\partial(\frac{v}{r})}{\partial \vartheta} \\ \varepsilon_r &= \frac{u}{r} + r\frac{\partial(\frac{u}{r})}{\partial r} \\ \gamma_{r\vartheta} &= \frac{\partial(\frac{u}{r})}{\partial \vartheta} + r\frac{\partial(\frac{v}{r})}{\partial r}, \end{aligned}\right\} \begin{matrix} \text{Strain} \\ \text{Displacement} \end{matrix} \qquad (5.2)$$

Rationalize these by making the five equations STRAIN oriented and by using the definitions

$$d = \frac{Eu}{r} \qquad\qquad g = \frac{Ev}{r} \qquad (5.3)$$

(d and g are here similar to D and G defined in paragraph 4.3.3).

Equilibrium; Since $\sigma_\vartheta = \frac{E}{(1+\nu)(1-2\nu)}\left[(1-\nu)\varepsilon_\vartheta + \nu\varepsilon_r\right]$

$$\sigma_r = \frac{E}{(1+\nu)(1-2\nu)}\left[(1-\nu)\varepsilon_r + \nu\varepsilon_\vartheta\right]$$

$$\tau_{r\vartheta} = \frac{\gamma_{r\vartheta}}{G} = \frac{E\gamma_{r\vartheta}}{2(1+\nu)}$$

then equations (5.1) become

$$\left.\begin{aligned} \frac{(1-\nu)}{(1-2\nu)}\frac{\partial \varepsilon_\vartheta}{\partial \vartheta} + \frac{\nu}{(1-2\nu)}\frac{\partial \varepsilon_r}{\partial \vartheta} + 0.5\, r\frac{\partial \gamma_{r\vartheta}}{\partial r} + \gamma_{r\vartheta} &= 0 \\ \frac{(1-\nu)}{(1-2\nu)}\, r\frac{\partial \varepsilon_r}{\partial r} + \frac{\nu}{(1-2\nu)}\, r\frac{\partial \varepsilon_\vartheta}{\partial r} + 0.5\frac{\partial \gamma_{r\vartheta}}{\partial \vartheta} + \varepsilon_r - \varepsilon_\vartheta &= 0. \end{aligned}\right\} (5.4)$$

Using the definitions (5.3) in (5.2) gives with (5.4)

$$\left.\begin{aligned} \frac{(1-\nu)}{(1-2\nu)}\frac{\partial \varepsilon_\vartheta}{\partial \vartheta} + \frac{\nu}{(1-2\nu)}\frac{\partial \varepsilon_r}{\partial \vartheta} + 0.5\, r\frac{\partial \gamma_{r\vartheta}}{\partial r} + \gamma_{r\vartheta} &= 0 \\ \frac{(1-\nu)}{(1-2\nu)}\, r\frac{\partial \varepsilon_r}{\partial r} + \frac{\nu}{(1-2\nu)}\, r\frac{\partial \varepsilon_\vartheta}{\partial r} + 0.5\frac{\partial \gamma_{r\vartheta}}{\partial \vartheta} + \varepsilon_r - \varepsilon_\vartheta &= 0 \\ \varepsilon_\vartheta &= d + \frac{\partial g}{\partial \vartheta} \\ \varepsilon_r &= d + r\frac{\partial d}{\partial r} \\ \gamma_{r\vartheta} &= \frac{\partial d}{\partial \vartheta} + r\frac{\partial g}{\partial r}\,. \end{aligned}\right\} (5.5)$$

Thus the five equations (5.5) have five unknowns ε_r, ε_r, $\gamma_{r\vartheta}$, d, g. The original idea was to divide the field into polar elements and solve these successively or in groups.

5.2.2 Solution of Elements

Element $\alpha(1, 2, 3, 4)$ is first solved as follows; (refer to fig. 5.2). Assume ε_ϑ, ε_r given on notch surface — $\varepsilon_{\vartheta_1}$, $\varepsilon_{\vartheta_2}$, ε_{r_1}, ε_{r_2} known. From symmetry and the condition of no shear on the notch surface — $\gamma_{r\vartheta_1} = \gamma_{r\vartheta_2} = \gamma_{r\vartheta_3} = 0$, and $g_1 = g_3 = 0$. Thus for element α there are ten unknowns d_2, g_2, $\varepsilon_{\vartheta_3}$, ε_{r_3}, d_3, $\varepsilon_{\vartheta_4}$, ε_{r_4}, $\gamma_{r\vartheta_4}$, d_4, g_4. Symmetry across the $\measuredangle$ gives $\frac{\partial \varepsilon_\vartheta}{\partial \vartheta} = \frac{\partial \varepsilon_r}{\partial \vartheta} = \frac{\partial d}{\partial \vartheta} = 0$, and a condition of asymmetry exists for $\gamma_{r\vartheta}$.

With all these conditions, application of equations (5.5) along the sides of the element yield only seven equations and three more must be found to solve the ten unknowns. A further assumption can be made —

viz $$\left(\frac{\partial g}{\partial \vartheta}\right)_1 = 0 \quad \Rightarrow \quad \varepsilon_{\vartheta_1} = d_1.$$

Also two 'estimates' must be made

viz $$\varepsilon_{\vartheta_4} = 0.945\ \varepsilon_{\vartheta_3}$$

and $$d_2 - d_1 = d_4 - d_3.$$

The ten equations were solved by an elimination procedure and not surprisingly the results were not very good. Nonetheless, element β was solved with the values at points 2 and 4 from α.

With $\varepsilon_{\vartheta 5}$, ε_{r5} being given and $\gamma_{r\vartheta 5} = 0$, element β had seven unknowns, d_5, g_5, $\varepsilon_{\vartheta 6}$, ε_{r6}, $\gamma_{r\vartheta 6}$, d_6, g_6. Six equations can be found from equations (5.5) applied along the sides of β. The seventh equation as above comes from the 'estimate'

$$d_6 - d_4 = d_5 - d_2.$$

The solution of these equations produced bad results for β and this approach was dropped.

An attempt was made to solve elements α and β together but this approach was dropped for similar reasons.

In conclusion, solution by elements was abandoned due to the lack of equations. Also the strain boundary conditions on the inner surface made it difficult to use the stress conditions $\tau_{r\vartheta} = \sigma_r = 0$. It was felt, in addition, that working around the perimeter of each element made the 'linking' of variables at opposite points difficult (e.g. points 1 to 4 and 2 to 3) and the use of centred difference gradients inaccurate.

5.3 Solution by Interlacing Grids

In response to the above comment on boundary conditions the equations (5.2) were STRESS oriented using the elastic stress strain relations

$$E\varepsilon_\vartheta = (1 - \nu^2)\sigma_\vartheta - \nu(1 + \nu)\sigma_r$$

$$E\varepsilon_r = (1 - \nu^2)\sigma_r - \nu(1 + \nu)\sigma_\vartheta$$

$$E\gamma_{r\vartheta} = 2(1 + \nu)\tau_{r\vartheta}.$$

At this stage the variables were non-dimensionalized as shown in paragraph 4.3.3 where $AS = \frac{\sigma_\vartheta}{\sigma_Y}$ etc. and $D = \frac{Eu}{\sigma_Y R}$, $G = \frac{Ev}{\sigma_Y R}$.

Thus the five equations are now

$$\frac{\partial AS}{\partial \vartheta} + R\frac{\partial CS}{\partial R} + 2CS = 0 \qquad (5.6)$$

$$R\frac{\partial BS}{\partial R} + \frac{\partial CS}{\partial \vartheta} + BS - AS = 0 \qquad (5.7)$$

$$D + \frac{\partial G}{\partial \vartheta} = (1-\nu^2)AS - \nu(1+\nu)BS \qquad (5.8)$$

$$\frac{\partial (RD)}{\partial R} = (1-\nu^2)BS - \nu(1+\nu)AS \qquad (5.9)$$

$$\frac{\partial D}{\partial \vartheta} + R\frac{\partial G}{\partial R} = 2(1+\nu)CS. \qquad (5.10)$$

In order to achieve some 'linking' between points which appeared to lack in the previous method, an interlacing net was introduced as shown in the fig. 5.3. This grid system also allowed better centring of difference gradient formulae. Coordinates K,L define positions on the grids.

The boundary condition of zero radial and shear loading on the inner surface gives

$$BS = CS = 0$$

and on the $\not\in$ the symmetry gives

$$G = CS = 0.$$

The variables are assigned at particular intersections on the two grids, such that equations (5.6) to (5.10) can be used to advantage as is shown below, assuming solution of the field proceeds in the positive ϑ and positive R directions. When values are required at particular intersections, where no value is assigned, then an interpolation is carried out between neighbouring intersections.

i) Use of equation (5.6) to determine $\boxed{CS}$ (K,L) — fig. 5.4. The equation is centred at $\triangle$(K − 1, L)

therefore $$\left(\frac{\partial AS}{\partial \vartheta}\right)_{K-1,L} + \left(R\frac{\partial CS}{\partial R}\right)_{K-1,L} + 2CS_{K-1,L} = 0.$$

ii) Use of equation (5.7) to determine $\boxed{BS}$ (K,L) — fig. 5.5.

The equation is centred at $\triangle$ (K−1,L)

therefore $$(R\frac{\partial BS}{\partial R})_{K-1,L} + (\frac{\partial CS}{\partial \vartheta})_{K-1,L} + (BS - AS)_{K-1,L} = 0.$$

(iii) Use of equation (5.8) to determine $\boxed{G}$ (K,L) – fig. 5.6. The equation is centred at $\triangle$(K,L−1)

therefore $$D_{K,L-1} + (\frac{\partial G}{\partial \vartheta})_{K,L-1} = (1-\nu^2)AS_{K,L-1} - \nu(1+\nu)BS_{K,L-1}.$$

(iv) Use of equation (5.9) to determine $\boxed{D}$ (K,L), radially – fig. 5.7. The equation is centred at $\triangle$(K−1,L)

$$(\frac{\partial(RD)}{\partial R})_{K-1,L} = (1-\nu^2)BS_{K-1,L} - \nu(1+\nu)AS_{K-1,L}.$$

(v) Use of equation (5.10) to determine $\boxed{D}$ (K,L), circumferentially – fig. 5.8. The equation is centred at $\triangle$(K,L−1)

$$(\frac{\partial D}{\partial \vartheta})_{K,L-1} + (R\frac{\partial G}{\partial R})_{K,L-1} = 2(1+\nu)CS_{K,L-1}.$$

Essentially this method is similar to the last one in that the solution progresses from one boundary, in this case the inner surface to an outer boundary as yet undefined. In order to do this the value of AS must be assumed known on K = 2 and 4 (OR 2 and 3). With this assumption and the assumption that $(\frac{\partial G}{\partial \vartheta})_{2,2} = 0$, the solution can progress successively from one K line to the next having first solved all variables on that K line for $\vartheta = 0^o$ to $\frac{\pi}{2}$.

It will be noted above that the use of equations (5.6) to (5.10) does not show any way of progressing AS forward. This must be done in a simultaneous fashion as follows:–

Referring to fig. 5.9.

(a) (G) is found at (K,L+1) from (5.10).

(b) Assume AS has a value x.

(c) (BS) is found at (K,L) from (5.7).

(d) (D) is found at (K+1,L) from (5.9).

(e) (G) is found at (K,L+1) from (5.8).

Matching of the values of G from (d) and (e) gives x, i.e. AS (K,L).

This method proved reasonably successful, a trial field being solved, moving from the inner boundary K = 2 out to K = 14, solving circumferentially from L = 2 to L = 14 for each K line -- fig. 5.10.

The results are shown below for uniaxial tension at infinity; the bracketed values are the exact values from the analytical solution.

Note **

K	Radius × r_o	L = 2 AS	L = 2 BS	L = 3 CS	L = 10 AS	L = 10 BS	L = 11 CS
2	1.00	1.125†	0.00*	0.00*	0.375†	0.00*	0.00*
3	1.06			0.015 (0.015)			0.075 (0.075)
4	1.13	0.874†	0.096 (0.094)		0.336†	0.039 (0.039)	
5	1.20			0.034 (0.034)			0.171 (0.171)
6	1.27	0.703 (0.711)	0.133 (0.131)		0.298 (0.304)	0.071 (0.071)	
7	1.34			0.043 (0.043)			0.218 (0.218)
8	1.42	0.589 (0.604)	0.143 (0.141)		0.270 (0.279)	0.094 (0.096)	
9	1.51			0.047 (0.047)			0.238 (0.240)
10	1.60	0.512 (0.534)	0.133 (0.133)		0.246 (0.261)	0.113 (0.114)	
11	1.70			0.049 (0.049)			0.240 (0.246)
12	1.80	0.458 (0.486)	0.118 (0.119)		0.223 (0.246)	0.128 (0.129)	
13	1.91			0.047 (0.049)			0.231 (0.246)
14	2.03	0.418 (0.454)	0.099 (0.103)		0.201 (0.233)	0.143 (0.143)	

† fixed boundary values of $\frac{\sigma_\theta}{\sigma_Y}$.

*given zero boundary conditions for $\frac{\sigma_r}{\sigma_Y}$ and $\frac{\tau_{r\theta}}{\sigma_Y}$.

** Note all the numerical results given in this chapter are based on the elastic plane strain solution of the hole in tension at the point of yielding, i.e. $\bar{\sigma}_{22} = \sigma_Y$.

In conclusion, however, it was noted that accuracy diminished as R and θ increased. This would be attributed to the decreasing effect of the boundary lines K = 2 and L = 2. No heed was taken about merging the K lines at L = 14 into the known analytical solution. Nevertheless the apparent success of this method led on to an attempt at an elasto-plastic solution, which proved unstable. Better methods were thus sought to improve evaluation of extrapolated values.

5.4 Solution of Fields by Extrapolation and Correction

5.4.1 Introduction

The two similar methods detailed below attempted to extrapolate from the outer boundary correcting the K lines successively by using the first order equations in a reiterative technique. The equations were STRESS oriented viz. equations (5.6) to (5.10).

In the first method much use is made of the Trapezoidal Rule (TR); circumferentially this rule can be used to find the value of functions at neighbouring points from (see fig. 5.11) $X_2 = X_1 + \frac{H}{2}(XH_1 + XH_2)$. It can also be used radially. In place of the gradients, expressions from equations (5.6) to (5.10) can be used. Finally it is used to find gradients, e.g. $XH_2 = \frac{2}{H}(X_2 - X_1) - XH_1$.

5.4.2 Method 1

The field used is as shown in fig. 5.12. The geometric ratio of radii was 1.125 and the equal circumferential spacing, $\frac{\pi}{32}$. This time no intermediate net was used. The ratio 1.125 means that the radii of adjacent I lines are such that $\frac{R_{I+1}}{R_I} = 1.125 = T$, say.

Initially the following boundary conditions were fed in —

(a) On the I = 8,9 lines AS, BS, CS, D, G, ASN, BSN, CSN.

(b) On the L = 10,11 lines AS, BS, CS, ASH, CSH,
where $ASH = \frac{\partial AS}{\partial \theta}$ and $ASR = R\frac{\partial AS}{\partial R}$ etc.

The following steps indicate the general technique for moving from a $I + 1$ line to a I line.

(1) D_I is found at $L = 10,11$ using the TR and equation (5.9)
GH_I is found at $L = 10,11$ from equation (5.8).

(2) G_I is found at $L = 11$ with the TR and equation (5.10)
G_I at $L = 10$ is found by integration from $L = 11$.

(3) GN_I is found at $L = 10,11$ using the TR between I and $I + 1$
DH_I is found at $L = 10,11$ using equation (5.10).

(4) AS, BS, CS, G are extrapolated onto line I for $L = 2, 10$ using the values of each variable at $I + 1$ and $I + 2$ and also the normal gradient at $I + 1$. The extrapolation formula used was

$$X_I = \frac{1}{T^2}\left[X_{I+2} + (T^2 - 1)X_{I+1} - T(T^2 - 1)XN_{I+1}\right]$$

(5) Since the values of the variables in (4) will show a discrepancy at $L = 10$, a correction factor is applied along the I line to each of the variables to equate the values at this boundary.

(6) D_I is calculated for $L = 2,10$ using the TR.

On the I line the points are scanned from $L = 9$ into $L = 3$ and at each point the following steps (7) to (15) are looped 4 times. Also the overall calculation along the I line is looped 8 times in order to achieve accuracy.

Thus for each L point on the I line

(7) ASH_I is found using equation (5.6).

(8) AS_I is calculated by integration using the TR from $L + 1$ to L.

(9) BS_I is found using the TR radially and equation (5.7).

(10) D_I is found using the TR radially and equation (5.9).

(11) GH_I is calculated using equation (5.8).

(12) G_I is found by integration.

(13) GN_I is calculated from the TR radially from I + 1.

(14) CS_I is found from equation (5.10).

(15) BH_I is found by a circumferential difference formula.

(16) Corrections are made for the L = 2 boundary.

(17) Radial gradients ASN_I, BSN_I, CSN_I are found using the TR radially, for use in the extrapolation formulae when moving onto the I − 1 line.

Despite all the careful formulation of the technique this method lost stability very quickly, when the calculations are started on I = 8, the results, on reaching the I = 6 and I = 5 lines show the initiation of a violent oscillation.

5.4.3 Method 2

Method 2 is similar to Method 1. Both methods start at an outer boundary assuming that all the variables AS, BS, CS, D, G and their gradients are known, and both endeavour to move into the inner boundary solving all circumferential lines successively. Method 2, however, differs in 4 aspects.

(1) The grid dimensions are altered, making $T = (1.125)^{\frac{1}{2}}$ in the hope of stabilizing the advance along the radial lines. The circumferential spacing is still $\frac{\pi}{32}$.

(2) Various forms of radial gradient calculation were used in the hope of achieving better directional stability — see paragraph 5.4.4.

(3) Method 1 solved all the variables at a point by an iterative technique whereas in Method 2, this is done by a matrix elimination process.

(4) There is a better 'knitting' effect when working circumferentially.

Referring to (1) above, the field dimensions are as shown in fig. 5.13. Due to the change ratio T, the circumferential lines are again denoted by K.

5.4.4 Gradient Formulae

Consider now the formulation of the gradient formulae and the better extrapolation formula for any variable X.

(a) Radial gradients.

One of the simpler formulae is based on the values X and gradients XN at adjacent points on an L line. The points are on lines K + 1 and K, i.e. at radii R_{K+1} and R_K ($R_{K+1} > R_K$) – fig. 5.14. Denote the ratio of radii by T, and the distance between the lines by H_R

therefore $$T = \frac{R_{K+1}}{R_K}$$

and $$H_R = R_{K+1} - R_K = R_K(T - 1).$$

Using the TR $$X_{K+1} = X_K + \frac{H_R}{2}\left(\left(\frac{\partial X}{\partial R}\right)_{K+1} + \left(\frac{\partial X}{\partial R}\right)_K\right).$$

Thus $$X_{K+1} = X_K + \frac{(T-1)}{2}\left(R_K\left(\frac{\partial X}{\partial R}\right)_{K+1} + R_K\left(\frac{\partial X}{\partial R}\right)_K\right)$$

Since $$R_K\left(\frac{\partial X}{\partial R}\right)_K = XN_K$$

and $$R_K\left(\frac{\partial X}{\partial R}\right)_{K+1} = \frac{1}{T} R_{K+1}\left(\frac{\partial X}{\partial R}\right)_{K+1} = \frac{XN_{K+1}}{T},$$

Then $$X_{K+1} = X_K + \frac{T-1}{2}\left(\frac{XN_{K+1}}{T} + XN_K\right)$$

OR $$XN_K = \frac{2}{T-1}(X_{K+1} - X_K) - \frac{XN_{K+1}}{T}. \qquad (5.11)$$

This formula however can be improved upon by inclusion of the value of X at K + 2, this making it accurate up to the cubic, viz.

$$XN_K = \frac{1}{T^2(T^2-1)} X_{K+2} + \frac{2T^3+3T^2-1}{T^2(T^2-1)} X_{K+1} - \frac{(2T+3)}{(T^2-1)} X_K - \frac{T+1}{T^2} XN_{K+1}. \quad (5.12)$$

While evaluating the gradient $\frac{\partial(RD)}{\partial R}$ it was found that the values obtained were always more accurate than for the other variables. It was concluded that the field variables must bear some relationship to $(\frac{1}{R})^n$. The effect of this can be nullified by taking the gradients of XR, XR^2 or XR^3 instead of X. The value of XN could then be extracted from the resulting relationship.

On an XR^2 basis this results in

$$XN_K = \frac{T^2}{T^2-1} X_{K+2} + \frac{T+1}{T-1} X_{K+1} - \frac{2T^2+2T+1}{T^2-1} X_K - XN_{K+1}(T+1). \quad (5.13)$$

On an XR^3 basis this results in

$$XN_K = \frac{T^4}{T^2-1} X_{K+2} + \frac{T(2+T-T^2)}{T-1} X_{K+1} - \frac{T(2+3T)}{T^2-1} X_K - T(T+1)\ XN_{K+1}. \quad (5.14)$$

As a check on the accuracy of each of these formula, the gradient $R\frac{\partial CS}{\partial R}$ at the point K = 13, L = 10, was evaluated using exact quantities and comparing the results with the analytical solution

Method	Value	Error
Analytical	-0.0367093	-
Formula (5.11)	-0.0379339	3.2%
Formula (5.12)	-0.0370029	0.75%
Formula (5.13)	-0.0367828	0.20%
Formula (5.14)	-0.0367238	0.04%

Although formula (5.14) gives the best result, the formula (5.13) was selected as being the optimum since -

(i) it was proposed to use this formula generally for all variables and some variables such as CS and BS near the K = 2 line do not conform to the $(\frac{1}{R})^n$ pattern,

(ii) any inaccuracies would be exagerated more by multiplying by R^3.

Confirmation of this choice is shown in paragraph 5.4.6.

(b) Circumferential gradients.

Two types of circumferential gradient formulae were required, depending on the position of available values. If H is the circumferential spacing – fig. 5.15, the two formulae are

$$XH_L = \frac{1}{2H}(X_{L+2} + 4X_{L+1} - 5X_L) - 2XH_{L+1} \qquad (5.15)$$

and

$$XH_L = \frac{1}{2H}(2.5\ X_{L+1} - 2\ X_L - 0.5\ X_{L-1}) - 0.5\ XH_{L+1}. \qquad (5.16)$$

These formulae are of use when traversing the K line in a negative ϕ direction. When traversing in a positive ϕ direction, similar gradients can be found.

(c) Extrapolation formula.

Using the XR^2 basis, a better formula can be found for evaluating an extrapolated value on a K line from

$$X_K = -\frac{T(T^2+T+1)}{(T+1)} X_{K+1} + (T^2+T+1)X_{K+2} - \frac{T^2}{T+1} X_{K+3} - \frac{T^3-1}{T} XN_{K+1}. \qquad (5.17)$$

5.4.5 Method 2 – Method of Solution

The solution of any K line starts at L = 11 and works into the ϕ.

As an example of the general method a description is given below of the solution of the variables at the point (K,L) – fig. 5.16.

For convenience the equations (5.6) to (5.10) are re-written here

$$ASH + CSH + 2CS = 0 \qquad (5.6)$$

$$BSV + CSH + BS - CS = 0 \qquad (5.7)$$

$$D + GH = (1-\nu^2)AS - \nu(1+\nu)BS \qquad (5.8)$$

$$D + DH = (1-\nu^2)BS - \nu(1+\nu)AS \qquad (5.9)$$

$$DH + GN = 2(1+\nu)CS \qquad (5.10)$$

In solving the variables AS, BS, CS, D, G each of these equations is evaluated at point (K,L). Look at each in turn

(5.6) The gradient ASH cannot be discretized using a central difference formula since AS_{L-1} has not yet been solved and so formula (5.15) is used. Gradient CSN uses one of the formulae (5.12), (5.13) or (5.14).

(5.7) BSN like CSN uses one of the formulae (5.12), (5.13) or (5.14). CSH can like ASH use formula (5.15). However bearing in mind that central difference formulae are more accurate, formula (5.16) was used with the value of CS at L-1. Originally this value of CS was found through the normal gradient CSN by applying equation (5.6) at the point (K+1,L-1). Later however the extrapolation formula (5.17) was used.

(5.8) Gradient GH similarly to CSH above used the central difference formula (5.16) with the value of G at L-1 being found originally from equation (5.10) applied at point (K+1,L-1). Finally the extrapolated value was found using formula (5.17).

(5.9) The gradient DN is discretized by use of formula (5.12), (5.13) or (5.14), with the value of DN at (K+1,L) being replaced by $\left[(1-\nu^2)BS_{K+1,L} - \nu(1+\nu)AS_{K+1,L} - D_{K+1,L}\right]$.

(5.10) DH like CSH and GH above uses a value at point L-1. This value of D was originally extrapolated through DN in equation (5.9) which was applied at (K+1,L-1) but was finally found using formula (5.17). GH is discretized by use of formula (5.12), (5.13) or (5.14).

Having applied these equations, the values of AS, BS, CS, D and G at (K,L) are set in terms of the other known variables and gradients at the points shown on fig. 5.16.

The five equations are then solved by a matrix elimination process.

At points (K,L+1),(K,L+2),(K+1,L) and (K+2,L) all values are known whereas at the point (K,L-1) the values of CS, D, G are extrapolated from values at (K+1,L-1) and (K+2,L-1). However on progressing to point (K,L-1), solution of CS, D, G allows variables at (K,L) to be more accurately calculated; in this way a better 'knitting' effect is achieved.

5.4.6 Method 2 - Results

To compare the relative effects of the various gradient formulae (5.12), (5.13) and (5.14), the radial line L = 7 was selected since it is in the centre of the field. Values at the points (14,7) and (13,7) are compared with the exact values

Point (14,7)	AS	BS	CS	D	G
Exact	0.35580	0.12060	0.20408	0.53100	-0.06328
Formula(5.12)	0.35559	0.12064	0.20409	0.53096	-0.06328
Formula(5.13)	0.35561	0.12064	0.20408	0.53096	-0.06328
Formula(5.14)	0.35561	0.12064	0.20406	0.53096	-0.06328

Point (13,7)	AS	BS	CS	D	G
Exact	0.36641	0.12264	0.20621	0.56494	-0.74419
Formula(5.12)	0.36608	0.12274	0.20726	0.56498	-0.74456
Formula(5.13)	0.36604	0.12278	0.20693	0.56498	-0.74438
Formula(5.14)	0.36604	0.12278	0.20698	0.56498	-0.74438

Although it is not very clearly shown, the formula (5.13) gives slightly better results over either (5.12) or (5.14).

However it can be clearly seen that the errors at point (13,7) are greater than at (14,7). It is this build up of error as the procedure progresses radially in, which causes the instability. This can be seen below where the values of AS on L = 7 are given in contrast to the exact values. This trend is characteristic of all the other variables.

Values of AS on L = 7 in field

K	Radius r_o	Exact	Calculated
14	2.03	0.3558	0.3556
13	1.91	0.3664	0.3660
12	1.80	0.3791	0.3793
11	1.70	0.3941	0.3936
10	1.60	0.4122	0.4067
9	1.51	0.4340	0.4049
8	1.42	0.4602	0.3364
7	1.34	0.4920	0.1980
6	1.27	0.5305	-1.1429
5	1.20	0.5775	-5.0375
4	1.13	0.6349	-17.3899
3	1.07	0.7053	-54.8406
2	1.00	0.7917	-162.5741

Method 1 and 2 thus lack stability. Initially they start off well but there is a build up of error which is not self-correcting. Some variation of the ratio T was attempted but to no avail. It was finally decided that the instability was essentially due to there being no second order curvature term involved in the radial progression. Initially this was not contemplated because our aim was the use of first order equations.

The relative stability of the method using interlacing nets must be mentioned. Although this did appear to show stability, it was noted at the time the slight build up in error. This method certainly has some merits but overall it appears that even the errors here are not self-correcting.

It was at this point in the study that it was decided to proceed on two fronts. As has been pointed out earlier the equations of Mixed-Plasticity are either elliptical or hyperbolic or a mixture of both. Thus the two approaches attempted were along these lines

(a) hyperbolic
(b) elliptic.

The elliptic or boundary-value approach proved to be the correct one, and the development of that method is outlined in the next chapter.

The hyperbolic or initial-value approach is basically an extension of the methods already attempted, except that a curvature term is now included. As it is an extension of these previous methods it is detailed in this chapter — section 5.5 below.

5.5 Solution by Lax-Wendroff Method

5.5.1 Introduction

The Lax-Wendroff approach to initial value problems is to expand the function in the direction of solution as a Taylor series up to the curvature term and apply this at the last estimated point. For example, consider any function $X = f(x,y)$ and its expansion in the x direction between points 1 and 2 at a distance k apart (fig. 5.17).

Thus

$$X_2 = X_1 + \frac{k}{1!}\left(\frac{\partial X}{\partial x}\right)_1 + \frac{k^2}{2!}\left(\frac{\partial^2 X}{\partial x^2}\right)_1 + - - - \ .$$

The series is truncated at the curvature term. Now suppose that there exists a first order partial differential equation relating the gradients of X in the x and y directions then

$$\left(\frac{\partial X}{\partial x}\right)_1 = f\left(X_1, \left(\frac{\partial X}{\partial y}\right)_1\right)$$

$$\left(\frac{\partial^2 X}{\partial x^2}\right)_1 = f\left(X_1, \left(\frac{\partial X}{\partial y}\right)_1, \left(\frac{\partial^2 X}{\partial y^2}\right)_1\right)$$

and the expansion can be written

$$X_2 = a_1 X_1 + a_2\left(\frac{\partial X}{\partial y}\right)_1 + a_3\left(\frac{\partial^2 X}{\partial y^2}\right)_1$$

where a_1, a_2, a_3 are constant coefficients.

When the y derivatives are discretized, using values of X at points 3 and 4, distance h apart, then X_2 can be

expressed as a function of the values of X at 1, 3 and 4 and the constants h and k

$$X_2 = f(X_1, X_3, X_4, k, h).$$

In hyperbolic equations, there can be found a relationship between k and h, within which the solution is stable but out of which instability will ultimately occur. The relationship is found by evaluating the characteristics of the system of equations. In our equations, however, the characteristics are all imaginary (see paragraph 4.3.6). The meaning of this cannot be explained in practical terms. However, in hyperbolic problems it is good guideline to keep $\frac{k_c}{h}$ around or less than 1. With a characteristic fixed, line 3,2 for example, the solution must work within this to retain stability. Thus with point 3 being a boundary value the solution to points 6 and 7 will not violate this stability condition.

5.5.2 Field Sizes

The dimension of the field used is shown in fig. 5.18.

The radial ratio $T = 1.125^{\frac{1}{2}}$

$= 1.06066.$

The circumferential spacing is $H = \frac{\pi}{32}$

$= 0.9811.$

At any radius r the ratio of '$\frac{k}{h}$' differs whether moving radially or circumferentially - fig. 5.19. Radially $(\frac{k_r}{h_r}) = \frac{0.061}{0.098} = 0.62.$ Circumferentially $(\frac{k_c}{h_c}) = \frac{0.098}{0.061} = 1.61.$

5.5.3 Formulation of Taylor Series for Grid Dimensions

The proposed direction of solution is either in the negative x or negative r directions. The formulae below are for any variable X.

(a) Circumferentially:-

The series expansion from point (K,L+1) to (K,L)

at distance H apart, fig. 5.20 is

$$X_L = X_{L+1} - H\left(\frac{\partial X}{\partial \vartheta}\right)_{L+1} + \frac{H^2}{2}\left(\frac{\partial^2 X}{\partial \vartheta^2}\right)_{L+1}$$

$$= X_{L+1} - H.XH_{L+1} + \frac{H^2}{2} X2H_{L+1}. \qquad (5.18)$$

(b) Radially:-

The series expansion from point (K+1,L) to (K,L) at distance $(R_{K+1}-R_K)$ apart, fig. 5.20 is

$$X_K = X_{K+1} - (R_{K+1}-R_K)\left(\frac{\partial X}{\partial R}\right)_{K+1} + \frac{(R_{K+1}-R_K)^2}{2}\left(\frac{\partial^2 X}{\partial R^2}\right)_{K+1}.$$

But $R_{K+1} = T.R_K$, therefore $R_{K+1} - R_K = R_K(T-1)$.

Therefore $X_K = X_{K+1} - \frac{T-1}{T} XN_{K+1} + \frac{(T-1)^2}{2T^2} X2N_{K+1}.$

However remembering the benefit gained in the last method by developing the formulae on an XR^2 basis the above equation is altered as follows

$$(R^2X)_K = (R^2X)_{K+1} - \frac{T-1}{T} R_{K+1}\left(\frac{\partial}{\partial R}(R^2X)\right)_{K+1} + \frac{(T-1)^2}{2T^2} R^2_{K+1}\left(\frac{\partial^2}{\partial R^2}(R^2X)\right)_{K+1}$$

giving $X_K = X_{K+1} + (T-2)(T-1)XN_{K+1} + \frac{(T-1)^2}{2} X2N_{K+1}.$ (5.19)

5.5.4 Reformulation of Equations for Lax-Wendroff Method

For this hyperbolic approach to the solution, the five first order equations were reduced to four first order equations by the introduction of the variable F.

From chapter 4, the equations (4.28) are repeated here, considering only the elastic case where AS = A etc.

$$CN + AH + 2C = 0$$
$$BN + CH + B - A = 0$$
$$V3AN - V4BN - FH + (V3+V4)(A-B) = 0$$
$$V5CN - FN - V3BH + V4AH + V5C = 0,$$

These equations have to be reformed, to give the radial or circumferential curvature and gradient of any variable in terms of the four variables and their circumferential or radial curvatures and gradients respectively.

The radial gradients and curvatures are thus

$$\left.\begin{aligned} AN &= B - A - V2CH + \frac{FH}{V3} \\ BN &= A - B - CH \\ CN &= -AH - 2C \\ FN &= -V5C - (V5-V4)AH - V3BH \end{aligned}\right\} \qquad (5.20)$$

$$\left.\begin{aligned} A2N &= 3A - 3B - (\frac{V5}{V3} + 1 - 4V2)CH - \frac{2FH}{V3} - 2A2H - B2H \\ B2N &= -3A + 3B + (4-V3)CH + \frac{FH}{V3} + A2H \\ C2N &= 4AH - BH + V2C2H + \frac{F2H}{3} + 6C \\ F2N &= -3V5C - (V3+2V4-3V5)AH - V4BH + (1+2V2)C2H \\ &\qquad - (2+V2)F2H \end{aligned}\right\} \qquad (5.21)$$

The circumferential gradients and curvatures are thus

$$\left.\begin{aligned} AH &= -CN - 2C \\ BH &= (4+2V2-V5)C + (2+V2)CN - \frac{FN}{V3} \\ CH &= A - B - BN \\ FH &= (V3+V4)(A-B) + V3AN - V4BN \end{aligned}\right\} \qquad (5.22)$$

$$\left.\begin{aligned} A2H &= -2A + 2B - AN + 4BN + B2N \\ B2H &= -6A - 8B + 5BN - A2N - 2B2N \\ C2H &= BH - 6C - 3(V2+3)CN - (2+V2)C2N + \frac{3FN}{V3} - \frac{F2N}{V3} \\ F2H &= (V4-V3)BN - 2(V3+3V4)C - (4V3+3V4V2+9)CN \\ &\qquad - (V3+2V4+V4V2)C2N + 3V2FN - V2F2N \end{aligned}\right\} \qquad (5.23)$$

where $V2 = \frac{\nu}{1-\nu}$ $\quad V3 = 1-\nu^2$ $\quad V4 = \nu(1+\nu)$ $\quad V5 = 2(1+\nu)$

ν = Poisson's ratio.

5.5.5 First Method of Solution, Fig. 5.21

Two methods of solution were attempted. The first had a certain amount of sophistication and the experience gained from this led to the second, which is dealt with in paragraph 5.5.6.

The analytical boundary values and gradients are fed in on the K = 10,11 lines and the L = 10,11 lines. The solution now proceeds as follows:-

(a) Area I is first solved by moving in radially to line K = 6. Using the concept of characteristics area I only extends up to the line p_1p_2. The $\not\in$ is a line of symmetry or asymmetry and so the solution can move up to L = 2. On moving to a K line from a K+1 line the following steps are used:-

(i) On the K+1 line the circumferential gradients and curvatures of the variables are evaluated.

(ii) The normal gradients and curvatures of each variable are found at each point using equations (5.20) and (5.21).

(iii) The values of the variables are found at each point on the K line (up to the line p_1p_2) using the Lax-Wendroff equation (5.19).

(b) The direction of solution now changes and area II is solved by moving circumferentially from line L = 10. The characteristic lines are now p_1p_2 and p_2p_6. On moving from an L+1 line to an L line the equations (5.22) and (5.23) are used.

(c) Areas III and IV are calculated similarly to step (a), and values at point (2,9) are found by interpolation.

In this way the Lax-Wendroff process can progress across the field from its outer boundary into the inner boundary.

Results

Comparison is made between the solved values and analytical values on the line K = 2 at positions L = 2, 4, 6 and 8. It should be remembered that on the K = 2 line, B and C should be zero.

Method	Variable	L = 2	L = 4	L = 6	L = 8
Analytical (Exact)	A	1.1251	1.0680	0.9053	0.6619
	B	0.0	0.0	0.0	0.0
	C	0.0	0.0	0.0	0.0
	F	0.0	−0.2612	−0.4826	−0.6306
Lax–Wendroff	A	1.1177	1.0618	0.9101	0.6623
	B	0.0053	0.0047	−0.0045	−0.0013
	C	0.0	0.0028	0.0024	0.0023
	F	0.0	−0.2653	−0.4356	−0.6392

These values compare favourably.

5.5.6 The Second Method of Solution

Although the results above look favourable, the overall field showed greater errors in the area II near the radial L = 9,10 lines. It will be remembered that in this region the solution is progressing circumferentially and during this process the ratio $(\frac{k_c}{h_c}) = 1.61$ as calculated in the paragraph 5.5.2 on field sizes. This is an unfavourable ratio for the Lax–Wendroff method. Two ways of overcoming this are –

(i) to re-shape the grid size to give

$$(\frac{k_r}{h_r}) \doteq (\frac{k_c}{h_c}) \doteq 1$$

or (ii) to progress purely in a radial direction.

Since the field was already set up the latter way was chosen. The difficulty of progressing only radially is that the field is successively contracting due to the characteristic lines. This however was overcome in different ways for the hole and the keyhole:–

(a) Consider first the hole problem – fig. 5.22. Due to symmetry, as has already been mentioned, the values of A and B are symmetrical and C and F asymmetrical over the $\mathcal{L}_1$ boundary. However these conditions also exist over the $\mathcal{L}_2$ boundary and so the solution can proceed from the

K = 11 boundary into the K = 2 boundary, solving all point L = 2 to 18 on each K line.

(b) For the keyhole (fig. 5.23) the above symmetry does not exist. However starting on the outer K = 11 boundary and using the full symmetrical half (L = 2 to 34), the solution can still proceed into the inner K = 2 boundary. The characteristic line p_1p_2 means that area II remains unsolved. This area is small, the point p_2 having coordinates (2,25); the notch surface, line L = 34, has prescribed stress conditions.

Thus in order to match area II into area I with a view to reversing the direction of solution, smoothing formulae were developed. These formulae, although developed here for this particular application, are used in the elliptical elasto-plastic solutions, which are dealt with in Chapter 7.

The process, when used in reverse (fig. 5.24), can solve area III, starting from the smoothed K = 2 boundary values and restricting the solution to within the characteristic line p_3p_4. On reaching the K = 11 boundary the area IV can be smoothed in between area III and the L = 34 boundary.

Once again this solution gave favourable results on the K = 2 boundary as well as in the field.

5.5.7 Conclusion

If, as in the above cases, the values and gradients on the outer boundary are known then certainly the solution using Lax-Wendroff will produce good results. Possibly the non-zero values of B and C on K = 2 could be reversed and the procedure attempted in the opposite direction, on an incremental basis. The process is, however, not self correcting - errors in initial values will tend to be exaggerated. If one reversed the sign of B and C on K = 2, the values of A and F would also require a corrective increment and, in the elasto-plastic solution

contemplated, A and F cannot be assumed to be known. Consequently applying the procedure in reverse is useless.

This means that the procedure can only be applied one way. In the elastic case, this appears to give a reasonable result. The solution to the elasto-plastic problem is a different matter because the initial boundary values cannot reflect the presence of a yielded zone with different governing equations. This will thus tend to minimise the extent of plasticity.

Since the solution depends so much on the initial boundary values and gradients, an attempt was made to alter the values of A and AN on the outer boundary for the elasto-plastic solution. The alteration of A and AN was attempted using a perturbation technique which was intended to minimise the values of σ_r and $\tau_{r\theta}$ on the inner surface. The complexities of this technique mounted without showing much beneficial result and, with the elliptical approach at this time showing hopeful results, it was decided to suspend any further attempt at a hyperbolic elasto-plastic solution.

The enormous effort that went into the work detailed in this chapter did produce some useful results. The idea of applying a X^2R basis for gradients developed in paragraph 5.4.4 are applied directly into the elliptical approach. Similarly the smoothing formulae, both radial and circumferential, which were developed and found necessary to give the hyperbolic method any chance, are also of use in the elliptical approaches, especially the elliptical elasto-plastic problem.

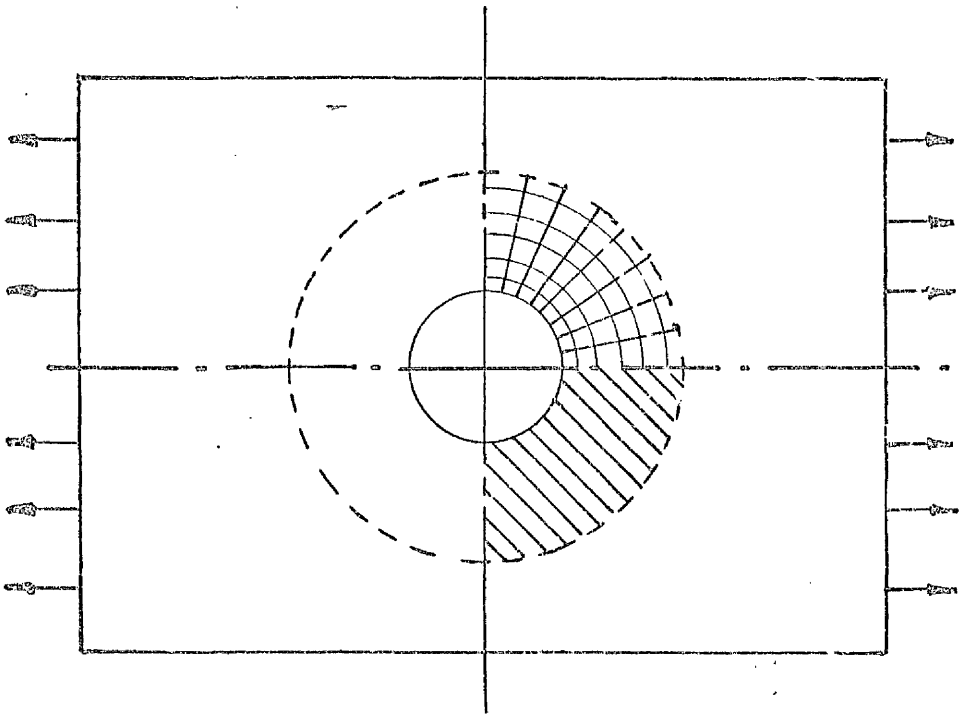

Fig 5.1

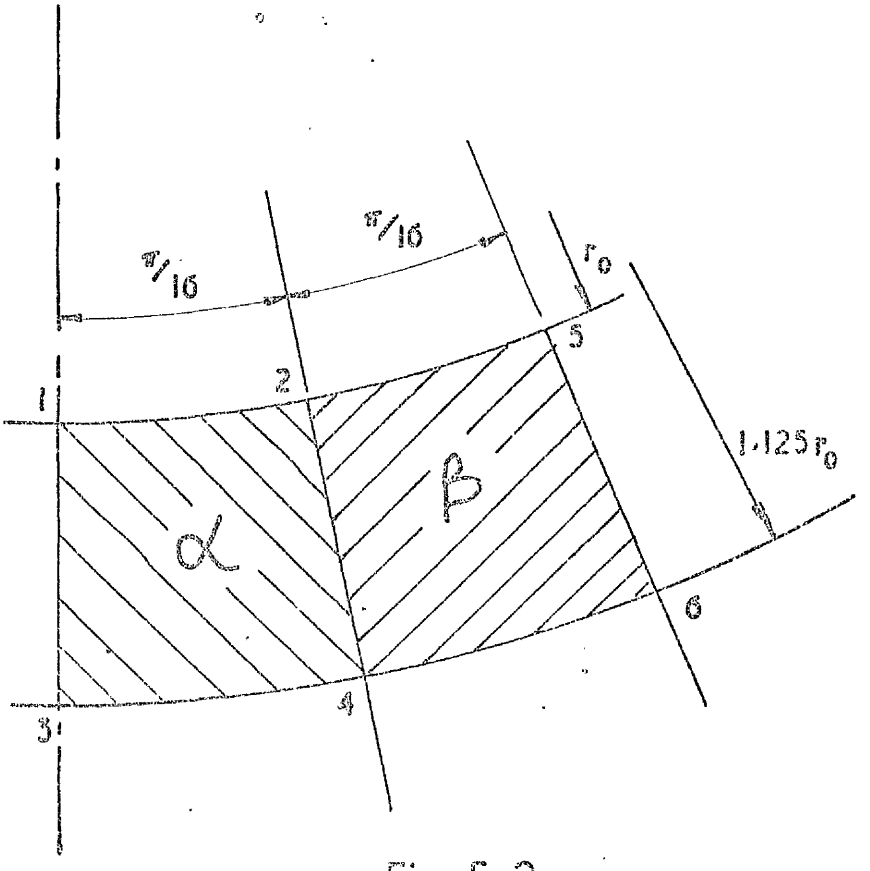

Fig 5.2

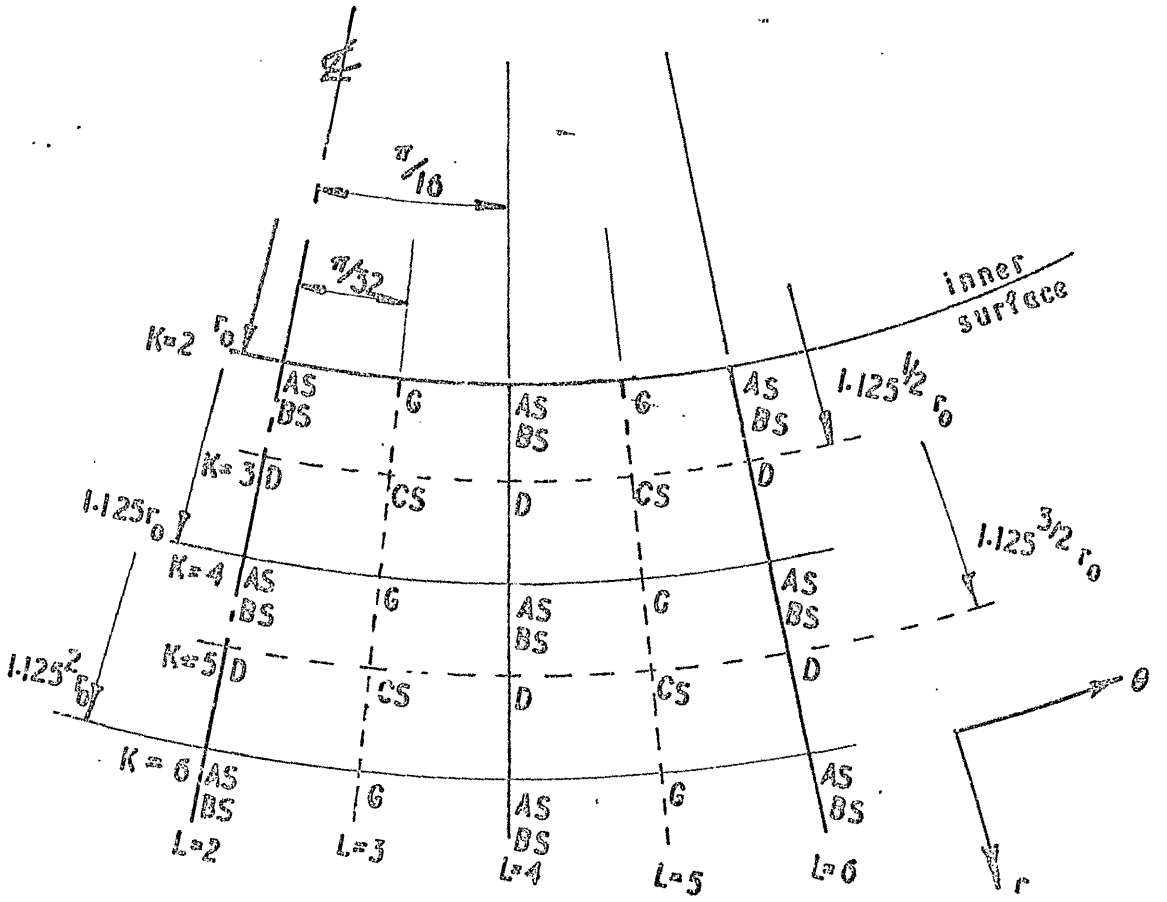

Fig 5.3

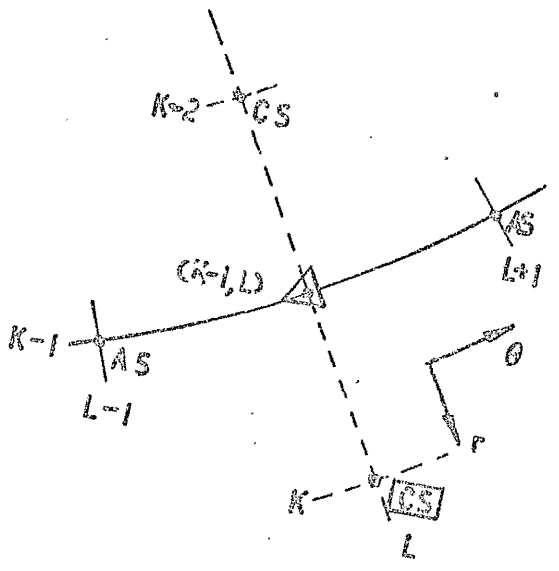

Fig 5.4

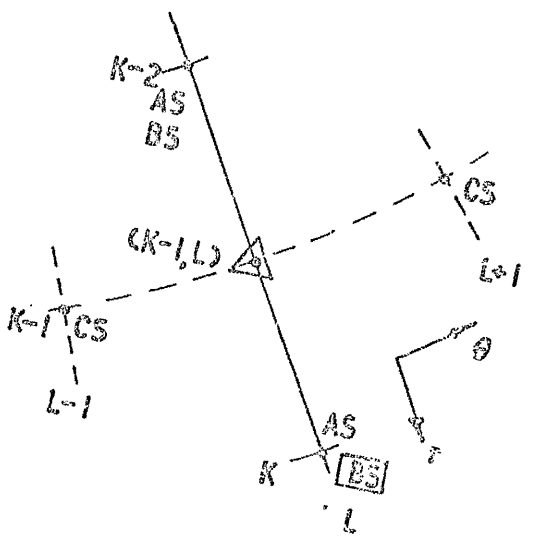

Fig 5.5

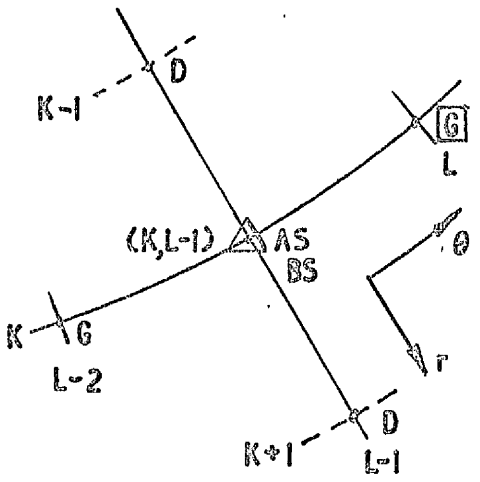

Fig 5.6

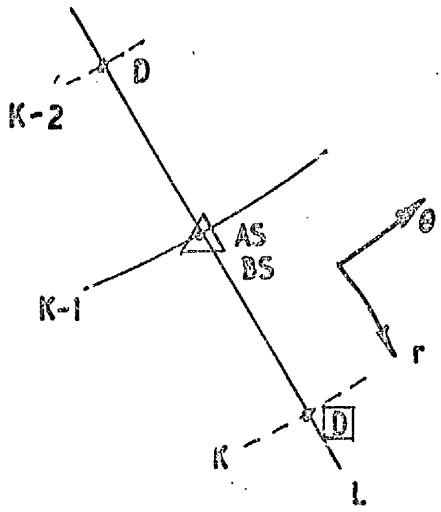

Fig 5.7

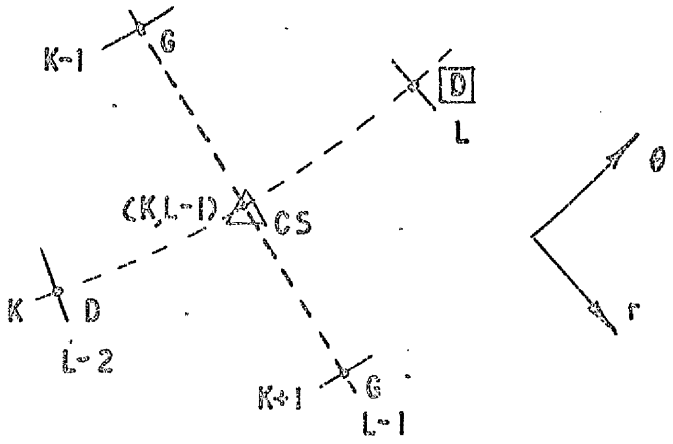

Fig 5.8

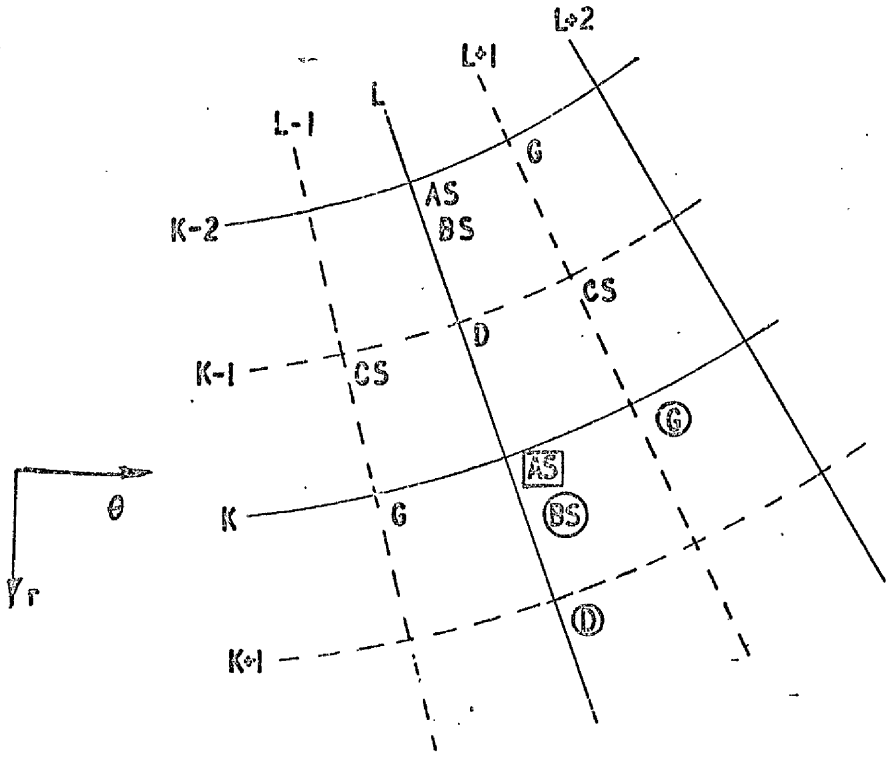

Fig 5.9

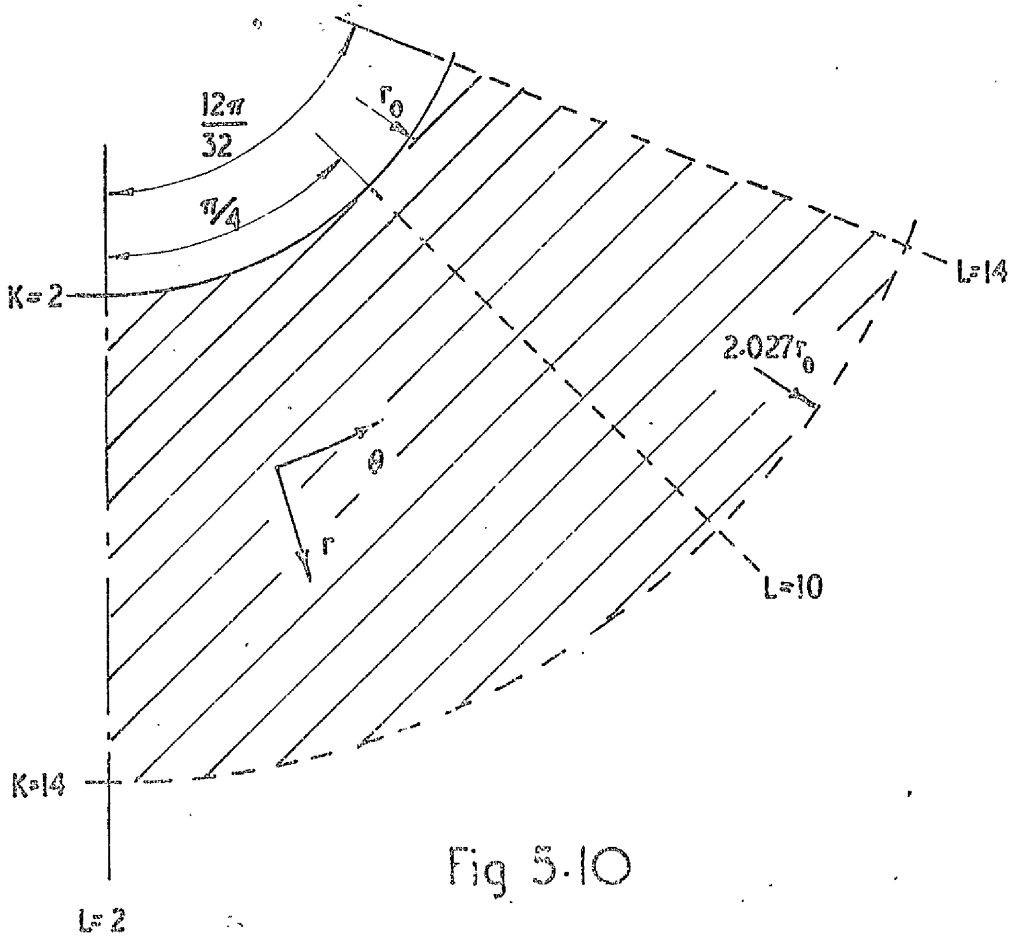

Fig 5.10

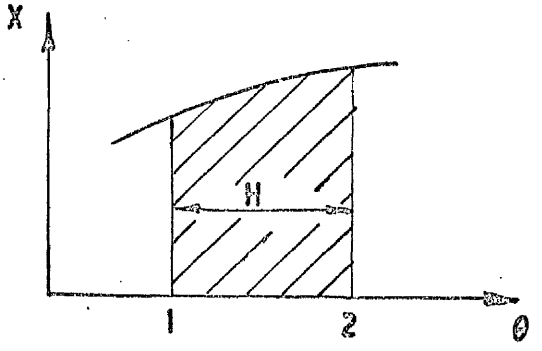

Fig 5.11

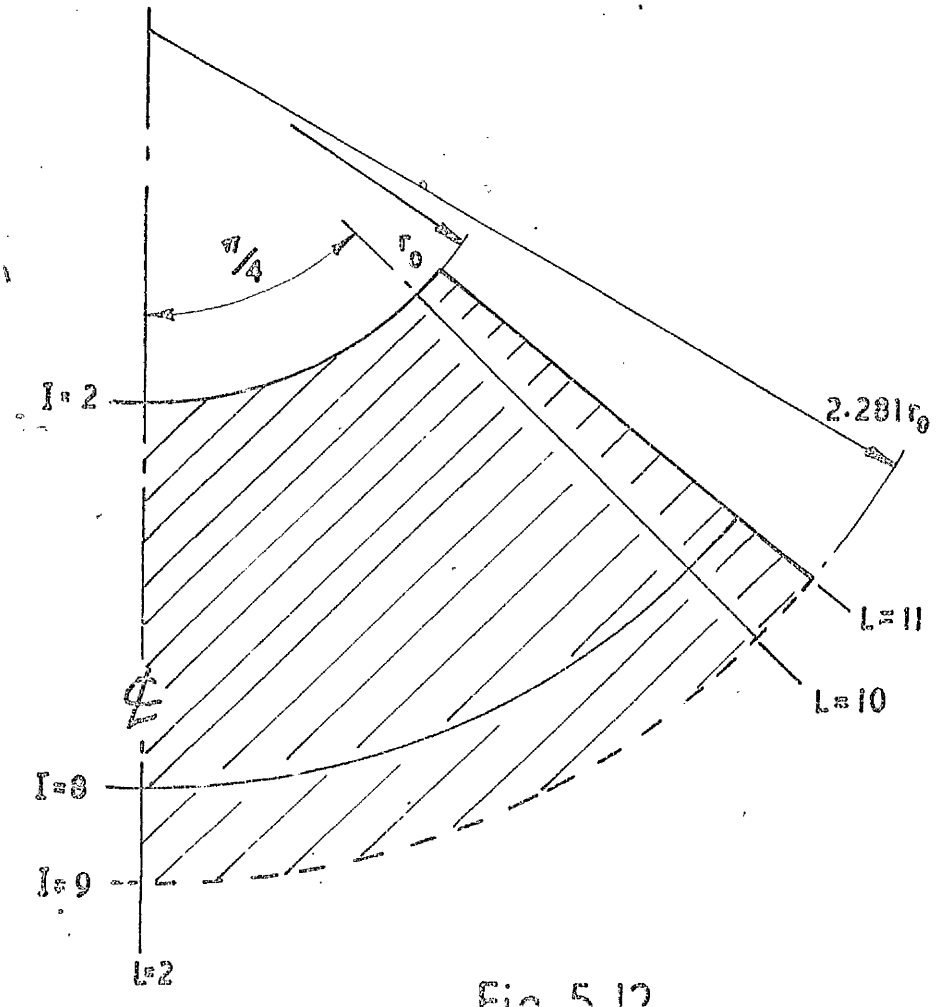

Fig 5.12

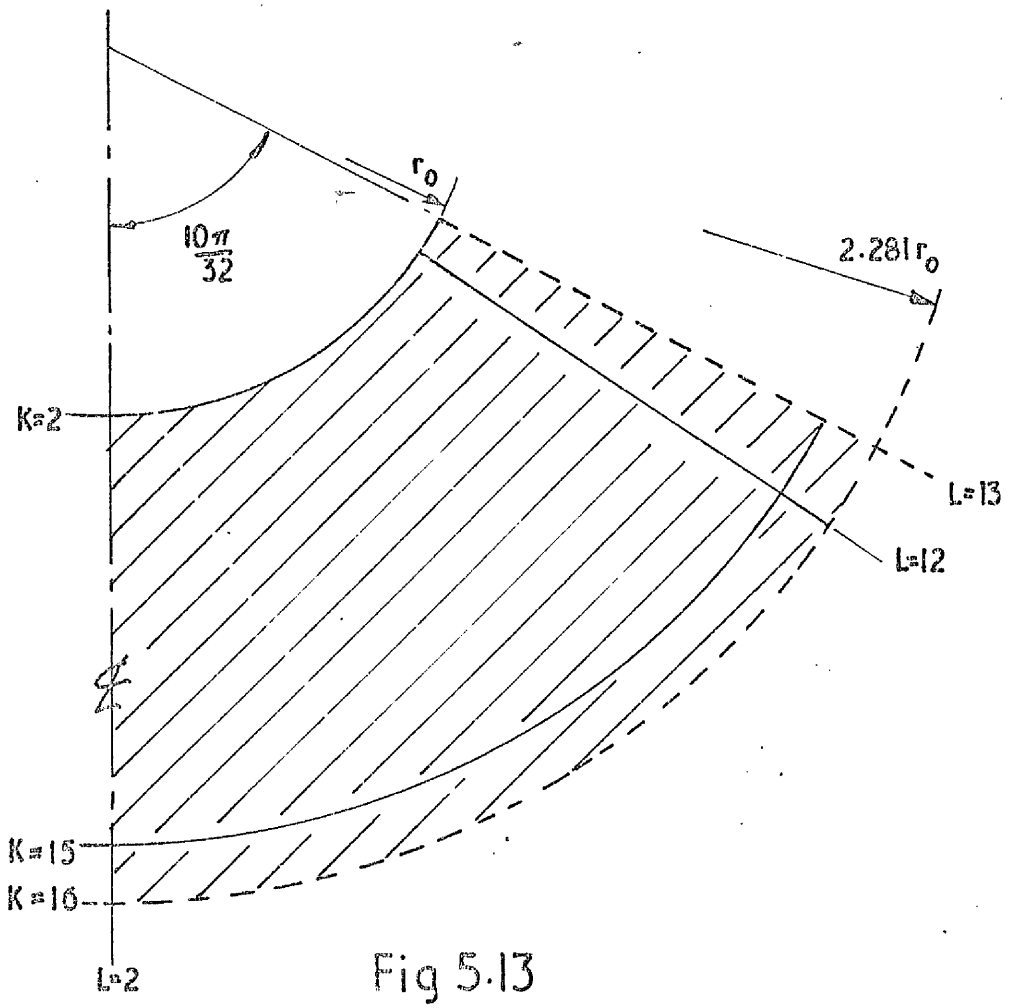

Fig 5.13

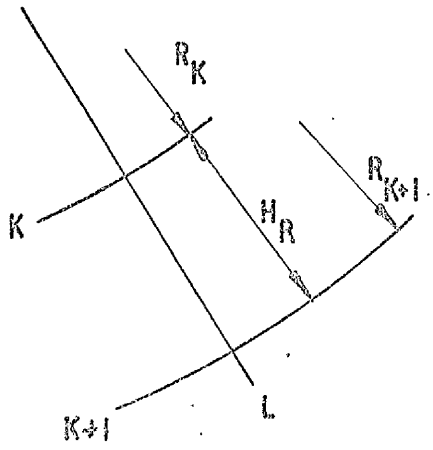

Fig 5.14

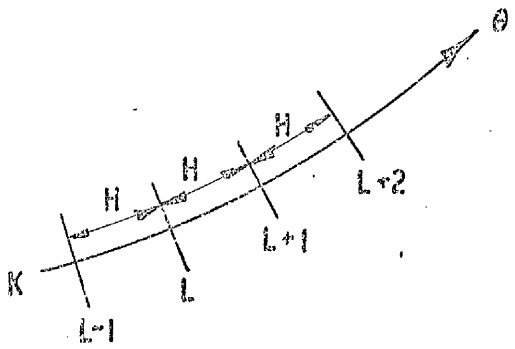

Fig 5.15

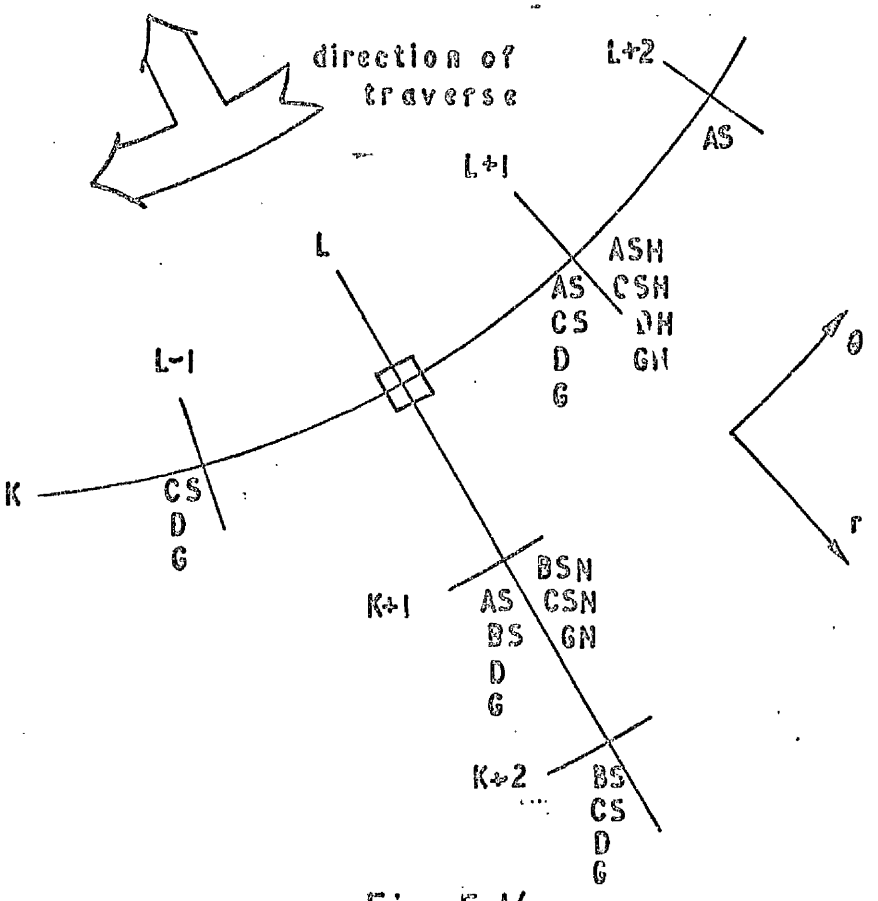

Fig 5.16

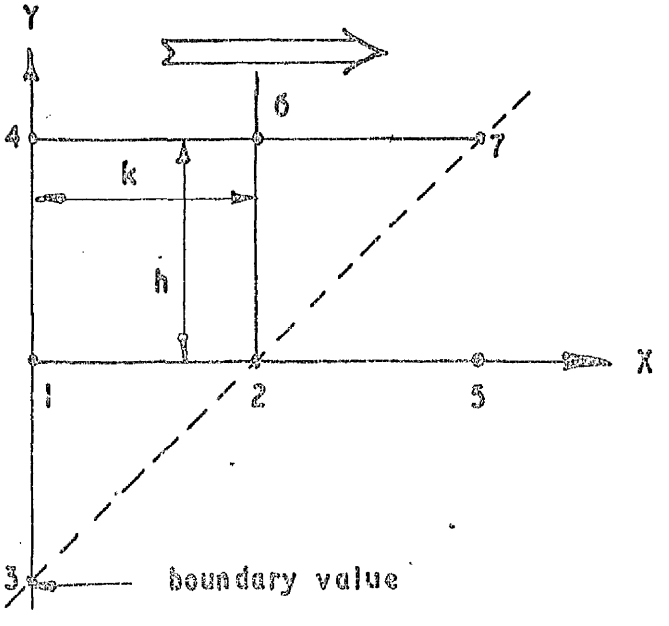

Fig 5.17

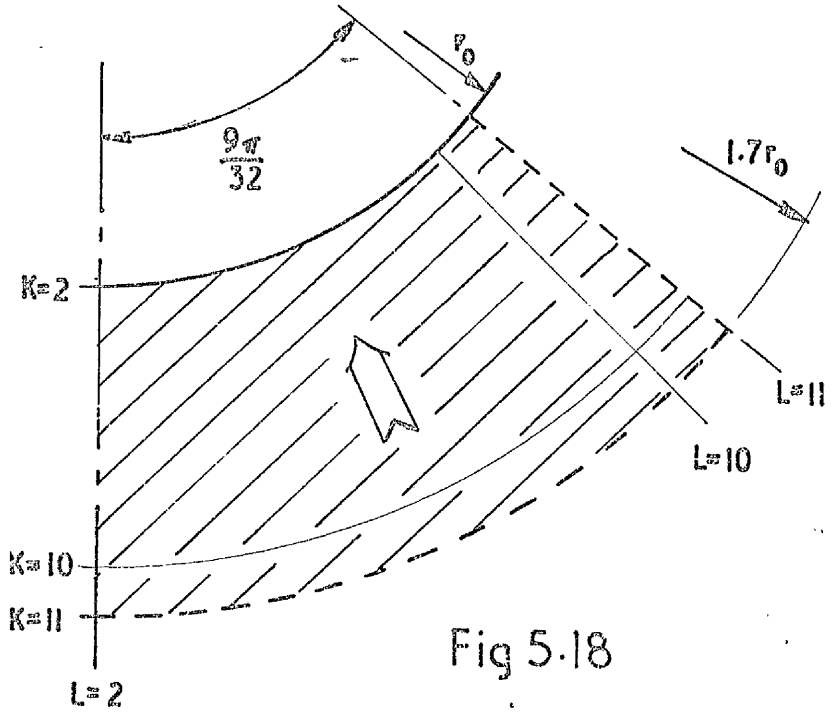

Fig 5.18

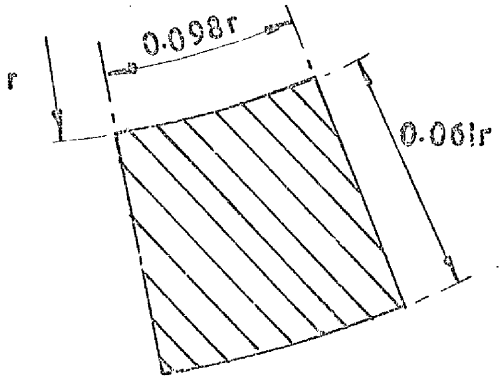

Fig 5.19

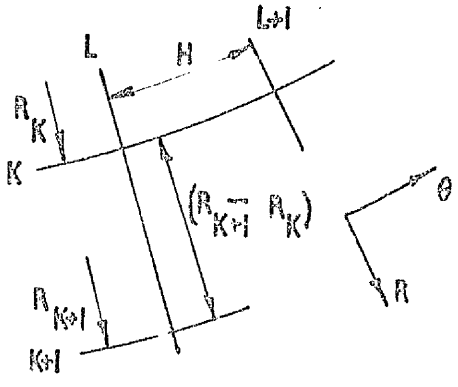

Fig 5.20

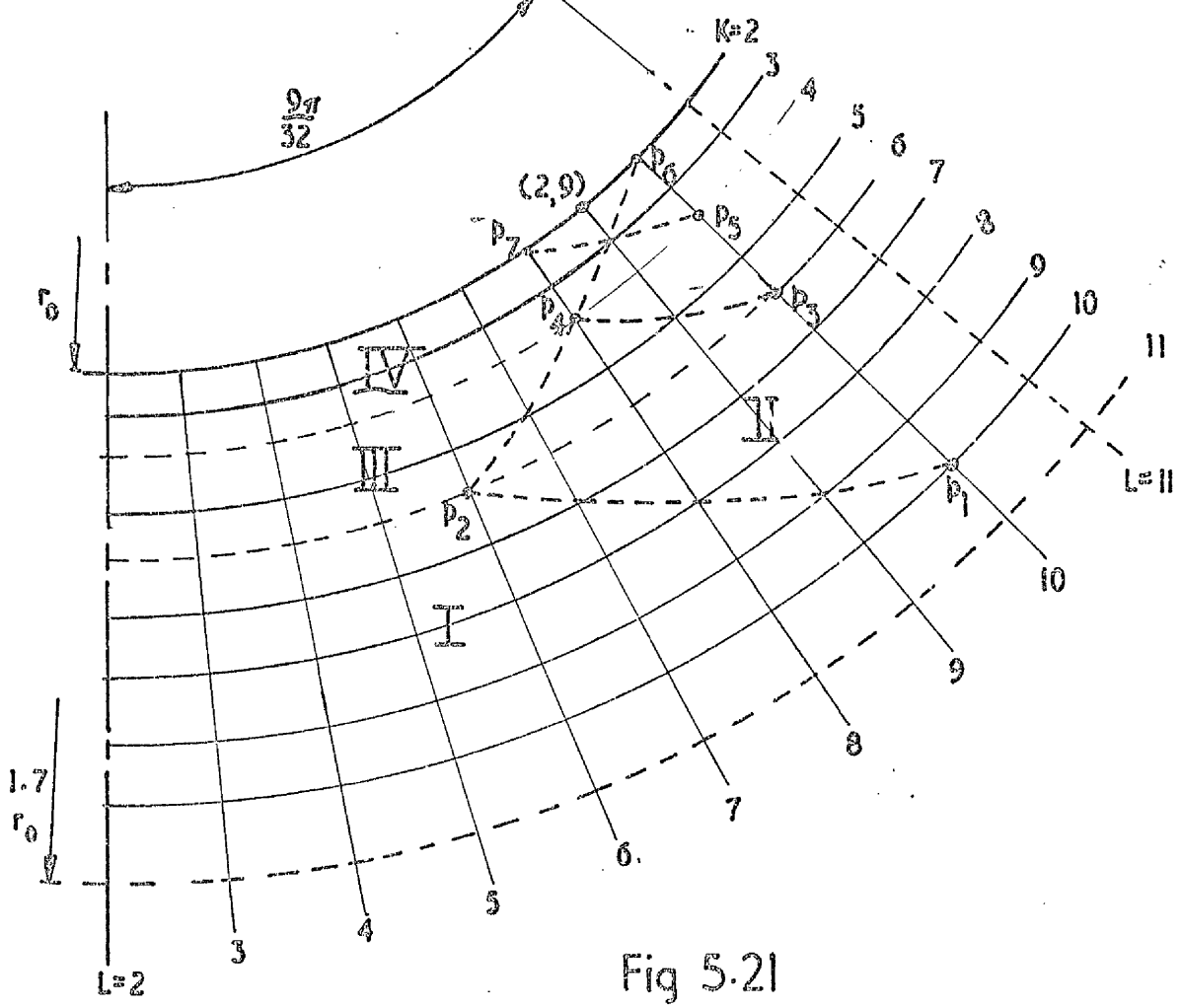

Fig 5.21

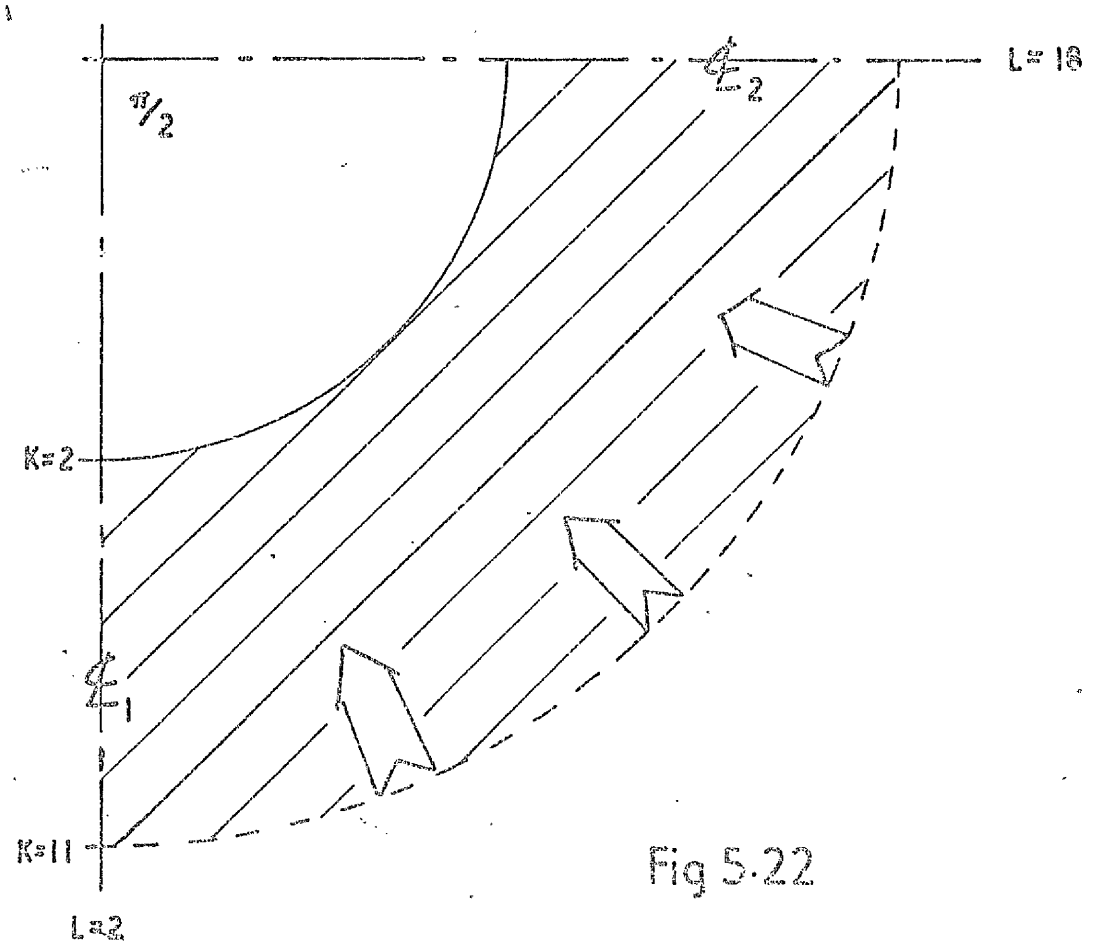

Fig 5.22

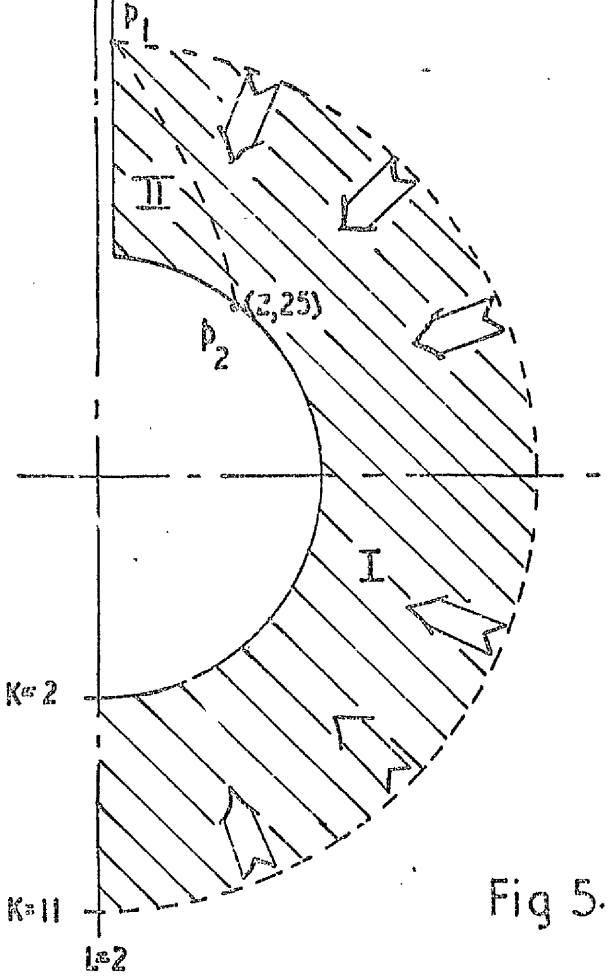

Fig 5.23

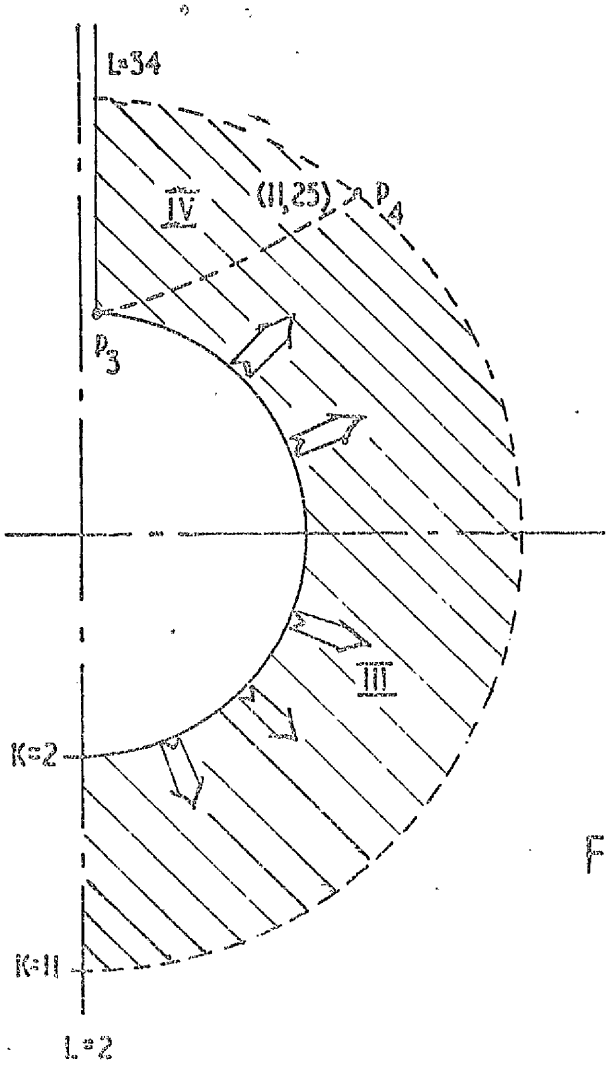

Fig 5.24

CHAPTER 6

ELLIPTICAL APPROACH TO THE ELASTIC PROBLEM

CHAPTER 6

ELLIPTICAL APPROACH TO THE ELASTIC PROBLEM

6.1 Introduction

In contrast to the last chapter, which essentially dealt with attempts at initial-value solutions, this chapter deals with the elliptical or boundary-value approach. With initial-value problems, all the necessary information is amassed on one boundary from which the solution progresses. On the other hand, boundary-value problems have the necessary boundary information divided among its enclosing boundaries.

In elliptical problems there are two main subproblems which must be recognised:-

(a) types of boundary conditions — 6.1.1
(b) field equations — 6.1.2.

Before dealing with these, consider the usual method of classifying second order partial differential equations, e.g. Mitchell[22].

Suppose that $\mathbb{R}$ is a bounded region in the (x_1,x_2) plane with the boundary ∂R. The equation

$$a(x_1,x_2)\frac{\partial^2 u}{\partial x_1^2} + 2b(x_1,x_2)\frac{\partial^2 u}{\partial x_1 \partial x_2} + c(x_1,x_2)\frac{\partial^2 u}{\partial x_2^2} = d\left(x_1,x_2,\frac{\partial u}{\partial x_1},\frac{\partial u}{\partial x_2}\right) \qquad (6.1)$$

is said to be elliptic in $\mathbb{R}$ if $b^2 - ac < 0$ for all points (x_1,x_2) in $\mathbb{R}$. It is worth noting the importance of the signs of the coefficients a and c because if $ac < 0$ then $b^2 - ac > 0$ and the equation is then classified as hyperbolic; if $b^2 = ac$ it is said to be parabolic.

6.1.1 Types of Boundary Conditions

Two distinct problems involving equation (6.1)

arise depending on the boundary conditions prescribed on ∂R

(i) the first boundary value-problem or Dirichlet problem, requires only a solution of equation (6.1) which takes on prescribed values

$$u = f(x_1, x_2)$$

on the boundary ∂R.

(ii) the second boundary-value problem, or Neumann problem requires

$$\frac{\partial u}{\partial n} = g(x_1, x_2)$$

on ∂R . Here $\frac{\partial}{\partial n}$ refers to differentiation along the normal to ∂R directed away from the interior of R .

As an example of the use of these conditions, if one looks back to the solution of the biharmonic equation (which is elliptic), it can be seen that two boundary conditions were required on each boundary since it was a fourth order equation. The $\nabla^4\psi$ equation required the function ψ and its normal gradient to be specified on each boundary — Dirichlet and Neumann Problems.

6.1.2 Field Equations

Using again, as an example, the biharmonic solution it was seen how the $\nabla^4\psi = 0$ equation was discretized in such a way that the value at a nodal point 0 could be expressed in terms of the values at its twelve neighbouring points — see fig. (6.1)

$$\psi_o = \frac{1}{20}\left[8(\psi_1+\psi_2+\psi_3+\psi_4) - 2(\psi_5+\psi_6+\psi_7+\psi_8) - (\psi_9+\psi_{10}+\psi_{11}+\psi_{12})\right] \quad (6.2)$$

If one looks at the harmonic equation $\nabla^2\psi = 0$ (Laplace's Equation), in cartesian coordinates —

$$\nabla^2\psi = \frac{\partial^2\psi}{\partial x^2} + \frac{\partial^2\psi}{\partial y^2} = 0$$

this can be discretized to give the value at a nodal point 0 in terms of the values at its four neighbouring points (fig. 6.1) viz.

$$\psi_o = \frac{1}{4}(\psi_1 + \psi_2 + \psi_3 + \psi_4). \qquad (6.3)$$

In both of these examples the effect of equations (6.2) and (6.3) is to 'balance' the values at 0 from its neighbouring points. This however cannot be effectively done with a first order equation. For example, the equation

$$\frac{\partial \psi}{\partial x} + \frac{\partial \psi}{\partial y} = 0$$

would be simply discretized, to give (see fig. 6.1)

$$\psi_3 + \psi_2 - \psi_1 - \psi_4 = 0$$

with no ψ_o term present.

It was this absence of ψ_o that prompted the use of second order field equations based on the differentiation of the first order equations. It should be pointed out here that the first order equations do give values of function gradients over the field and these in fact can be integrated, but this is not the elliptical field equation approach.

The question now arises as to how to simultaneously solve several variables. In the examples just quoted there was only one variable ψ and so it could be continously and methodically recalculated throughout the field until convergence was achieved. If there are several field variables then there must be an interaction among them since each equation is a function of two or more. If convergence is achieved with one variable, while the others are held constant, then as soon as any of these other variables are recalculated this disrupts the solution of the first. The answer to this difficulty is to scan the field a few times recalculating one variable while holding the others constant and then scan the field a few times again, recalculating another variable with the better values of the first, and the most recently calculated values of the rest being held constant. And so on through all the variables and back to the first. It was felt that between 5 and 10 scans of the field for each variable should allow time for any disturbances in the field to transmit their effects to all points.

In view of the rapid increase in the number of interactions with increasing number of variables, it was decided to reduce the number from five to four by introducing the variable F (defined in paragraph 4.3.5).

Since this was a new method of solution, once again the elastic solution was exhaustively investigated using the analytical solution of the hole under tension as a check on accuracy. Consequently all the variables can be simplified by inserting into the equilibrium equations

$$AS = A, \quad BS = B \text{ and } CS = C$$

(defined in 4.3.3). The four variables are now A, B, C and F.

6.2 Boundary Conditions

Since only the solution in the vicinity of the high stress point is sought, the small hatched area in fig. 6.2 is that of interest.

For absolute freedom of the boundaries, the minimum boundary conditions are as follows -- fig. 6.3

(i) K = 2 boundary. Since there is no normal or shear surface loading

$$\sigma_r = \tau_{r\vartheta} = 0.$$

(ii) K = KE. For equilibrium with the surrounding field to be maintained, on this boundary the values of σ_r and $\tau_{r\vartheta}$ must be fixed.

(iii) L = LE. For equilibrium with the surrounding field to be maintained, on this boundary the values of σ_ϑ and $\tau_{r\vartheta}$ must be fixed.

(iv) L = 2. From arguments of symmetry, $\tau_{r\vartheta} = F = 0$. Also conditions of symmetry for σ_r and σ_ϑ and asymmetry for $\tau_{r\vartheta}$ and F exist over this boundary.

The above boundary conditions also exist for the keyhole notch geometry. However, for the hole in tension, if the

LE boundary coincides with the centreline $\mathcal{L}_2$, the conditions of symmetry and asymmetry will exist over this boundary as in (iv).

These boundary conditions expressed above are the minimum conditions. It is conceivable that in addition to the above, two more conditions could be added as follows

(v) K = KE — σ_θ fixed.

(vi) L = LE — σ_r fixed.

The effect of these two additions is to apply restraints to the system, resulting in a concentration of effects in the field due to there being no possibility of boundary relaxation. The only argument in favour of the addition of these two constraints is, that, if the effect of any disturbance such as plasticity in the field dies away quickly, the change on the boundary values will be minimal.

The reason why the above is contemplated is that unless these stresses (v) and (vi) are known the boundary value problem goes from the simpler Dirichlet type to the much more complex Neumann type. Before applying the (v) and (vi) constraints however an attempt was made to solve the field using four variables and the minimum boundary conditions (i) to (iv) -- <u>called hereafter free boundaries in contrast to fixed boundaries with conditions (i) to (vi).</u>

6.3 Elliptical Solution with Four Variables and Free Boundaries

6.3.1 Field Equations

The equations for four variables are repeated here foiEquilibriumce (see Chapter 4)

Equilibrium

$$AH + CK + 2C = 0 \qquad (6.4)$$

$$EN + CH + B - A = 0 \qquad (6.5)$$

Strain/Displacement

$$V5CN - FN - V3EH + V4AH = -V5C \qquad (6.6)$$

$$V3AN - V4BN - FH = (V3+V4)(B-A) \qquad (6.7)$$

These above equations are differentiated and added in such a fashion as to give a cross-curvature relationship for each variable — a similar form to the harmonic ∇^2. Looking at each variable in turn —

(a) For A, differentiating (6.4) w.r.t. ϑ and (6.7) w.r.t. R, then adding, gives

$$A2H + V3A2N + (2V3 + V4)AN = V4B2N + (V3 + 2V4)BN + FNH - CNH - 2CH. \quad (6.8)$$

Notice that the two equations are added giving coefficients a, b, c of equation (6.1) as $a = 1$. $b = 0$, $c = V3$
therefore $b^2 - ac = -V3 < 0$ — elliptical.
If the two equations are subtracted the coefficients would be $a = 1$, $b = 0$, $c = -V3$
and $b^2 - ac = +V3 > 0$ — hyperbolic.

The subtilities of this were not investigated and the additive form of equation (6.8) was taken.

(b) For B, differentiating (6.5) w.r.t. R and (6.6) w.r.t. ϑ, then adding, gives

$$V3B2H + B2N + 2BN = AN + V5CH - FNH + V4A2H + (V5 - 1)CNH. \quad (6.9)$$

(c) For C, differentiating (6.4) w.r.t. R and (6.5) w.r.t. ϑ, then adding, gives

$$C2H + C2N + 3CN = -ANH + AH - BH - BNH. \quad (6.10)$$

(d) For F, differentiating (6.6) w.r.t. R and (6.7) w.r.t. ϑ, then adding, gives

$$F2H + F2N + FN = (V3 + V4)(ANH + AH - BNH - BH) + (V5 + 1)CN + V5C2N. \quad (6.11)$$

Equations (6.8) to (6.11) thus form the four field equations for the four variables. These have to be discretized to express the values of nodal points in terms of the values at the four neighbouring points and the constant right hand sides.

For example, any variable X at 0 (fig. 6.1) can be written

$$X_o = f(X_1, X_2, X_3, X_4, RHSX_o)$$

where X_i is the values of X at the neighbouring point i and $RHSX_o$ is the value, at point 0, of the constant right hand side, which is a function of all the other variables, their gradients and their curvatures.

In this form the equation is similar to the stress function biharmonic difference equation and consequently the same method of solution is used viz. Successive Over-Relaxation. This entails the use of an accelerator q. The above equation thus becomes

$$X_o = q.f(X_1, X_2, X_3, X_4, RHSX_o) - (q - 1)X_o.$$

The optimum value of q in the biharmonic field was approximately 1.7 and this value is also used for each of the variable field equations although some variation was made to check its effect on the solution.

6.3.2 New Gradient and Curvature Formulae

The gradient and curvature formulae developed in the last chapter have a 'spread' of three points and also include a gradient of a neighbouring point. For the elliptical approach the field equations require simpler compact formulae. These are now shown below. In addition to the central difference formulae, backward and forward difference formulae are given as these are required at boundaries. The radial gradients and curvature are expressed on a R^2X basis as previously. All the formulae are expressed in terms of any variable X.

(a) Radial Gradients:— see fig. 6.4.

Central Difference —

$$XW_K = RC1\ X_{K+1} - RC2\ X_{K-1} - X_K \qquad (6.12)$$

where $RC1 = \frac{T^2}{(T^2-1)}$ and $RC2 = \frac{1}{(T^2-1)}$.

Forward Difference —

$$XN_K = RF1\ X_{K+1} - RF2\ X_{K+2} - RF3\ X_K \qquad (6.13)$$

where $RF1 = \frac{T(T+1)}{(T-1)}$, $RF2 = \frac{T^3}{(T^2-1)}$, $RF3 = \frac{T(2T+1)}{(T^2-1)}$.

Backward Difference —

$$XN_K = RB1\ X_K + RB2\ X_{K-2} - RB3\ X_{K-1} \qquad (6.14)$$

where $RB1 = \frac{(T+2)}{(T^2-1)}$, $RB2 = \frac{1}{T(T^2-1)}$, $RB3 = \frac{(T+1)}{T(T-1)}$.

(b) Radial Curvature:—

Central Difference —

$$X2N_K = RCC1\ X_{K+1} + RCC2\ X_K + RCC3\ X_{K-1} \qquad (6.15)$$

where $RCC1 = \frac{2T^2(2-T)}{(T^2-1)(T-1)}$

$$RCC2 = \frac{2(T^2-3T+1)}{(T-1)^2}$$

$$RCC3 = \frac{2(2T-1)}{(T^2-1)(T-1)}.$$

The backward and forward difference forms were not explicitly developed since there was little use for them. However, if required, they could be found by using equations (6.13) or (6.14) twice, e.g.

$$X2N = R^2 \frac{\partial^2 X}{\partial R^2}$$

$$R \frac{\partial}{\partial R}\left(R \frac{\partial X}{\partial R}\right) = R \frac{\partial X}{\partial R} + R^2 \frac{\partial^2 X}{\partial R^2}$$

$$= XN + X2N$$

therefore $$X2N = R \frac{\partial}{\partial R}\left(R \frac{\partial X}{\partial R}\right) - XN.$$

Therefore using equation (6.14) with XN gradients will give

$$X2N_K = RB1XN_K + RB2XN_{K-2} - RB3XN_{K-1} - XN_K$$

(c) Circumferential Gradients — see fig. 6.5

Central Difference —

$$XH_L = \frac{1}{2H}(X_{L+1} - X_{L-1}). \qquad (6.16)$$

Forward Difference —

$$XH_L = \frac{1}{2H}(4X_{L+1} - X_{L+2} - 3X_L). \qquad (6.17)$$

Backward Difference —

$$XH_L = \frac{1}{2H}(-4X_{L-1} + X_{L-2} + 3X_L). \qquad (6.18)$$

(d) Circumferential Curvature:—

Central Difference —

$$X2H_L = \frac{1}{H^2}(X_{L+1} + X_{L-1} - 2X_L). \qquad (6.19)$$

The comments expressed for the radial case regarding backward and forward curvature formulae similarly apply here.

The formulae (6.12) to (6.19) are the ones chosen to be used hereafter in both elastic and elasto-plastic solutions.

6.3.3 Boundary Conditions for Each of the Variables

Having four field equations, means that there are four sets of boundary conditions. Using the boundary conditions mentioned in section 6.2, (i) to (iv), consider each variable separately; reference should be made to fig. 6.3.

(a) For A (or σ_ϑ).

On the L = LE boundary σ_ϑ is held and so this is a Dirichlet Boundary condition. Due to symmetry over the $\not\in$ L = 2 boundary AH = 0 and $A_{L=1} = A_{L=3}$. On both K boundaries, however, no fixed σ_ϑ value exists and so the boundary control comes from AH, evaluated from equation (6.7). These are Neumann Boundary conditions.

(b) For B (or σ_r).

On both K = 2 and K = KE, the value of σ_r

is fixed; indeed on $K = 2$, $\sigma_r = 0$.

Like σ_ϑ, σ_r is symmetrical over the centreline. On $L = LE$, however, a Neumann boundary condition exists for B, control can be exercised only by BH, evaluated from equation (6.6).

(c) For C (or $\tau_{r\vartheta}$).

The shear stress $\tau_{r\vartheta}$ has by far the best boundary conditions and is consequently the most numerically stable variable. On the $K = 2$, $K = KE$ and $L = LE$ boundary Dirichlet conditions exist and on the $K = 2$ boundary $\tau_{r\vartheta}=0$. Due to asymmetry, $\tau_{r\vartheta} = 0$ on the $\not\in$ $L = 2$ boundary and $C_{L=1} = -C_{L=3}$.

(d) For F (or $\frac{\partial v}{\partial R}$).

In contrast to C above, F has the weakest of boundaries. A Dirichlet condition exists on the $\not\in$ $L = 2$ boundary where $F = 0$, but the other three are normal gradient controlled Neumann conditions. On the $K = 2$ and $K = KE$ boundaries, FN is found from (6.6) and on the $L = LE$ boundary FH is found from (6.7).

As far as the attempts at a free boundary four variable solution, the values of K and L at their outer boundaries were

$$KE = 9 \qquad LE = 12.$$

6.3.4 Neumann Boundary Problem

Now several ways exist of solving the Neumann Boundary Problem. Several methods were tried and these are listed below using as an example any variable X at a K boundary defined by XN — fig. 6.6. (Similar formulae can be found for any variable X at an L boundary defined by XH).

(1) Using central difference formula at point (K-1,L), from equation (6.12)

$$X_K = \frac{1}{RC1}(RC2\ X_{K-2} + X_{K-1} - XN_{K-1}).$$

(2) Using backwards difference formula at point (K,L), from equation (6.14)

$$X_K = \frac{1}{RB1}(RB3\ X_{K-1} - RB2\ X_{K-2} + XN_K).$$

Methods (1) and (2) imply the use of the field equation for X up to the line K-1 and then the use of one of the above evaluations for X_K. However, the concept of an external point can be utilised in order that the field equation be used up to the line K. The external point is then calculated from (3) below.

(3) Using an external point with the central difference formula applied at point (K,L) gives

$$X_{K+1} = \frac{1}{RC1}(RC2\ X_{K-1} + X_K - XN_K).$$

6.3.5 Attempts at the Solution with Four Variables and Free Boundaries

Consider first the general framework of the method of solution.

(a) Boundary values are fed in on all four boundaries.

(b) The field equations (6.8) to (6.11) are used, the field being scanned 10 times for each variable to allow a certain amount of settling.

(c) Corrections are made on the LE boundary for B and F using BH and FH.

(d) Corrections are made on the K = 2 and KE boundaries for A and F using AN and FN.

(e) At the points (2,LE) and (KE,LE) the value of F is found as the mean of the values obtained by extrapolating F along K = 2 and L = LE and K = KE and L = LE respectively.

(f) Return to step (b) until convergence is achieved.

The very first run of the program was to search for errors in the field equations. For this all the boundaries for all the variables had a Dirichlet condition. Convergence was achieved within 10 main iterations of the field. Accuracy was good as can be seen by comparing the analytical values with the calculated values of ABC and F at the sample point (6,7) — central in the field.

Note ⁂

Value / Method	A(6,7)	B(6,7)	C(6,7)	F(6,7)
Analytical	0.53053	0.10461	0.16828	-0.13553
Numerical	0.53068	0.10449	0.16798	-0.13629

The boundaries were now freed. The boundary corrections in steps (c) and (d) above could be carried out in three ways viz. Method (1), (2) or (3).

Each of these ways was tried in programs in which 1000 main iterations were carried out and the following are the results:-

Method (1): After 1000 iterations the field was not settled, e.g.

	A(2,2)	A(6,7)	B(6,7)	C(6,7)	F(6,7)
Analytical / Number of Iterations	1.12510	0.53053	0.10461	0.16828	-0.13553
900	1.29593	0.49446	0.11258	0.20558	-0.49065
999	-	0.47991	0.11618	0.22043	-0.62471
1000	1.37970	0.47983	0.11621	0.22059	-0.62627

The values of F were well out.

Method (2): After 1000 iterations, once again the field was not settled, e.g.

	A(2,2)	A(6,7)	B(6,7)	C(6,7)	F(6,7)
Analytical / Number of Iterations	1.12510	0.53053	0.10461	0.16828	-0.13553
900	0.99737	0.52819	0.10071	0.15722	-0.00405
999	-	0.52841	0.10033	0.15666	+0.06351
1000	0.99227	0.52841	0.10031	0.15664	+0.06456

The most disturbing feature is the error in F.

⁂ Note all the numerical results given in this chapter are based on the elastic plane strain solution of the hole in tension on the point of yielding, i.e. $\bar{\sigma}_{2,2} = \sigma_Y$.

Method (3): This method resulted in violent oscillation leading to divergence.

It was decided at this stage to look more closely at A and F, both of which have weak boundary controls. Another method of evaluating a boundary point was used viz. by a Taylor's expansion from its neighbouring point in the field. When looking at each of these variables, the exact values of all the other three variables were fixed. Consider A first. The field was scanned 500 times for A alone and still convergence was not achieved, e.g.

	A(2,2)	A(6,7)
Analytical / Number of Iterations	1.12510	0.53053
400	1.08129	0.51283
500	1.08137	0.51287

With F, not only was convergence not achieved but the field values were moving away from their correct values. With these trends in A and F it was decided to look at the effects of fixing various boundaries. For F, the effect on the point (6,7) is shown for various fixed boundary conditions – (for reference see fig. 6.3).

Boundary Conditions	F(6,7)	Number of Iterations to Settle
Analytical	-0.13553	–
L = LE fixed	-0.12714	170
K = 2, KE fixed	-0.13757	30
All fixed	-0.13624	30

From the above, the effect of boundaries on the stability of numerical procedures is obvious.

With the knowledge that F has the weakest boundaries and that F can be eliminated, two approaches presented themselves:–

(a) Since F cannot be restrained physically on any of its free boundaries, the extra boundary conditions for σ_r and σ_θ – (v) and (vi) of section 6.2 – could be introduced.

OR (b) F could be eliminated and the solution be attempted in terms of the three varibles A, B and C.

The first approach is dealt with in section 6.4 below and the second approach in section 6.5.

6.4 Elliptical Solution with Four Variables and Fixed Boundaries

6.4.1 Introduction

Essentially this section is very similar to section 6.3. The field equations are identical as are the gradient and curvature formulae. The main difference lies in the simplification of the σ_r and σ_ϑ boundary conditions on the lines LE and KE respectively. Instead of the difficult Neumann condition we now have the simpler Dirichlet condition. The method of successive over-relaxation is used again for tackling field equations.

However the above does not alleviate the difficulty of dealing with F which still has its zero value on the L = 2 and three Neumann Boundary conditions. Also A still has it Neumann Boundary control on the K = 2 boundary. It was felt that a different approach sould be taken to F and this led to the circumferential interation method which is shown in paragraph 6.4.2.

6.4.2 Circumferential Integration

Consider the variable X along a K line – fig. 6.5. If, at all points along that line, the value of XH, $(\frac{\partial X}{\partial \vartheta})$, is known then by integration one can find X

$$X = \int (\frac{\partial X}{\partial \vartheta}) d\vartheta.$$

This numerical integration of the gradients XH between points (L+1) and (L-1) will give the relationship between X_{L+1} and X_{L-1}, viz. using the Simpson's Rule.

$$X_{L+1} - X_{L-1} = \frac{H}{3}(XH_{L+1} + 4XH_L + XH_{L-1}). \quad (6.20)$$

Or between points L and L-1 using the Trapezoidal Rule gives

$$X_L - X_{L-1} = \frac{H}{2}(XH_L + XH_{L-1}). \quad (6.21)$$

Thus for F, FH can be found from equation (6.7)

$$FH = V3AN - V4BN + (V3+V4)(A-B)$$

and along any K line — fig. 6.7, since $F_2 = 0$

$$F_3 = \frac{H}{2}(FH_2 + FH_3)$$

$$F_4 = \frac{H}{3}(FH_2 + 4FH_3 + FH_4)$$

$$F_5 = F_3 + \frac{H}{3}(FH_3 + 4FH_4 + FH_5)$$

etc.

This could similarly be done for A by integrating A from its given value on LE, negatively into the $\not\in$ L = 2.

6.4.3 Attempts at the Solution with Four Variables and Fixed Boundaries

The general framework of the method of solution was as follows

(a) Boundary values are fed in on all four boundaries.

(b) The field equation (6.10) is used for C and the field is scanned 10 times.

(c) The field equation (6.9) is used for B and the field is scanned 10 times.

(d) The following steps are executed 10 times for A
- values of AN and A2N are calculated on the line K = 3
- values of A on K = 2 are calculated as a Taylor series expansion from K = 3
- the field is scanned calculating A (excluding values on K = 2) using field equation (6.8).

(e) Values of FH are calculated over the whole field and the values of F found by circumferential integration from $\not\in$ L = 2.

(f) Return to step (b) until convergence is attained.

The field size was now enlarged to KB = 11, LE = 17.

Three attempts are worthy of note. In each of them a different method of calculating A on the line

K = 2 is used. The first is as detailed above. The second evaluates A on K = 2 by integrating the values of AH on that line from L = LE back into $\mathcal{L}$ L = 2 — using equation (6.20). The third merely extrapolates the values of A on the lines K = 3, K = 4, K = 5 onto the line K = 2 using

$$A_2 = (T^2+T+1)A_3 - T(T^2+T+1)A_4 + T^3A_5. \quad (6.22)$$

The first program only executed the main loop 80 times with an accelerator of 1.7. The last two programs executed the main loop 200 times with the same accelerator. The results are as follows. Once again sample points (2,2) and (6,7) are shown

Method of Calculating $A_{K=2}$	Number of inter-ations	$A_{2,2}$	$A_{6,7}$	$B_{6,7}$	$C_{6,7}$	$F_{6,7}$
Analytical Values		1.12510	0.53053	0.10461	0.16828	-0.13553
Taylor Series	70	0.99266	0.52254	0.05001	0.16335	-0.03341
Taylor Series	80	0.99212	0.52528	0.04573	0.16350	-0.02968
Integration	190	1.11624	0.54028	0.08580	0.16734	-0.13378
Integration	200	1.11624	0.54028	0.08580	0.16734	-0.13378
Extra-polation	190	1.12194	0.54486	0.08651	0.16729	-0.13768
Extra-polation	200	1.11947	0.54285	0.08790	0.16714	-0.13791

From the above it can be seen that the first set of results rules out the Taylor Series expansion method on both convergence and accuracy grounds. The integration along K = 2 gave a convergent result which had reasonably good agreement with the analytical solution. The extrapolation method, by 200 iterations, had not quite converged.

In parallel to this study of four variables with fixed boundaries, a study of the three variable field was being undertaken, the details of which now follow.

6.5 Elliptical Solution with Three Variables and Fixed Boundaries

6.5.1 Introduction

On abandoning the four variable free boundary attempts as lacking stability, two approaches were proposed. These were tackled in parallel, with this three varible approach starting slightly later than the four variable fixed boundary approach (Section 6.4). Consequently, the idea of integrating variable gradients had been established. Originally it had not been decided whether or not to fix the boundaries in this case and so the idea of using a radial integration for B was considered. It will be remembered that for free boundary conditions σ_r (or B in the elastic case) is quoted only on the K = 2 and K = KE boundaries — fig. 6.3. In the fixed boundary case B is also quoted on the L = LE boundary.

However a radial integration could be performed outward from K = 2 where $\sigma_r = 0 = B$ using the following Simpson's Rule formula along the L line (fig. 6.4)

$$B_{K+1} = B_{K-1} + \frac{T^2-1}{6T}\left(T(2-T)BN_{K-1} + \frac{(T+1)^2}{T}BN_K + \frac{(2T-1)}{T^2}BN_{K+1}\right). \qquad (6.23)$$

Due to numerical approximations the value of B obtained at K = KE would differ slightly from the given boundary value, but this could be corrected by adjustment back along the L line.

This approach was initially tried but found to lead to instability. Consequently it was dropped and the boundaries fixed.

6.5.2 Field Equations

The elastic equations for three variables are repeated here for convenience (see equations (4.39) with zero P terms)

Equilibrium

$$AH + CN + 2C = 0 \qquad (6.24)$$

$$BN + CH + B - A = 0 \qquad (6.25)$$

Strain/Displacement

$$A2N + A2H + AN + B2N + B2H + BN = 0 \qquad (6.26)$$

In a similar fashion to the four variable cases above, the field equations require a cross-curvature relationship. In equation (6.26) can be found the field equations for A and B in an elliptical form. Thus

(a) For A the field equation is

$$A2N + A2H + AN = -B2H - B2N - BN. \qquad (6.27)$$

(b) For B the field equation is

$$B2N + B2H + BN = -A2N - A2H - AN,$$

To break the obvious inbreeding of this equation and (6.27) the A2H term is replaced by $-(CNH + 2CH)$ which is found from equation (6.24) by differentiation w.r.t. ϑ, therefore

$$B2N + B2H + BN = -A2N - AN + CNH + 2CH. \qquad (6.28)$$

(c) For C the two equilibrium equations (6.24) and (6.25) are differentiated w.r.t. R and ϑ respectively and the two equations added to give

$$C2N + C2H + 3CN = -ANH + AH - BNH - BH. \qquad (6.29)$$

Equations (6.27) to (6.29) thus form the three field equations for the three variables A, B and C. As for the four variable case, these equations are discretized to express the values of nodal points in terms of the values at the four neighbouring points and the constant right hand sides. The method of solving these equations is once again Successive Over-relaxation using an accelerator of 1.7.

6.5.3 Fixed Boundary Conditions for Three Variables

The outer boundaries are located as in the four variable fixed boundary case at K = 11 and L = 17.

With the fixing of the boundaries the boundary conditions (i) to (vi) of section 6.2 are enforced. Consider each variable in turn — fig. 6.8.

(a) For A (or σ_ϑ).

On both the L = 17 and K = 11 boundaries the simple Dirichlet condition holds and on the $\not\in$ L = 2

boundary symmetry exists. However the K = 2 boundary still remains a problem since essentially it is a Neumann boundary condition with AN being the control; several different methods are used to overcome the difficulty.

(b) For B (or σ_ϑ).

Symmetry exists over the $\not\in$ L = 2 boundary and the simple Dirichlet condition controls the other three boundaries.

(c) For C (or $\tau_{r\vartheta}$).

Similarly to B, Dirichlet conditions control the L = A, K = 2, K = 11 boundaries. However, asymmetry exists for C over the $\not\in$ L = 2.

These then are the boundary controls for the three variables for all the solutions referred to below.

6.5.4 Solutions for Three Variables and Fixed Boundaries

With the obvious weakness of the K = 2 boundary for A all effort was concentrated on searching for the best way of solving this boundary. Bearing in mind the results illustrated in paragraph 6.4.3, only two methods of solving A on K = 2, were considered. These were –

(1) by integrating AH circumferentially along K = 2 from L = 17 to $\not\in$ L = 2 using equation (6.20),

(2) by extrapolation from values of A on the K = 3, 4 and 5 lines using equation (6.22).

However, since A on K = 2 is found by integration why should all the other K lines not be solved by the same way? This was tried and found successful. To iron out any disturbances due to the integration a circumferential smoothing was introduced for A after every 50 iterations.

The general framework of the method of solution is thus:–

(a) Boundary values are fed in on all four boundaries.

(b) The field values of A are calculated in one of the three following ways

Method (1) the following steps are executed 10 times

- values of A on K = 2 are found by extrapolation using equation (6.22)
- the field is scanned calculating A (excluding values on K = 2) using field equation (6.27).

OR Method (2) values of A on K = 2 are calculated by integration along that line using equation (6.20) and then the field is scanned 10 times calculating A (excluding values on K = 2) using field equation (6.27).

OR Method (3) values of A on all K lines are calculated by integration along these K lines from L = 17 to L = 2. Values of A on each K lines are smoothed circumferentially.

(c) The field equation (6.29) is used for C and the field is scanned 10 times.

(d) The field equation (6.28) is used for B and the field is scanned 10 times.

(e) Return to step (b) until convergence is attained.

The order of solution of variables in steps (b), (c), (d) is A, C, and then B since field equations (6.27) and (6.28) are very similar as pointed out in paragraph 6.5.2.

The results below indicate the accuracy and speed of convergence. Once again the values of A at point (2,2) and A, B and C at point (6,7) give a good indication of field behaviour. The method number refers to the method of solving the A field as indicated in step (b) above and the column 'Iterations' refers to the number of main

iterations at which the values of A, B, C are given

Method	Iterations	A(2,2)	A(6,7)	B(6,7)	C(6,7)
Analytical		1.12510	0.53053	0.10461	0.16828
(1)	990	1.11026	0.52943	0.10011	0.16712
	1000	1.11005	0.52948	0.09998	0.16712
(2)	90	1.08418	0.52973	0.08893	0.16618
	100	1.08439	0.53978	0.08897	0.16620
(3)	190	1.08926	0.53053	0.09041	0.16646
	200	1.08926	0.53053	0.09041	0.16646

Method (1); Even after 1000 main iterations it has not quite settled, although the values at this stage are reasonably accurate.

Method (2); This program was only run for 100 iterations, but from the results obtained at 100 iterations, it appears that the values are not quite so accurate. However, quicker convergence was achieved using the integration of AH on K = 2 to give A boundary values.

Method (3); The field settled after 200 iterations, the program being run for a few hundred more to check this convergence. Although some of the values are not as accurate, it appears that this method is a good compromise between methods (1) and (2) as far as accuracy and speed of convergence are concerned.

To show the effect of the Methods (1) and (3), the distributions of $A(=\frac{\sigma\phi}{\sigma Y})$ on K = 2, are plotted against the exact value on fig. 6.11 from L = 2 up to L = 10. This indicates clearly that the maximum error exists at the point (2,2).

It was of interest to check the accuracy of larger fields. Two larger fields were solved using method (3).

(a) Fig. 6.9 – the outer boundary was taken out to K = 20 (or 2.89 r_o).

(b) Fig. 6.10 – the ratio of radii T was increased to 1.125 from $\sqrt{1.125}$ (= 1.06066). The same number of radial divisions (say KK lines) were used. Thus the outer boundary was at KK = 11 (or 2.89 r_c) like (a).

The outer L boundary was maintained at L = 17 with the circumferential division H still at $\frac{\pi}{32}$.

Both of these solutions settled within the 200 iterations and the values below compare the results of the analytical with those of methods (1), (3), (3)(a) and (3)(b). The latter one having a larger T ratio means that the point KK = 4, L = 7 corresponds to point K = 6, L = 7 on the following table –

Method	Iterations	A(2,2)	A(6,7) A(4,7) for(3)(b)	B(6,7) B(4,7) for(3)(b)	C(6,7) C(4,7) for(c)(b)
Analytical	–	1.1250	0.53053	0.10461	0.16828
(1)	1000	1.11006	0.52948	0.09998	0.16712
(3)	Settled	1.08926	0.53053	0.09041	0.16646
(3)(a)	Settled	1.08733	0.52637	0.08946	0.16551
(3)(b)	Settled	1.03620	0.52699	0.06139	0.16320

From the above it is obvious that the change of ratio is detremental to accuracy and that the best way to increase field size is by increasing the number of K lines. The distribution of $A(=\frac{\sigma_\theta}{\sigma_Y})$ on K = 2 is plotted for methods (1), (3)(a) and (3)(b) against the exact values, on fig. 6.12.

6.6 Conclusion

The thorough investigation in this chapter was essential in order that experience and confidence in procedure stability could be gained. The ideas of initially solving a field having free boundary conditions has now been ruled out but the question of using three or four variables is not yet settled. Undoubtedly working with three variables is much simpler than with four. Since the field equations are of second order anyway, the existence of a second order governing equation in the three variable case is not a disadvantage whereas the existence of the F with its weak boundary conditions is.

With the introduction of the complexities of the plasticity relations, it was felt that using the simpler three variable approach would minimise the difficulties and the interaction among the variables. The elasto-plastic method of solution dealt with in the next chapter thus utilizes exclusively the elliptical three variable fixed boundary approach.

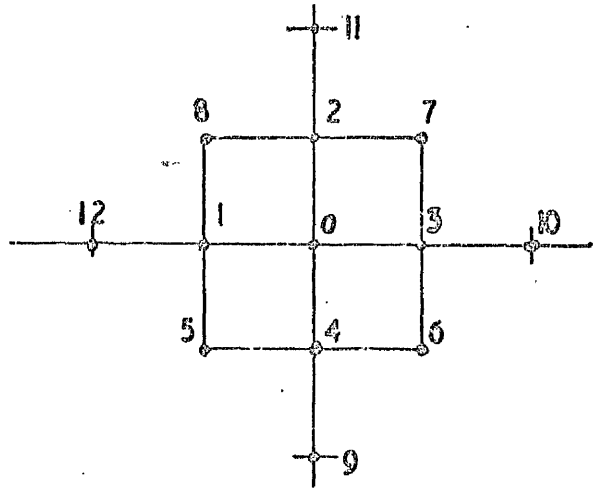

Fig 6.1

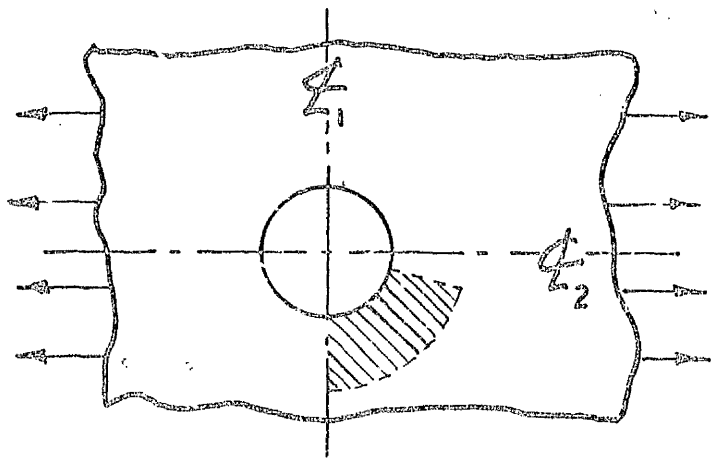

Fig 6.2

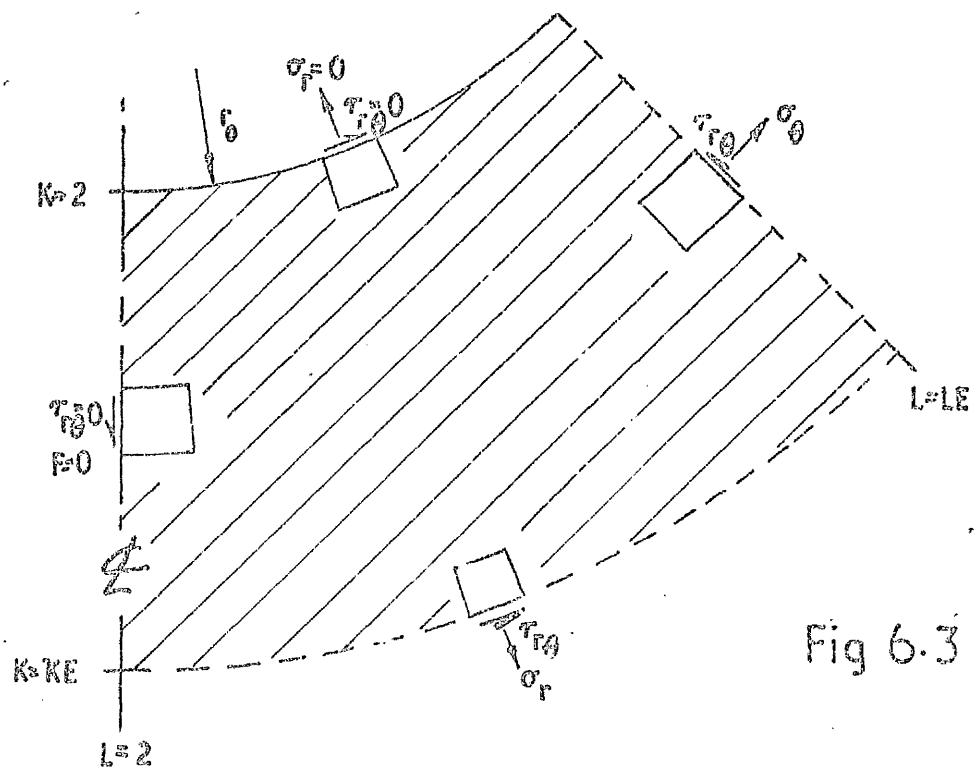

Fig 6.3

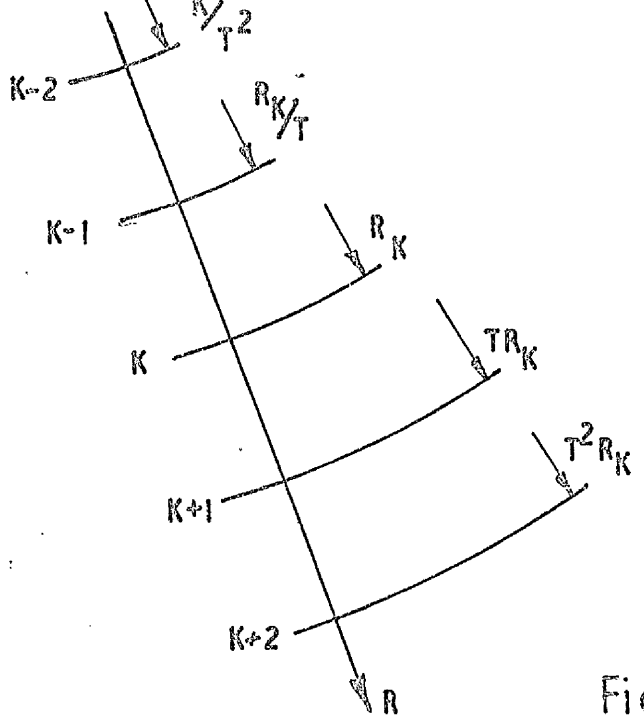

Fig 6.4

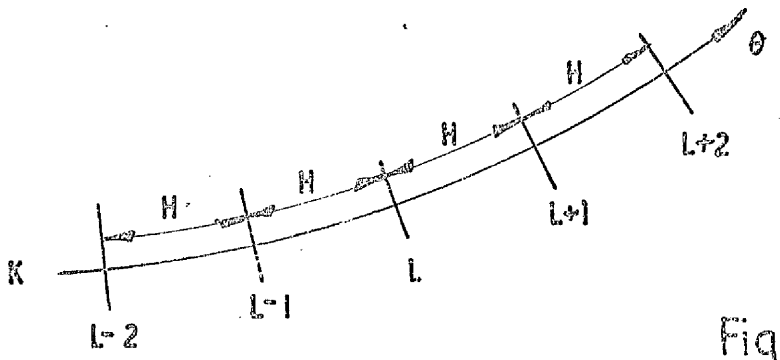

Fig 6.5

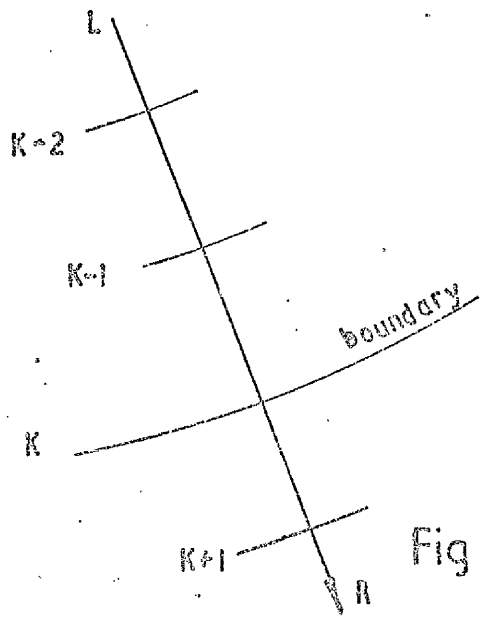

Fig 6.6

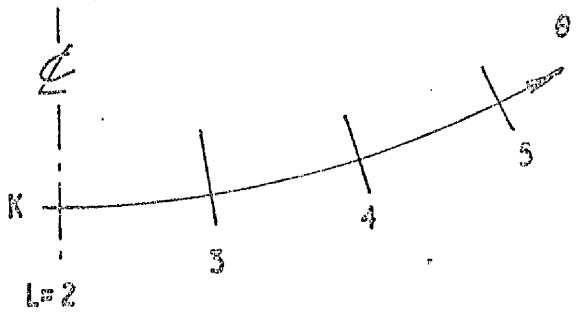

Fig 6.7

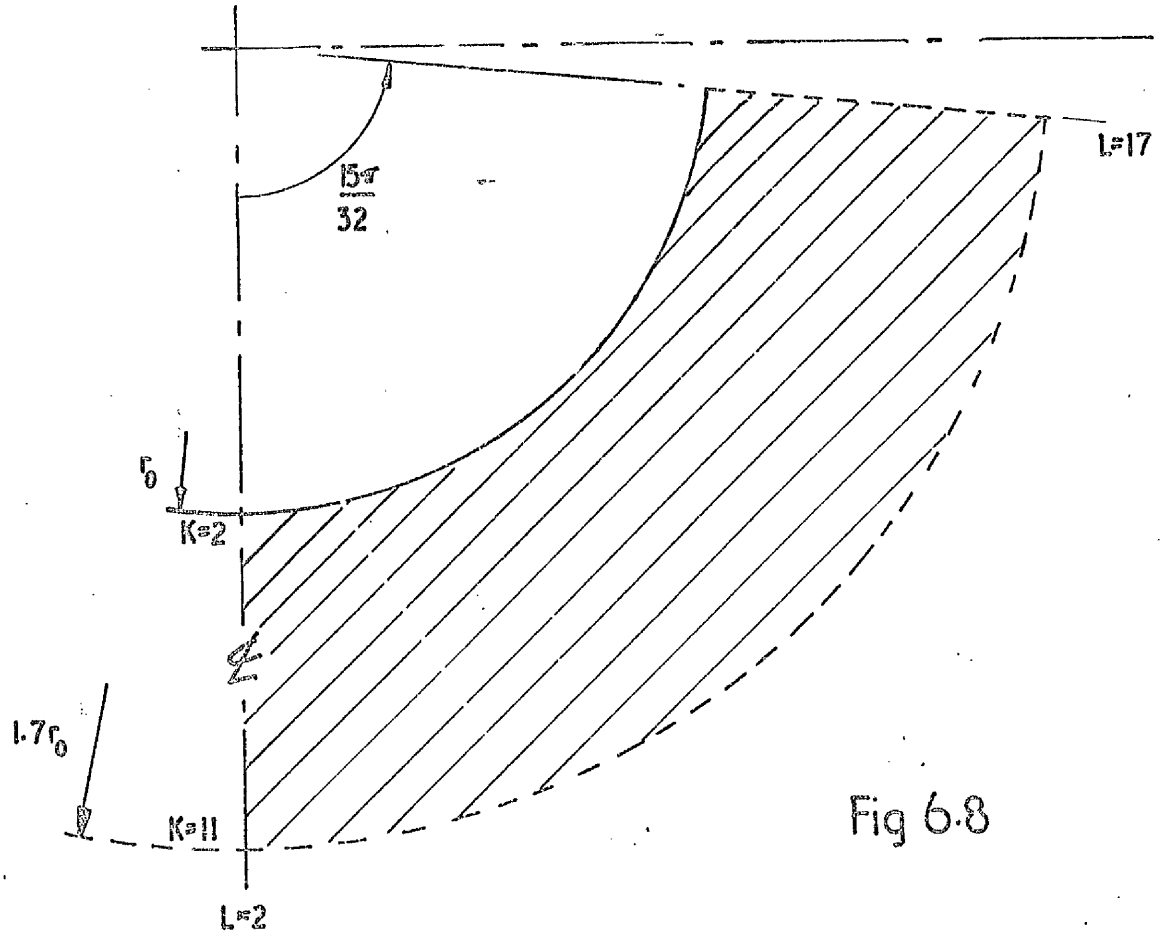

Fig 6.8

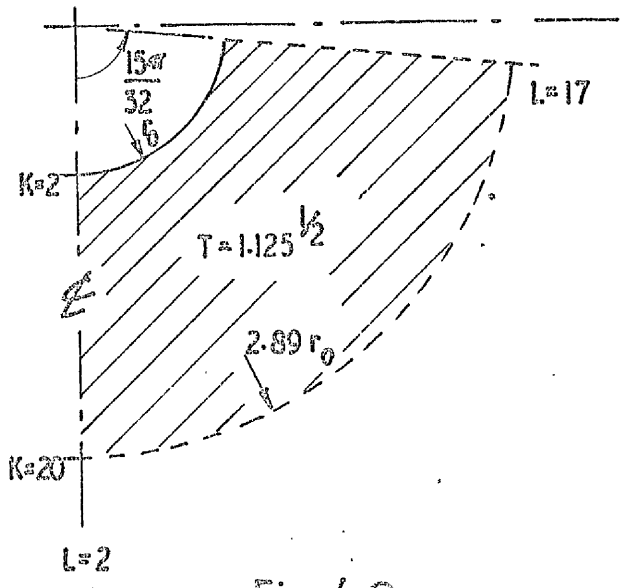

Fig 6.9

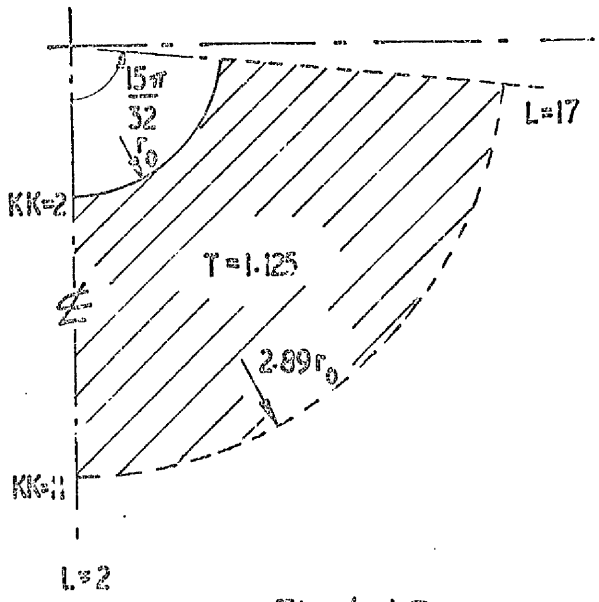

Fig 6.10

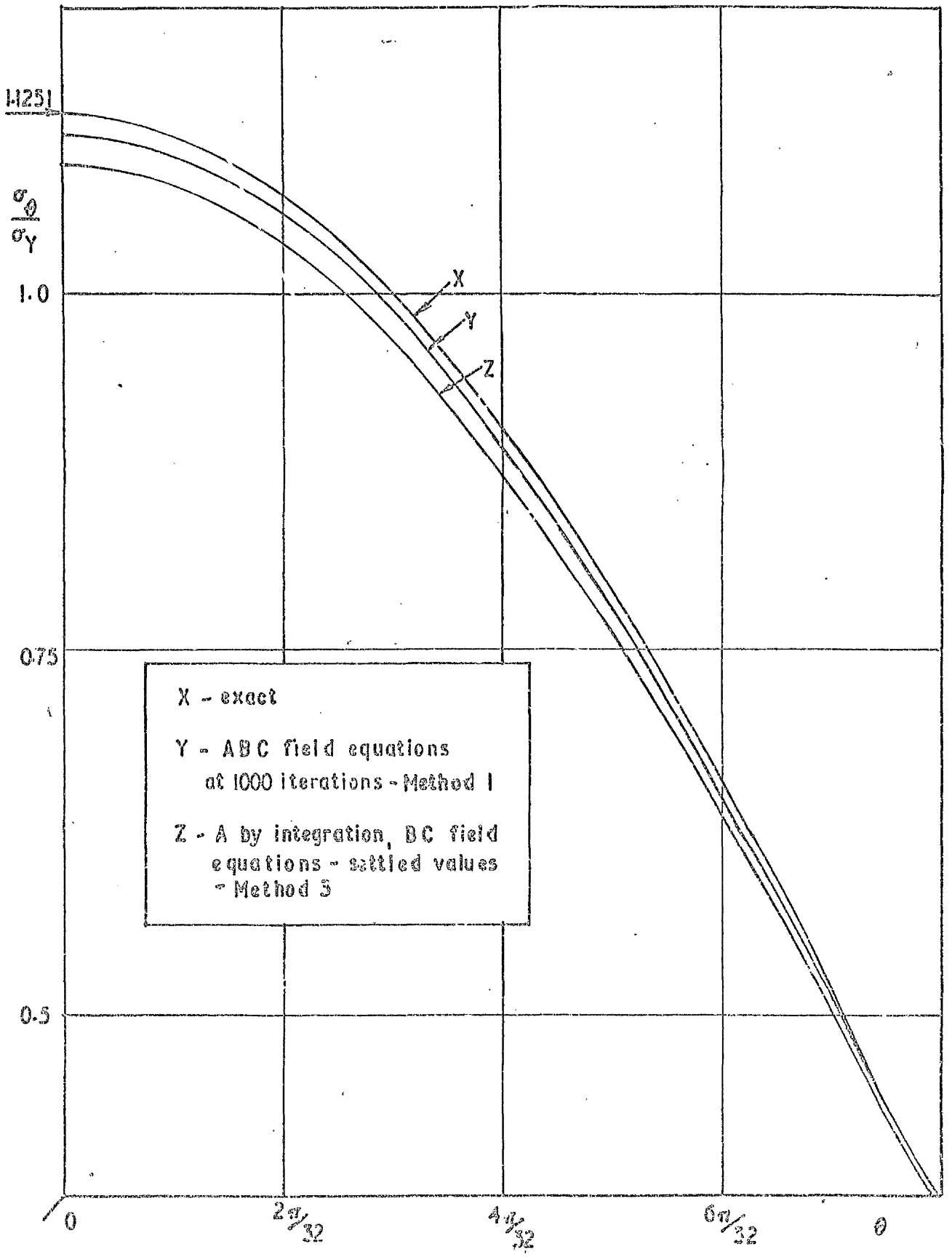

Fig 6-11 Distribution of σ_θ/σ_Y along inner surface for various boundary conditions

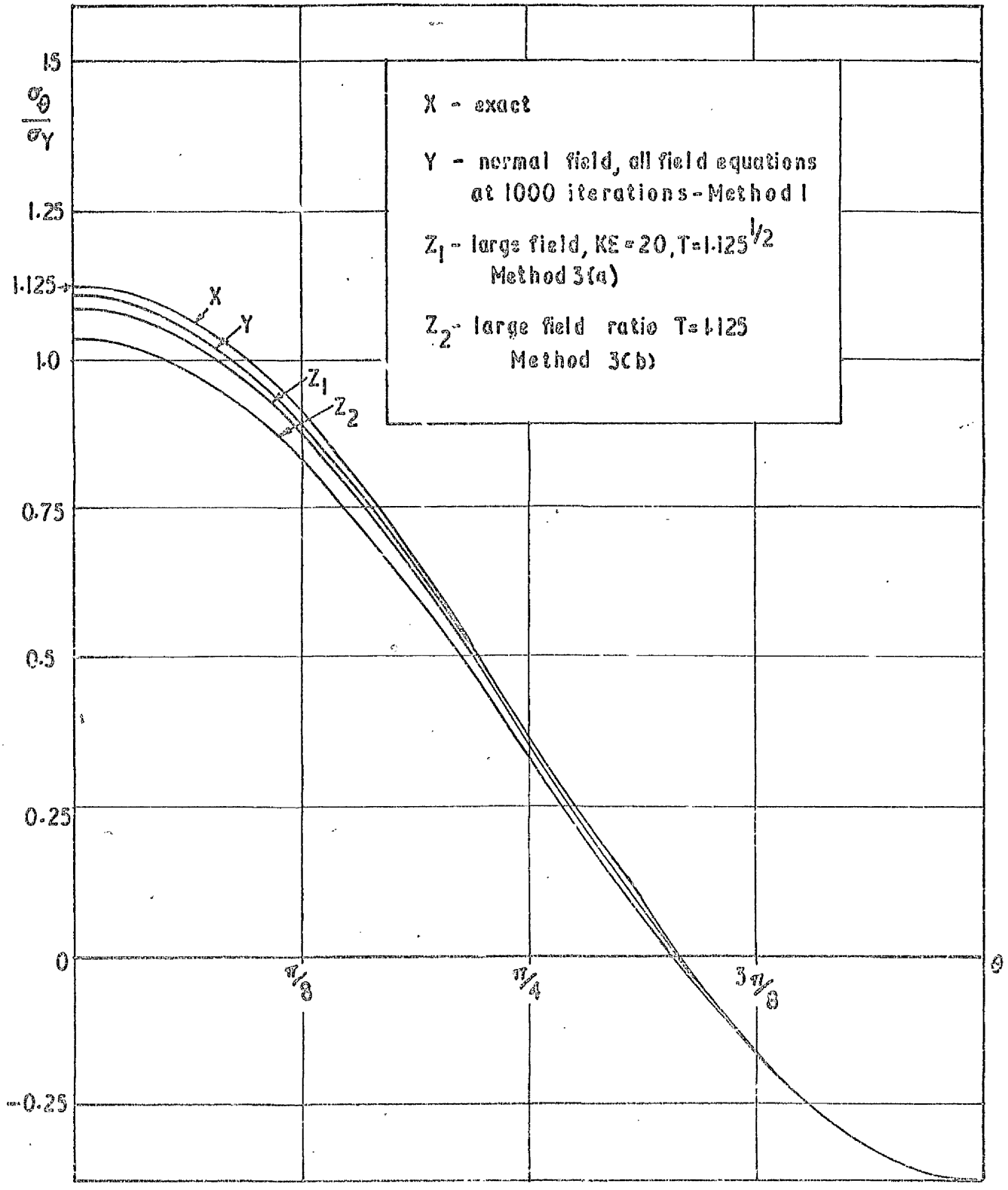

Fig 6.12 Distribution of σ_θ/σ_Y along inner surface for various field sizes

CHAPTER 7

ELASTO-PLASTIC SOLUTIONS -- ELLIPTICAL PROCESS

CHAPTER 7

ELASTO-PLASTIC SOLUTIONS — ELLIPTICAL PROCESS

7.1 Introduction

The solutions to problems in plasticity can be tackled from three approaches

(a) Completely. This involves satisfying all conditions of equilibrium, compatibility and stress/strain relations — simultaneously.

(b) Energy Approach. Instead of satisfying the condition of equilibrium and compatibility simultaneously, one condition is satisfied overall, while the other is satisfied in isolation. For example, if a solution satisfying equilibrium, is combined with any compatible solution, the answer will provide a lower bound to the problem. The closer the compatible solution comes to the correct one, the higher will be the lower bound and so closer to the answer. The alternative approach is to combine a compatible solution with any equilibrium solution and hence achieve an upper bound to the problem. Optimisation of the two approaches should converge to the required solution, when the upper and lower bounds are equal.

(c) Slip-line Fields. This approach is similar to (b), in general leading to an upper bound on the applied load. Lower bound solutions have been attempted but are far from numerous and comprehensible. This approach is mostly used for metal forming problems where an upper bound on the applied load gives a designer the maximum required capacity of the forming machinery. However when

the approach is applied to notches etc. it is the lower bound which is required to keep the maximum stress within the prescribed factor of safety; this bound is very difficult to find due to the difficulty of matching stresses over the plastic-rigid boundary. In addition, it should be remembered that the solution is only applicable for large scale yielding where the effects of elastic strains can be neglected. In addition the material characteristics are assumed to be rigid plastic with the unreal condition of zero work-hardening. Bearing these latter restrictions in mind, a slip line solution can be considered as one extreme, the other one being the elevated elastic solution; between both of these extremes should be the work-hardening elasto-plastic solution. For these reasons, a slip line solution is given for the keyhole notch in Chapter 10.

Of the three approaches mentioned it is the complete solution which is attempted here. In the last chapter, the elastic solution was obtained by employing three strain variables A, B, C (defined in section 4.3) in the three governing equations (two equilibrium and the third essentially strain-displacement). The stress strain relations were implicit in the formulation of these equations, which were solved simultaneously with fixed boundary conditions.

The elasto-plastic governing equations are similar, the only difference being the inclusion of plastic terms; a similar approach can thus be taken to their solution. The field grid size remains the same as the elastic solution although the outer radial boundary was taken as L = 18 (fig. 7.1), to take advantage of the symmetry over this centre line in the case of the hole in tension.

The circumferential boundaries were also treated similarly to the elastic solutions; they were chosen to be K = 2 and K2 (now increased) = 14.

7.2 The Complete Solution Attempt to Elasto-plastic Problems

Consider first, the iterative procedure for determining plastic strain components. In most cases the solution of elasto-plastic problems is by the method of successive approximation. The following outlines the method, the stress and strain components being referred to the more familiar cartesian coordinates as in the first part of chapter 4:-

The loading path is divided into a number of load increments, if the incremental theory of plasticity is being used. If the deformation theory is used, it is assumed that between yield and the required load the ratios of the stresses remains constant and only one large load increment need be considered in the solution. In what follows, only the incremental theory is employed.

For the first load increment, guessed values of $d\varepsilon_x^p$† etc. are used, starting from zero values of ε_x^p† etc. Thus $d\bar{\varepsilon}^p$, and, from the stress strain curve, $\bar{\sigma}$ can be found. Equations (4.1) to (4.3) are solved as for an elastic problem except with non-zero values for $d\varepsilon_x^p$ etc. Thus a first approximation of stresses and total strains is obtained. From these stresses and the original values of $d\bar{\varepsilon}^p$ and $\bar{\sigma}$, the new values of $d\varepsilon_x^p$ etc. as a proportion of $d\bar{\varepsilon}^p$ can be evaluated using equations (4.4). These first approximations to $d\varepsilon_x^p$ etc. will give the new value of $d\bar{\varepsilon}^p$ and so $\bar{\sigma}$ can be found as before from the stress-strain curve. Also substitution of $d\varepsilon_x^p$ etc. into equations

---

† $d\varepsilon_x^p$ = current value of x-component of plastic strain increment etc.

ε_x^p = total value of x-component of plastic strain up to but not including the current strain increment etc.

$d\bar{\varepsilon}^p$ = effective plastic strain increment.

(4.1) to (4.4) will give new values of the R.H.S. The process proceeds until two consecutive approximations give a small enough change in component values for the process to be considered as having converged to a solution.

For second and subsequent load increments, the values of ε_x^p etc. are no longer zero but have fixed values while new values of the current $d\varepsilon_x^p$ etc. are guessed and then successively approximated as above until convergence is achieved. The complete stress strain history for any loading or unloading path is thus obtained.

Convergence is of paramount importance and consequently consideration should be given to possible sources of divergence in the use of the stress strain curve. In the discussion above, the value of $\bar{\sigma}$ was evaluated from $d\bar{\varepsilon}^p$ – $\overrightarrow{OKLM}$ on the bilinear stress–strain curve shown – fig. 7.2. Often, however, the governing equation or equations are in terms of stresses and it would be more convenient to calculate $\bar{\sigma}$ and then find $d\bar{\varepsilon}^p$ by $\overrightarrow{MLKO}$.

If one looks at real materials, <u>once the plastic regime has firmly established itself</u>, the work-hardening index m lies between 0.0 and 0.1. Thus in the latter method, small errors in $\bar{\sigma}$ would produce very large errors in $d\bar{\varepsilon}^p$. It is thus always better to evaluate $d\bar{\varepsilon}^p$ and extract $\bar{\sigma}$ from the curve. This is not to say that divergence will <u>not</u> occur.

The magnitude of load increment is of great importance for the following reason. Starting with the guessed values of $d\varepsilon_x^p$ etc., the values of $d\bar{\varepsilon}^p$ and $\bar{\sigma}$ are found. The values of $d\varepsilon_x^p$ etc. also enable equations (4.1) to (4.4) to be solved, giving values of σ_x etc. These stresses could be used to evaluate $\bar{\sigma}$ again but this $\bar{\sigma}$ will not in general agree with the first value obtained from the stress–strain curve – although, if the initial guess were exact, the values of $\bar{\sigma}$ would be identical. This discrepancy in $\bar{\sigma}$ will produce an inconsistency in the Levy Mises equations (4.4), which will produce large errors in the strains. If the load and thus the stresses

are large, this initial error can be enough to initiate divergence.

Elasto-plastic problems should thus be formulated to determine $\bar{\sigma}$ from $d\bar{\varepsilon}^p$ with care being taken to limit load increments. Mendelson and Manson[10] refined the above procedure of determination of plastic strains from total strains as was shown in Chapter 2.

The Mendelson Manson procedure is the one which is used here – see paragraph 7.3.5. It requires the input of total strains from which the plastic strains are extracted. The total strains are made up of elastic and plastic strains; the elastic part can be obtained directly from the current stresses.

Two approaches to the method of elasto-plastic solution thus present themselves –

(a) the stress oriented approach dealt with in section 7.3 below,

OR (b) the strain oriented approach dealt with in section 7.4 below.

7.3 Stress Oriented Approach

7.3.1 Introduction

What is intended by 'stress oriented approach' is that the governing equations are in terms of the stress components σ_r, σ_θ, $\tau_{r\theta}$. Obviously this approach is a favourable one where stress boundary conditions are directly applicable and thus give Dirichlet Boundary conditions. The complication lies in the use of the stress-strain curve, where low work-hardening rates produce large errors in determining effective plastic strain from approximate effective stress values. This was discussed more fully in the section 7.2.

However, referring back to the Chapter 2, therein will be found the solution to the above difficulty. (Steps (a3) to (g3) in section 2.3). The stress field values at

the end of any iteration are used to give the elastic strains to which are added the total plastic strains calculated before the current iteration thus giving a new value of total strain. This total strain is then fed into the Mendelson Manson procedure which produces the current plastic strain increment, to which can be added the values at previous load stages, thus giving a current estimate of total plastic strains. These total plastic strains are now added to the calculated elastic strains following the field iteration.

The use of this device allows the stress oriented solution to deal successfully with the typical low work-hardening material.

7.3.2 Outline of Program for Stress Oriented Solution

It is probably better at this stage to give an outline of the method of solution and then to deal with points of detail later. This then is the program outline;

(a) Constant coefficients and field parameters are fed in or assigned.

(b) The elastic field values of the stress components are read in.

(c) An initial estimate is made of P, X, Y, and Z (defined in paragraph 4.3.3) and the yield stress SY is fixed at the value of $\bar{\sigma}$ at the point of maximum stress ($\bar{\sigma}_{max}$).

(d) The load is incremented by a fixed amount and, as a first estimate, all the stresses are incremented by the same amount.

(e) Initial estimates of total strains are made using P, X, Y, Z.

(f) The values of total strains are fed into the Mendelson Manson procedure, from which are found values of X, Y, Z and the plastic increment P.

(g) The component plastic strain increments can now be

found using P, X, Y, Z – for example $d\varepsilon_\vartheta^p \equiv P(1+\nu)X$.

(h) The plastic strain gradients required in the stress field equations are now found over the whole field and then zeroed at non-plastic points.

(i) The field is scanned ten times evaluating BS† at each point using its field equation.

(j) The field is scanned ten times evaluating CS† at each point using its field equation.

(k) Values for AS† at each point in the field are found by integrating ASH† circumferentially from the L = LE boundary.

(l) Steps (i) to $(l)_1$ are performed 50 times to settle the AS, BS, CS fields using the current estimates of the plastic strains and gradients.

(m) The values of AS, BS and CS are smoothed circumferentially along the K lines to iron out any second order ripples especially in AS.

(n) From the stresses AS, BS, CS (evaluated in the (i) to (l) loop) and the values of plastic strains, both current (step (g)) and from previous load stages (if any), the value of σ_z can be calculated over the field.

(o) The component elastic strains are evaluated from the stresses and added to the current plastic strain increments (from step (g)) and any accumulated increments from previous load stages. This gives new values of total strains – for example $\varepsilon_\vartheta = \varepsilon_\vartheta^e + d\varepsilon_\vartheta^p + \varepsilon_\vartheta^p$ where $\varepsilon_\vartheta^p = \sum_{k=1}^{n-1} d\varepsilon_\vartheta^p$ during the n^{th} load stage.

---

† AS is defined as $(\frac{\sigma_\vartheta}{\sigma_Y})$, BS as $(\frac{\sigma_r}{\sigma_Y})$ and CS as $(\frac{\tau_{r\vartheta}}{\sigma_Y})$.

ASH is defined in paragraph 4.3.3 as $\frac{\partial(AS)}{\partial\vartheta} = \frac{\partial(\sigma_\vartheta/\sigma_Y)}{\partial\vartheta}$.

(p) With the new values of total component strains the program returns to step (f) and steps (f) to (p) are performed enough times to allow convergence at any particular load stage.

(q) Total plastic strain quantities and their gradients are updated by the current increments, which are then set to zero.

(r) Steps (d) to (r) are performed until the correct number of load stages has been executed, after which the program stops.

Certain points of detail are amplified in the following sections:-

(1) The field equations for BS and CS and the integration of AS - see paragraph 7.3.3; steps (i), (j) and (k) of the outline.

(2) The gradients of plasticity P - see paragraph. 7.3.4; step (h) of the outline.

(3) The extraction of plastic strains from total strains using the Mendelson-Manson procedure - see paragraph 7.3.5; step (f) of the outline.

(4) The evaluation of the stress σ_z - see paragraph 7.3.6; step (n) of the outline.

(5) The calculation of total strains - see paragraph 7.3.7; step (o) of the outline.

7.3.3 Stress Field Equations

Re-writing the equations (4.40) from Chapter 4

$$\left.\begin{aligned} AS2N + ASN + AS2H + BS2N + BSN + BS2H &= \frac{1}{1-\nu} P_4 \\ CSN + ASH + 2CS &= 0 \\ BSN + CSH + BS - AS &= 0 \end{aligned}\right\} \quad (7.1)$$

The similarity of these with the elliptical elastic three variable governing equations is obvious. The only difference in form is that the first equation has now a non-zero right hand side. Consequently the same

form of field equations is used:

(a) for BS, the first equation is used and, as in the last chapter, the AS2H term is replaced using the differentiated form of the second equation: thus

$$BS2N + BSN + BS2H = -AS2N - ASN + CSNH + 2CSH + \frac{1}{1-\nu} P_4 \qquad (7.2)$$

(b) for CS, the last two equations are differentiated with respect to R and θ respectively and then added to give

$$CS2N + CS2H + 3CSN = -ASNH - BSNH + ASH - BSH. \qquad (7.3)$$

For AS, no field equation was used since, as a compromise of accuracy and speed of convergence, it was decided from the three variable elastic solution to integrate AS circumferentially into the ℓ I = 2.
The gradient ASH was evaluated from the second equation viz.

$$ASH = -CSN - 2CS. \qquad (7.4)$$

As before these equations are discretized and the method of solution used in steps (i) and (j) of the program outline is one of Successive Over relaxation.

One further point must be made regarding the field equation for BS. The right hand side contains P_4 which is a function of the gradients and curvatures of P, X, Y and Z. This point is now dealt with in paragraph 7.3.4 below.

The boundary conditions are similar to those used in the last chapter for the elliptical three variable fixed boundary approach, the only difference being that the boundary variables are in terms of stresses AS, BS and CS. These boundary definitions give the very favourable condition that along the inner K = 2 boundary BS = CS = 0.

7.3.4 The Gradients of Plasticity P

In the first of equations (7.1) is the term P_4. This when expanded as in equation (4.40) gives

$$P_4 = -(1-\nu)PX2N + \nu PX2H - (2-\nu)PXN + \nu PY2N$$
$$-(1-\nu)PY2H + (1+\nu)PYN + 2PZH + 2PZNH$$

where $P = \frac{\Sigma d\bar{\varepsilon}^p}{(1-\nu)}$, $PXN = R\frac{\partial(PX)}{\partial R}$, $PZH = \frac{\partial(PZ)}{\partial \vartheta}$ etc.

As can be seen the evaluation of curvatures is required. This problem is not unique to this approach to elasto-plastic problems, as second order terms also exist when the stress function governing equation is used. However, in this formulation the equation for P_4 is in terms of P, X, Y and Z. The difficulties and their solution to them are detailed below.

(a) Size of plastic zone. Take as an example, the case of a 50% increase of load over load at first yield for the hole in uniaxial tension. The size of plastic zone is shown in fig. 7.3; this is a relatively small zone for such a load increase. This poses great difficulties in trying for example to take a radial gradient or curvature at the point (2,8) since at the points (3,8), (4,8) etc. zero plasticity is registered.

The solution to this difficulty is found by evaluating the values P at all points in the field; at elastic points, instead of zeroing the negative P values, retain them.

What do these negative values represent? Consider the stress-strain curve ONS in fig. 7.4 and let the strain hardening part NS be continued back to M. For the normal plastic point with stress σ_T, the point T on the stress-strain curve would indicate a positive plasticity P_T. However for an elastic point with stress σ_W, the point W on the part MN of the stress-strain curve would give a negative plasticity P_W as indicated in the figure.

In this way P can now be considered as a continuous function over the elasto-plastic boundary. Due to the greater steepness of part ON on the stress-strain curve, the distribution of the negative P values in the elastic zone will show reduced gradients and curvatures. In fig. 7.5 this is illustrated qualitatively in the line ABC of a sample distribution of P along a circumferential

line. When gradients are taken over the elasto-plastic boundary at B, this different character of the distribution BC will falsify the values slightly. In order to reduce this error, the values of P over the whole field were smoothed circumferentially then radially and finally circumferentially again. The effect of this is to change the distribution from ABC to ADE, and increase the plastic zone by $d\theta$, length BD; however, the gradients are expected to be more accurate.

The smoothing formulae use are those developed in Chapter 5 on the Initial-Value Approach.

(b) The gradients and curvatures. In section (a) only general reference was made to the plastic gradients and curvatures; in this a detailed look is taken at these quantities.

The quantities comprising P_4 are gradients and curvatures of the products P and each of X, Y and Z. These would appear on first glance to be easily evaluated but a closer look at the problem produces some anomalies. Normally one would multiply the values of X, Y and Z at each point with the values of P, which is considered continuous (as discussed in (a) above). The gradients and curvatures of PX, PY and PZ could then be found using the formulae developed in Chapter 5.

However, due to there being zero surface shear loading and due to the asymmetry of the shear stress over the ϕ. L = 2, all the values of Z on L = 2 and K = 2 are zero. This in itself does not disrupt the continuity of Z but the values of the product PZ along these lines will now also be zero. The anomaly arises when dealing with a point like (2,8) in fig. 7.3, since now PZ is zero at this point and the term for PZRH will have dubious accuracy.

With the above considerations in mind it was decided to split the gradients and curvatures of the products into the gradients and curvatures of each of P, X, Y and Z, finally combining them through the following

formulae.

Since $\frac{\partial(PX)}{\partial \vartheta} = P\frac{\partial X}{\partial \vartheta} + X\frac{\partial P}{\partial \vartheta}$ etc. then

$$PXH = P \times XH + X \times PH$$
$$PXN = P \times XN + X \times PN$$

Similarly
$$PX2H = P \times X2H + X \times P2H + 2 \times PH \times XH$$
$$PX2N = P \times X2N + X \times P2N + 2 \times PN \times XN$$
$$PXNH = PN \times XH + P \times XNH + X \times PNH + XN \times PH$$

Similarly for PY and PZ.

Once all the gradients and curvatures have been found, these values at all elastic points are zeroed.

In this way, the continuous character of each variable is best used.

(c) Interpretation of P. One final point must be considered in using the values of P in P_4; if there is more than one load stage then what does P represent?

In P_4, P is a function of the sum of the effective plastic strain increments up to and including the current load stage. From the Mendelson-Manson procedure (paragraph 7.3.5) only the current effective plastic strain increment $d\bar{\varepsilon}^p$ is evaluated and so to this must be added to the total up to but not including this load stage, before the gradients are taken.

Defining $\bar{\varepsilon}^p$ as the total up to but not including the current load stage, allows one to define

$$P = \frac{1}{1+\nu}(\bar{\varepsilon}^p + d\bar{\varepsilon}^p).$$

However X, Y and Z similarly vary from one load stage to the next, and in fact the products PX, PY and PZ are directly proportional to the sum of the circumferential plastic strain increments, the radial plastic strain increments and the shear plastic strain increments respectively. Thus for n load stages

$$PX = \sum_{i=1}^{n} P_i X_i \propto \sum_{i=1}^{n} d\varepsilon_{\vartheta_i}{}^p \quad \text{etc.}$$

When one evaluates the gradients and curvatures -- PXH, for

example, they can be found by

either (a) Summing all the values of $P_i X_i$ up to and including the present load stage and taking the gradient from the sum.

or (b) Retaining the sum of the gradients PXH_i up to but not including the current load stage and adding this to the value of PXH found using the current increment $\frac{d\bar{\varepsilon}^p}{(1+\nu)}$ and the current value of X.

The latter method was used.

7.3.5 The Mendelson-Manson Procedure †

In section 2.3 is detailed the use of the Levy Mises Equations to extract component plastic strain increments ($d\varepsilon_\vartheta^p$ etc.) from the effective plastic strain increment $d\bar{\varepsilon}^p$ and, also discussed, is the use of the stress-strain curve. Mendelson et al[10,13], however, take a very different approach. Total strains (ε_ϑ etc.) are fed into the procedure and the value of $d\bar{\varepsilon}^p$ is extracted along with values of x, y, z (see equations (4.20)).

Essentially the procedure is incremental and so from the input of total strains are subtracted the accumulated plastic strains up to but not including the current load stage. This idea can best be visualised by reference to the stress-strain curve, fig. 7.6. After the first load stage, imagine that a point has reached the stress state defined by point 2. During the second load stage the stress state moves from point 2 to point 3 with an effective plastic strain increment of $d\bar{\varepsilon}_2^p$. In the Mendelson-Manson procedure, the strains are 'modified' — for example $\varepsilon_\vartheta' = \varepsilon_\vartheta - \varepsilon_\vartheta^p$; this is equivalent, in the second load stage, to working on the stress-strain curve 0'25 (with yield stress $\bar{\sigma}_2$) and finding $d\bar{\varepsilon}_2^p$. This, however, would be

---

† In this paragraph, the stress and strain symbols stand for their usual meaning and are not non-dimensionalized.

for one particular point. Another point in the field may have the stress state of point 3 and in this case the stress–strain curve would be equivalent to O"45 with yield stress $\bar{\sigma}_4$. For <u>all</u> elastic points the stress–strain curve used would be O15 with the actual yield stress $\bar{\sigma}_1 = \sigma_Y$.

From the above description, it will be seen that, at <u>each</u> point in a field, certain other information must be fed into the procedure, if at a previous load stage yielding had been exceeded –

viz. (1) the accumulated plastic strains, ε_ϑ^p etc.

(2) the effective stress at the end of the previous load stage e.g. $\bar{\sigma}_2$, $\bar{\sigma}_4$ etc. or σ_Y for the above example – fig. 7.6.

Consider now the steps in the procedure, which is written <u>for the i^{th} load stage and any one point in a field</u>;–

(1) Total strains ε_ϑ etc. are fed in.

(2) The modified strains are formed – for example $\varepsilon'_\vartheta = \varepsilon_\vartheta - \varepsilon_\vartheta^p$. (Remember $\varepsilon'_z = -\varepsilon_z^p$).

(3) The effective total strain ε_{et} is calculated from (2.15).

(4) The effective plastic strain increment is evaluated from (2.16).

viz.
$$d\bar{\varepsilon}^p = \frac{\left(\varepsilon_{et} - \frac{2}{3}\frac{(1+\nu)}{E}\bar{\sigma}_{i-1}\right)}{1 + \frac{2}{3}(1+\nu)\,Q}$$

where $\bar{\sigma}_{i-1} > \sigma_Y$ if yielding had occurred at a previous load stage

$= \sigma_Y$ if elastic conditions existed at the end of the $(i-1)^{th}$ load stage.

and $Q^{\dagger} = \frac{1}{E}\left(\frac{d\bar{\sigma}}{d\bar{\varepsilon}^p}\right)_{i-1}$ — gradient of the effective stress/effective plastic strain curve at the position reached at the end of the $(i-1)^{th}$ load stage.

(5) The value of p can thus be found

$$p = \frac{E d\bar{\varepsilon}^p}{(1+\nu)}$$

and the plastic strain/total strain relations give the component plastic strain increments — for example

$$d\varepsilon_\vartheta^p = \frac{d\bar{\varepsilon}^p}{3\varepsilon_{et}}(2\varepsilon'_\vartheta - \varepsilon'_r - \varepsilon'_z).$$

(6) The ratios x, y, z can also be found

$$x = \frac{(2\varepsilon'_\vartheta - \varepsilon'_r - \varepsilon'_z)}{3\varepsilon_{et}} \quad \text{etc.}$$

The gradients of x, y, z and of p can this be calculated and combined to give P_4 (paragraph 7.3.4).

---

† Note regarding work-hardening coefficients;—

Consider the bilinear stress-strain curve shown — the gradients of the two bits are $\tan^{-1}E$ and $\tan^{-1}mE$. Thus for a jump from point 1 to point 2

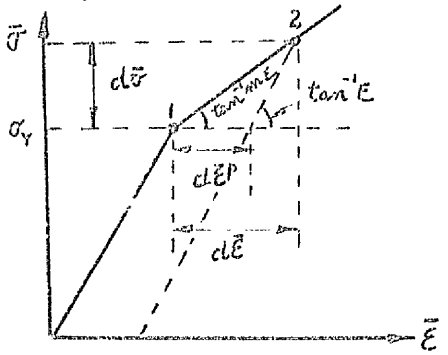

$$mE = \frac{d\bar{\sigma}}{d\varepsilon}$$

therefore $d\bar{\sigma} = mE d\bar{\varepsilon}$. (a)

Also $E = \frac{d\bar{\sigma}}{(d\bar{\varepsilon} - d\bar{\varepsilon}^p)}$, therefore $d\bar{\sigma} = E(d\bar{\varepsilon} - d\bar{\varepsilon}^p)$. (b)

This eliminating $d\bar{\varepsilon}$ from (a) and (b) gives

$$d\bar{\varepsilon}^p E = d\bar{\sigma}\left(\frac{1}{m} - 1\right). \quad \text{But} \quad \frac{d\bar{\varepsilon}^p}{d\bar{\sigma}} = Q.E$$

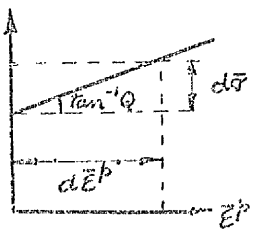

therefore $m = \frac{Q}{(1+Q)}$.

Q is the gradient of the effective stress-effective plastic strain curve.

During this i^{th} load stage ster (1) to (6) are executed for each point after 50 main iterations of the field equations until convergence is achieved, after which the $(i+1)^{th}$ load stage can be tackled, the accumulated plastic strains having been incremented with the current plastic strain increments $(\varepsilon_\vartheta^p + d\varepsilon_\vartheta^p)$.

7.3.6 Evaluation of Stress σ_z.

From the previous paragraph it can be seen that $\bar{\sigma}_{i-1}$ is required and this in turn requires a value for σ_z. In plane strain $\varepsilon_z = 0$ but $d\varepsilon_z^p$ is not zero and after one load stage ε_z^p is non-zero also. Thus after the i^{th} load stage

$$\varepsilon_z = 0 = \frac{1}{E}\left[\sigma_z - \nu(\sigma_r + \sigma_\vartheta)\right] + \varepsilon_z^p + d\varepsilon_z^p$$

and from considerations of constant volume plastic flow

$$\varepsilon_z^p = -(\varepsilon_r^p + \varepsilon_\vartheta^p) \text{ and } d\varepsilon_z^p = -(d\varepsilon_r^p + d\varepsilon_\vartheta^p).$$

Thus $$\sigma_z = \nu(\sigma_r + \sigma_\vartheta) + E(\varepsilon_r^p + \varepsilon_\vartheta^p) + E(d\varepsilon_r^p + d\varepsilon_\vartheta^p).$$

7.3.7 Calculation of Total Strains

From the stresses can be found the elastic strains and to these are added the accumulated plastic strains up to but not including the current load stage and the current plastic strain increments which are found from the Mendelson Manson procedure immediately before the latest settling of field variables. Thus — for example

$$\varepsilon_\vartheta = \frac{1}{E}\left[\sigma_\vartheta - \nu(\sigma_r + \sigma_z)\right] + \varepsilon_\vartheta^p + d\varepsilon_\vartheta^p$$

and of course $\varepsilon_z = 0$.

7.4 Strain Oriented Approach

7.4.1 Introduction

Essentially the stress and strain oriented approaches are very similar. In this case, however, the governing equations are in terms of the total strain functions A, B and C. This at first glance appears to be in the more useful form, since, from the settled field

variables A, B, C can be extracted the total strains which are then fed directly into the Mendelson Manson procedure, from which are found P, X, Y and Z. This means that only strains need be considered in the solution of any one load stage.

Due to the similarity with the stress oriented approach the outline of the method is similar and is not given here. Similarly the sections dealing with the gradients of P, the Mendelson Manson procedure and the evaluation of σ_z, are applicable to this approach and so no comment is made regarding these topics. However the topics unique to this approach are now dealt with below.

7.4.2 Strain Field Equations

For convenience the elasto-plastic strain governing equations (4.39) are repeated here

$$\left.\begin{aligned} AH + CN + 2C &= PZN + PXH + 2PZ \\ CH + BN + B - A &= PZH + PYN + PY - PX \\ A2N + A2H + AN + B2N + B2H + BN &= \frac{P_3}{(1-\nu)} \end{aligned}\right\} \quad (7.5)$$

where $P_3 = -PXN + PX2H + 2PYN + PY2N + 2PZH + 2PZNH.$

The field equations for B and C are formed in a similar way to the stress field equations and once again a circumferential integration of AH is used to calculate A. The equations are as follows

$$B2N + B2H + BN = -A2N - AN + CNH + 2CH - PX2H - PZNH - 2PZH + \frac{1}{(1-\nu)} P_3 \quad (7.6)$$

$$C2N + C2H + 3CN = AH - ANH - BNH - BH + PXNH - PXH + PYNH + PYH + PZ2N + PZ2H + 3PZN \quad (7.7)$$

$$AH = -CN - 2C + PZN + PXH + 2PZ. \quad (7.8)$$

As before equations (7.6) and (7.7) are discretized and the method of solution is one of Successive Over relaxation. The solution of A by circumferential integration is by the technique previously discussed.

7.4.3 Boundary Conditions

The boundaries are very similar to the three variable fixed boundary case dealt with in the last chapter. Consider each boundary fig. 7.1;

(a) On the K = KE bounday B and C are fixed. In addition A is fixed although it will be shown later how this may be 'loosened'.

(b) Over the L = 2 boundary A and B are symmetrical whereas C is asymmetrical and in addition due to symmetry of loading C is zero along this boundary.

(c) On the L = LE boundary C and A are fixed. In addition B is fixed although like A in (a) above, it will be shown later how this may be 'loosened'.

(d) On the K = 2 boundary, C is zero due to there being no shear loading on that boundary. A is not known and is found by circumferential integration like the rest of the field. On the other hand B causes some problem. If one looks at the definition of B viz.

$$B = BS + PY$$

it will be seen that it is made up of the stress BS, which will be zero on this surface due to there being no radial loading, and the plastic strain PY. If part of the notch or hole surface is plastic then B is non-zero and B = PY otherwise in the elastic part B = 0.

The non-zero boundary condition for B on K = 2 has a detrimental effect on the numerical stability. In the method of solution, the K = 2 boundary is treated as a Dirichlet boundary by assigning to B on the plastic part of K = 2 the value of PY from the Mendelson Manson procedure.

7.4.4 Calculation of Total Strains and Stress Components

The governing equations are in terms of A, B and C which are functions of total strains, and from these the total strain components must be extracted to be fed into the Mendelson Manson procedure. This can easily be done by referring back to the definitions of A, B and C and in particular equations (4.22) which are written here in their non-dimensional form

$$\left.\begin{aligned} \frac{E\varepsilon_\vartheta}{\sigma_Y} &= (1-\nu^2)A - \nu(1+\nu)B \\ \frac{E\varepsilon_r}{\sigma_Y} &= (1-\nu^2)B - \nu(1+\nu)A \\ \frac{E\gamma_{r\vartheta}}{\sigma_Y} &= 2(1+\nu)C. \end{aligned}\right\} \quad (7.9)$$

The stress components AS, BS and CS can easily be found from equations (4.24)

$$\left.\begin{aligned} AS &= A - PX \\ BS &= B - PY \\ CS &= C - PZ. \end{aligned}\right\} \quad (7.10)$$

These stresses are of course required after the end of a load stage in order to calculate the effective stress, which in turn is required in the Mendelson Manson procedure for the next load stage.

7.5 The Loosening of the Boundaries

In paragraph 7.4.3 above, mention was made of 'loosening' the boundaries. It will be remembered that two additional boundary restraints were applied –

(a) A or AS was fixed on the K = KE boundary
(b) B or BS was fixed on the L = LE boundary.

Once the stress or strain fields are settled it might be possible to 'loosen' these two constraints gradually to avoid any numerical instability. Consider each in turn

(a) The loosening of A or AS on the KE boundary is achieved easily by merely extending the circumferential integration of AH or ASH out as far as this boundary.

(b) With B or BS, the loosening of the LE boundary is not so easy, since B and BS have field equations and the Neumann boundary condition should be avoided. Different approaches are taken for the Hole and the Keyhole problems.

(1) Hole fig. 7.1

Due to the two axes of symmetry in this problem, B and BS are symmetrical over both the $\mathfrak{L}_1$ and $\mathfrak{L}_2$. In order to use this symmetry condition over the boundary the field is extended to L = 18 = LE and so, over the two $\mathfrak{L}$ boundaries —

$$B_{L=1} = B_{L=3} \quad \text{and} \quad B_{L=19} = B_{L=17}$$
$$BS_{L=1} = BS_{L=3} \quad \text{and} \quad BS_{L=19} = BS_{L=17}.$$

(2) Keyhole fig. 7.7

Unlike the hole, the keyhole configuration has only one line of symmetry — the L = 2 line over which

$$B_{L=1} = B_{L=3} \quad \text{and} \quad BS_{L=1} = BS_{L=3}.$$

However on the open surface, line L = 34, BSH = BH = 0 and so the values of B or BS in areas I and II can be smoothed between the condition of BSH = BH = 0 on L = 34 to the condition of BSH = BH = 0 on L = 2.

In this way a certain amount of constraint could be removed from the field.

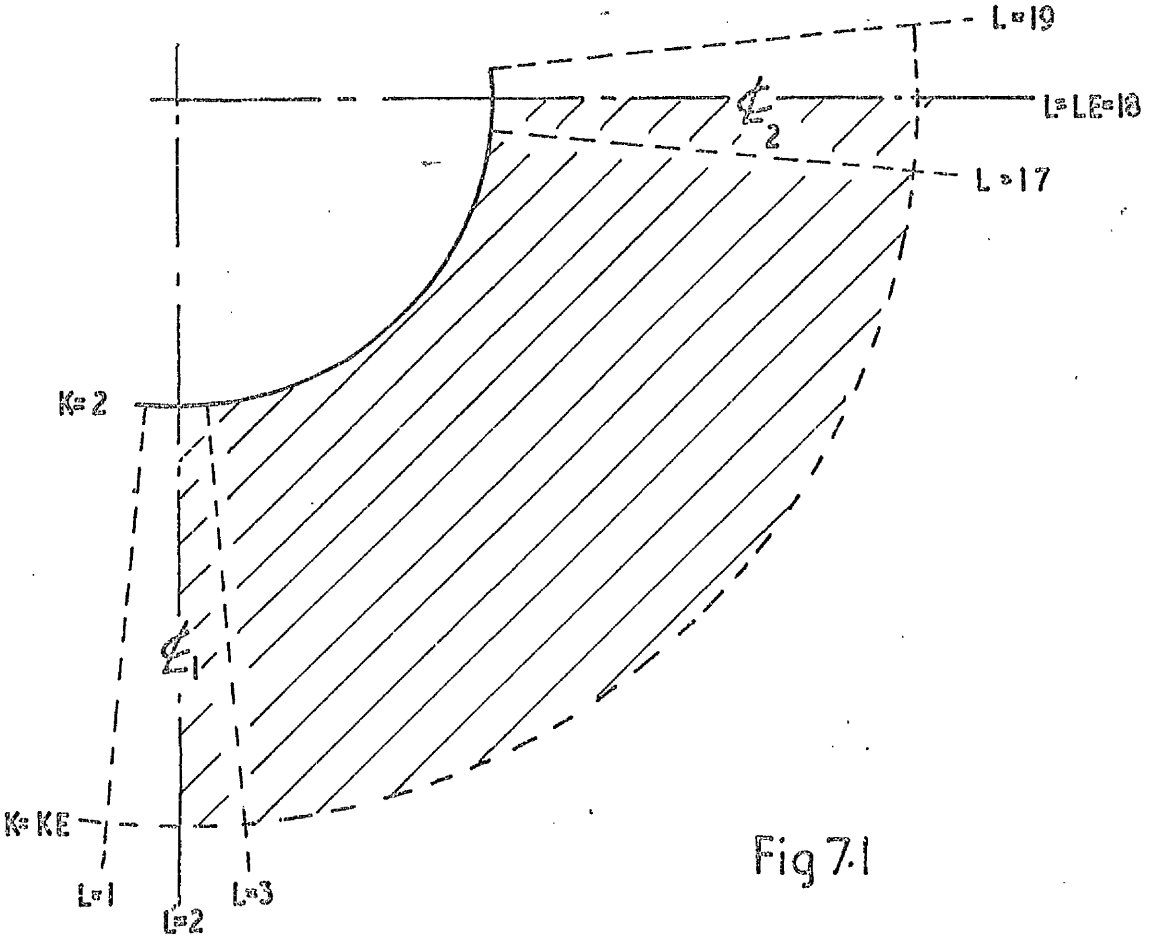

Fig 7.1

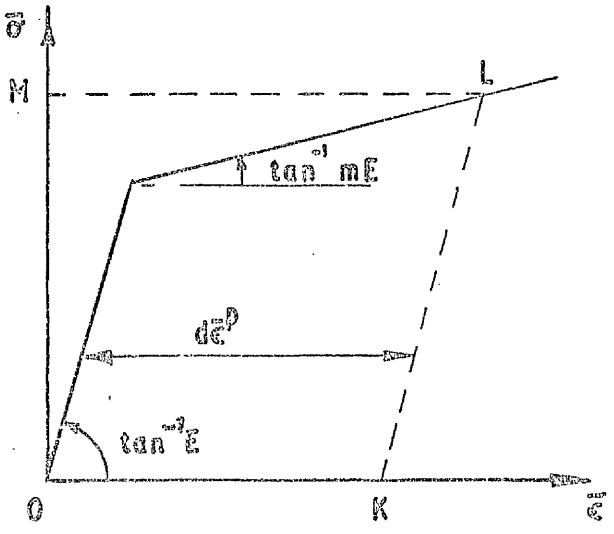

Fig 7.2

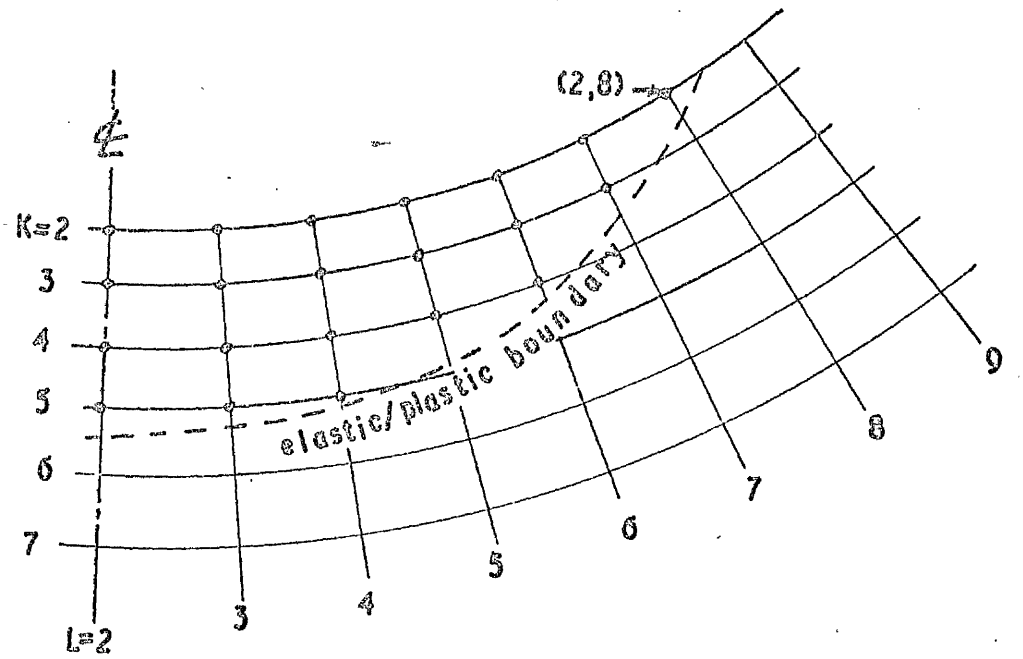

Fig 7.3

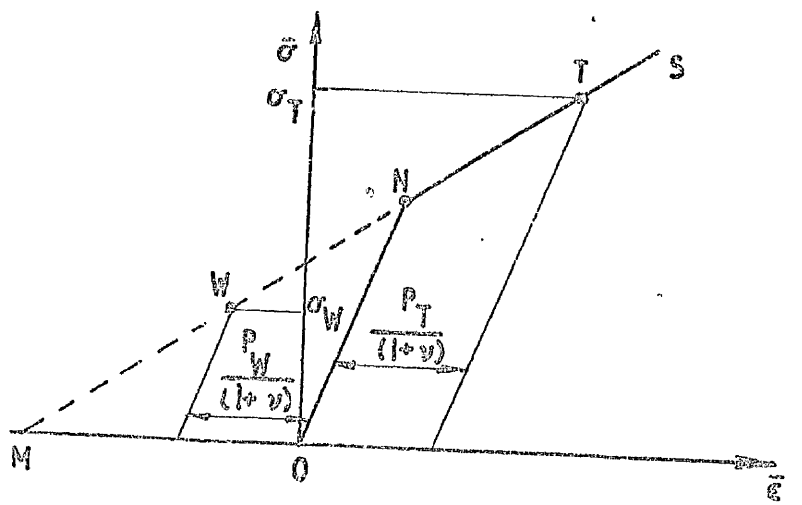

Fig 7.4

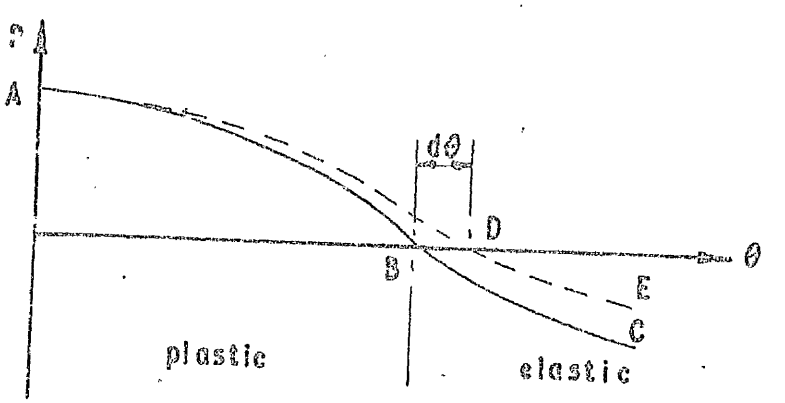

Fig 7.5

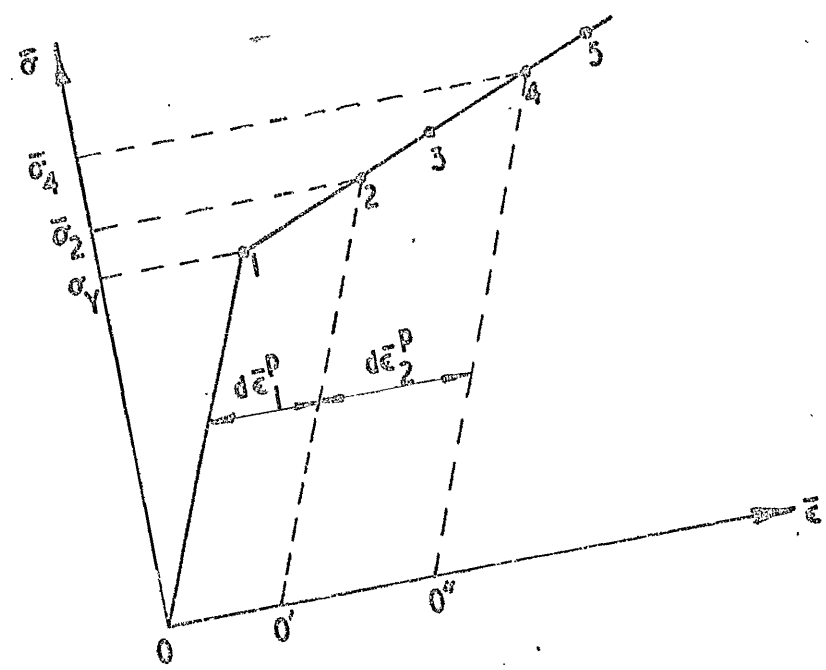

Fig 7.6

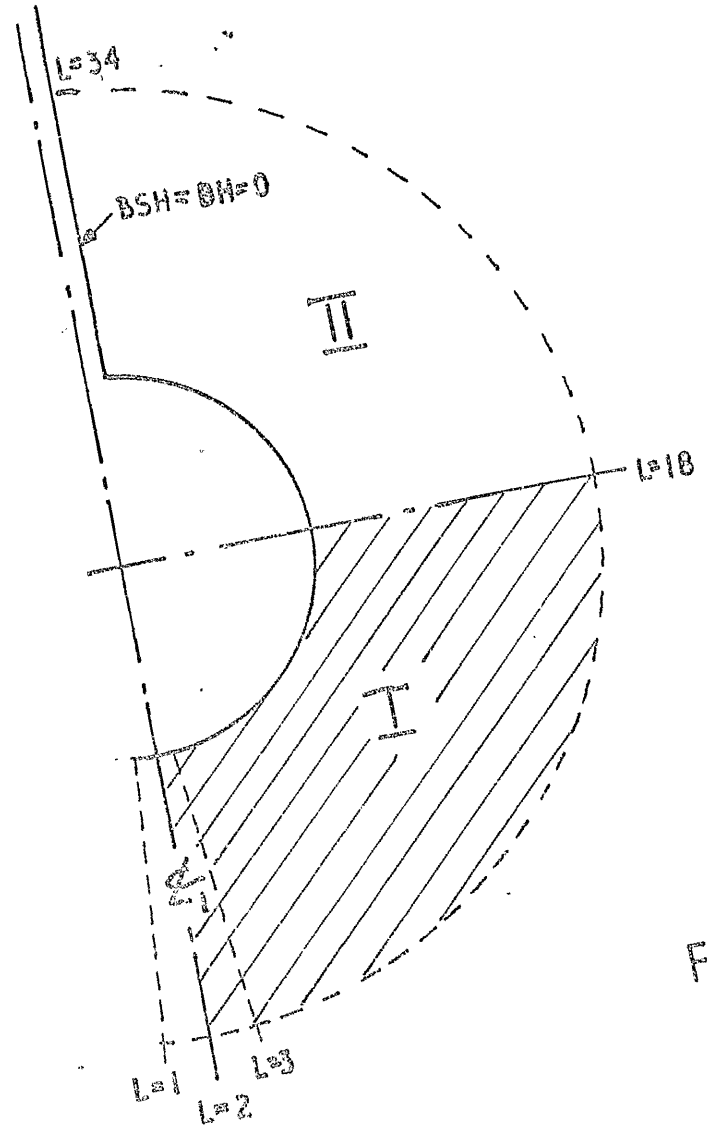

Fig 7.7

CHAPTER 8

RESULTS OF ELASTO-PLASTIC SOLUTIONS

CHAPTER 8

RESULTS OF ELASTO-PLASTIC SOLUTIONS

8.1 Introduction

8.1.1 Main Aims

Two configurations were studied, a hole under uniaxial tension and a keyhole notched specimen in bending. In both, the conditions were plane strain, by making the strain in the through thickness direction equal to zero. The results reflect our interest in the initial stages of plasticity, where the plastic zone is enclosed by an elastic material.

The four main aims were:-

1. To produce a convergent elasto-plastic solution which uses first and second order partial differential equations and which is stable at low work-hardening indexes (Q).
2. To determine values of stress and strain concentration factors for various loads and Q values.
3. To find the variation of plastic zone size and effective plastic strain distribution with load and Q value.
4. To ascertain the state of stress under the surface and, in particular, plot the distribution of the mean to effective stress ratio at various loads and Q values.

Before proceeding with the results in section 8.2, the method of indicating load is detailed in paragraph 8.1.2.

Section 8.3 discusses in more detail the specification of the method and program used.

8.1.2 Method of Indicating Loads

Following the lines of the elastic solution, the boundaries had fixed stress or strain values imposed on them. Fig. 8.1 illustrates the point in the case of the hole in tension, where the boundaries SQ and NS have fixed stress values (AS, BS, CS) and strain values (A, B, C).

As the applied load P increases from zero, the boundary values increase linearly; the effective stress ($\bar{\sigma}$) at M will be the first to exceed yield (σ_Y). Thus at the limit of elasticity $(\frac{\bar{\sigma}}{\sigma_Y})_M = 1.0$, and this loading condition will be denoted by 100%, the applied stress and strain along VW being σ_o and ε_o. If the load is now increased to 150%, for example, the stress σ_o and the still elastic boundary stresses and strains on SQ and NS are incremented by 50%.

Next consider the case of the keyhole notched specimen – fig. 8.2. In chapter 3 the elastic solution was formulated and solved with a scale based only on the radius r_o. The solution covered the field NUVW. To link it up to the test specimen geometry it was assumed that a moment M_Y had been applied to give first yielding at the point N. Using (a) the elastic value of stress concentration, (b) the stress distribution on NU from the elastic solution and (c) an assumed stress distribution on UZ, an approximate value of $M_Y = 2.1$ kNm was obtained (paragraph 3.1.3).

The value of notch opening displacement obtained in paragraph 3.4.4 is plotted against M_Y on fig. 8.3, which also shows the slip line result and the experimental results. It is clear that although yielding has initiated at 2.1 kNm, the overall effect of the elastic mass of material is to give a linear response up to approximately 9 kNm.

For the elasto-plastic solutions the outer boundary UV was brought in to PS (fig. 8.2), fixed stress and strain boundary conditions being imposed along PS and ST. The loading condition corresponding to M_Y will be denoted by 100%. To increment the load, it is assumed that, for example, a 50% increase in M_Y will give a 50% increase in

the reference bending stress (σ_b), and the boundary stresses and strains on PS and ST. This loading condition would thus be denoted by 150%.

The question now arises as to how to relate the solution to fig. 8.3. The yield displacement 0.108 mm was calculated by integrating around the inner surface and up the notch side (NTW – fig. 8.2); this displacement could however have been found by an integration of strains around say UVW or PSS'. In the elasto-plastic solutions, the values of strains along PSS are merely proportionally incremented and so also must be the displacement. Thus if a load of 230% is applied the moment can be assumed to be 2.1 x 2.3 = 4.8 kNm, giving a displacement of approximately 0.2 mm. The reason for this approach is that the effects of plasticity are very local in these initial stages, in which our interests lie.

8.2 Results

8.2.1 Introduction

All results were produced using

(a) the stress oriented approach
(b) a field size with $(\frac{r}{r_o})_{\text{outer}} = 2.281$
(c) fixed boundaries
(d) incremental theory: initial load increment of 50% followed by 20% increments.

Discussion on points (a) to (d) is contained in section 8.3.

In the case of the hole in tension the loading was stopped at 210% since overall yielding occurs at 300%. The keyhole specimen was loaded up to 230%. For both configurations solutions were obtained for the following work-hardening indices –

$$Q = 0.3,\ 0.2,\ 0.1,\ 0.05^{\dagger}$$

---

† The Q values are sometimes quoted as m values where, referring to the figure

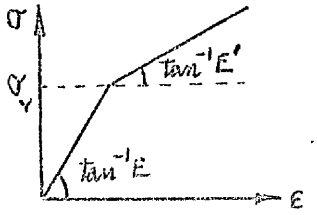

$$m = \frac{E'}{E} = \frac{Q}{1+Q}$$

therefore m value equivalent of Q values above = 0.23, 0.17, 0.09, 0.048.

These Q values might be considered to be on the high side for real materials, but the main interest in this study is the initial stages of plasticity and reference to fig. 8.4 shows that for an aluminium alloy, the value of m only drops to 0.2 (Q = 0.25) at a stress of 1.25 σ_Y.

For all the above Q values and up to the maximum loads for the two configurations convergent solutions were obtained although greater difficulty was experienced at low work-hardening and high loads. The program was run on a UNIVAC 1108 computer and each solution took approximately 25 minutes and cost approximately £ 50.

8.2.2 Stress and Strain Concentration Factors

The stress and strain concentration factors are defined differently for each configuration

(i) Hole in Tension:-

Referring back to fig. 8.1 the stress concentration factors are:-

Circumferential - $K\sigma_\vartheta$ is the ratio of the circumferential stress at M to the applied stress σ_o on the line VW

$$K_{\sigma_\vartheta} = \frac{(\sigma_\vartheta)_M}{\sigma_o} \quad (= 3 \text{ in the elastic case}).$$

Effective - $K_{\bar{\sigma}}$ is the ratio of the effective stress at M to the applied stress σ_o

$$K_{\bar{\sigma}} = \frac{(\bar{\sigma})_M}{\sigma_o} \quad (= 2.66 \text{ in the elastic case}).$$

The strain concentration factor $K_{\varepsilon_\vartheta}$ is defined as the ratio of the total circumferential strain at M to the strain ε_o along VW

$$K_{E_\vartheta} = \frac{(\varepsilon_\vartheta)_M}{\varepsilon_o} \quad (= 3 \text{ in the elastic case}).$$

(ii) Keyhole Notch Specimen:-

Referring back to fig. 8.2 the stress concentration factors are:-

Circumferential - K_{σ_ϑ} is the ratio of the circumferential stress at N to the reference bending stress σ_b

$$K_{\sigma_\vartheta} = \frac{(\sigma_\vartheta)_N}{\sigma_b} \qquad (\doteq 4.7 \text{ in the elastic case}).$$

Effective — $K_{\bar{\sigma}}$ is the ratio of the effective stress at N to the reference bending stress σ_b

$$K_{\bar{\sigma}} = \frac{(\bar{\sigma})_N}{\sigma_b} \qquad (\doteq 4.18 \text{ in the elastic case}).$$

The strain concentration factor $K_{\varepsilon_\vartheta}$ is defined as the ratio of the total circumferential strain at N to the strain ε_b, due to σ_b and the plane strain σ_z component

$$K_{\varepsilon_\vartheta} = \frac{(\varepsilon_\vartheta)_N}{\varepsilon_b} \qquad (\doteq 4.7 \text{ in the elastic case}).$$

Figs. 8.5 and 8.6 show the variation of K_{σ_ϑ} and $K_{\bar{\sigma}}$ with load and Q index for the hole in tension and figs. 8.9 and 8.10 show the similar graphs for the keyhole notch specimen. In both cases is displayed the unusual feature of the 'tail' which tends to rise, the turning point being at higher loads the lower the Q value. The explanation, of which the proof is given in paragraph 9.4.2, is that it is due to the effect of the linear work-hardening.

Figs. 8.7 and 8.11 show the strain concentration factors $K_{\varepsilon_\vartheta}$ for the hole and keyhole respectively for varying loads and Q values. The very large increase especially at low Q values is probably due to plane strain conditions.

In the case of the hole in tension, comparison of plane stress and plane strain, stress and strain concentration factors is given on fig. 8.8. The plane stress curves are from Tuba[19] for a steel and an aluminium alloy with Q values of around 0.05; Tuba's results are compared favourably in his paper with experimental results. The most notable feature is the large rise in strain concentration due to the $\varepsilon_z = 0$ restriction.

8.2.3 Effective Plastic Strain

Fig. 8.12 and 8.14 illustrate the development with

load of effective plastic strain for hole and keyhole respectively using a work-hardening index $Q = 0.1$. The variation of effective plastic strain distribution and shape of elastic-plastic boundary with Q is given for the hole in fig. 8.13 and for the keyhole in fig. 8.15. Some common features emerge from the latter graphs;-

(a) the similar shape of the strain distribution both along the surface $r = r_o$ and down the $\mathbb{C}$ $\vartheta = 0^o$ in each solution

(b) the very small change in extent of plastic zone on the surface $r = r_o$ with different loads and Q values in both solutions

(c) the very little difference in size and shape of plastic zone with varying Q at the same load in each solution

(d) the noticeable difference in the value of effective plastic strain at the point $r = r_o$, $\vartheta = 0^o$ with varying Q at the same load, in each solution.

For the hole in tension, fig. 8.13(c) shows the comparison of plane stress and plane strain plastic zone based on the results of Tuba[19] for SAE 4130 steel at approximately the same load. Tuba's results in turn favourably compare with the experimental results of Theocaris and Marketos[33]. Of interest is the formation of the plastic 'wing' at higher loads, this being due on the one hand to the build up of mean stress along the $\mathbb{C}$ $\vartheta = 0^o$ and on the other hand to the higher shear stress values existing in the centre of the field.

On fig. 8.15(c) for the keyhole is included the plastic zone obtained from the slip line solution of chapter 10. It was noted from experiment (fig. 10.4) that the extent of yielding was approximately 70^o on either side of the $\mathbb{C}$; it will be seen that this is borne out by the elasto-plastic solution. No value of effective plastic strain from the slip line solution are plotted on figs. 8.14 or 8.15 due to the difficulty of matching up displacement boundary conditions, but the shape of the curves on fig. 10.12 gives some confirmation.

8.2.4 Distribution of $\frac{\sigma_m}{\bar{\sigma}}$ along $\measuredangle\, \vartheta = 0^o$

The mean to effective stress ratio $\frac{\sigma_m}{\bar{\sigma}}$ is of interest in our fracture studies in that it gives an indication of stress state and ductility as well as being of use in the void growth formula. Figures 8.16 and 8.17 give the distribution, along the $\measuredangle\, \vartheta = 0^o$, of $\frac{\sigma_m}{\bar{\sigma}}$ at various loads, with Q values 0.1 and 0.05 respectively for the hole in tension. Similar graphs for the keyhole notch specimen are given in figs. 8.18 and 8.19.

Two unusual features are immediately obvious in these four sets of graphs

(i) in the region of the elastic plastic boundary there is a 'kink' in the curves

(ii) there is a noticeable rise over the elastic (100%) value at a radius $\frac{r}{r_o} = 1.8$ at 150% load, this rise reducing with increasing load.

Consider these features separately –

(i) To explain this feature reference should be made to Chapter 9, in which the mean to effective stress distribution for the thick sphere under pressure also shows a 'kink' in the vicinity of the elastic plastic boundary. This is investigated thoroughly in paragraph 9.4.3 and the conclusion arrived at is that it is due to 'the continuous derivatives being taken over the elastic/plastic boundary'.

(ii) This feature cannot be so easily explained as (i) above. However a clue can be found by noticing that the effect is more noticeable in the hole than the keyhole (e.g. figs. 8.16 and 8.18) and that the shape of the plastic zone for each configuration is markedly different (e.g. figs. 8.12(c) and 8.14(c)).

It is known that, in the elastic case, a smaller radius r_o will give a higher rise in the value of $\frac{\sigma_m}{\bar{\sigma}}$ under the surface. When plasticity developes, the value of $\frac{\sigma_m}{\bar{\sigma}}$ at $r = r_o$ will rise to approximately 0.58 for very large

plastic strains ($\nu \Rightarrow 0.5$). However this does not explain the rise under the surface. Referring to fig. 8.12(c), for example, it will be seen that at the early stages of plasticity (150% load), the 'mean' radius of the elastic–plastic boundary is just over 0.6 r_o. If one assumes that the material within this boundary is unable to sustain its proportion of the load then this means that the equivalent inner radius for the remaining elastic zone is less than r_o and the $\frac{\sigma_m}{\bar{\sigma}}$ value under the surface is consequently higher. Referring to the keyhole – fig. 8.14(c) the mean radius of the elastic–plastic boundary at 150% is nearer r_o and so the difference of values of $\frac{\sigma_m}{\bar{\sigma}}$ at 100% and 150% is not so marked. In both configurations as plasticity developes the 'mean' elastic–plastic boundary radius increases and so reduces the value of $\frac{\sigma_m}{\bar{\sigma}}$ in the elastic region under the surface.

Included on figs. 8.18 and 8.19 for the keyhole is the distribution obtained from the slip line solution – fig. 10.13. It is clear that as the loading increases, the elasto–plastic distribution tends towards the rigid–plastic solution and more so with lower Q values, as expected.

8.3 Discussion

At the beginning of paragraph 8.2.1, the conditions under which the results were produced, were stated. Several checks were made, however, before the final decision was reached and these are detailed below.

Strain or Stress Oriented Approaches? Details of both approaches are found in Chapter 7. The main difference lies in the boundary conditions existing in the plastic region on the inner boundary; in the strain approach both $A^\dagger$ and $B^\dagger$ are unknown whereas in the stress approach only $AS^\dagger$ is

---

† $A = (1-\nu^2)\frac{E\varepsilon_\vartheta}{\sigma_Y} - \nu(1+\nu)\frac{E\varepsilon_r}{\sigma_Y}$, $\quad B = (1-\nu^2)\frac{E\varepsilon_r}{\sigma_Y} - \nu(1+\nu)\frac{E\varepsilon_\vartheta}{\sigma_Y}$.

$AS = \frac{\sigma_\vartheta}{\sigma_Y}$.

unknown. The result of this complexity in the former approach is that for any significant change in load, instability occurs due to the large increase in strain in the plastic regime. The stress oriented approach was thus used.

The boundary restriction on the strain oriented approach does not completely debar its used. The hole and the keyhole problems are essentially stress boundary defined and obviously the stress oriented approach is to be preferred; any problems with strain boundary controls would use the strain oriented approach.

At a load of 150% and a work-hardening index $Q = 0.3$, the plane strain elasto-plastic solution of the hole, gave almost identical results using both approaches.

Field Size and Boundaries. There was some doubt as to the size of field to be used; if the outer boundary PS (figs. 8.2 and 8.20) was too near the inner boundary the extent of plasticity could be affected. The L boundaries PN and ST were maintained.

As a check two solutions were obtained for the hole in tension at 150% load and $Q = 0.3$, with outer boundaries $\frac{r}{r_o} = 1.912$ and $\frac{r}{r_o} = 2.281$. The effect on plasticity was minimal, but it was decided to maintain the K = 14 outer boundary in case the effect was more noticeable at higher loads. Mendelson[3] confirms this finding in his solution of a crack in an infinite plate, where, in fact, his plastic zone approaches much closer to the boundary.

One final question regarding boundaries needs to be resolved. Can the boundaries be 'loosened' as suggested in section 7.5? To check this out, the solution for the hole in tension was solved for 150% load, $Q = 0.3$ and fixed boundaries; the outer L and K boundaries (ST and PS) were then freed in turn for BS and AS respectively. The effect in both cases was at worst, of the order of 2-3% and the slight perturbation slowly converged. Due to the minimal changes and the extra time and cost of running the programs longer, it was decided that the loosening of the boundaries

was not justified.

Incremental or Deformation Theories? In 1965, Tuba[14] gave his results for the elasto-plastic solution of a hole in an infinite plate under uniform stress. For this geometry he rightly points out that incremental and deformation theories coincide. Essentially the reason for this is the radial symmetry of loading and geometry as in the sphere (see Chapter 9). In a footnote Tuba states '... for the non-radial type of problems the two methods (incremental and deformation) can differ considerably from each other. The incremental theory should be used'. However in 1967 when dealing with the solution for the hole in a plate in uniaxial tension[19] he states 'although it is known that the incremental theories give more realistic solutions, the present examples are worked out for a deformation theory ...' because it '... requires less work than the incremental theory'.

It was decided to check the present solutions using both theories applied to the stress oriented solution of the hole in tension with $Q = 0.3$. It was done in the following way;-

Incremental:

(a) An elastic solution (100%) was incremented to 150% and then with three more load stages of 20% up to 210%.

Deformation:

(b) An elastic solution (100%) was loaded to 150% in one load stage. Another solution was loaded in one stage from 100% to 160% and another from 100% to 170% and so on up to 200%.

The minimum first load increment must be ~ 50% to allow the plastic zone to have significantly established. The effect of (a) and (b) above is clearly shown in two ways (1) concentration factors, (2) effective plastic strain.

(1) The stress concentration factor K_σ and strain concentration factor $K_{\varepsilon_\vartheta}$ are defined in paragraph

8.2.2. The graphs of these factors against load are given in figs. 8.21 and 8.22. A noticeable difference is obvious as the load increases over 150%.

(2) The effective plastic strain at 190% load is plotted along the $\measuredangle\ \vartheta = 0^{o}$ in fig. 8.23 and along the inner surface in fig. 8.24. Once again the incremental and deformation theories produce a noticeable difference at the high strain positions. It is interesting to note, however, that the extent of the plastic zone does not vary significantly.

The incremental theory should be used, but with what size of load increment. As has been stated a first load increment of 50% is necessary. The load increments thereafter are determined by two factors; if a particular load has to be reached one can either (i) take a few load stages and large load increments or (ii) take a large number of load stages of small load increments. Both ways produce inaccuracies and so a compromise of a 20% load increment was used for all the results.

The elasto-plastic solutions obtained for the hole in tension and the notched keyhole specimen are both under conditions of plane strain. It is the plane strain keyhole solution which is required by the fracture research program because there is no experimental way of finding the stress and strain fields under the notch in the centre of the thick bar.

In both configurations, experimental confirmation under plane strain conditions is not possible. One can however find experimental plane stress results; much information has been gathered by the aero-industry for perforated tension panels. Plane stress data for notch bend tests is not so readily available, and in any case the results from them are not very meaningful in this context.

Analytical or numerical confirmation of plane strain solutions is also not readily available; two papers by Wilshaw, Rau and Tetelman[30] and Griffiths and Owen[31]

tackle similar problems. The paper by Wilshaw et al uses Neuber's stress concentration factors and slip line fields; a similar slip line solution is given in Chapter 10 and this is used as a check of results. The paper by Griffiths and Owen deals with larger strains leading to overall yielding, also a very low work-hardening index is used.

8.4 Conclusions

In the introduction section 8.1, four aims were set down, these have all been achieved in section 8.2.

1. A solution is definitely possible right down to a Q of 0.05 although care must be taken at low Q values and large loads. The method is elliptic.
2. Stress and strain concentration factors have been evaluated and despite the 'tail' on K_{σ_ϑ} and $K_{\bar{\sigma}}$, the stress concentration factors show modest reductions while the strain concentration factors show a marked increase — all as expected.
3. Effective plastic strain distributions have been plotted and despite a noticeable difference of values with varying work-hardening the plastic zone size remains relatively similar.
4. The ratio of mean to effective stress distribution shows markedly different values for the hole and the keyhole and both show an initial increase under the surface; this increase decays with increasing load. In the keyhole the distribution is shown tending towards the slip line solution.

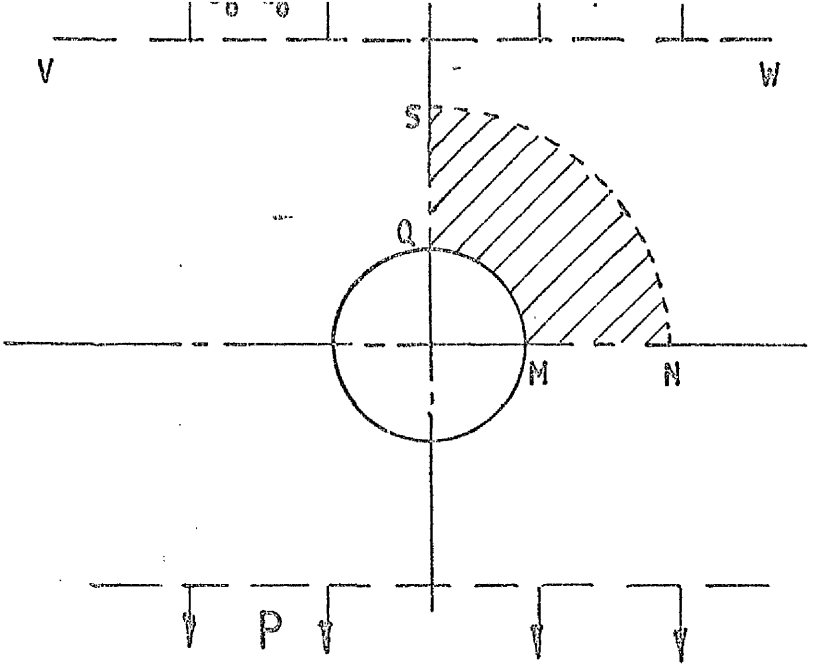

Fig 8.1

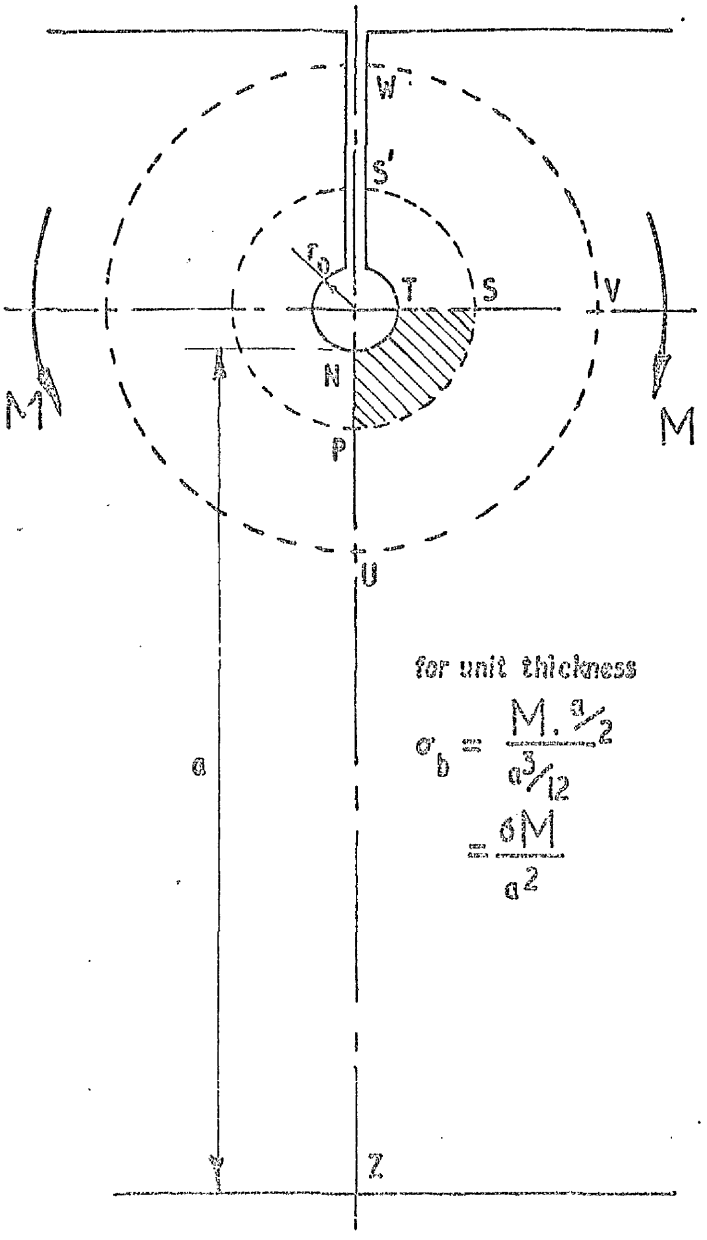

for unit thickness

$$\sigma_b = \frac{M \cdot a/2}{a^3/12} = \frac{6M}{a^2}$$

Fig 8.2

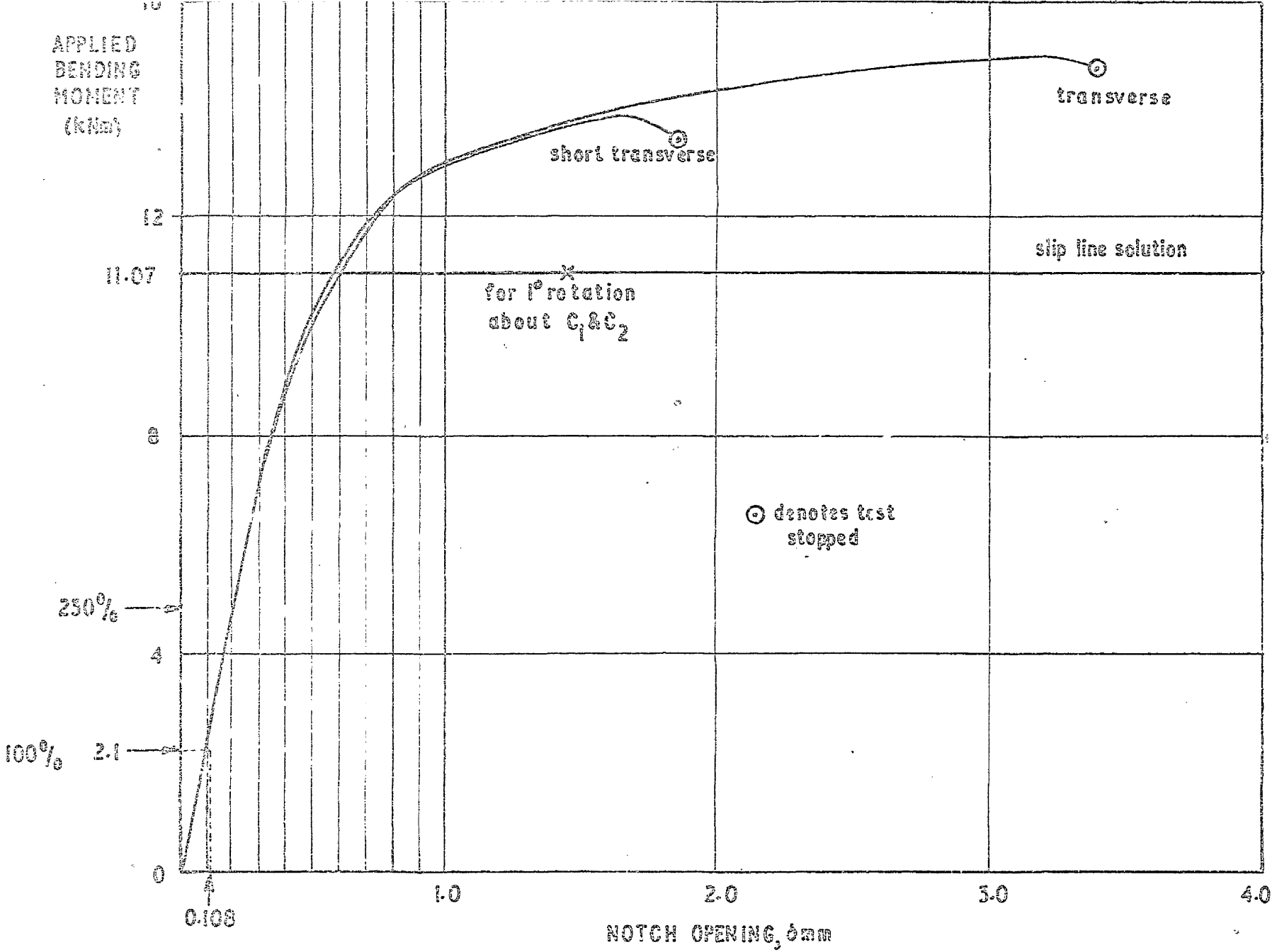

Fig 8.3 Notch bend tests (ref (42))

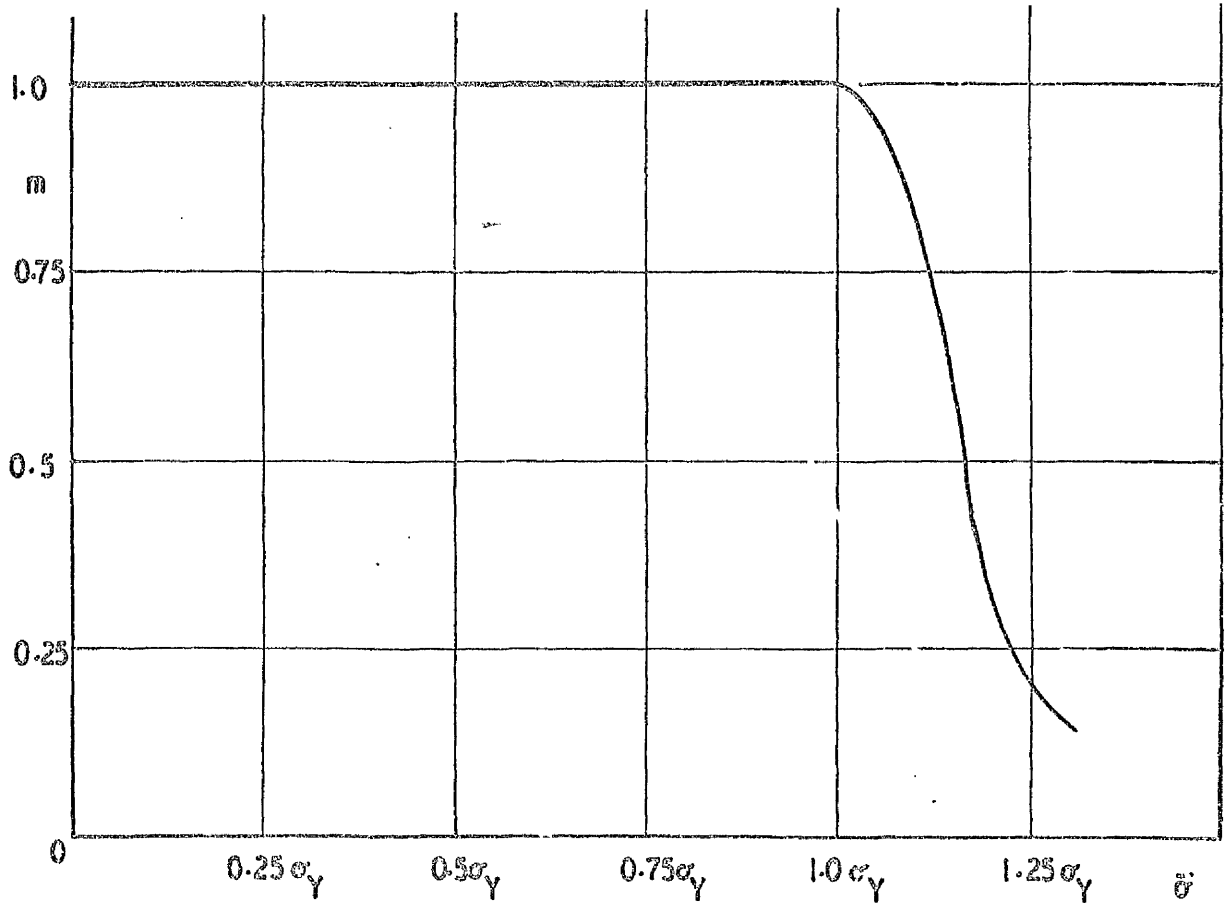

Fig 8.4 Values of m for 24S-T3 aluminium alloy (ref Stowell [32])

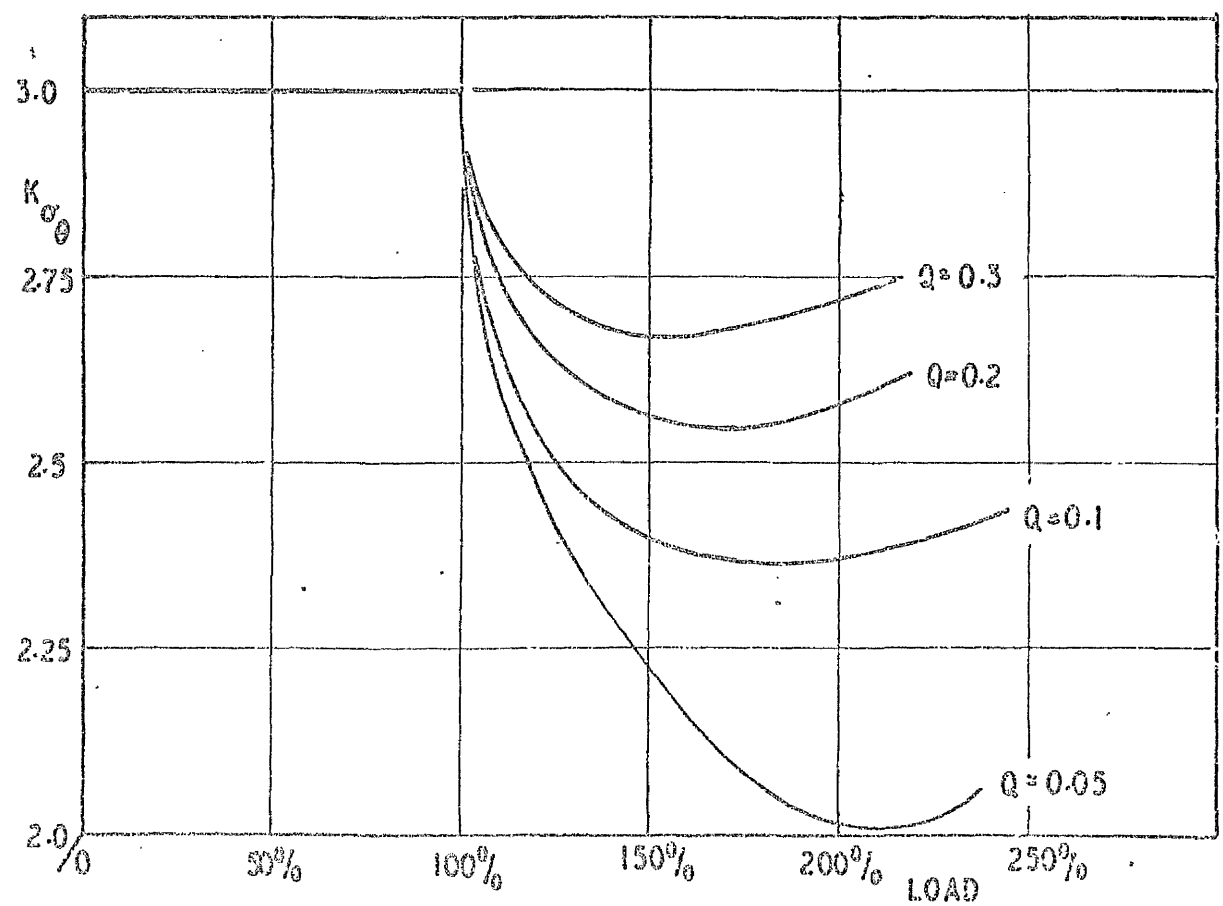

Fig 8.5 K_{σ_θ} for hole in tension - plane strain

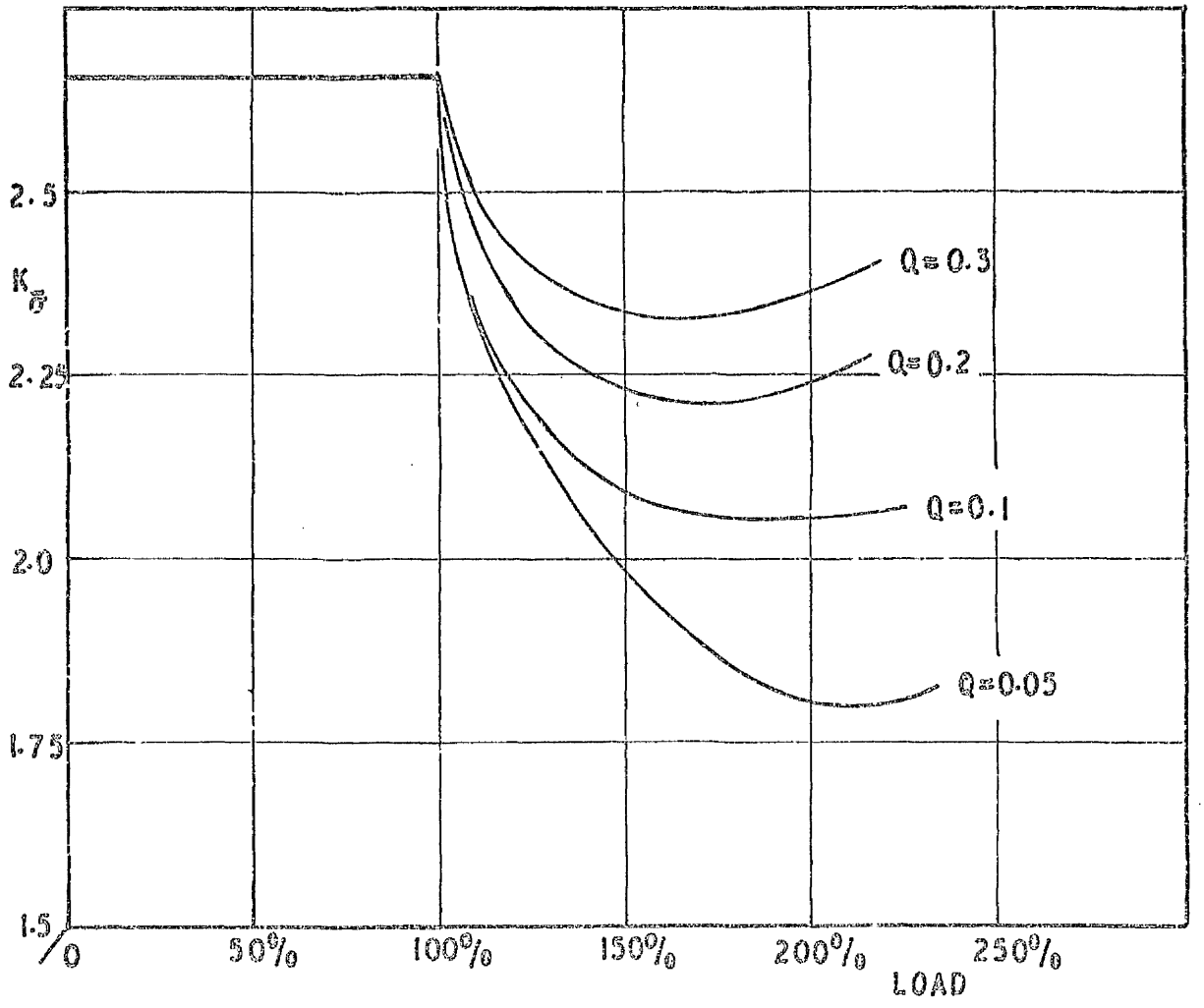

Fig 8.6 K_σ for hole in tension
– plane strain

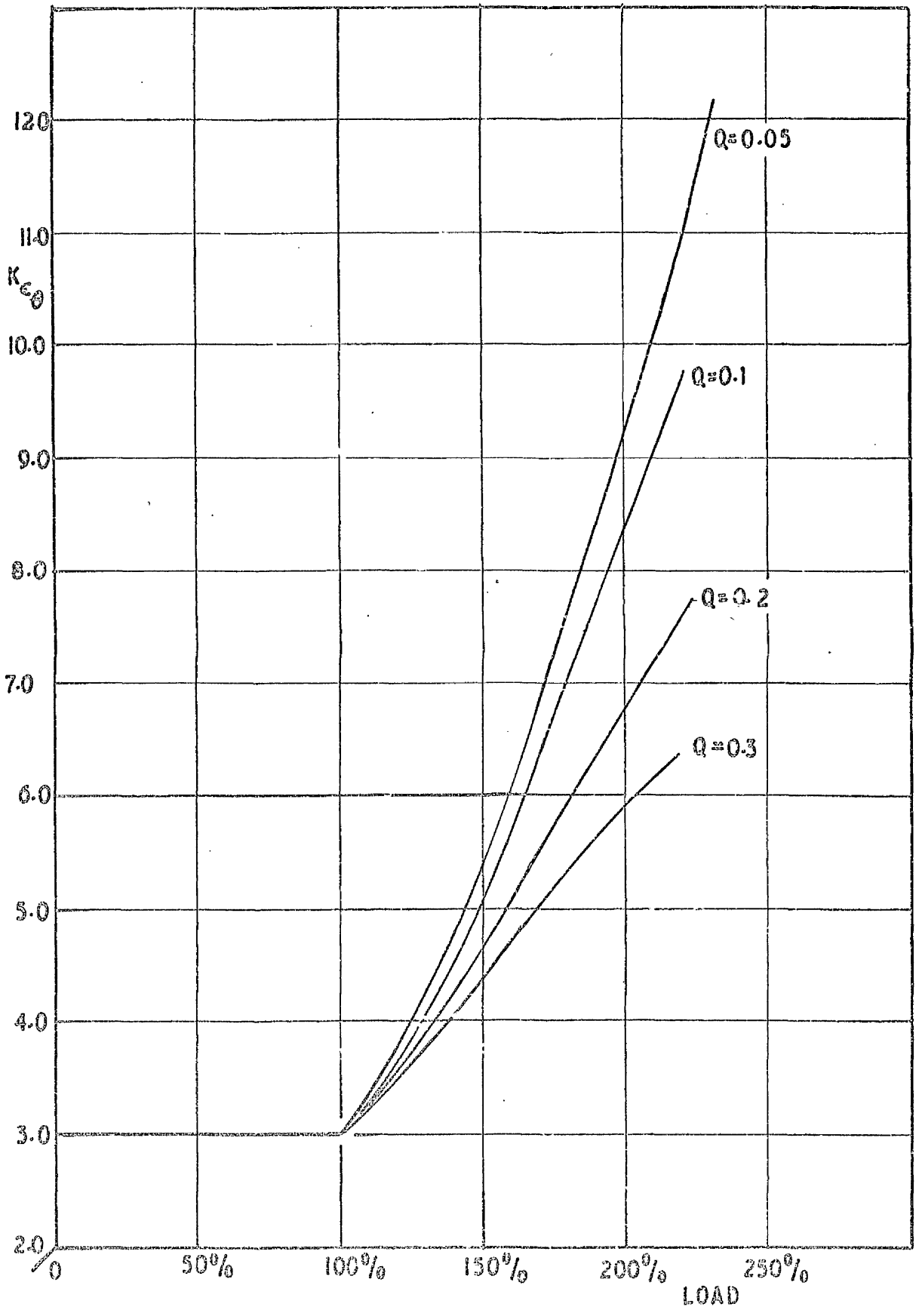

Fig 8.7 $K_{\epsilon\theta}$ for hole in tension - plane strain

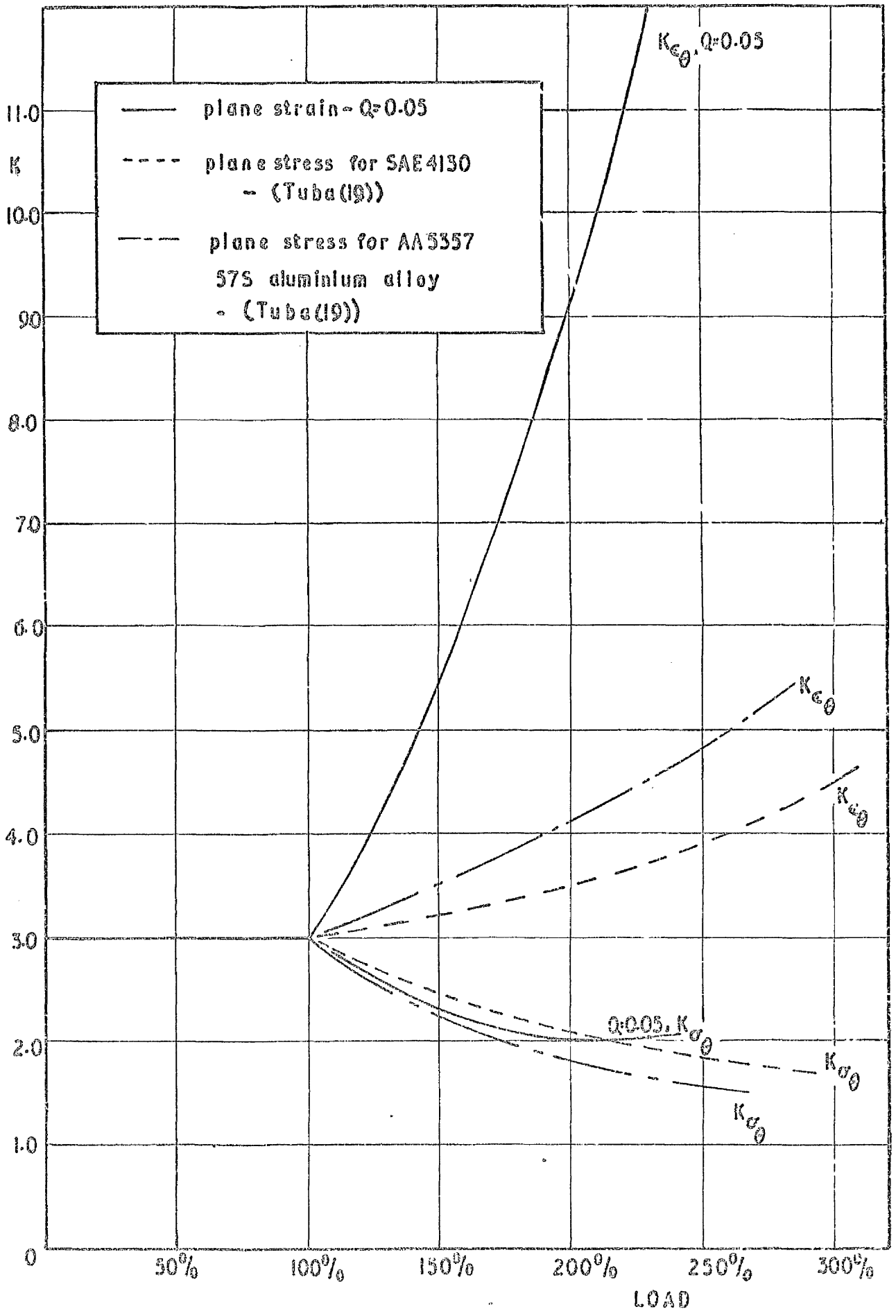

Fig 8.8 Comparison of $K_{\sigma\theta}$ and $K_{\epsilon\theta}$ under plane stress and plane strain

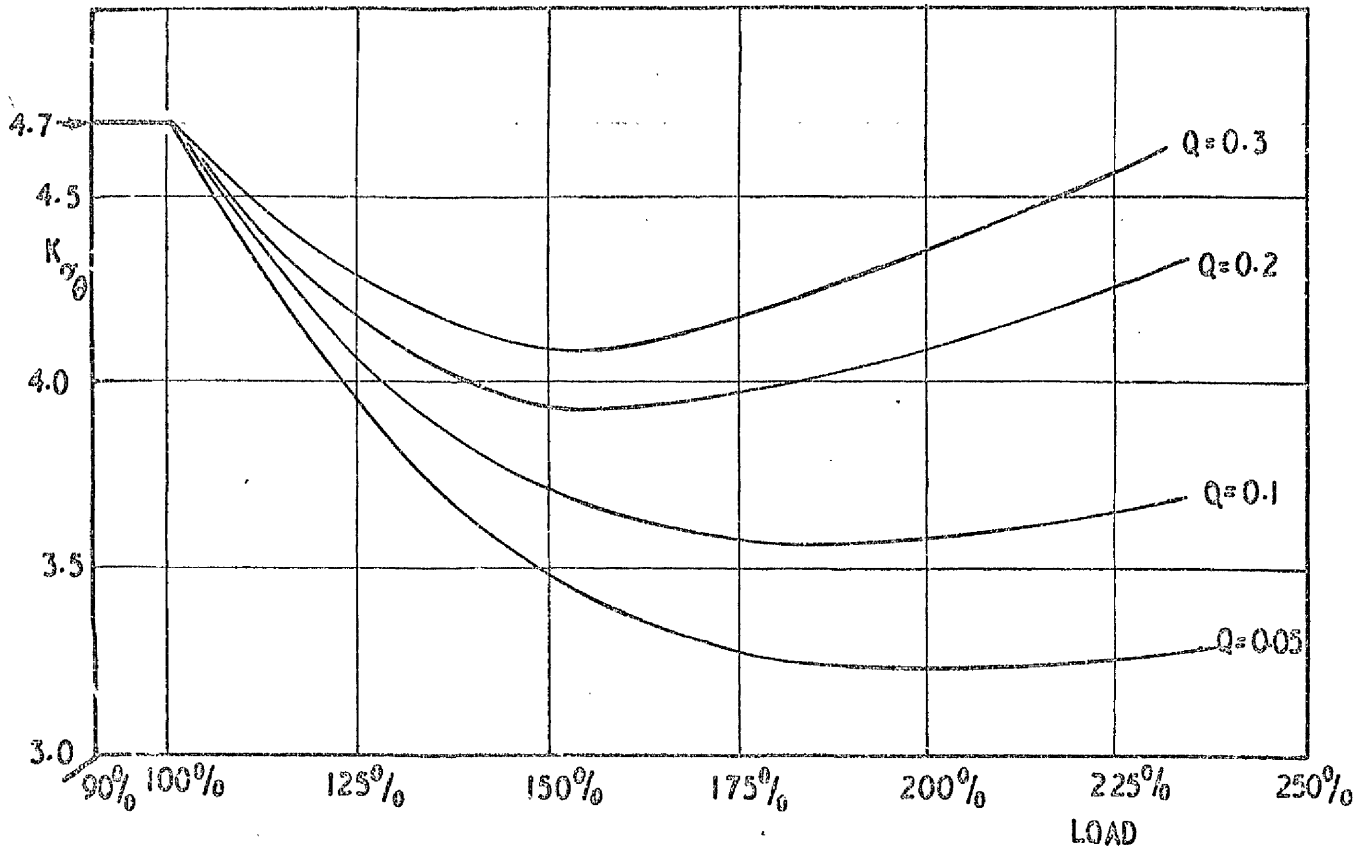

Fig 8.9 K_{σ_θ} for keyhole-plane strain

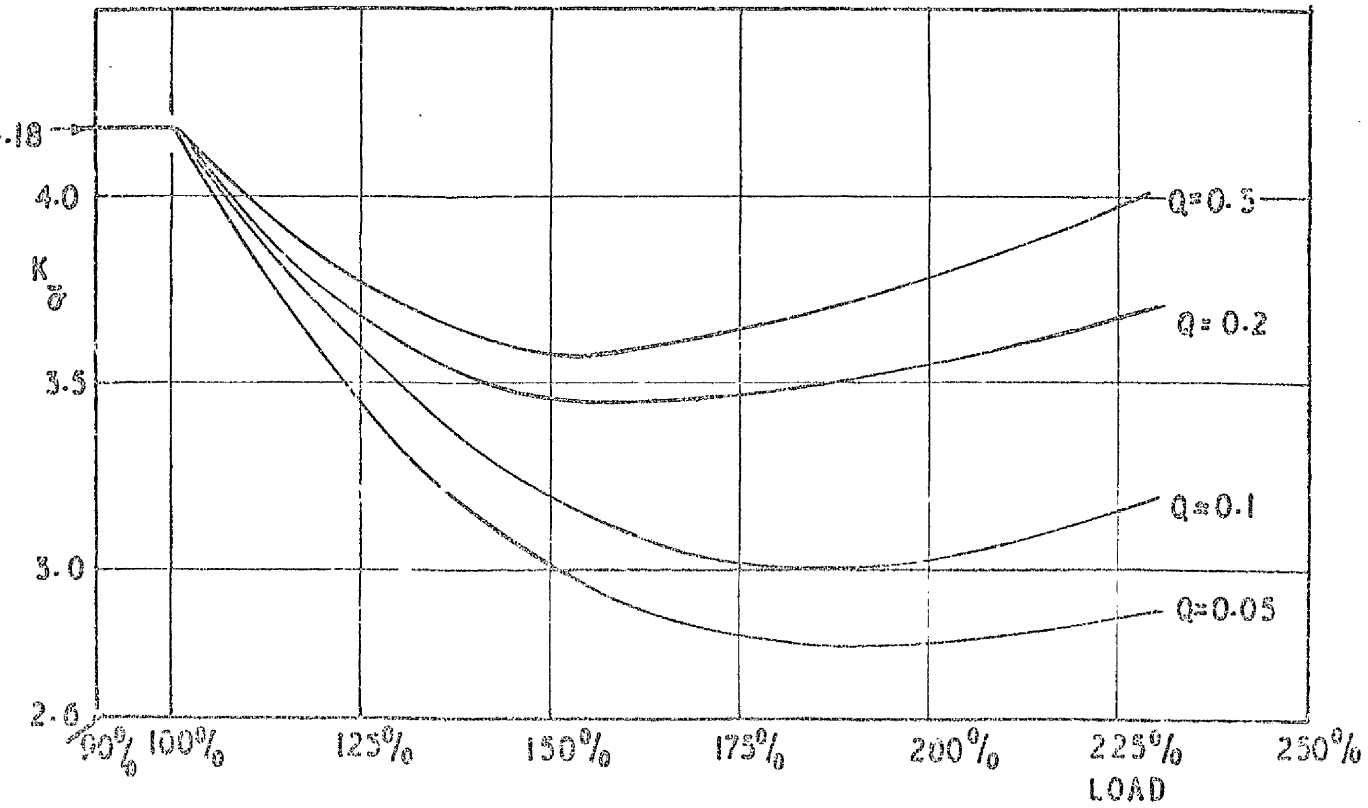

Fig 8.10 $K_{\bar{\sigma}}$ for keyhole-plane strain

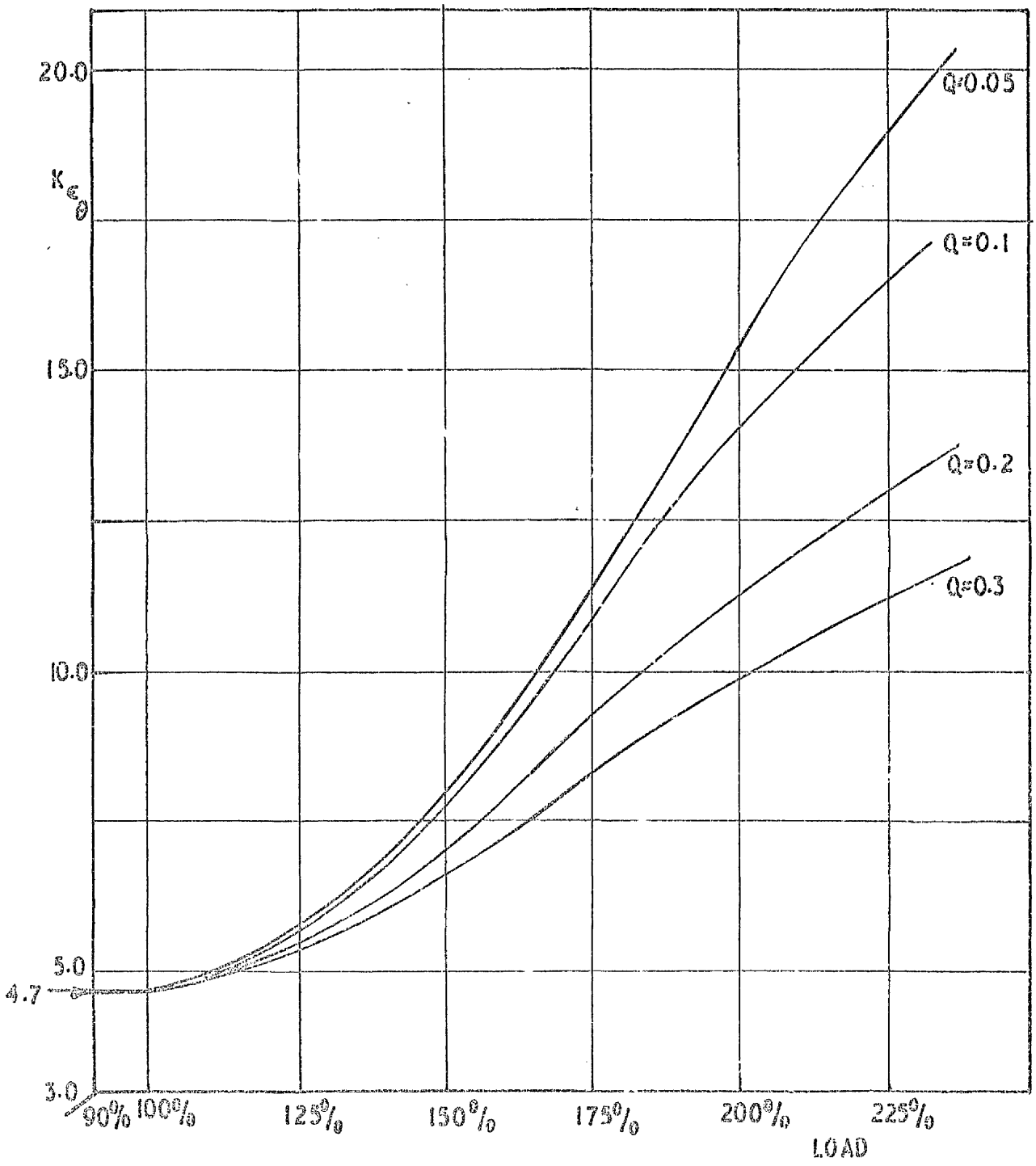

Fig 8.11 K_{ϵ_θ} for keyhole-plane strain

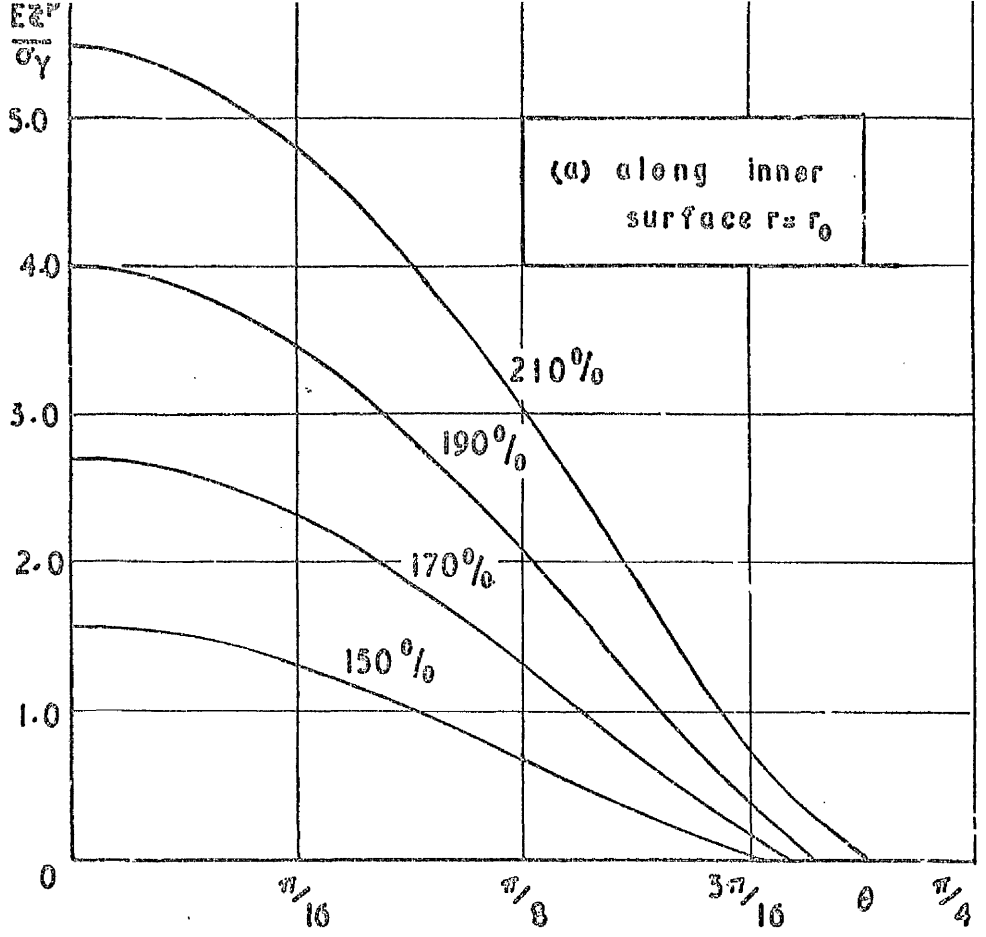

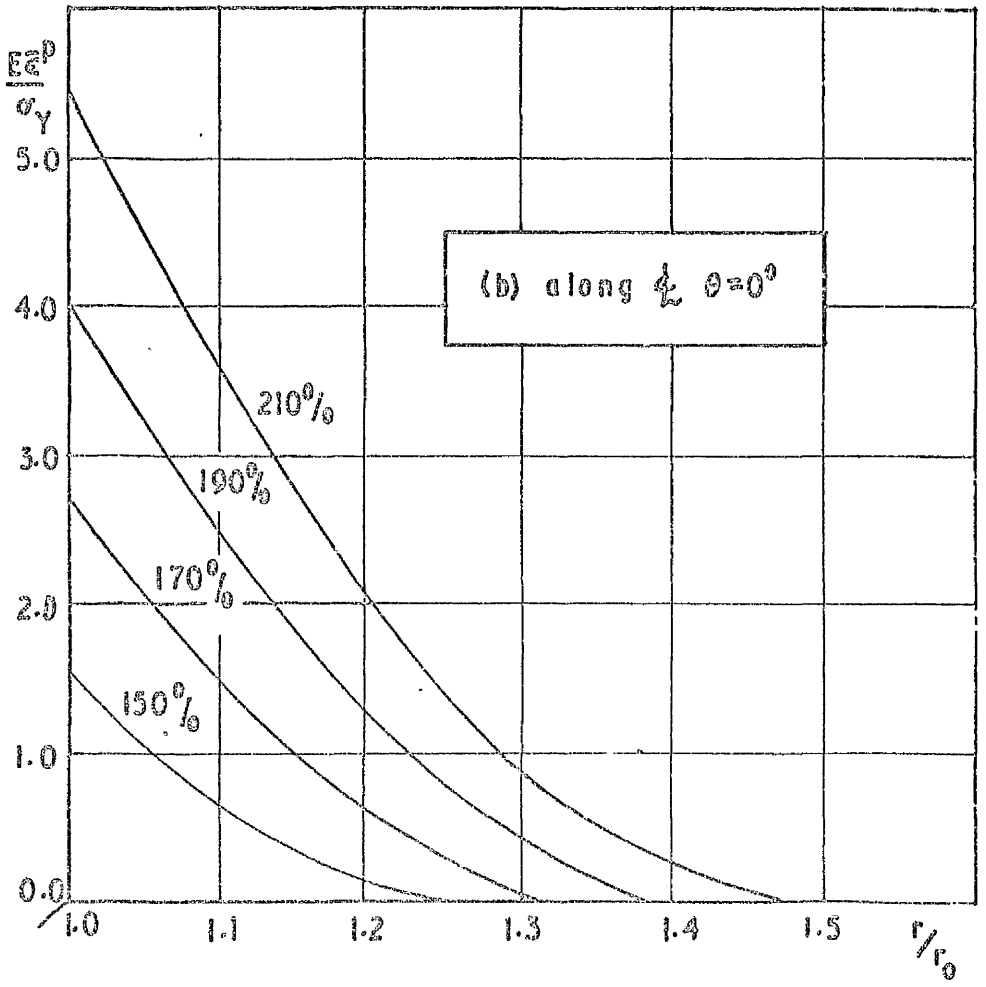

Fig 8.12 Development of effective plastic strain with load for hole in tension, Q=0.1

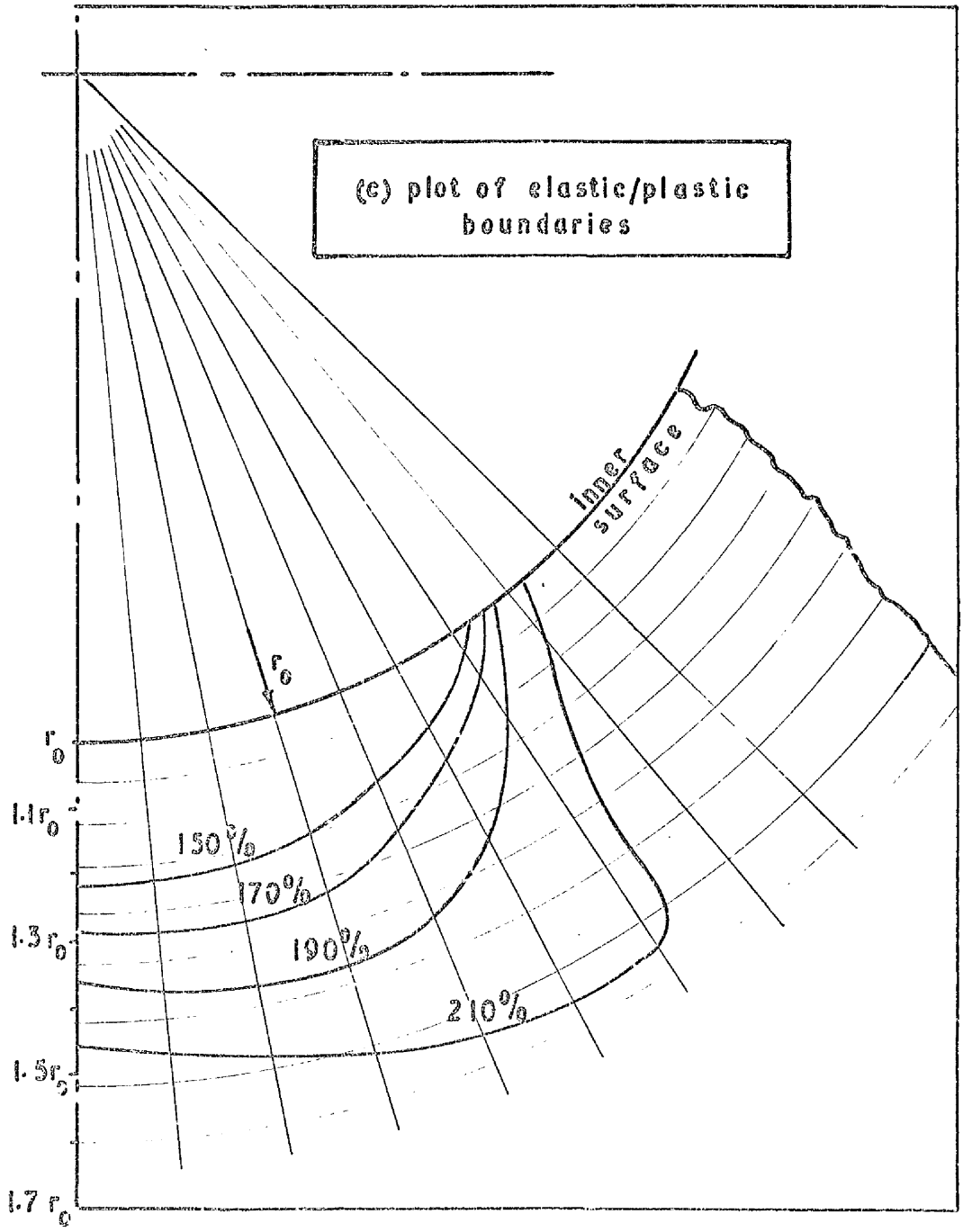

Fig 8.12 (continued)

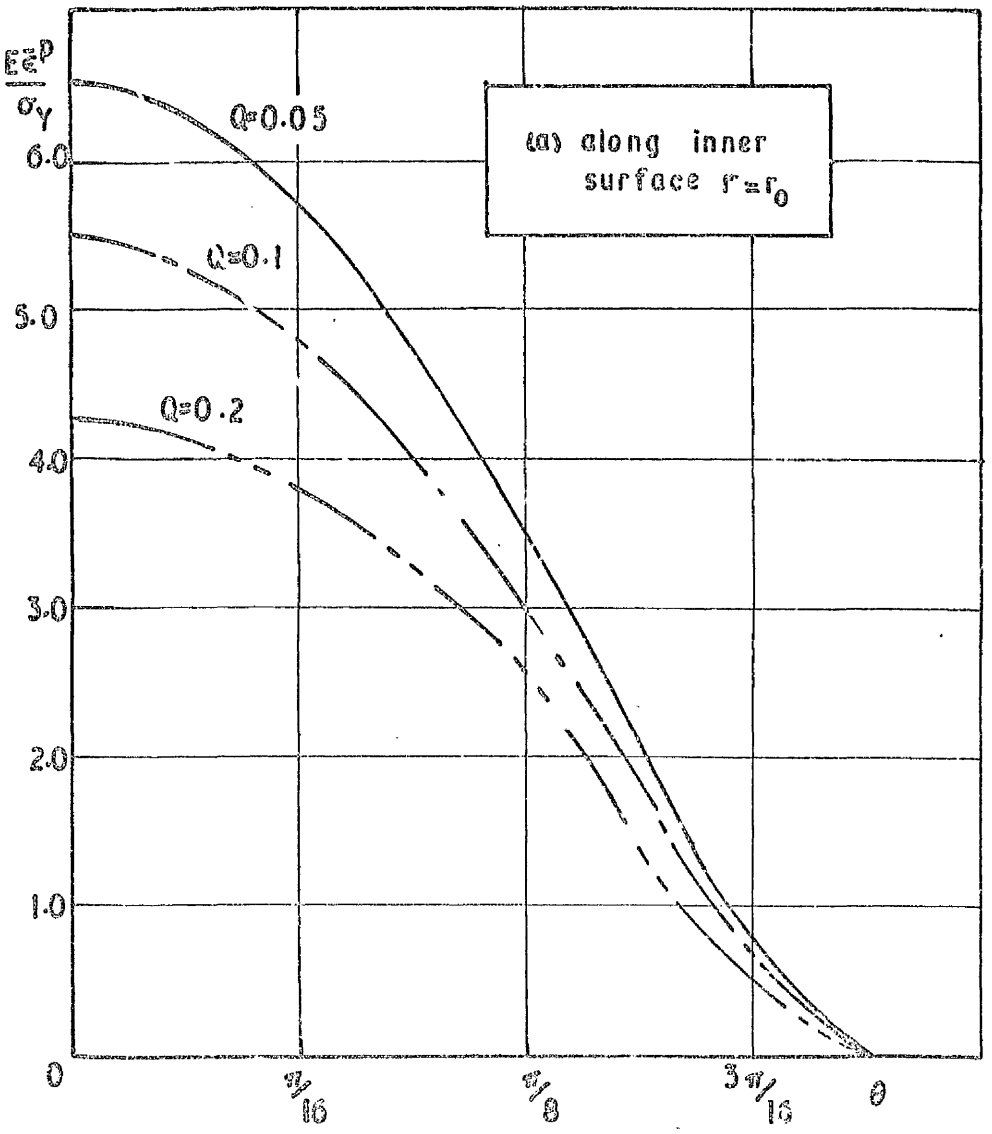

Fig 8·13 Variation of effective plastic strain with Q at 210% load for hole in tension

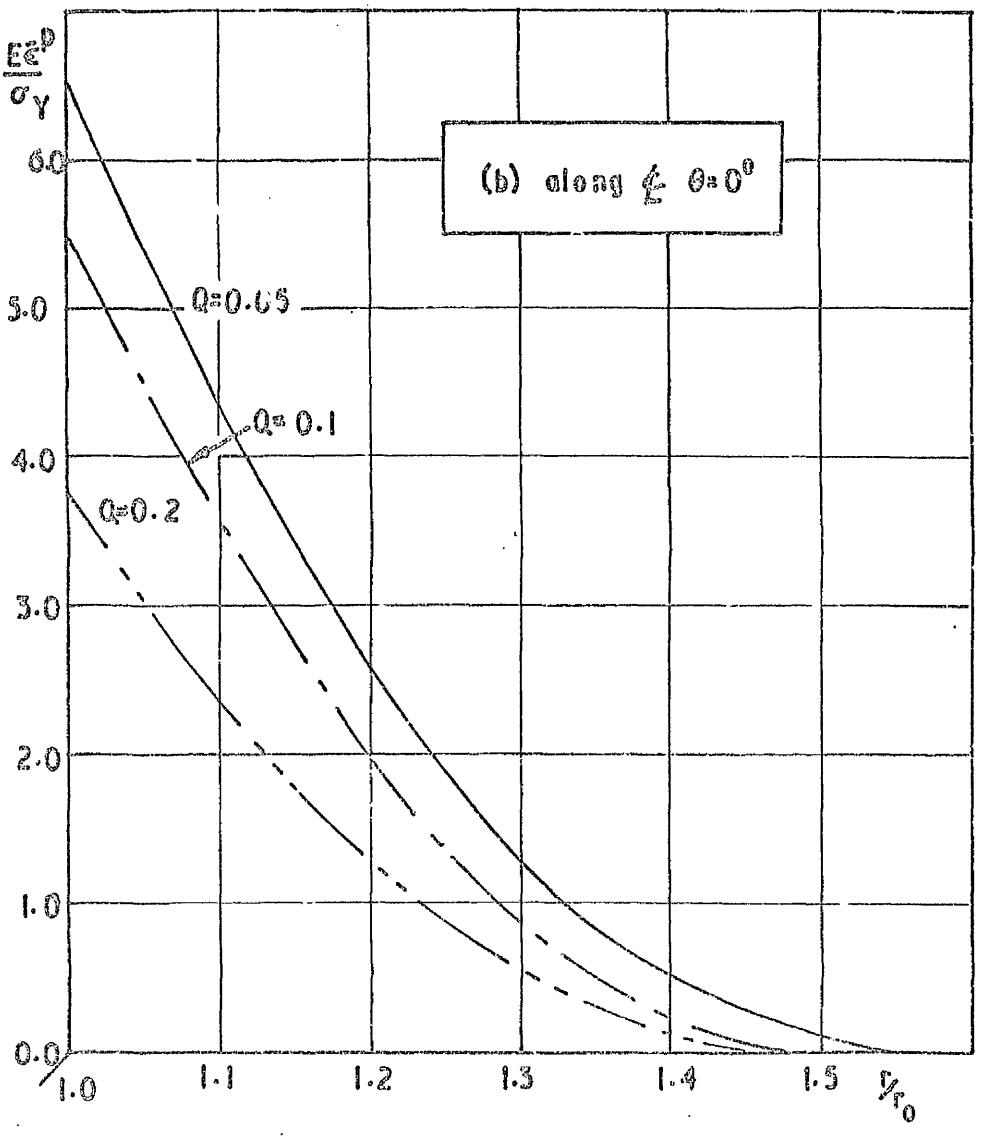

Fig 8.13 (continued)

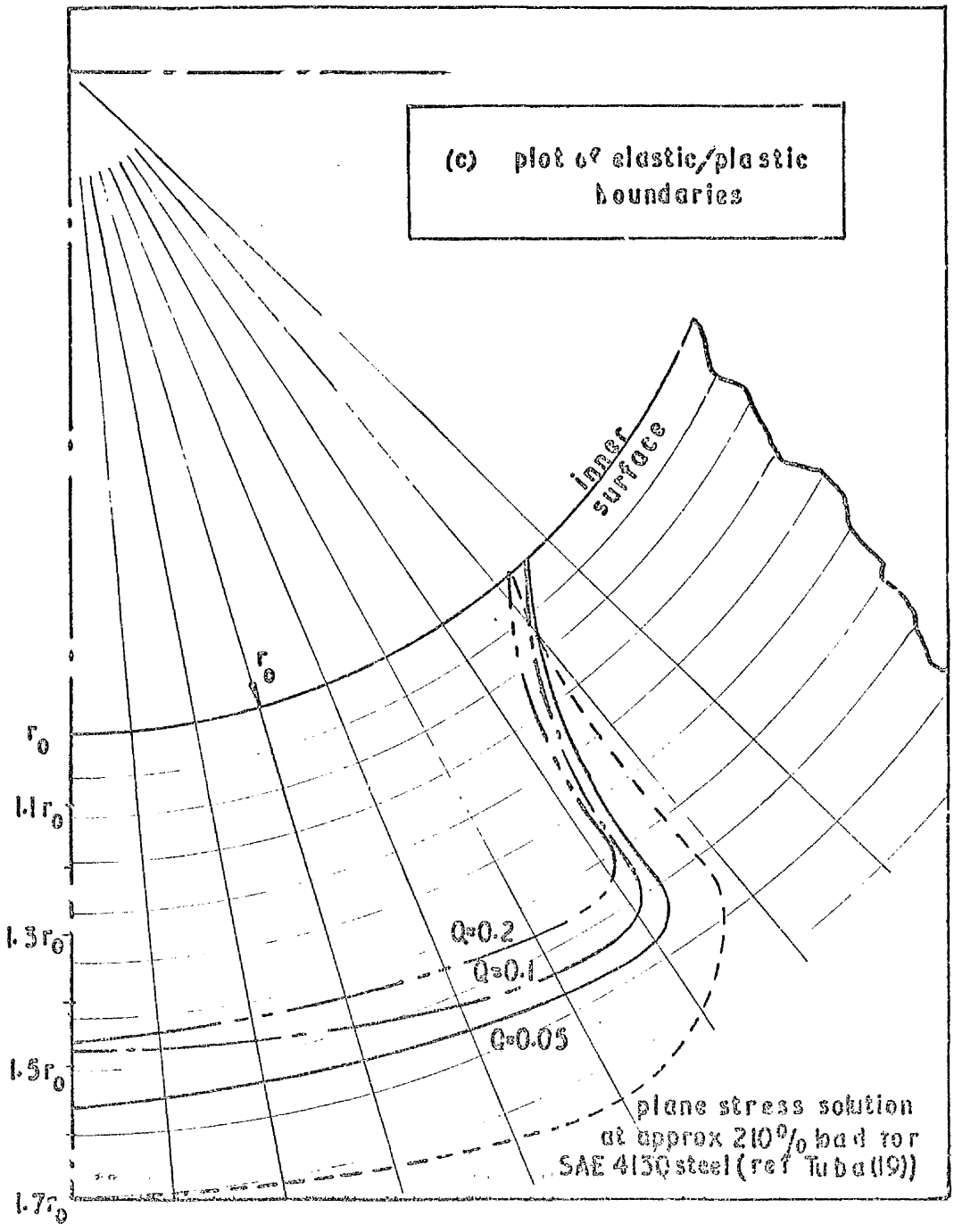

Fig 8.13 (continued)

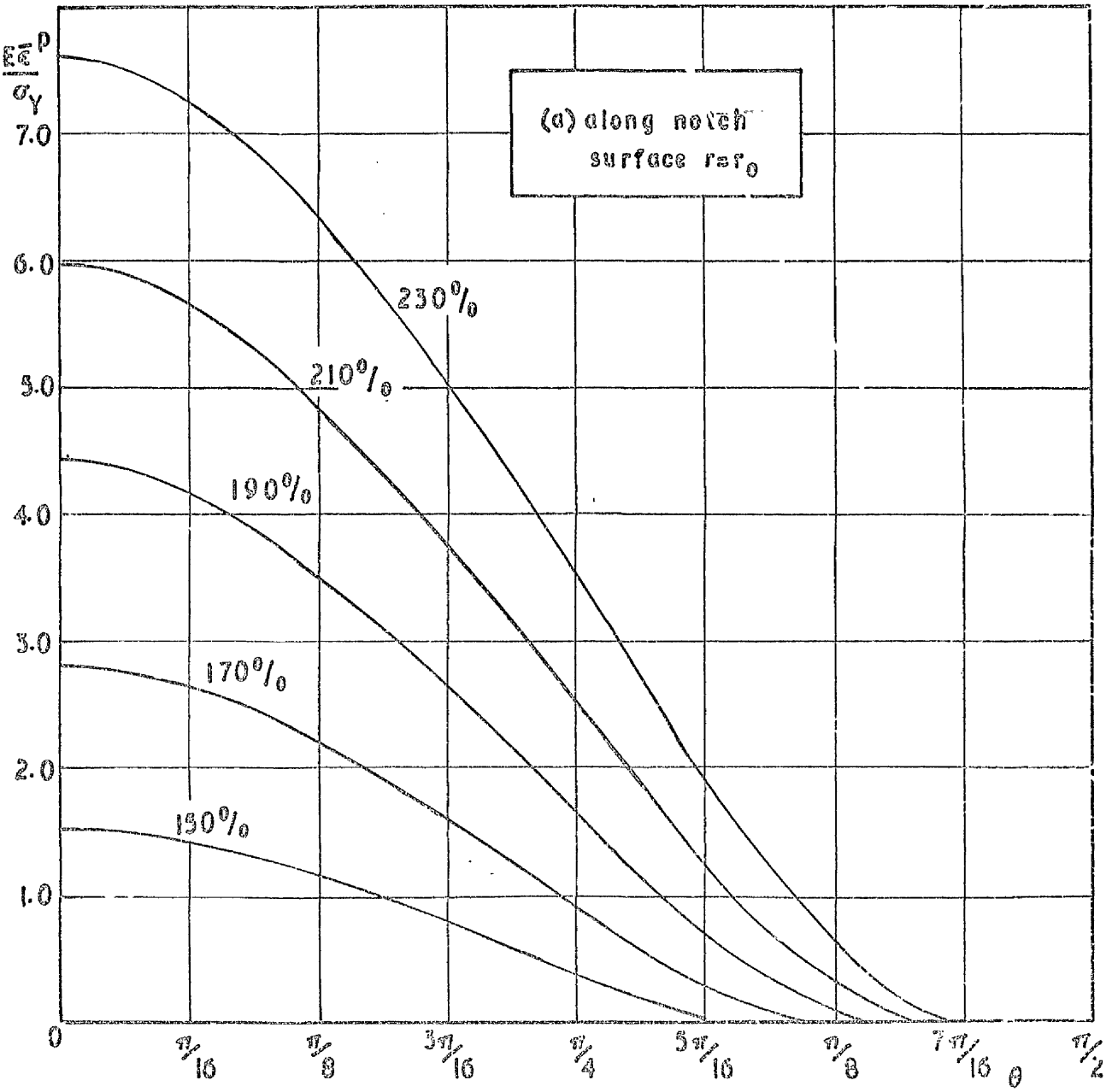

Fig 8.14 Development of effective plastic strain with load for keyhole, Q=0.1

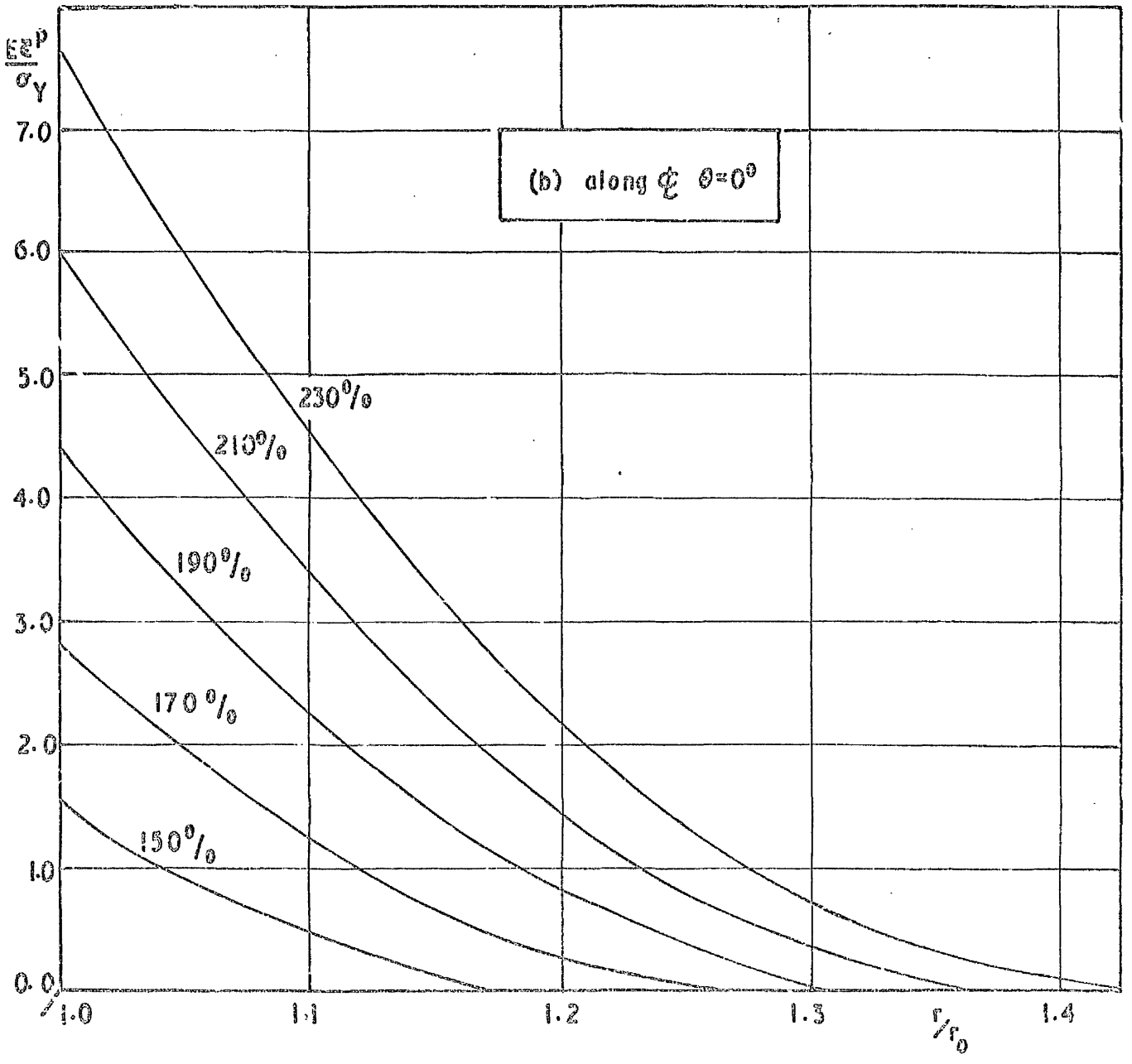

Fig 8.14 (continued)

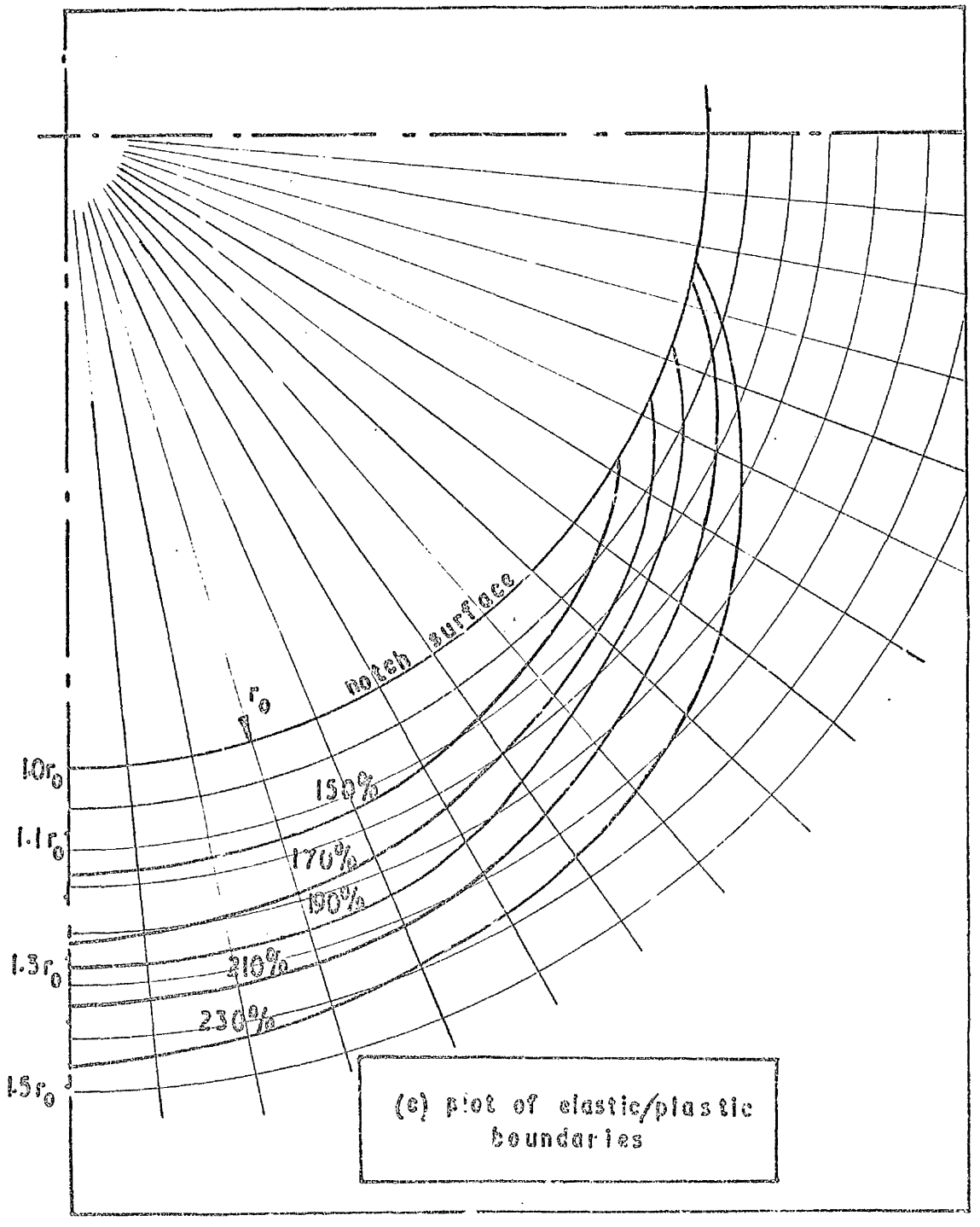

Fig 8.14 (continued)

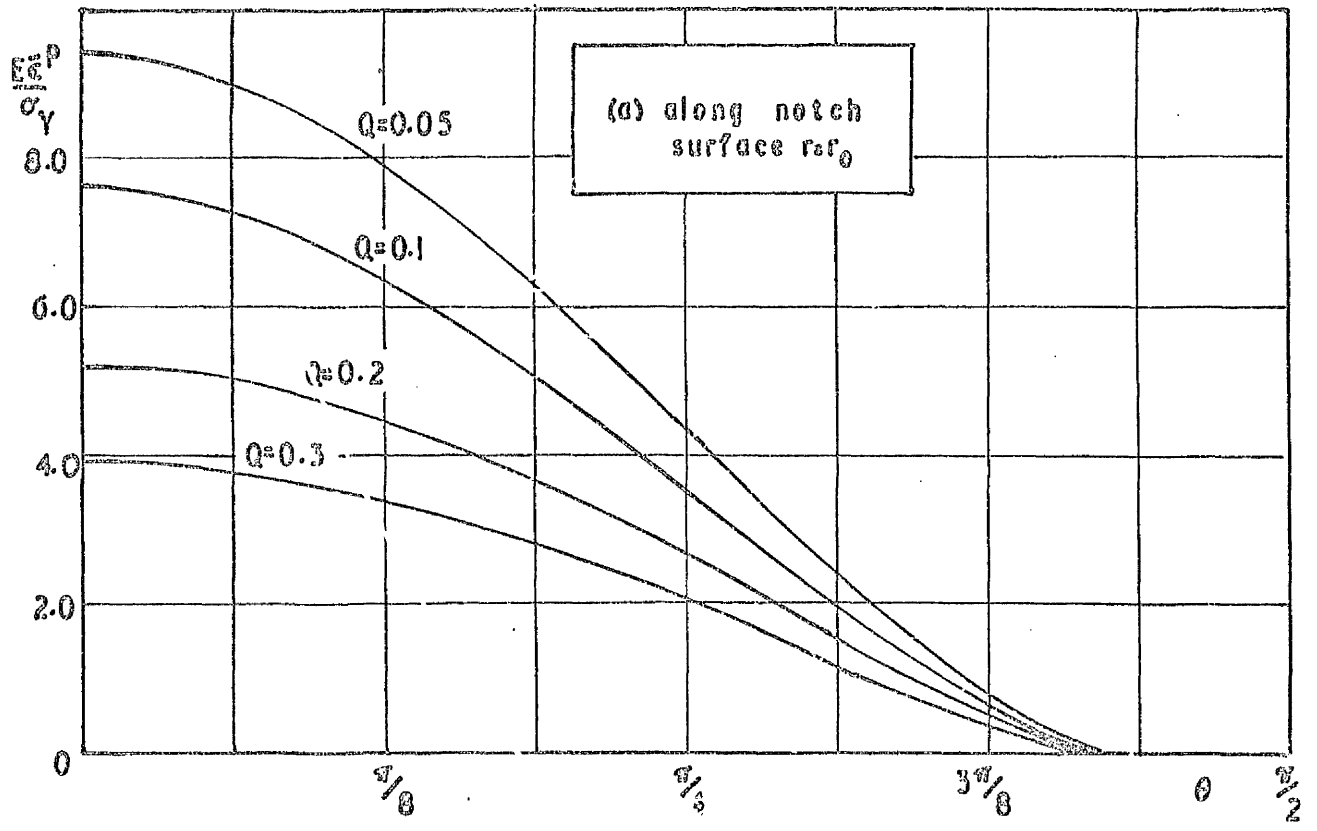

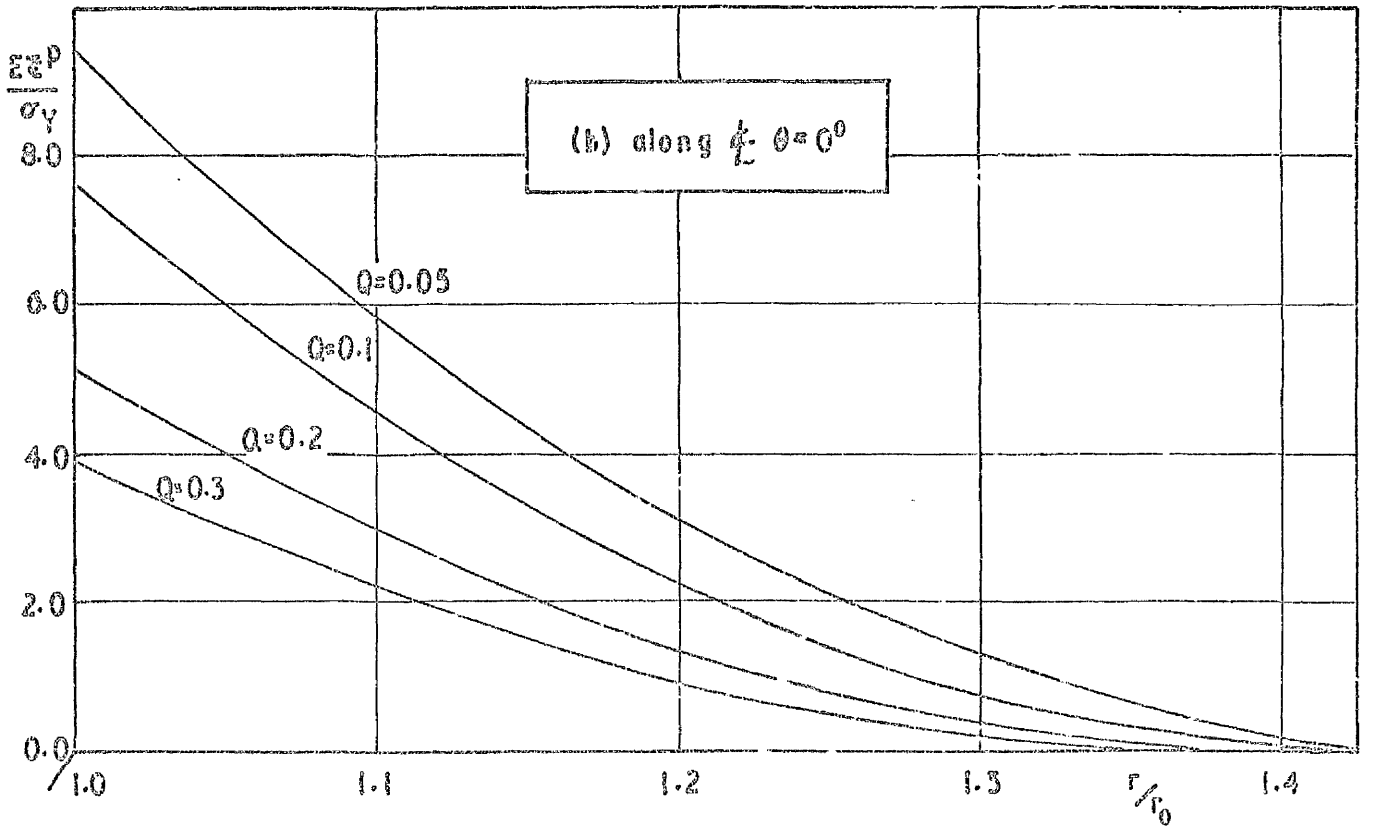

Fig 8.15 Variation of effective plastic strain with Q at 230% load for keyhole

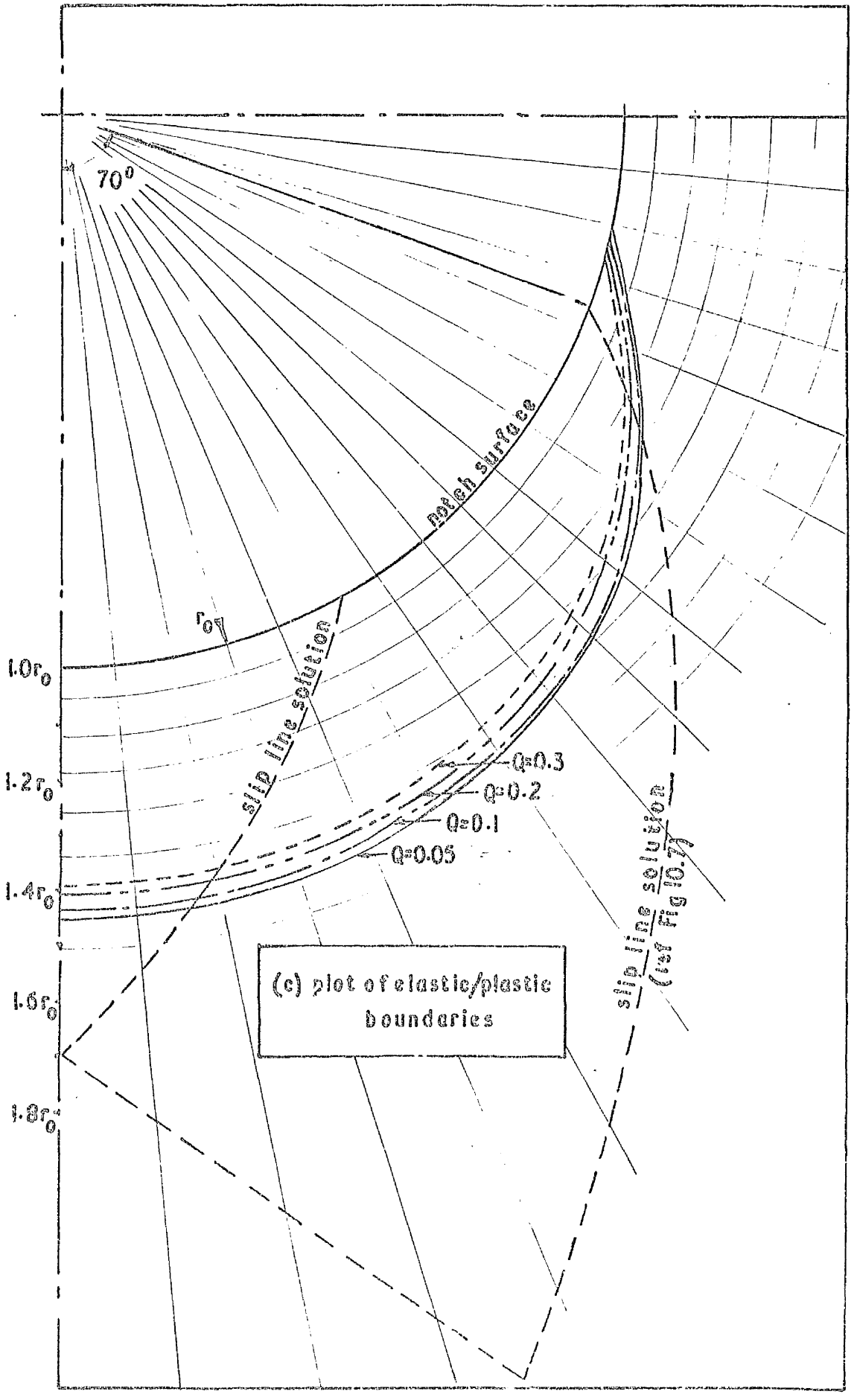

Fig 8.15 (continued)

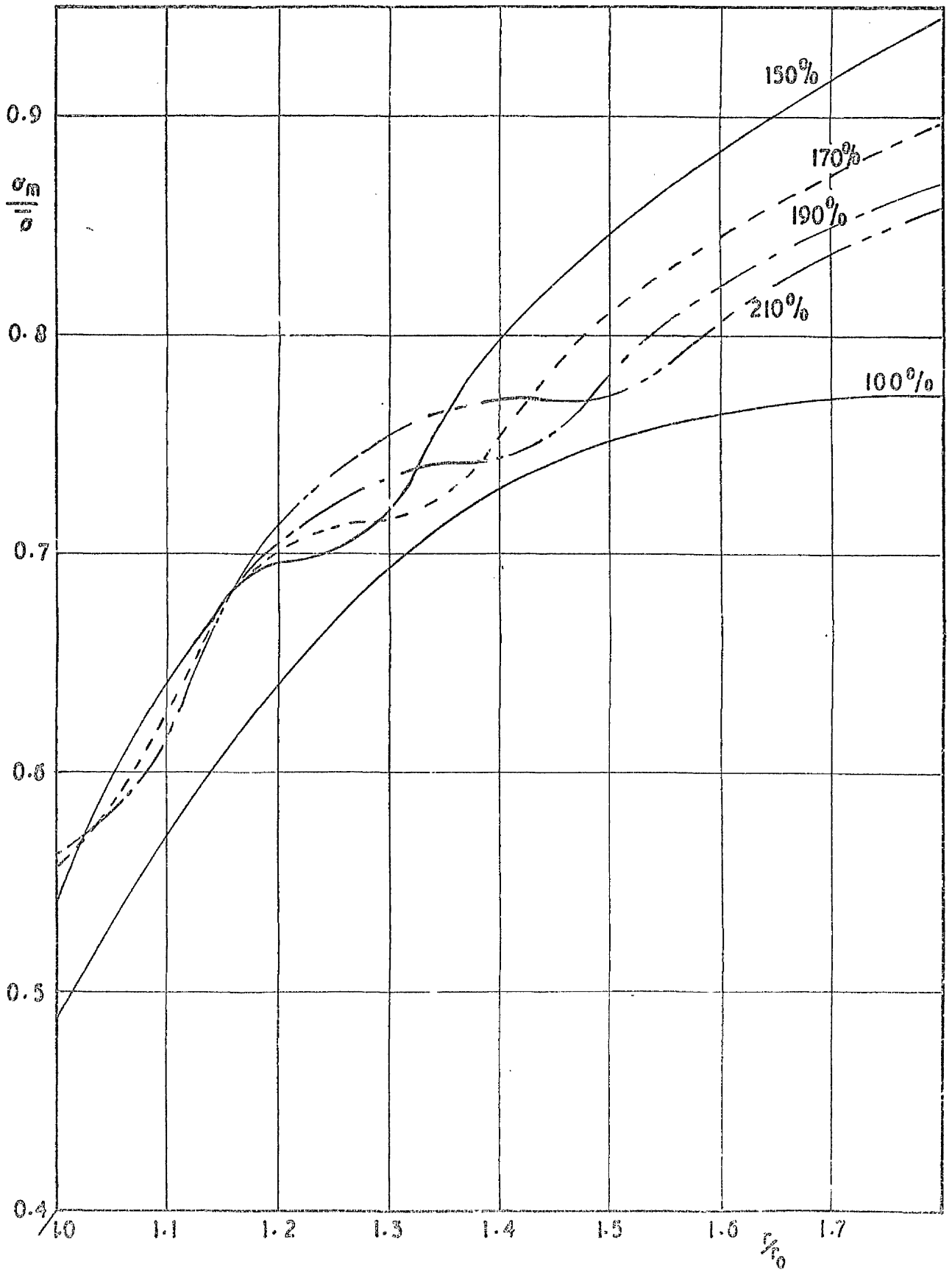

Fig 8.16 Distribution of σ_m/σ along ϕ $\theta=0^\circ$ for hole in tension - Q=0.1

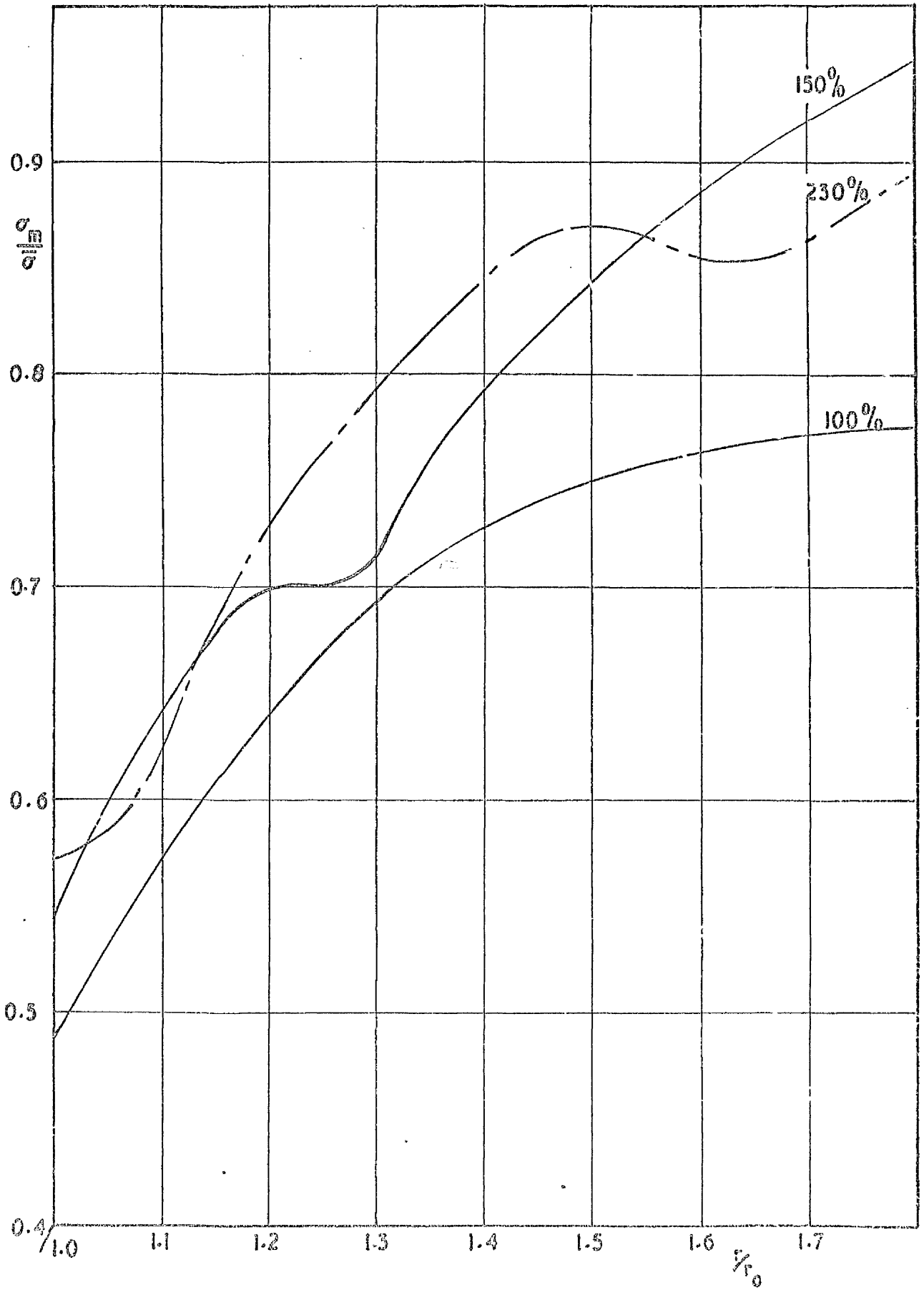

Fig 8.17 Distribution of $\frac{\sigma_m}{\sigma}$ along ϕ $\theta = 0^\circ$ for hole in tension - Q = 0.05

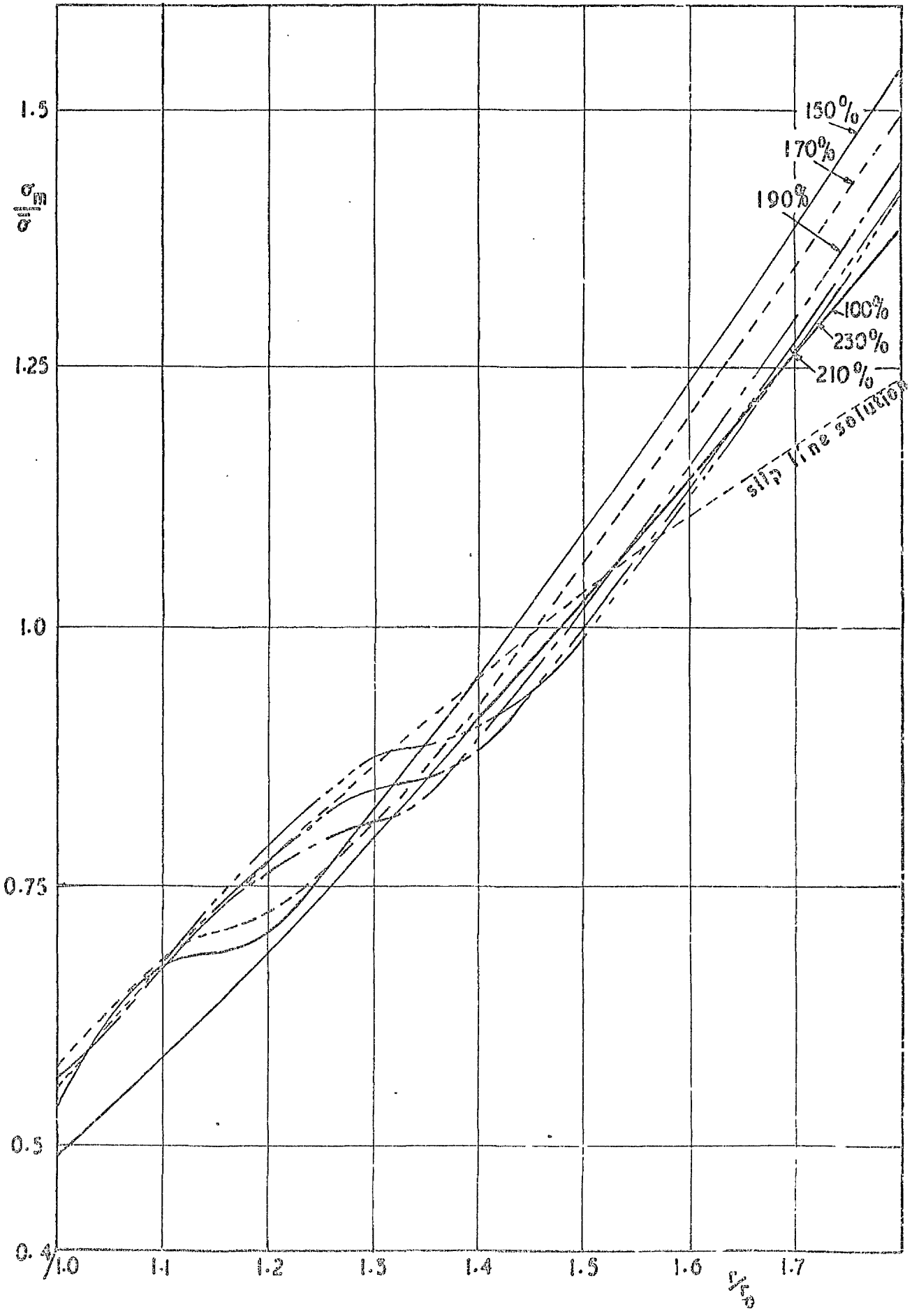

Fig 8.18 Distribution of $\frac{\sigma_m}{\sigma}$ along ϕ $\theta = 0^0$ for keyhole - $Q = 0.1$

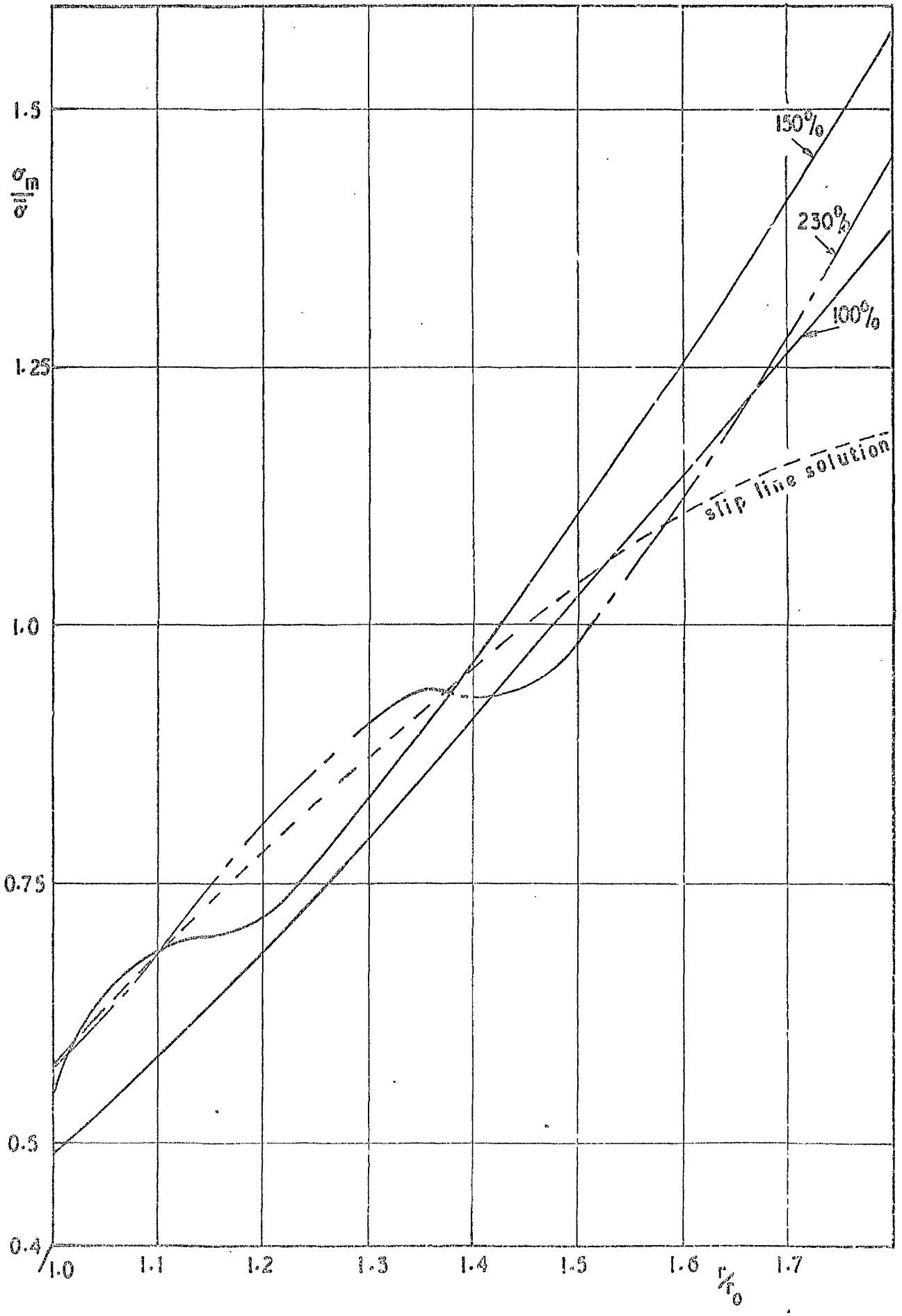

Fig 8.19 Distribution of $\frac{\sigma_m}{\sigma_{ref}}$ along $\mathfrak{L}$ $\theta = 0^0$ for keyhole - Q=0.05

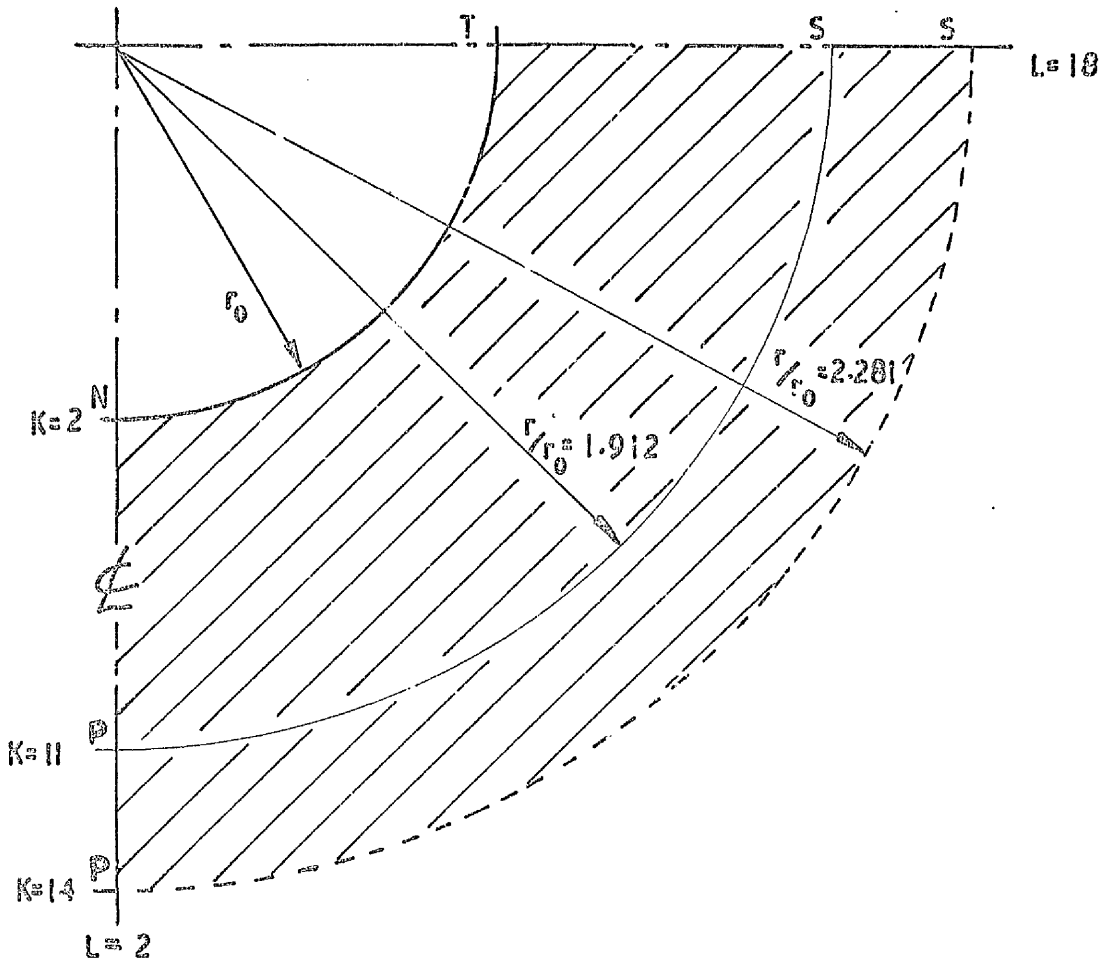

Fig 8.20

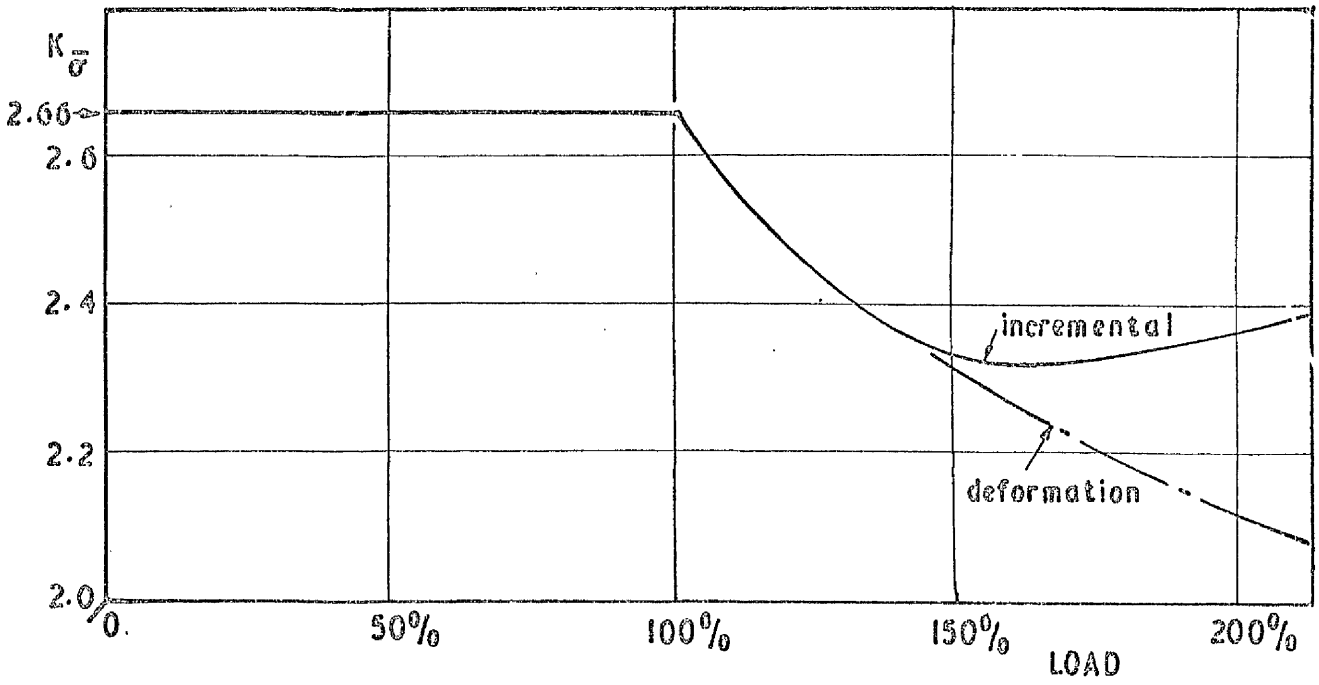

Fig 8.21

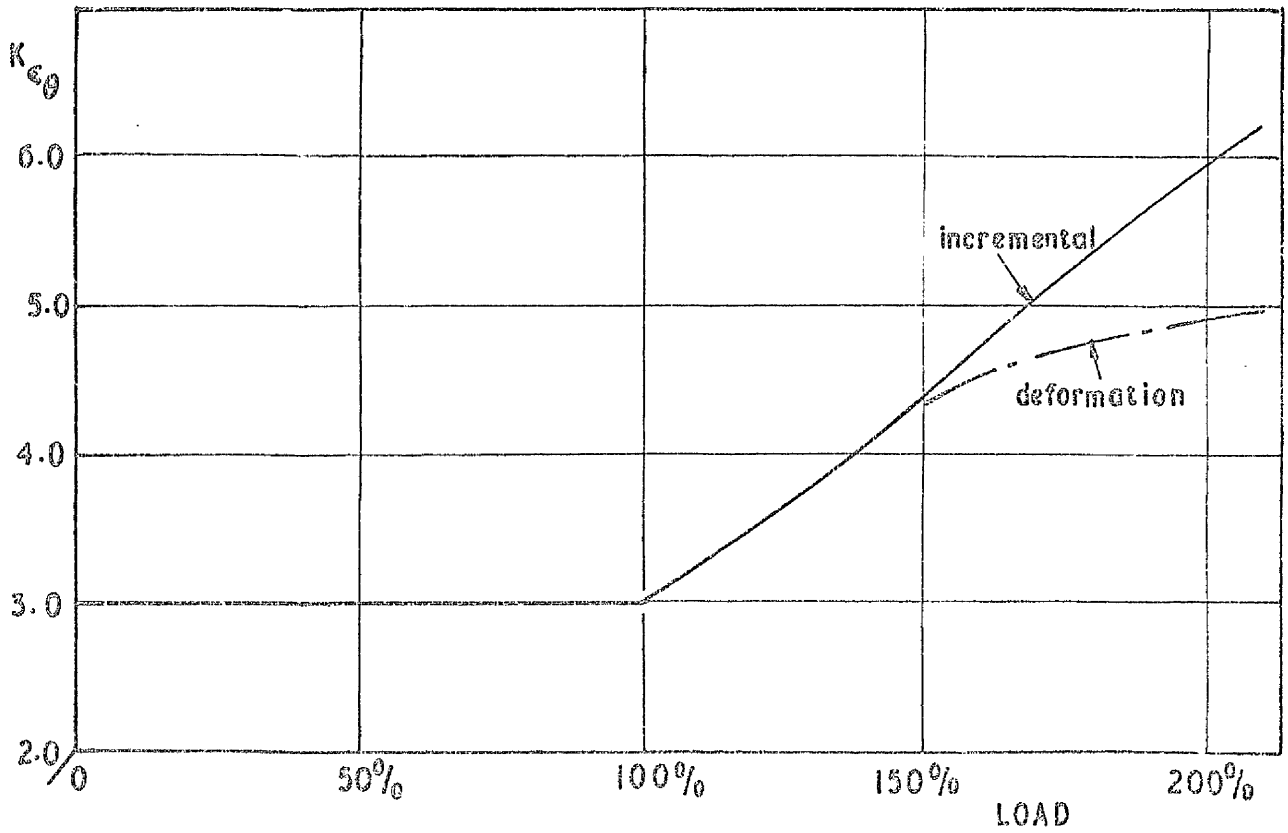

Fig 8.22

Effect of incremental & deformation theories on the stress and strain concentration factors for hole in tension - Q=0.3

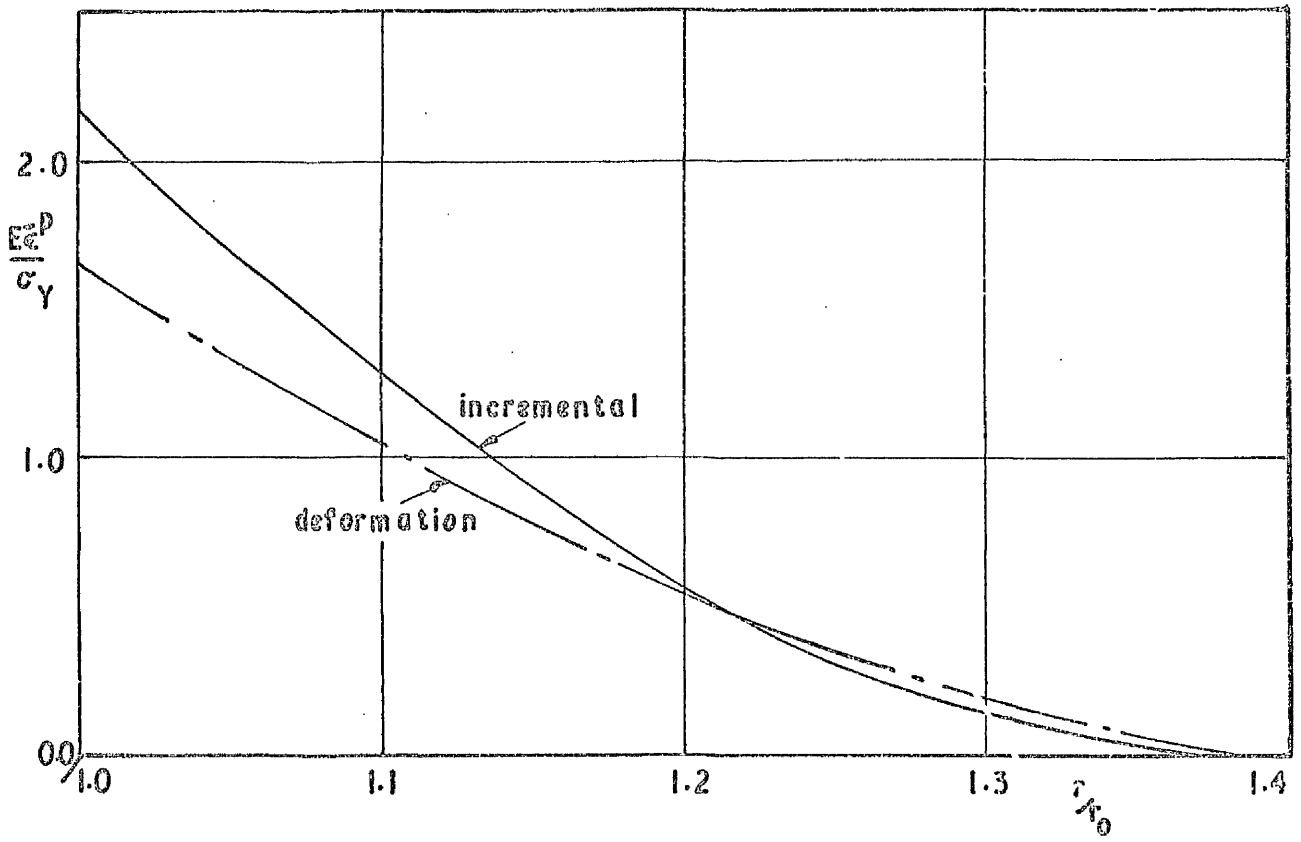

Fig 8.23 along $\measuredangle$ $\theta = 0^0$

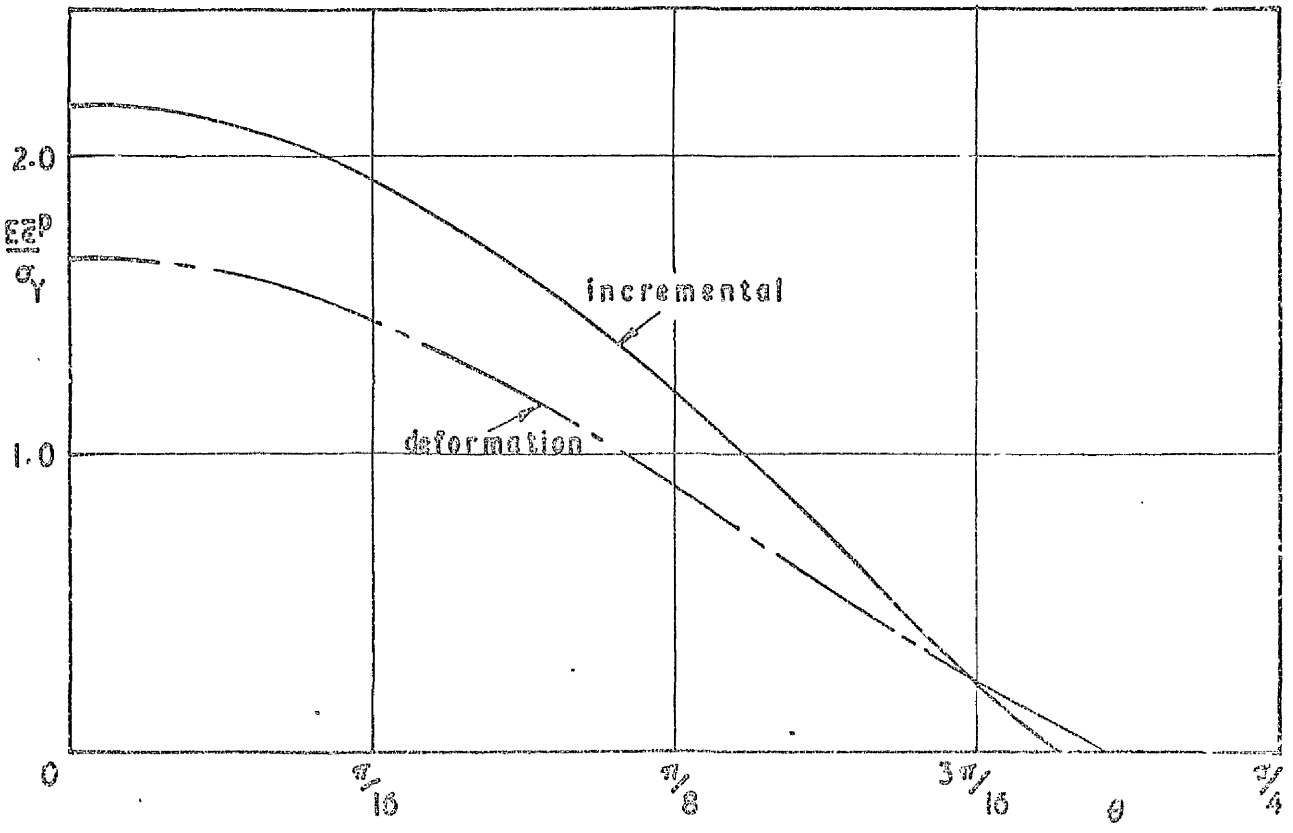

Fig 8.24 along inner surface $r = r_0$

Effect of incremental & deformation theories on the distribution of effective plastic strain for hole in tension at 190% load-Ω=0.3

CHAPTER 9

THE ELASTO-PLASTIC SOLUTION OF THE THICK SPHERE UNDER INTERNAL PRESSURE

CHAPTER 9

THE ELASTO-PLASTIC SOLUTION OF THE THICK SPHERE UNDER INTERNAL PRESSURE

9.1 Introduction

The main purpose of this chapter is to show that some of the unexpected variations of chapter 8 are repeated in the solution to the sphere especially

(i) the tendency for K_{σ_θ}, in fig. 8.5 , to rise with increasing load and increasing work-hardening

(ii) the 'dip' in the value of $\frac{\sigma_m}{\bar{\sigma}}$ in fig. 8.16 in the vicinity of the elastic/plastic boundary.

The thick sphere stressed by pressure is of course a one dimensional problem and therefore rather simpler than the two dimensional problems of chapter 8. It can be tackled in two ways, both are developed for reasons which will become apparent. The first method is analytical, the closed form of the solution has been demonstrated by both Mendelson[3] and independently by Orr[4] but this closed form solution depends on linear work-hardening. In order to overcome this, the author produced a numerical solution which can use any shape of stress-strain curve but which has the disadvantages of numerical approximation and the necessity of using continuous derivatives over the elastic/plastic boundary. The numerical solution of Tuba[2] employs a different technique involving the numerical evaluation of integrals.

Both of these methods of solution are used and the agreement between them is good, excepting the slight differences which will explain (ii) above. Before looking at the Analytical and Numerical Methods in detail in

sections 9.2 and 9.3 below, consider the general formulation of the problem.

The state of stress is described by a $\sigma_r:\sigma_\vartheta:\sigma_\vartheta$ system and due to symmetry, all shear stresses are zero and the normal stresses are dependent only on radius.

Fig. 9.1 defines the inner and outer radii r_i and r_o and indicates the internal pressure p. Equilibrium is given by

$$\frac{d}{dr}(r^2\sigma_r) - 2r\sigma_\vartheta = 0 \qquad (9.1)$$

and Compatibility by

$$\varepsilon_r = \frac{d}{dr}(r\varepsilon_\vartheta). \qquad (9.2)$$

The effective stress is given by

$$\bar{\sigma} = \sqrt{\tfrac{1}{2}\left[(\sigma_r-\sigma_\vartheta)^2 + (\sigma_\vartheta-\sigma_\vartheta)^2 + (\sigma_\vartheta-\sigma_r)^2\right]} = |\sigma_\vartheta-\sigma_r| \qquad (9.3)$$

Due to this simplification, the Mises and Tresca yield conditions coincide and the Levy Mises Equations (4.4) become

$$\left.\begin{aligned} d\varepsilon_\vartheta^{\,p} &= \frac{d\bar{\varepsilon}^p}{\bar{\sigma}}\left[\sigma_\vartheta - \tfrac{1}{2}(\sigma_r+\sigma_\vartheta)\right] = \tfrac{1}{2}d\bar{\varepsilon}^p \\ d\varepsilon_r^{\,p} &= \frac{d\bar{\varepsilon}^p}{\bar{\sigma}}\left[\sigma_r - \tfrac{1}{2}(\sigma_\vartheta+\sigma_\vartheta)\right] = -d\bar{\varepsilon}^p \end{aligned}\right\} \qquad (9.4)$$

where as elsewhere defined $d\varepsilon_\vartheta^{\,p}$, $d\varepsilon_r^{\,p}$, $d\bar{\varepsilon}^p$ are the circumferential, radial and effective plastic strain increments. From equations (9.4), the ratios of the component plastic strain increments to the effective plastic strain increment remains constant whatever the load increment. This means that incremental and deformation theories coincide.

The stress strain relations need contain only one plastic strain increment and are thus written

$$\left.\begin{aligned} \varepsilon_\vartheta &= \frac{1}{E}\left[\sigma_\vartheta(1-\nu) - \nu\sigma_r\right] + \tfrac{1}{2}d\bar{\varepsilon}^p \\ \varepsilon_r &= \frac{1}{E}\left[\sigma_r - 2\nu\sigma_\vartheta\right] - d\bar{\varepsilon}^p. \end{aligned}\right\} \qquad (9.5)$$

The above equations can be non-dimensionalised as follows:-

$$S_\vartheta = \frac{\sigma_\vartheta}{\sigma_Y}, \quad S_r = \frac{\sigma_r}{\sigma_Y}, \quad \bar{S} = \frac{\bar{\sigma}}{\sigma_Y}, \quad S_m = \frac{2\sigma_\vartheta+\sigma_r}{3\sigma_Y}$$

$$E_\vartheta = \frac{E\varepsilon_\vartheta}{\sigma_Y}, \quad E_r = \frac{E\varepsilon_r}{\sigma_Y}, \quad d\bar{E}^p = \frac{Ed\bar{\varepsilon}^p}{\sigma_Y}, \quad R = \frac{r}{r_i}$$

where σ_Y = yield stress
E = Young's Modulus.

The equilibrium and compatibility equations (9.1) and (9.2) thus become

$$\frac{d}{dR}(R^2 S_r) + 2RS_\vartheta = 0 \qquad (9.6)$$

$$E_r = \frac{d}{dR}(RE_\vartheta) \qquad (9.7)$$

and the stress–strain relations (9.5) become

$$\left.\begin{aligned} E_\vartheta &= S_\vartheta(1-\nu) - \nu S_r + \tfrac{1}{2}d\bar{E}^p \\ E_r &= S_r - 2\nu S_\vartheta - d\bar{E}^p. \end{aligned}\right\} \qquad (9.8)$$

9.2 Outline of Analytical Method

This method is formulated in terms of the stress and strain increments and so equations (9.8) become (where the dots signify the increment)

$$\left.\begin{aligned} \dot{E}_\vartheta &= \dot{S}_\vartheta(1-\nu) - \nu\dot{S}_r + \tfrac{1}{2}\dot{\bar{E}}^p \\ \dot{E}_r &= \dot{S}_r - 2\nu\dot{S}_\vartheta - \dot{\bar{E}}^p \end{aligned}\right\} \qquad (9.9)$$

which when re–arranged and inserted into the effective stress (9.3) give

$$\dot{\bar{S}} = \frac{1}{1+\nu}(\dot{E}_\vartheta - \dot{E}_r - 1.5\,\dot{\bar{E}}^p). \qquad (9.10)$$

From the stress–strain curve fig. 9.2, the effective plastic strain increment obtained from a 'jump' from p tc q is found from

$$\dot{\bar{S}} = Q\dot{\bar{E}}^p + (1-\bar{S})$$

where Q is the work–hardening index as previously defined in paragraph 7.3.5.

Using this relation in (9.10) eliminates $\dot{\bar{S}}$ to give

$$Q\dot{\bar{E}}^p + (1-\bar{S}) = \frac{1}{1+\nu}(\dot{E}_\vartheta - \dot{E}_r - 1.5\dot{\bar{E}}^p). \qquad (9.11)$$

Inserting equations(9.9) into the incremental form of the equilibrium equation (9.6) gives

$$2(\dot{E}_\vartheta - \dot{E}_r) - 3\dot{\bar{E}}^p = R\frac{d}{dR}\left(\frac{1-\nu}{1-2\nu}\dot{E}_r + \frac{2\nu}{1-2\nu}\dot{E}_\vartheta + \dot{\bar{E}}^p\right). \quad (9.12)$$

The incremental form of the compatibility equation is

$$\dot{E}_\vartheta - \dot{E}_r + R\frac{d\dot{E}_\vartheta}{dR} = 0. \quad (9.13)$$

There are now three equations (9.11), (9.12) and (9.13) in the three variables $\dot{E}_r$, $\dot{E}_\vartheta$ and $\dot{\bar{E}}^p$.

These can be simplified and solved by using the following relations

$$a = \dot{E}_\vartheta - \dot{E}_r, \qquad b = \dot{E}_\vartheta.$$

Thus (9.11) becomes

$$\dot{\bar{E}}^p = \frac{1}{\alpha}(a - (1+\nu)(1-\bar{S})) \quad (9.14)$$

where $\alpha = \dfrac{1}{1.5+Q(1+\nu)}$

– (9.12) becomes

$$2a - 3\dot{\bar{E}}^p = R\frac{d}{dR}\left(\frac{1+\nu}{1-2\nu}b - \frac{1-\nu}{1-2\nu}a + \dot{\bar{E}}^p\right) \quad (9.15)$$

–and (9.13) becomes

$$a + R\frac{db}{dR} = 0 \quad (9.16)$$

eliminating b from (9.15) and (9.16) gives

$$3\dot{\bar{E}}^p + R\frac{d\dot{\bar{E}}^p}{dR} = \frac{3(1-\nu)}{1-2\nu}a + \frac{1-\nu}{1-2\nu}R\frac{da}{dR}. \quad (9.17)$$

Now for elastic conditions $\bar{S} = \dfrac{1}{R^3}$ and so using this relationship in (9.14) and then substituting the expression for $\dot{\bar{E}}^p$ into (9.17) gives

$$3a + R\frac{da}{dR} = \frac{-3(1-\nu)}{\alpha\left(\frac{1-\nu}{1-2\nu} - \frac{1}{\alpha}\right)} = -3\beta \text{ say.} \quad (9.18)$$

Note: for fixed values of ν and Q, α and β are constants.

The solution to (9.18) is

$$\boxed{a = -\beta + \frac{C_1}{R^3}} \quad (9.19)$$

where C_1 is a constant of integration.

Back substitution of (9.19) into (9.16) gives

$$\frac{db}{dR} = -\frac{a}{R} = \frac{\beta}{R} - \frac{C_1}{R^4}$$

and integration leads to

$$\boxed{b = \beta \ln R + \frac{C_1}{3R^3} + C_2} \qquad (9.20)$$

where C_2 is a constant of integration.

Finally substitution of (9.19) into (9.14) gives

$$\boxed{\dot{\bar{E}}^p = \frac{1}{\alpha}\left[-\beta + \frac{C_1}{R^3} - (1+\nu)\left(1-\frac{1}{R^3}\right)\right]}. \qquad (9.21)$$

The three equations (9.19) to (9.21) represent the solution with only the constants C_1 and C_2 to be evaluated. This is done as follows –

(i) A value of $\dot{\bar{E}}^p$ is chosen at $R = 1$ and consequently C_1 is evaluated from (9.21). Essentially this step is equivalent to applying a load.

(ii) C_2 is evaluated by matching of strains at the elastic/plastic boundary, which can easily be found from (9.21), since at that radius $\dot{\bar{E}}^p = 0$.

Once C_1 and C_2 are found distributions of a, b and $\dot{\bar{E}}^p$ and thus $\dot{E}_\vartheta$, $\dot{E}_r$, $\dot{S}_r$, $\dot{S}_\vartheta$, $\dot{\bar{S}}$ etc. can be evaluated.

A short computer program was written for this method. Apart from the information regarding sphere size, work-hardening index and Poisson's ratio, the only 'load' indication fed in is a value of effective plastic strain increment $\dot{\bar{E}}^p$ $\left(= \frac{E d\bar{\varepsilon}^p}{\sigma_Y}\right)$ at the inner surface. For this reason, non-integral internal pressure values result, as will be seen in the graphs, at the end of this chapter.

9.3 Outline of Numerical Method

This method reduces the constitutive equations to one second order ordinary differential governing equation in the total stress S_r. This equation is found by substituting equations (9.8) into (9.7) and then eliminating S_ϑ by use of the equilibrium equation (9.6). Thus

$$\frac{R^2}{2}\frac{d^2S_r}{dR^2} + 2R\frac{dS_r}{dR} = -\frac{1}{1-\nu}\left(1.5\,\dot{\bar{E}}^p + \frac{R}{2}\frac{d\dot{\bar{E}}^p}{dR}\right). \qquad (9.22)$$

In order to solve this equation, it is discretized and then used on the sphere which has be divided up into a number of

equally spaced grid points along a radius (fig. 9.3). The difference form of equation (9.22) is then applied at each of these grid points, thus giving a set of simultaneous linear algebraic equations with the boundary conditions

$$\text{(a)} \quad \text{at } R = 1, \quad S_r = \frac{-p}{\sigma_Y}$$

$$\text{(b)} \quad \text{at } R = R_o, \quad S_r = 0.$$

These simultaneous equations are then expressed in matrix form and solved using a Triangulation or Banachiewicz Crout Method, thus giving a value of S_r at each grid point.

No mention has been made yet of the term $\dot{\bar{E}}^p$. Initially this must be estimated and then successively corrected. The method of solution is similar to that outlined in steps (a_1) to (g_1) of Chapter 2.

As has been mentioned in both Chapters 2 and 4 evaluation of $\dot{\bar{E}}^p$ from $\bar{S}$ is restrictive on numerical stability. However, this method is stable within the range of work-hardening indexes required to illustrate the necessary points. If more than one load stage is required for stability (9.22) can be re-written as

$$\frac{R^2}{2}\frac{d^2S_{rn}}{dR^2} + 2R\frac{dS_{rn}}{dR} = -\frac{1}{(1-\nu)}\left[1.5\left(\bar{E}^p_{(n-1)} + \dot{\bar{E}}^p_n\right) + \frac{R}{2}\left(\frac{d\bar{E}^p_{(n-1)}}{dR} + \frac{d\dot{\bar{E}}^p_n}{dR}\right)\right] \qquad (9.23)$$

where S_{rn} = total value of the radial stress at the end of the n^{th} load stage

$\bar{E}^p_{(n-1)}$ = total value of the effective plastic strain at the end of the $(n-1)^{th}$ load stage

$\dot{\bar{E}}^p_n$ = the effective plastic strain increment during the n^{th} load stage.

The value of $\dot{\bar{E}}^p$ is taken directly off the stress strain $(\bar{\sigma} - \bar{E}^p)$ curve and consequently any shape of curve can be used, unlike the analytical solution.

9.4 Results

Referring back to section 9.1, the purpose of this chapter is twofold and these are dealt with separately in the two paragraphs below – 9.4.2 and 9.4.3. All the results that follow are for a thick sphere of which the dimension $R_o = 6.0$.

9.4.1 Stress-Strain Curves

Common to paragraphs 9.4.2 and 9.4.3 below are several stress strain curves ($\bar{S} - \bar{E}^p$) and these are shown on fig. 9.4. The linear work-hardening curves $Q = 0.0$ to 0.6 are as described in paragraph 7.3.5. The parabolae (1) and (2) have the following equations.

Parabola (1)

$$\bar{E}^p = -1.3753 + 1.3753\ \bar{S}^2.$$

Parabola (2)

$$\bar{E}^p = 7.7935 - 15.5868\ \bar{S} + 7.7933\ \bar{S}^2.$$

Parabola (2) is the only one of the stress-strain curves which has no discontinuity at the yield point $\bar{S} = 1.0$.

9.4.2 Circumferential Stress Concentration Factor K_{σ_ϑ}.

It was noticed in fig. 8.5 for the hole in tension that the concentration factor K_{σ_ϑ} tended to rise with increased work-hardening Q and load. For the sphere K_{σ_ϑ} is defined as $K_{\sigma_\vartheta} = \frac{S_\vartheta}{p}$. A similar effect can be noticed on fig. 9.5 for Q values of 0.3 and 0.6 using the analytical solution. For $Q = 0.0$, no such effect exists.

The reason for this is best explained by reference to fig. 9.6 – a plot of the distributions of circumferential stress near the inner surface at various internal pressures and a work-hardening index of 0.3. As the pressure increases, there is a tendency for S_ϑ to 'hook' near the inner surface, thus K_{σ_ϑ} will also hook. This 'hooking' is due to the linear work-hardening as can be seen by comparing the stress distribution on fig. 9.6 to that of fig. 9.7 in which the stress-strain curve is that of parabola (1) in

fig. 9.4, making use of the numerical solution.

The linear work-hardening at higher loads tends to force the value of $\bar{S}$ higher and so produce the slight distortion.

Conclusion:- The rise in the stress concentration factor K_{σ_θ} is due to linear work-hardening and will be more noticeable at high values of work-hardening index and high loads.

9.4.3 Distribution of Mean to Effective Stress Ratio $\frac{S_m}{\bar{S}}$.

In fig. 8.16 for the solution to the hole in tension, a dip was noticed in the distribution of mean to effective stress ratio. A similar dip is noticed in fig. 9.8 for linear work-hardening Q = 0.3 using the numerical solution. The effect is not due to only the linear work-hardening as in paragraph 9.4.2 since the dip is also present when the parabola (1) stress-strain curve (fig. 9.4) is used - see fig. 9.9.

It was then thought that maybe it was due to the discontinuity existing in these two curves at the yield point and so the numerical solution was used again but this time with the stress-strain curve parabola (2), which has no discontinuity at the yield point - fig. 9.4. However here again the distribution of $\frac{S_m}{\bar{S}}$ shows a similar dip in the vicinity of the elastic/plastic boundary, fig. 9.10.

The use of linear work-hardening Q = 0.3 in the analytical solution gives the answer. The resulting $\frac{S_m}{\bar{S}}$ distribution in fig. 9.11, shows a sharp change in the curve at the elastic/plastic boundary and no dip. The difference between the numerical and the analytical methods of solution responsible for this change is as mentioned in section 9.1, that, in the numerical solution, the derivatives are taken as continuous over the elastic/plastic boundary. In the analytical solution, there result distinct equations for the elastic and plastic regions. The effect is small

and only affects the vicinity of the elastic/plastic boundary as can be seen by comparing figs. 9.8 and 9.11.

Conclusion:— The dip in the distribution of mean to effective stress ratio is due to continuous derivatives being taken over the elastic/plastic boundary.

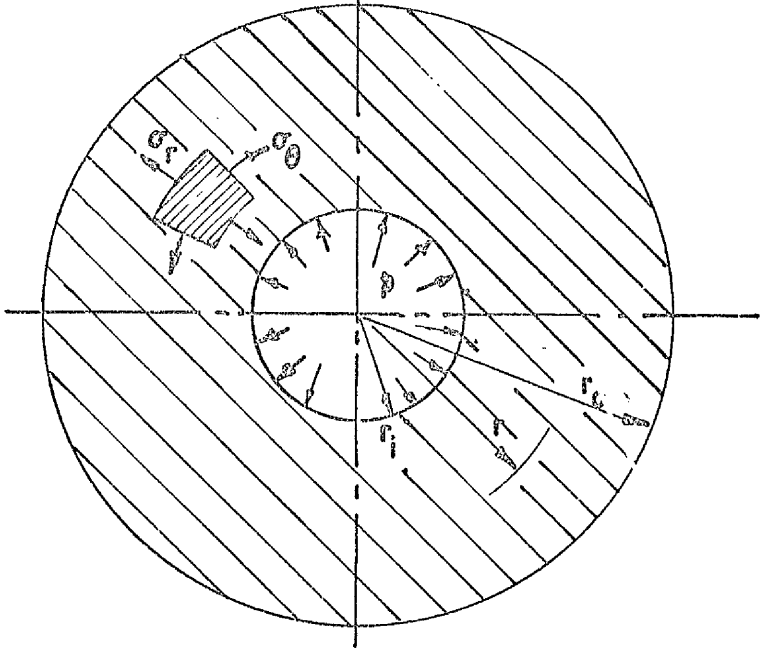

Fig 9.1

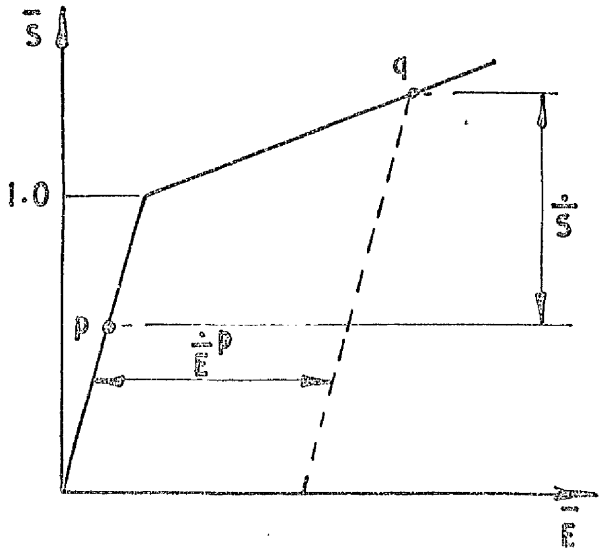

Fig 9.2

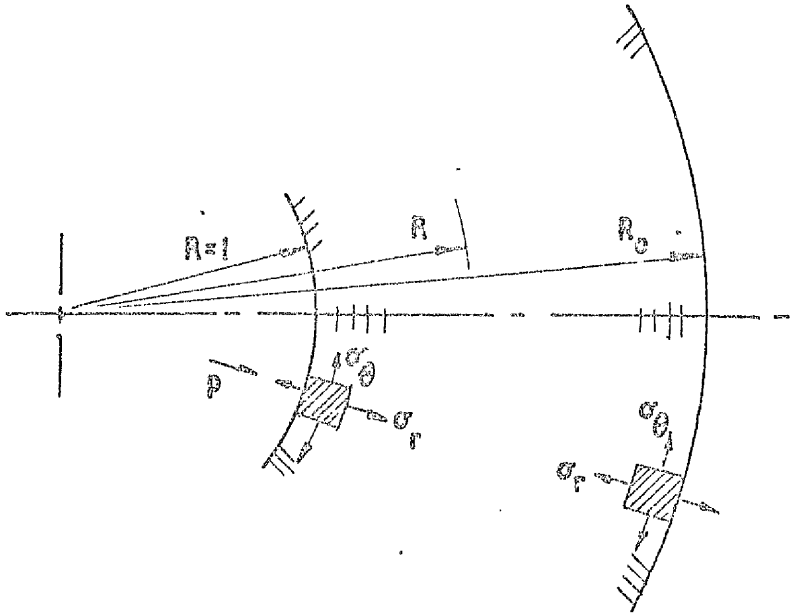

Fig 9.3

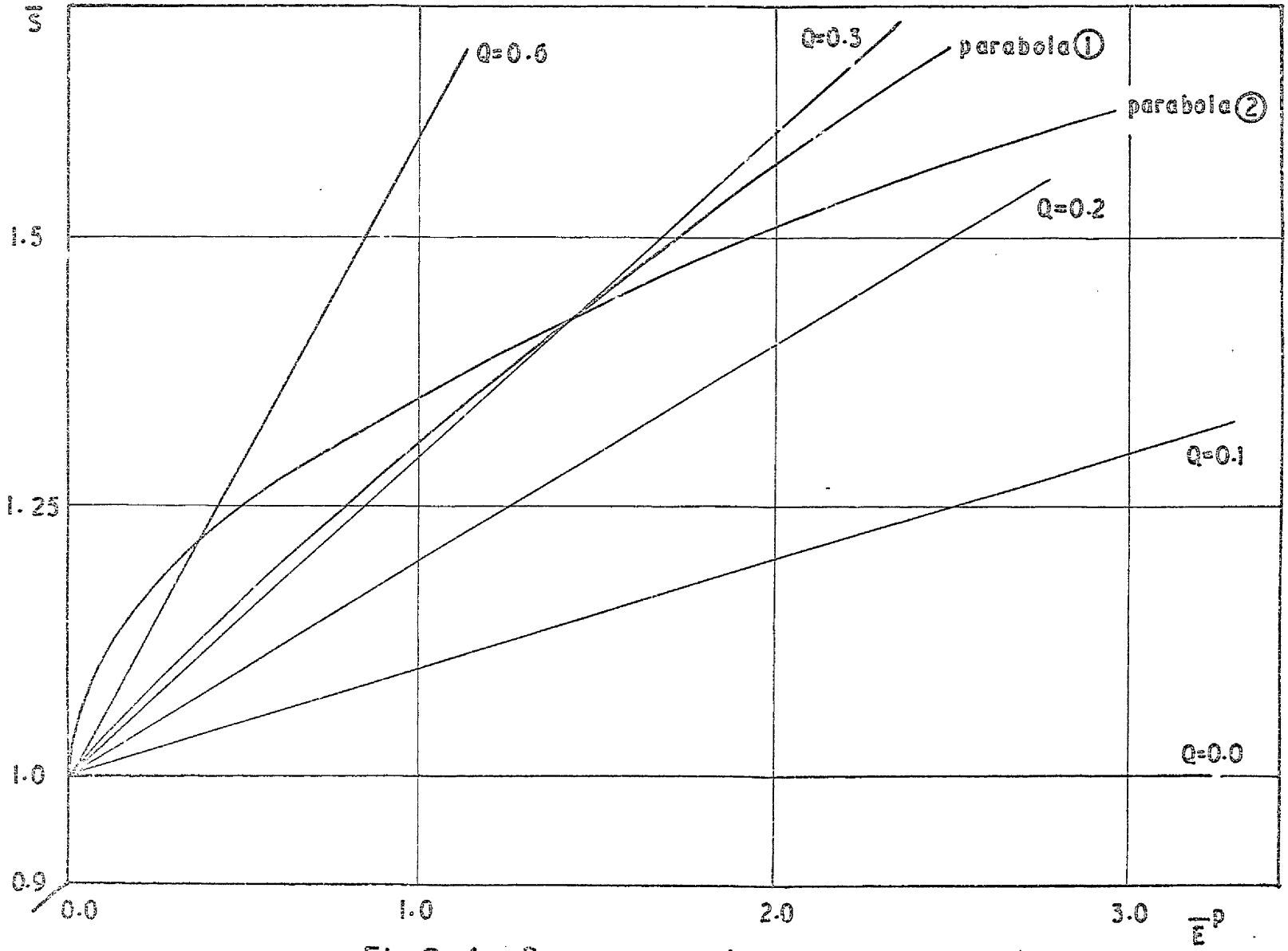

Fig 9.4 Stress-strain curves

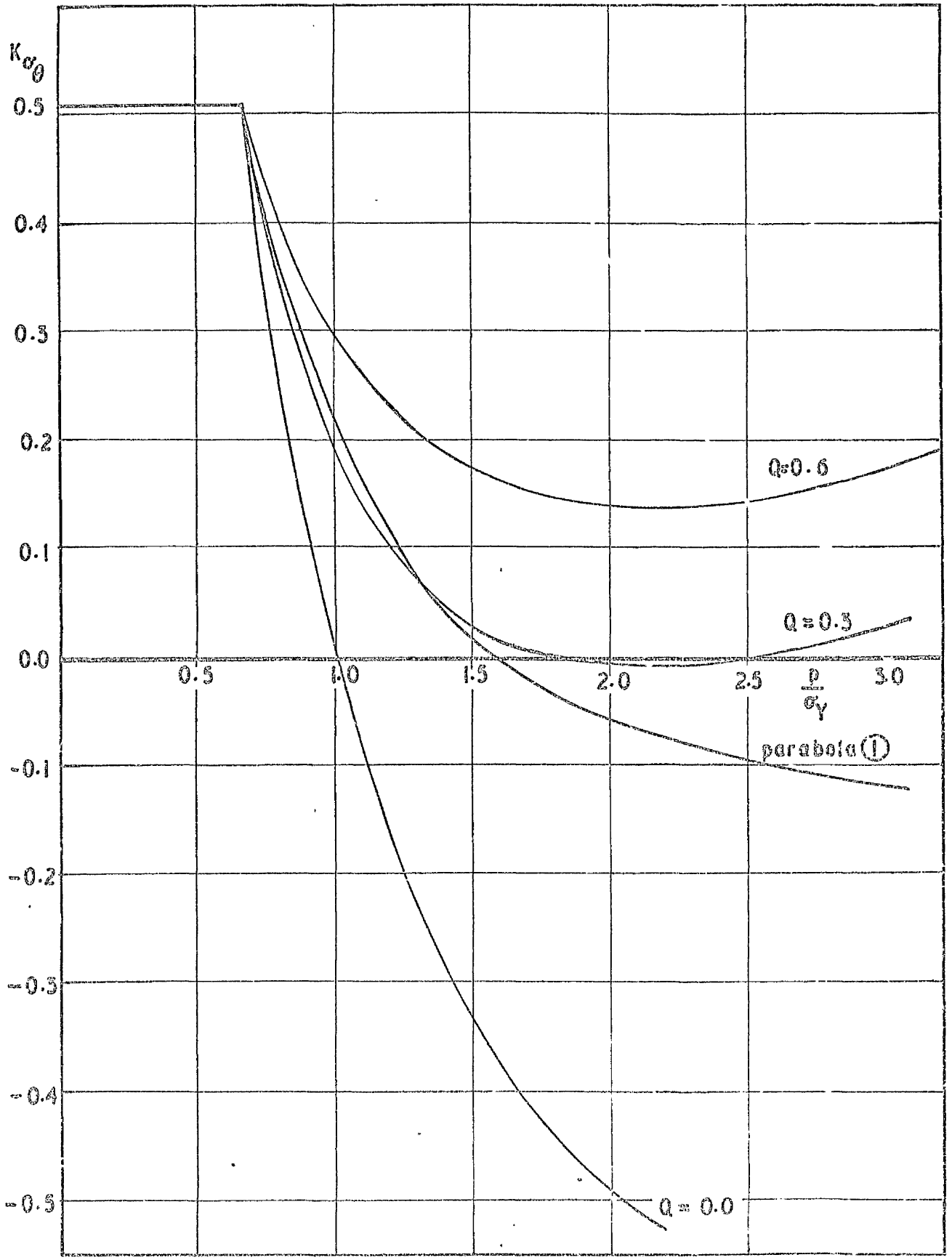

Fig 9.5 Variation of stress concentration factor K_{σ_θ} with pressure & Q-sphere $R_o = 6$

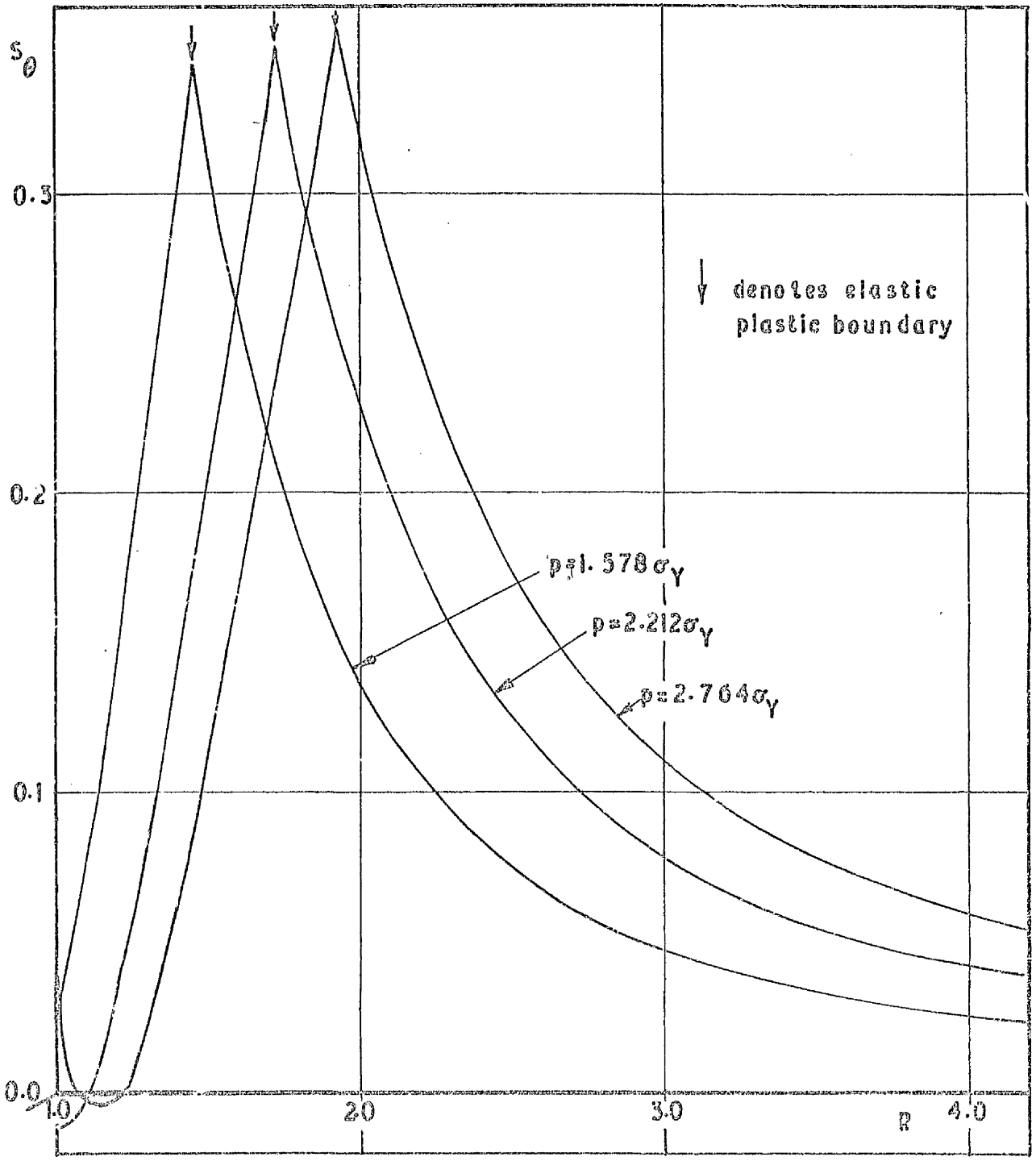

Fig 9.6 Distribution of S_θ for various loads - sphere, $Q=0.3$, $R_0=6$

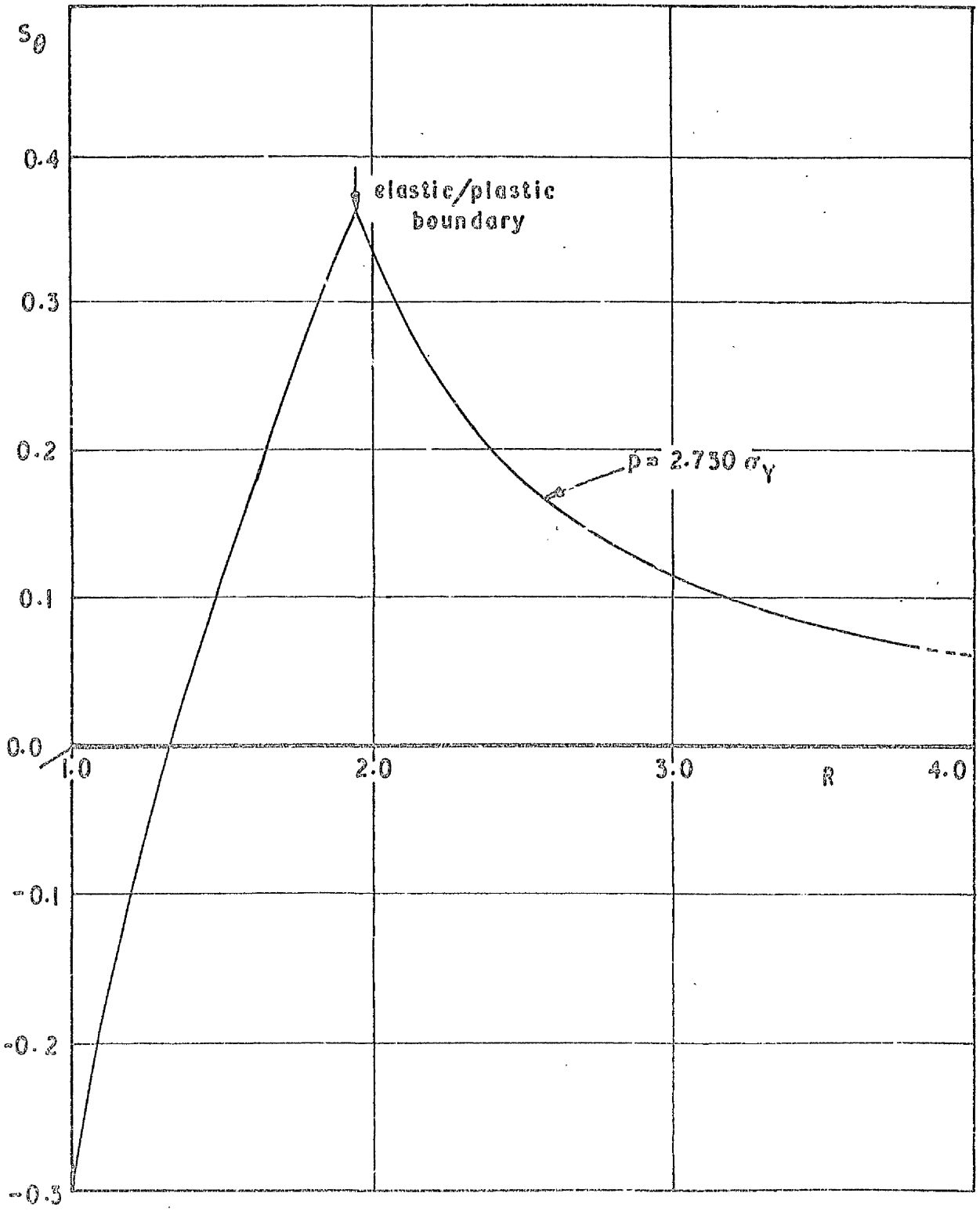

Fig 9.7 Distribution of S_θ at load $p = 2.73\sigma_Y$ using parabola ① - sphere, $R_0 = 6$

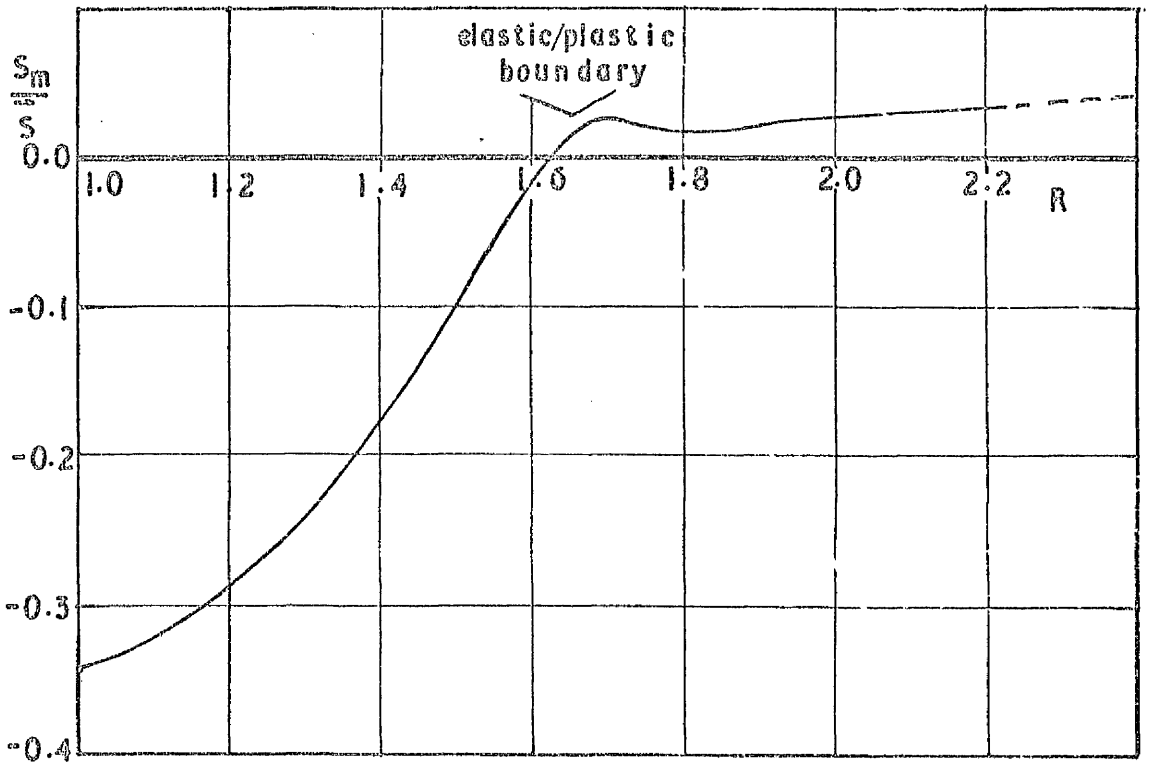

Fig 9.8 Numerical solution - Q=0.3, $p=2.04\sigma_Y$

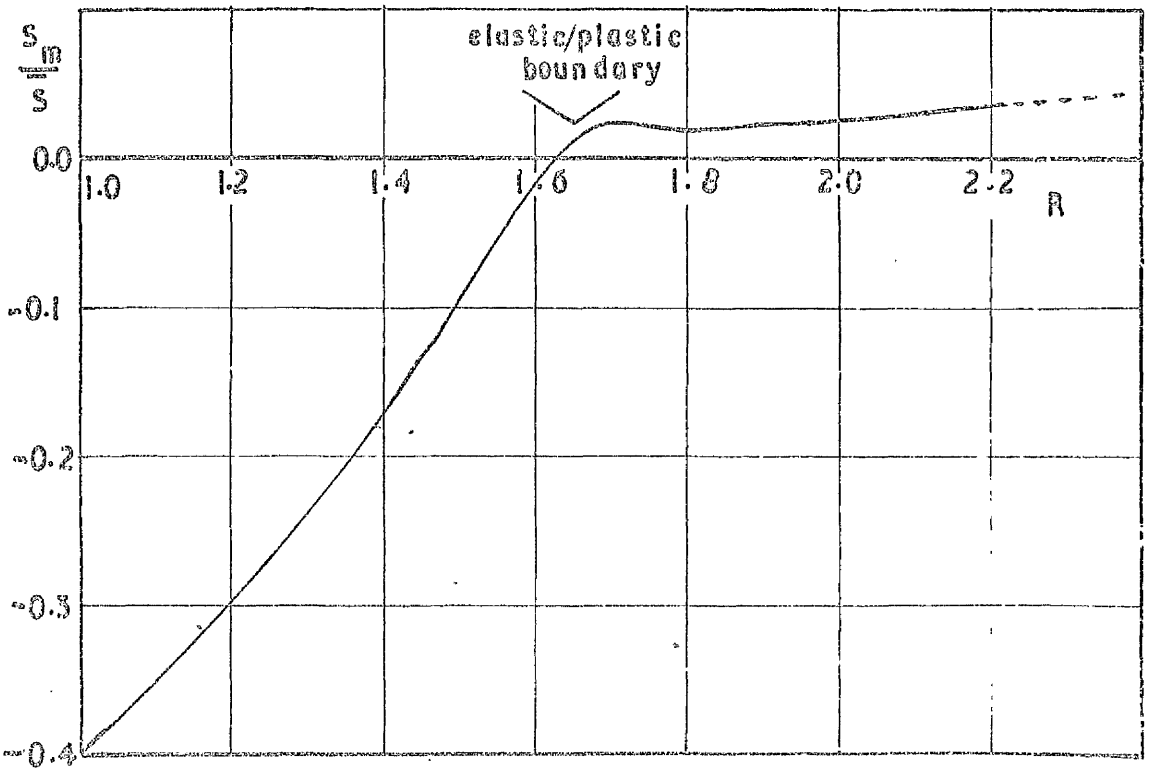

Fig 9.9 Numerical solution - parabola ①, $p=2.04\sigma_Y$

Radial distribution of S_m/S for sphere $R_o=6$ and different stress-strain curves

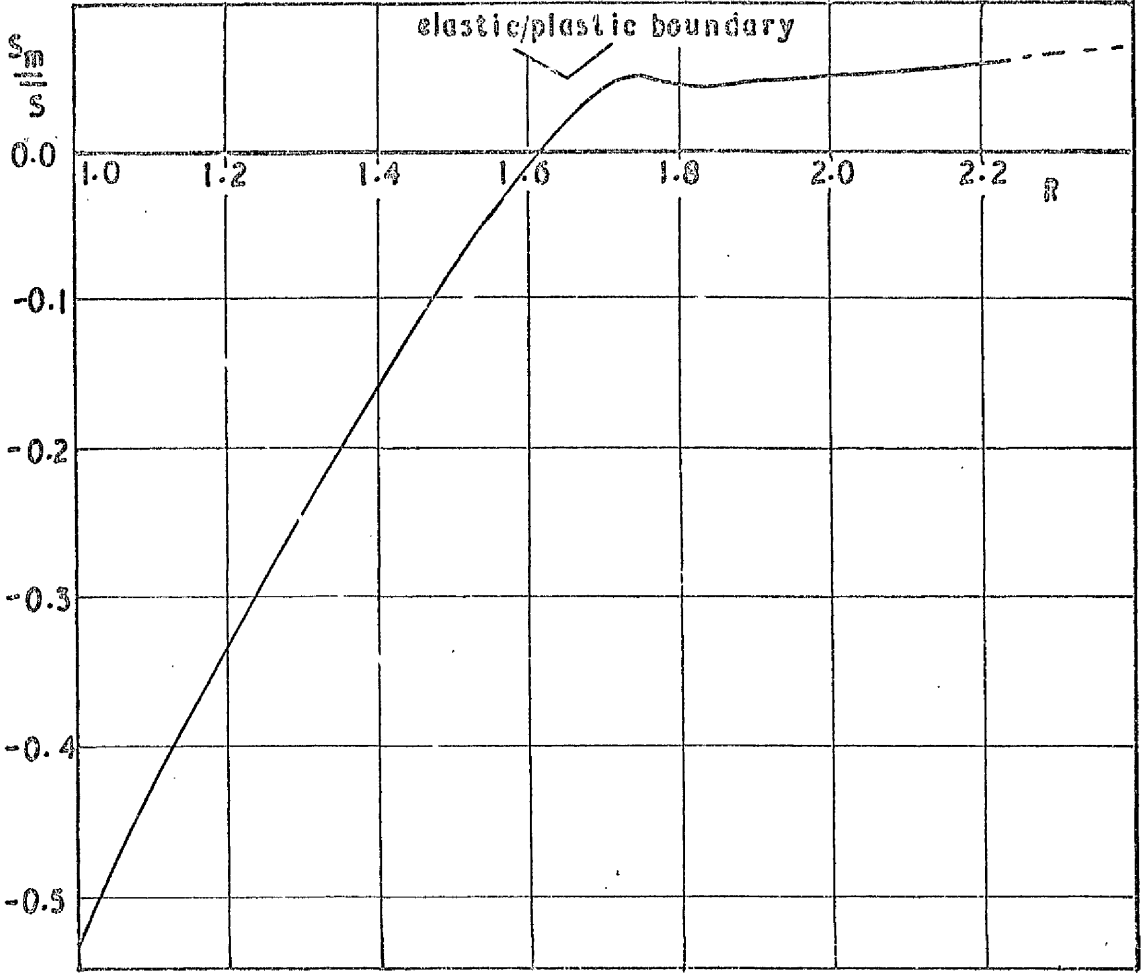

Fig 9.10 Numerical solution - parabola ②, $p = 2.04\sigma_Y$

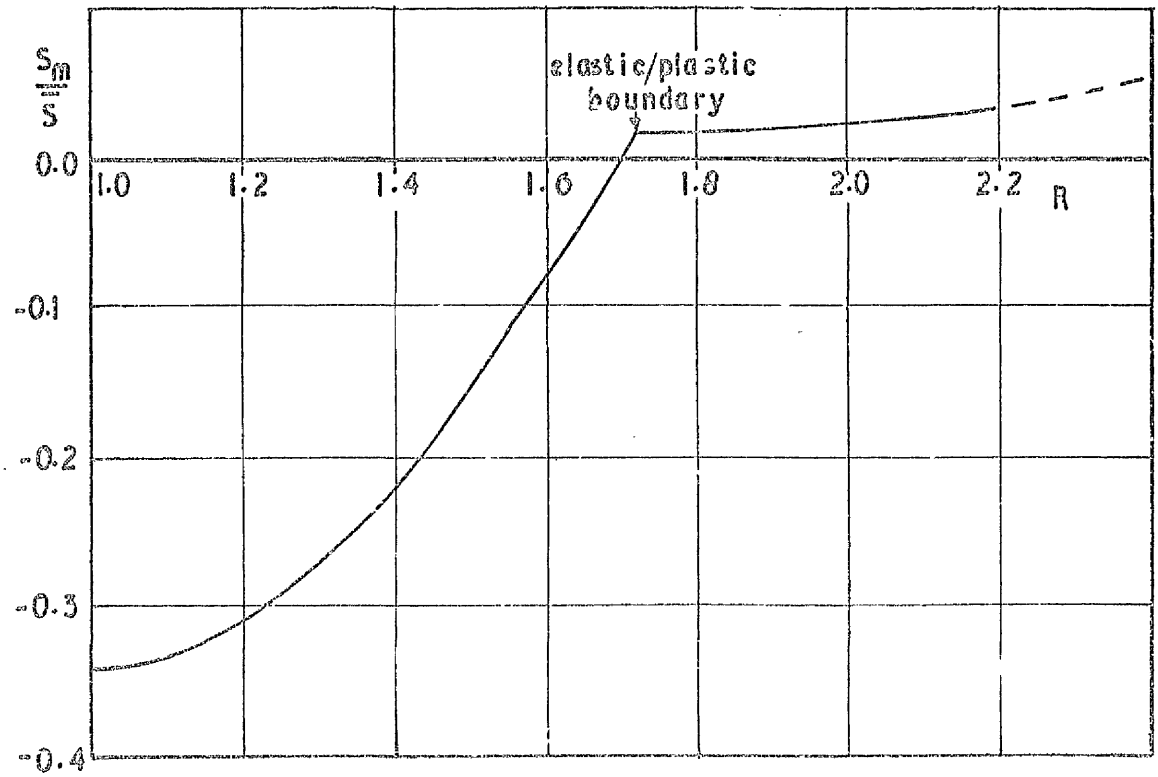

Fig 9.11 Analytical solution - $Q = 0.3$, $p = 2.21\sigma_Y$

Radial distribution of S_m/S for sphere $R_O = 6$ and different stress-strain curves

CHAPTER 10

SLIP LINE ANALYSIS FOR NOTCHED BAR IN BENDING

CHAPTER 10

SLIP LINE ANALYSIS FOR NOTCHED BAR IN BENDING

10.1 Introduction

This chapter details the work done in producing a plane strain slip line solution for a particular geometry of edge-notched bar. The geometry used was that of a series of four point bend specimens of Q1 Navy steel, tested as part of an overall programme of investigation carried out in the department by the fracture research group. The slip line solution was used initially to give a quick indication of the mean to effective stress ratio under the notch surface. Although of limited use, the solution represents one limit of plasticity solutions and helps to confirm other results.

Slip line theory dates back to work done by Coulomb in 1773. However, the velocity equations were not clearly formulated until 1930 by Geiringer[34]. Only in the early 1950's was a momentum created by the works of Hill[9] and Prager and Hodge[35]. In that decade several papers by A.P. Green were published and it is in one of these that the solutions for the edge notched bar in bending were first given.

As was mentioned in chapter 4 the essence of slip line theory is that the material is assumed to be rigid perfectly-plastic; this is a reasonable assumption when dealing with large strains in real low work-hardening materials. The governing equations (4.10) and (4.11) are hyperbolic, indicating that enough information can be found on one boundary for a solution to be determined by progressing from that boundary to another.

In his paper of 1953 Green[36] indicates that two solutions are required to cover the full range of bar sizes 'a'; see figs. 10.1 and 10.2. The first solution, fig. 10.1, is for bars in which the ratio $\frac{a}{r_o}$ is small and the angle $2\psi \leqslant 32^{\circ}41$. A is a point of stress discontinuity; regions (1) and (2) are tension and compression respectively, the remainder being rigid. When 2ψ exceeds this value, the solution at A becomes invalid and a solution of the form II, fig. 10.2, is required. As before there are tension and compression regions but these are now joined by continuous slip lines carried on circular arcs around a rigid region (3).

In 1956, Green and Hundy[37] considered the cases of three- and four-point bending and backed up their findings with excellent pictures of specimens etched by a technique they developed. In 1958, Lianis and Ford[38] tackled the problem of notches of any geometry, in bending, giving both the usual upper bound as well as a lower bound solution. In addition they included the hodographs for the type II solutions. (The use of the hodograph was first suggested by Green in 1954[39]). Checks were made on the solution by use of an internally etched grid. Work has carried on in the 1960's with papers by, for example, Ewing.

10.2 Method of Solution

Attempts to experimentally measure the plastic strains at the root of notches in bend specimens, proved very difficult. It was important for the group research on the 'fundamentals of fracture' to have some idea of the stress and strain pattern and it was thought that a slip line solution would be helpful even if strictly applicable only to rigid perfectly-plastic materials.

The notch geometry of the specimens used is shown in fig. 10.3 and the solution is of type II, due to the dimensions of the specimen. In order to start, an estimate must be made of the extent of yielding on the notch surface. This was done by sectioning strained specimens, photographing them and then tracing the profiles - fig. 10.4 for example.

From this it was decided to take the extent of yielding, η, as 140°.

10.2.1 Stress Solution

Knowing the stress state on the surface and the principal shear stress trajectories (α and β lines), enables the solution to proceed into the specimen. For this purpose equations (4.10) can be expressed in the following useful form:—

along an α line $d\sigma = 2kd\phi$

along a β line $d\sigma = -2kd\phi$

where σ, k, and ϕ are the parameters used in the solution.

Also $\sigma = \frac{1}{2}(\sigma_x+\sigma_Y) = \sigma_z = \frac{1}{2}(\sigma_1+\sigma_2)$

k = yield stress in pure shear

ϕ = angle between the X and α axes.

These quantities are shown on Mohr's circle and on an elemantal 'cube', in figs. 10.5 and 10.6.

The values of σ at all points a to p on fig. 10.7 are shown in Table I on fig. 10.10. From these can be found the principal stresses

$$\left.\begin{aligned} \sigma_1 &= \sigma \pm k \\ \sigma_2 &= \sigma \mp k \\ \sigma_z &= k \end{aligned}\right\} \Rightarrow \quad \begin{aligned} \bar{\sigma} &= \sqrt{3}k \text{ (effective stress)} \\ \sigma_m &= \sigma \text{ (mean stress)} \end{aligned}$$

The principal stress axes are at $(\phi \pm 45^{\circ})$.

The solution starts at the notch surface in a tension region and ends in a constant compressive stress region at the bottom of the bar — the slip line ABCD being continuous (fig. 10.3).

The angle 2λ (which is $\geqslant \frac{\pi}{2}$) and the radius R have to be adjusted to give the equilibrium condition that the σ_x distribution along the slip line ABCD gives no resultant force in the X-direction, while still maintaining right angles at B and C and the condition $2\lambda = 1+\psi$. Using a 10° division of the notch surface, the best approximate solution is as shown in figs. 10.3 and 10.7 with $2\psi = 100^{\circ}$. The σ_x distribution is shown on fig. 10.8.

The values of mean stress σ and the ratio $\frac{\sigma_m}{\bar{\sigma}}$ for all points a to p are given in Table I, fig. 10.10.

10.2.2 Velocity (or Displacement) Solution

The initial boundary displacements due to bending are fed into the field by assuming a $\delta\vartheta = 1^o$ rotation about centres C_1 and C_2 on fig. 10.3; this movement corresponds approximately to the movement of the strained specimen, the profile of which is shown in fig. 10.11. Fig. 10.7 gives the radii of each of the outer points about C_1 and the direction α_1 of the displacements. The values were obtained by geometric calculation based on the radius R (= 15.68 mm) and the angle between N and the other points on the slip line MN. The displacements are shown on the line MN of the hodograph, fig. 10.9, relative to a fixed node O. Essentially the hodograph is a graphical method of applying the compatibility equations (4.11).

Displacements in the outer plastic region lead to points a′ to g′ on the hodograph. The constant velocity discontinuity along a′g′ (fig. 10.7) brings the point a′ to a on the $\mathcal{L}$ and b′ to b etc. The solution then proceeds into the point p on the notch surface .

Checks have been made that the plastic work is positive throughout the field.

Estimates were made of the strains ε_ϑ and $\bar{\varepsilon}$ along the notch surface and the $\mathcal{L}$, along both of which the shear strain $\gamma_{r\vartheta}$ is zero. This entailed determining the original length ℓ_o, of the line (1) for example, on the real plane (fig. 10.7) and measuring its increase in length $\delta\ell$, in the ϑ direction, from the hodograph viz. line (1) on fig. 10.9. The average strain along ℓ_o was thus evaluated as

$$\varepsilon_\vartheta = \log_e \frac{\ell}{\ell_o} \quad \text{where } \ell = \ell_o + \delta\ell.$$

Since the solution is for plane strain ($\varepsilon_z = 0$) and there are no elastic strains (rigid) $\varepsilon_r = -\varepsilon_\vartheta$. Thus when the shear stresses $\gamma_{r\vartheta}$ are zero

$$\bar{\varepsilon} = \frac{2}{\sqrt{3}} \varepsilon_{\vartheta}.$$

The values for lines (1) to (6) are shown on Table II in fig. 10.10.

10.3 Results

It must be remembered that a plane strain slip line solution is approximate. The stress field is essentially a carefully calculated guess which takes no account of equilibrium between plastic and rigid regions, save checking that wedge-shaped rigid regions do not go plastic. Since the characteristics of the equilibrium and compatibility equations are the same the velocity or displacement solution is 'hooked' on to the slip lines of the stress solution. Here, however, the boundary displacements match up in plastic and rigid regions as well as the displacements in the plastic region obeying compatibility. The solution thus gives an upper bound on the applied moment.

A value of this moment can be found by numerical integration using the σ_x distribution in fig. 10.8; this gives a value of 244.88 $r_o^2 \sigma_Y$ kNm/m thickness. When the bar dimensions and the yield stress σ_Y are inserted, the moment is 11.07 kNm. When this value is plotted on the graphs of moment against notch opening (fig. 8.3) it is situated as expected, for a non-work-hardening material. The displacements on this graph are measured by a gauge placed at 3.2 mm above the upper surface of the bar (points P_1 and P_2 in fig. 10.3). For the slip line solution a rotation of 1^o about centres C_1 and C_2, the notch opening is 1.43 mm. This opening shows reasonable agreement with the curves in fig. 8.3 obtained from the testing of bars cut from the short and long transverse directions of thick plate.

The plots of $\bar{\varepsilon}$ along the $\mathcal{L}$ and along the notch surface are shown in fig. 10.12 and the plot of $\frac{\sigma_m}{\bar{\sigma}}$ along the $\mathcal{L}$, in fig. 10.13. The plots along the $\mathcal{L}$ show clearly a

significant drop in ductility within one radius of the notch surface, whereas along the notch surface the value of $\bar{\varepsilon}$ keeps a high value, dropping by only $\sim 10\%$ in 30° from the $\not{\mathrm{C}}$.

The curve of $\frac{\sigma_m}{\bar{\sigma}}$ is plotted on the graphs for the keyhole in Chapter 8 and shows good agreement. From the etched bands shown in fig. 10.11 an estimate of 20% for the effective strain at the notch root was made by Mackenzie[40]; this compares favourably with the 25% from the slip line solution.

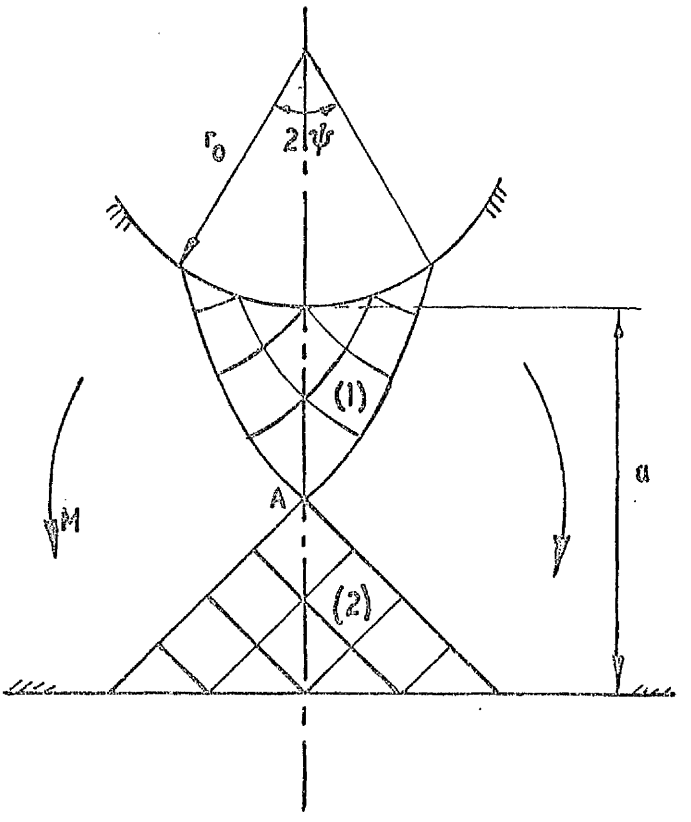

Fig 10.1 Solution I

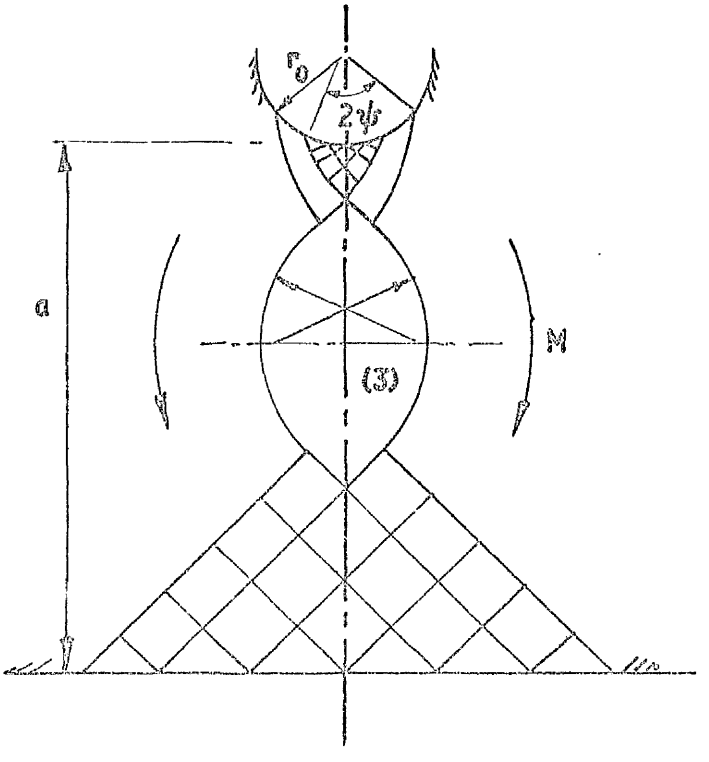

Fig 10.2 Solution II

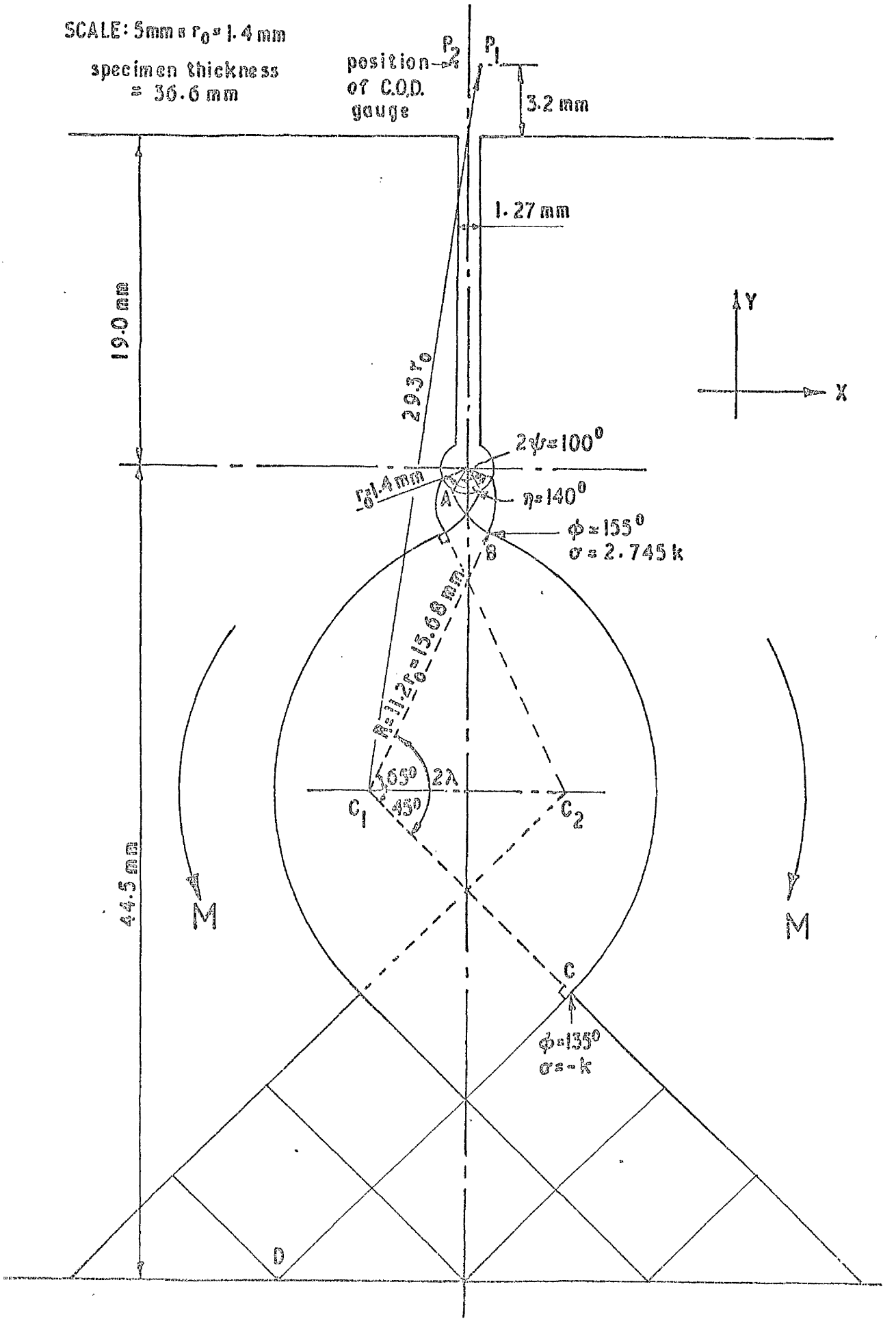

Fig 10.3 Overall geometry of slip line solution - edge notch bar in bending

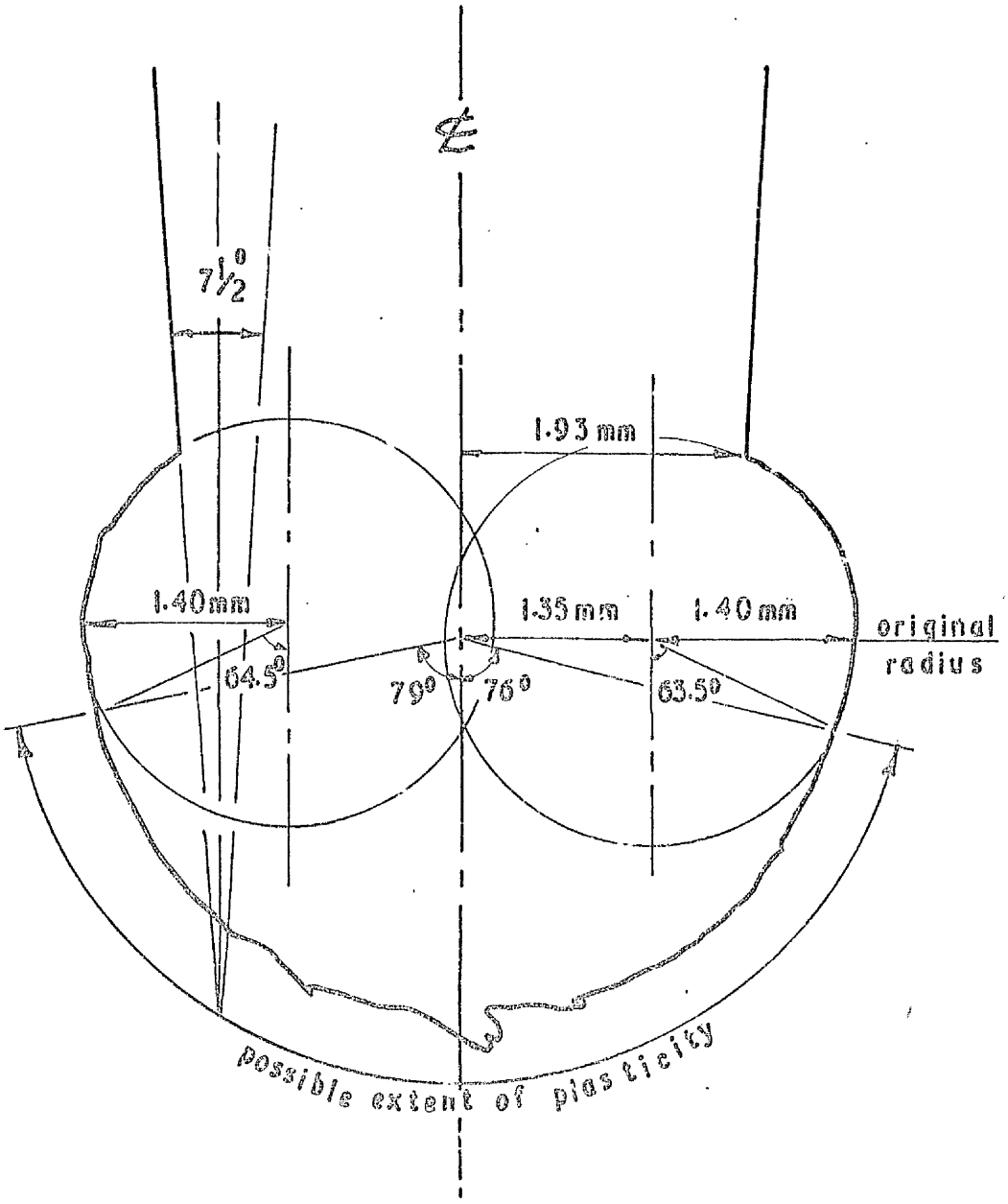

Fig 10·4 Traced profile of $7\frac{1}{2}^{\circ}$ strained bar

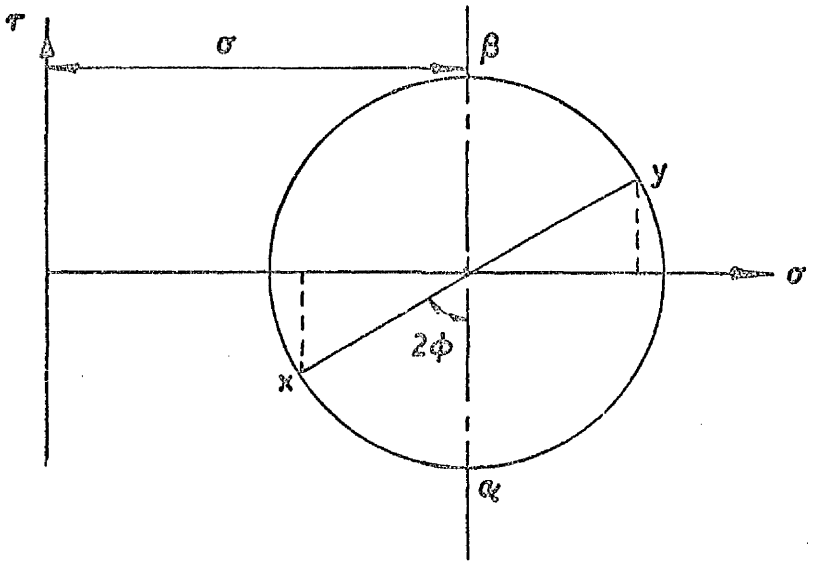

Fig 10.5

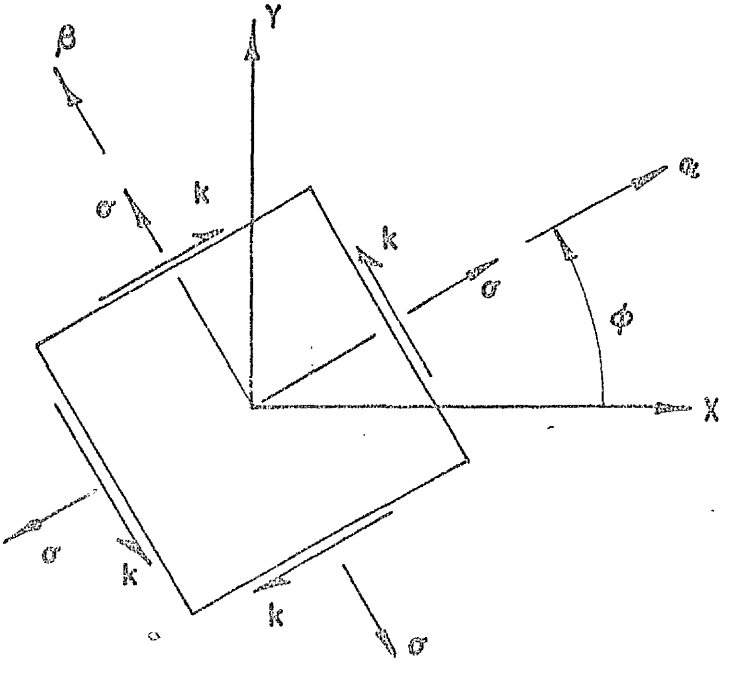

Fig 10.6

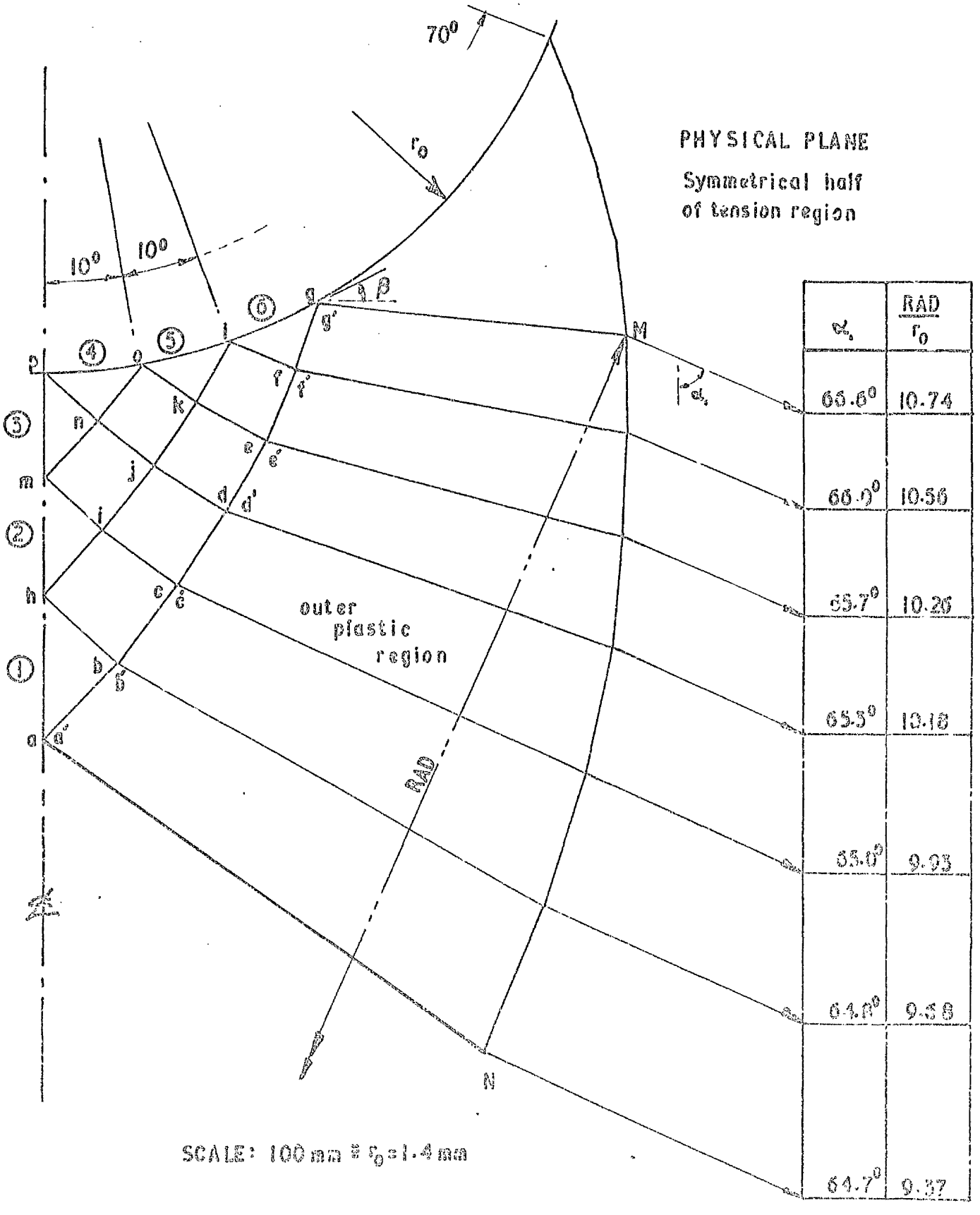

α_1	RAD / r_0
66·6°	10·74
66·0°	10·56
65·7°	10·26
65·5°	10·18
65·0°	9·93
64·8°	9·58
64·7°	9·37

Fig 10.7

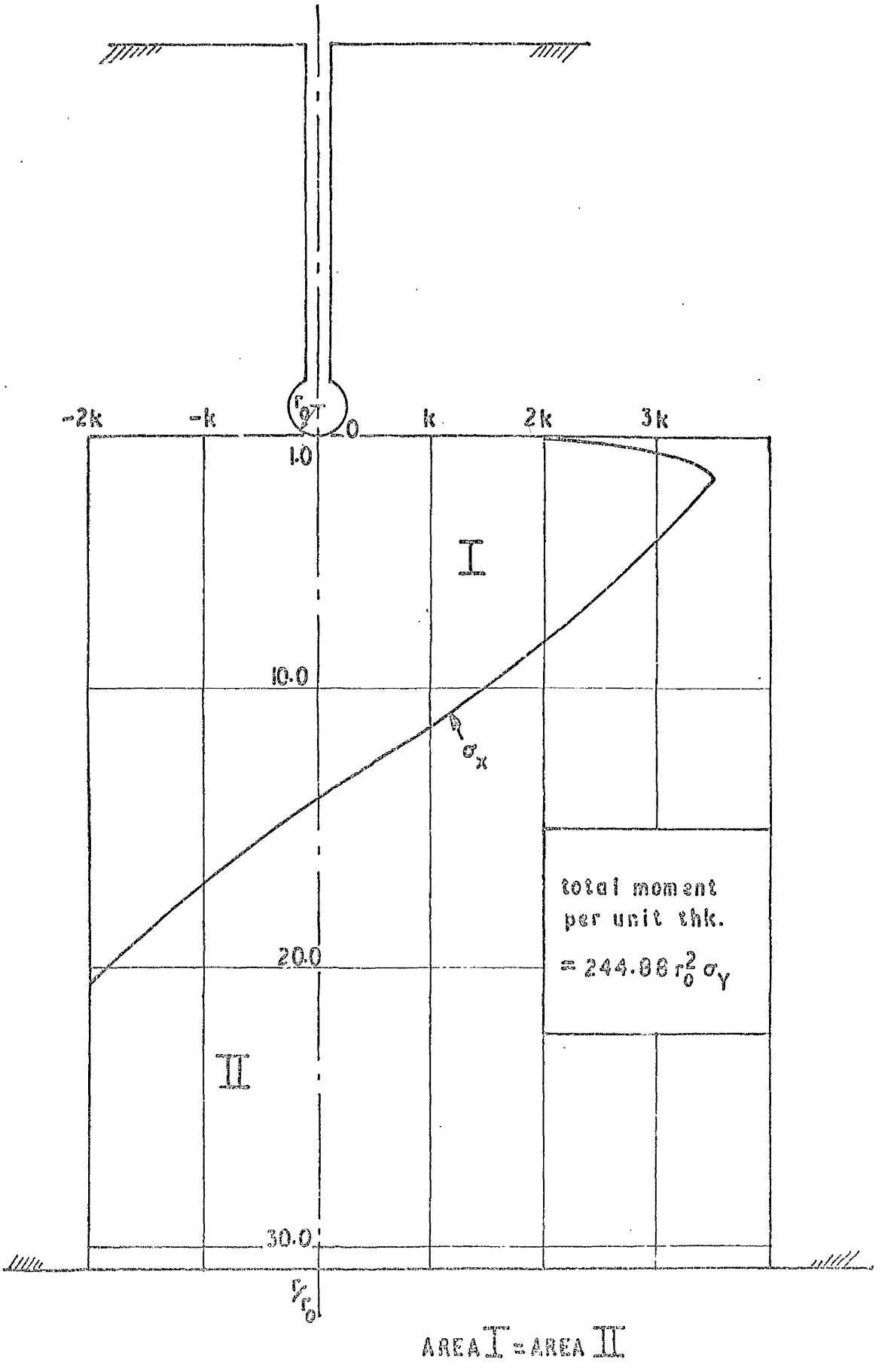

Fig 10.8 Distribution of σ_x across minimum section

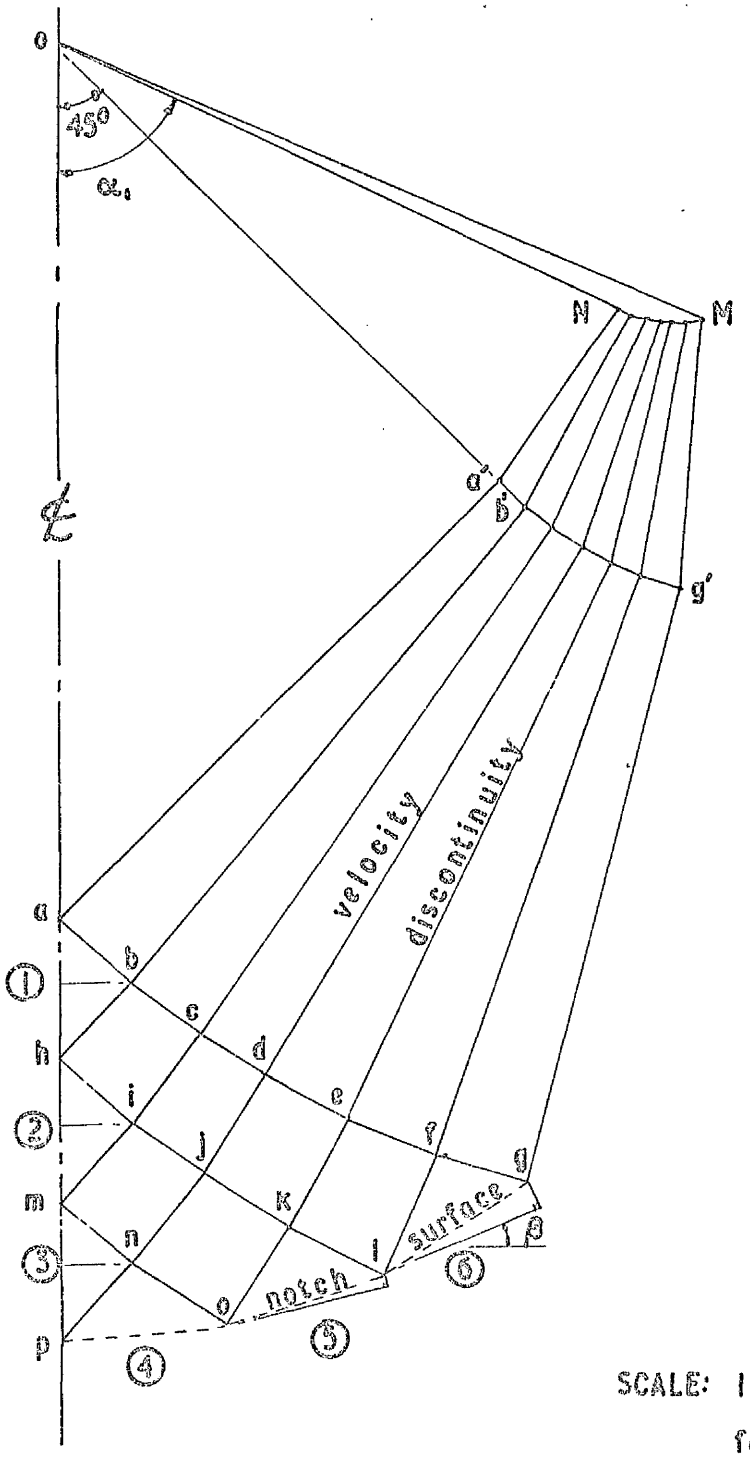

HODOGRAPH
symmetrical half
of tension region

SCALE: 1mm ≡ $2 \times 10^{-3} r_0$
for 1° opening

Fig 10.9

STRESSES

Points	Radius	σ	$\frac{\sigma_m}{\sigma} = \frac{\sigma}{\sqrt{3}k}$
p,o,l,g	$1.00r_0$	1.000k	0.578
n,k,f	$1.10r_0$	1.175k	0.678
m,j,e	$1.19r_0$	1.349k	0.778
i,d	$1.31r_0$	1.524k	0.880
h,c	$1.43r_0$	1.698k	0.980
b	$1.57r_0$	1.875k	1.080
a	$1.70r_0$	2.047k	1.180

TABLE I

STRAINS

Line	Radius	l_0	δl	$\epsilon_\theta = \log_e \frac{\delta l + l_0}{l_0}$	$\bar{\epsilon} = \frac{2}{\sqrt{3}} \epsilon_\theta$
①	$1.10r_0$	$0.105r_0$	$0.020r_0$	17.4%	20.1%
②	$1.31r_0$	$0.115r_0$	$0.019r_0$	14.5%	16.5%
③	$1.57r_0$	$0.145r_0$	$0.019r_0$	12.2%	14.1%
④	$1.00r_0$	$0.175r_0$	$0.044r_0$	22.3%	25.8%
⑤	$1.00r_0$	$0.175r_0$	$0.043r_0$	21.7%	25.1%
⑥	$1.00r_0$	$0.175r_0$	$0.043r_0$	21.7%	25.1%

TABLE II

Fig 10.10

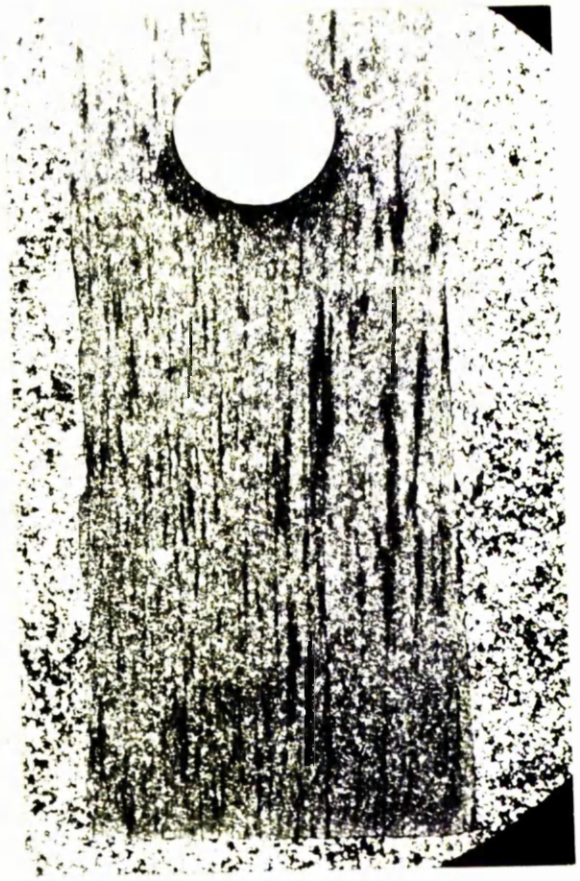

Fig 10·11 Etched section of notched bend specimen showing banding (ref (30))

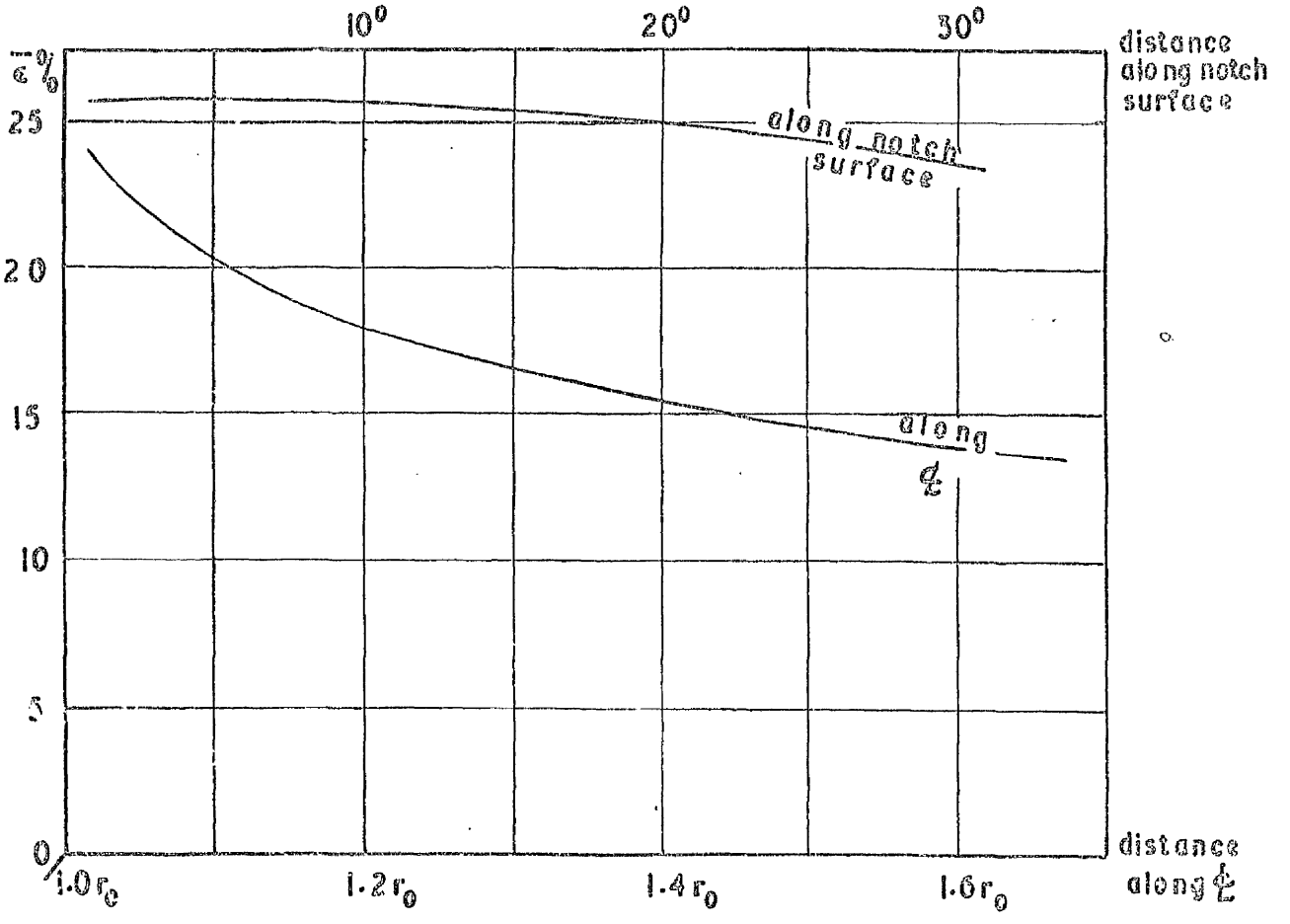

Fig 10.12 Distribution of effective plastic strain along notch surface and ℄

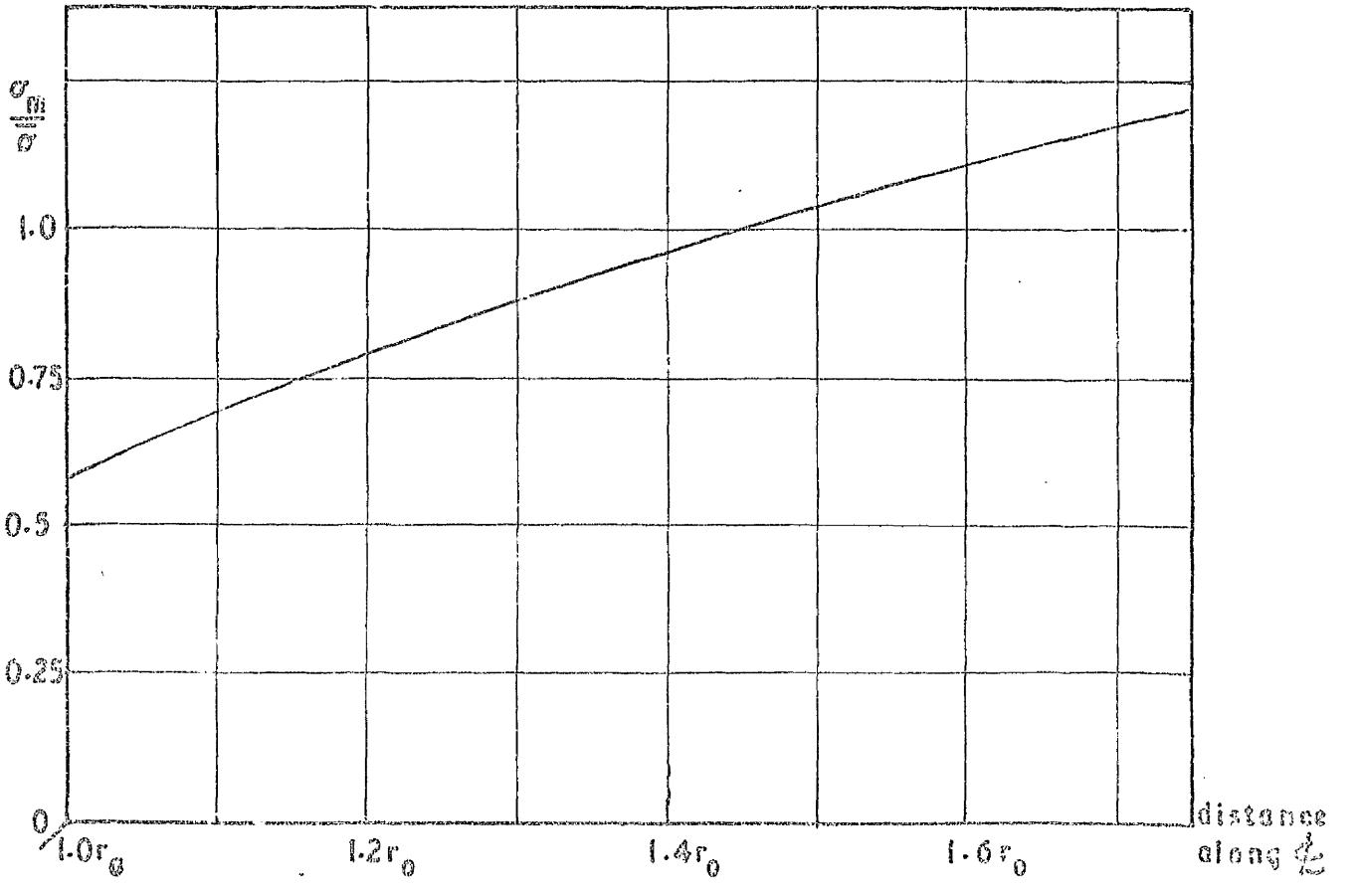

Fig 10.13 Distribution of $\frac{\sigma_m}{\sigma}$ along ℄

CHAPTER 11

ELLIPTICAL CREEP SOLUTION

CHAPTER 11

ELLIPTICAL CREEP SOLUTION

11.1 Introduction

The main purpose of this chapter is to illustrate how the elliptical three variable stress oriented approach could be applied to creep problems. It is not intended as a thorough study in creep but more as an illustration of the extension of the method; consequently it is dealt with briefly. Essentially the problem is one of initial stress redistribution in primary creep up to steady state conditions.

The formulation (section 11.2) is different from that of the elasto-plastic problem because of the constituitive equations being in stress and strain rates and including creep instead of plastic strains. The program (section 11.3) however is relatively similar with the three main variables once again being total stresses. The solution to the plain strain problem of the hole in tension is given as an illustration - section 11.4.

The other main difference is that the variables are now non-dimensionalized with respect to σ_o - the applied stress, instead of the yield stress σ_Y as in the elasto-plastic problem.

11.2 Formulation of the Creep Problem

11.2.1 The Governing Equations

Rewriting the equilibrium, stress/strain and strain/displacement equations in terms of rates gives:-

Equilibrium; $$r\frac{\partial \dot{\sigma}_r}{\partial r} + \frac{\partial \dot{\tau}_{r\vartheta}}{\partial \vartheta} + \dot{\sigma}_r - \dot{\sigma}_\vartheta = 0 \qquad (11.1)$$

$$r\frac{\partial \dot{\tau}_{r\vartheta}}{\partial r} + \frac{\partial \dot{\sigma}_\vartheta}{\partial \vartheta} + 2\dot{\tau}_{r\vartheta} = 0 \qquad (11.2)$$

where $\dot{\sigma} = \frac{d\sigma}{dt}$ etc.

Stress/strain; For plane strain $\varepsilon_z = 0 = \dot{\varepsilon}_z$ and using the assumption that creep strains produce no volume change gives –

$$E\dot{\varepsilon}_\vartheta = (1-\nu^2)\dot{\sigma}_\vartheta - \nu(1+\nu)\dot{\sigma}_r + E(1-\nu)\dot{\varepsilon}_{\vartheta_c} - \nu E\dot{\varepsilon}_{r_c} \qquad (11.3)$$

$$E\dot{\varepsilon}_r = (1-\nu^2)\dot{\sigma}_r - \nu(1+\nu)\dot{\sigma}_\vartheta + E(1-\nu)\dot{\varepsilon}_{r_c} - \nu E\dot{\varepsilon}_{\vartheta_c} \qquad (11.4)$$

$$E\dot{\gamma}_{r\vartheta} = 2(1+\nu)\dot{\tau}_{r\vartheta} + \dot{\gamma}_{r\vartheta_c} \qquad (11.5)$$

where ε_{r_c} etc. are creep strain components
and $\dot{\varepsilon} = \frac{d\varepsilon}{dt}$ etc.

Ellimination of $\dot{\varepsilon}_{r_c}$ from (11.3) and (11.4) gives

$$\frac{1}{(1+\nu)(1-2\nu)}\left[E(1-\nu)\dot{\varepsilon}_\vartheta + E\nu\dot{\varepsilon}_r\right] = \dot{\sigma}_\vartheta + \frac{E\dot{\varepsilon}_{\vartheta_c}}{1+\nu}$$

$$= \dot{a} \text{ by definition (11.6)}$$

Similarly $$\dot{b} = \dot{\sigma}_r + \frac{E\dot{\varepsilon}_{r_c}}{1+\nu} = \frac{1}{(1+\nu)(1-2\nu)}\left[E(1-\nu)\dot{\varepsilon}_r + E\nu\dot{\varepsilon}_\vartheta\right] \qquad (11.7)$$

and $$\dot{c} = \dot{\tau}_{r\vartheta} + \frac{E\dot{\gamma}_{r\vartheta_c}}{2(1+\nu)} = \frac{E\dot{\gamma}_{r\vartheta}}{2(1+\nu)}\,. \qquad (11.8)$$

Strain/displacement;

$$\dot{\varepsilon}_r = \frac{\dot{u}}{r},\quad \dot{\varepsilon}_\vartheta = \frac{\dot{u}}{r} + \frac{1}{r}\frac{\partial \dot{v}}{\partial \vartheta},\quad \dot{\gamma}_{r\vartheta} = \frac{1}{r}\frac{\partial \dot{u}}{\partial \vartheta} + \frac{\partial \dot{v}}{\partial r} - \frac{\dot{v}}{r}\,.$$

Elimination of the displacements gives the equation of compatibility of strain rates

$$\frac{\partial^2(r\dot{\gamma}_{r\vartheta})}{\partial r\partial \vartheta} - r\frac{\partial^2(r\dot{\varepsilon}_\vartheta)}{\partial r^2} - \frac{\partial^2 \dot{\varepsilon}_r}{\partial \vartheta^2} + r\frac{\partial \dot{\varepsilon}_r}{\partial r} = 0. \qquad (11.9)$$

Now from the definitions of $\dot{a}$, $\dot{b}$, $\dot{c}$ (equations (11.6), (11.7), (11.8))

$$E\dot{\varepsilon}_\vartheta = (1-\nu^2)\dot{a} - \nu(1+\nu)\dot{b}$$

$$E\dot{\varepsilon}_r = (1-\nu^2)\dot{b} - \nu(1+\nu)\dot{a}$$

$$E\dot{\gamma}_{r\vartheta} = 2(1+\nu)\dot{c}.$$

Substituting these relations into (11.9) gives

$$2\left(\frac{\partial \dot{c}}{\partial \vartheta} + r\frac{\partial^2 \dot{c}}{\partial \vartheta \partial r}\right) - (1-\nu)r^2\frac{\partial^2 \dot{a}}{\partial r^2} + \nu r^2\frac{\partial^2 \dot{b}}{\partial r^2} - (1-\nu)\frac{\partial^2 \dot{b}}{\partial \vartheta^2}$$
$$+ \nu\frac{\partial^2 \dot{a}}{\partial \vartheta^2} - r\frac{\partial \dot{a}}{\partial r}(2-\nu) + r\frac{\partial \dot{b}}{\partial r}(1+\nu) = 0 \qquad (11.10)$$

Equation (11.10) can be expressed in terms of stress rates by substitution of equations (11.6), (11.7) and (11.8) giving

$$2\left(\frac{\partial \dot{\tau}_{r\vartheta}}{\partial \vartheta} + r\frac{\partial^2 \dot{\tau}_{r\vartheta}}{\partial \vartheta \partial r}\right) - (1-\nu)r^2\frac{\partial^2 \dot{\sigma}_\vartheta}{\partial r^2} + \nu r^2\frac{\partial^2 \dot{\sigma}_r}{\partial r^2} - (1-\nu)\frac{\partial^2 \dot{\sigma}_r}{\partial \vartheta^2}$$
$$+ \nu\frac{\partial^2 \dot{\sigma}_\vartheta}{\partial \vartheta^2} - r\frac{\partial \dot{\sigma}_\vartheta}{\partial r}(2-\nu) + r\frac{\partial \dot{\sigma}_r}{\partial r}(1+\nu)$$
$$= -\frac{E}{(1+\nu)}\left[\left(\frac{\partial \dot{\gamma}_{r\vartheta c}}{\partial \vartheta} + r\frac{\partial^2 \dot{\gamma}_{r\vartheta c}}{\partial r \partial \vartheta}\right) - (1-\nu)r^2\frac{\partial^2 \dot{\varepsilon}_{\vartheta c}}{\partial r^2} + \nu r^2\frac{\partial^2 \dot{\varepsilon}_{rc}}{\partial r^2}\right.$$
$$\left. - (1-\nu)\frac{\partial^2 \dot{\varepsilon}_{rc}}{\partial \vartheta^2} + \nu\frac{\partial^2 \dot{\varepsilon}_{\vartheta c}}{\partial \vartheta^2} - r(2-\nu)\frac{\partial \dot{\varepsilon}_{\vartheta c}}{\partial r} + r\frac{\partial \dot{\varepsilon}_{rc}}{\partial r}(1+\nu)\right]$$
$$= \text{RHS}. \qquad (11.11)$$

The shear stress rate $\dot{\tau}_{r\vartheta}$ can be eliminated from this equation by use of the derivatives of equations (11.1) and (11.2). Thus

$$(-1+\nu)\left[r\frac{\partial \dot{\sigma}_r}{\partial r} + r^2\frac{\partial^2 \dot{\sigma}_r}{\partial r^2} + r\frac{\partial \dot{\sigma}_\vartheta}{\partial r} + \frac{\partial^2 \dot{\sigma}_\vartheta}{\partial \vartheta^2} + r^2\frac{\partial^2 \dot{\sigma}_\vartheta}{\partial r^2}\right.$$
$$\left. + \frac{\partial^2 \dot{\sigma}_r}{\partial \vartheta^2}\right] = \text{RHS} \qquad (11.12)$$

where RHS is as defined in (11.11).

Equations (11.1), (11.2) and (11.12) now form the three governing equations in $\dot{\sigma}_r$, $\dot{\sigma}_\vartheta$ and $\dot{\tau}_{r\vartheta}$, in a similar way to the stress formulation of the elasto-plastic problem.

Creep Relations; These are usually given as

$$\dot{\varepsilon}_{\vartheta_c} = A(t)\bar{\sigma}^{n-1}\left[\sigma_\vartheta - \frac{1}{2}(\sigma_r + \sigma_z)\right]$$
$$\dot{\varepsilon}_{r_c} = A(t)\bar{\sigma}^{n-1}\left[\sigma_r - \frac{1}{2}(\sigma_\vartheta + \sigma_z)\right]$$
$$\dot{\gamma}_{r\vartheta_c} = A(t)\bar{\sigma}^{n-1}\,3\tau_{xy}$$

where the creep law $\dot{\bar{\varepsilon}} = A(t)\bar{\sigma}^n$ is assumed.

Also $\dot{\varepsilon}_{z_c} = -\dot{\varepsilon}_{r_c} - \dot{\varepsilon}_{\vartheta_c} = A(t)\bar{\sigma}^{n-1}\left[\sigma_z - \frac{1}{2}(\sigma_r+\sigma_\vartheta)\right]$.

Non-dimensionalizing of Variables;

Let $dT = \frac{EA(t)dt\sigma_o^{n-1}}{1-\nu}$ where σ_o = some reference loading stress,

and $S_r = \frac{\sigma_r}{\sigma_o}$, $S_\vartheta = \frac{\sigma_\vartheta}{\sigma_o}$, $S_{r\vartheta} = \frac{\tau_{r\vartheta}}{\sigma_o}$, $\bar{S} = \frac{\bar{\sigma}}{\sigma_o}$.

Stress rates become $\dot{S}_r = \frac{dS_r}{dT}$ etc.

Non-dimensionalizing the three governing equations gives

$$(11.1) \Rightarrow r\frac{\partial}{\partial r}\left(\frac{dS_r}{dT}\right) + \frac{\partial}{\partial\vartheta}\left(\frac{dS_{r\vartheta}}{dT}\right) + \left(\frac{dS_r}{dT}\right) - \left(\frac{dS_\vartheta}{dT}\right) = 0 \qquad (11.13)$$

$$(11.2) \Rightarrow r\frac{\partial}{\partial r}\left(\frac{dS_{r\vartheta}}{dT}\right) + \frac{\partial}{\partial\vartheta}\left(\frac{dS_\vartheta}{dT}\right) + 2\left(\frac{dS_{r\vartheta}}{dT}\right) = 0 \qquad (11.14)$$

$$(11.12) \Rightarrow r^2\frac{\partial^2}{\partial r^2}\left(\frac{dS_\vartheta}{dT}\right) + r\frac{\partial}{\partial r}\left(\frac{dS_\vartheta}{dT}\right) + \frac{\partial^2}{\partial\vartheta^2}\left(\frac{dS_\vartheta}{dT}\right) + r^2\frac{\partial^2}{\partial r^2}\left(\frac{dS_r}{dT}\right) + r\frac{\partial}{\partial r}\left(\frac{dS_r}{dT}\right) + \frac{\partial^2}{\partial\vartheta^2}\left(\frac{dS_r}{dT}\right) = \left(r^2\frac{\partial^2}{\partial r^2} + r\frac{\partial}{\partial r} + \frac{\partial^2}{\partial\vartheta^2}\right)(\dot{S}_\vartheta+\dot{S}_r)$$

$$= \nabla^2(\dot{S}_\vartheta+\dot{S}_r) = \text{RHSN} \qquad (11.15)$$

where

$$\text{RHSN} = \frac{1}{1+\nu}\Big[\left(\frac{\partial}{\partial\vartheta} + r\frac{\partial^2}{\partial r\partial\vartheta}\right)(3\bar{S}^{n-1}S_{r\vartheta}) + \left(-(1-\nu)r^2\frac{\partial^2}{\partial r^2} + \nu\frac{\partial^2}{\partial\vartheta^2} - (2-\nu)r\frac{\partial}{\partial r}\right)\left(\bar{S}^{n-1}\left[S_\vartheta - \frac{1}{2}(S_r+S_z)\right]\right) + \left(\nu r^2\frac{\partial^2}{\partial r^2} + (1+\nu)r\frac{\partial}{\partial r} - (1-\nu)\frac{\partial^2}{\partial\vartheta^2}\right)\left(\bar{S}^{n-1}\left[S_r - \frac{1}{2}(S_\vartheta+S_z)\right]\right)\Big] \qquad (11.16)$$

Equations (11.13) to (11.16) are in terms of stress rates $\dot{S}_r$, $\dot{S}_\vartheta$ and $\dot{S}_{r\vartheta}$; they can also be expressed in terms of stress increments and this is the form in which they are used.

Thus

$$\boxed{\begin{aligned} &r\frac{\partial S'_r}{\partial r} + \frac{\partial S'_{r\vartheta}}{\partial\vartheta} + S'_r - S'_\vartheta = 0 \\ &r\frac{\partial S'_{r\vartheta}}{\partial r} + \frac{\partial S'_\vartheta}{\partial\vartheta} + 2S'_{r\vartheta} = 0 \\ &\left(r^2\frac{\partial^2}{\partial r^2} + r\frac{\partial}{\partial r} + \frac{\partial^2}{\partial\vartheta^2}\right)(S'_r + S'_\vartheta) = \text{RHSN}.dT \end{aligned}} \qquad (11.17)$$

where stress increment $S' = \delta S$.

Equations (11.17) form the three governing equations in terms of stress increments S'_ϑ, S'_r, $S'_{r\vartheta}$. The similarity of these equations with equations (4.40) for the elasto-plastic problem should be noted in that the method of solution by field equations and integration can be similarly applied.

11.2.2 Evaluation of S_z

It can be seen from equation (11.16) that S_z is required. In order to show the evaluation it must be realised that the solution of the equations (11.17) proceeds in finite time steps dT and that the quantities $\bar{S}$, S_ϑ, S_r, $S_{r\vartheta}$ and S_z in (11.16) refer to the values of these total stresses at the end of the previous time interval.

Thus consider the i^{th} and $(i+1)^{th}$ time intervals and let e_{zc_i} represent the total z creep strain at the end of the i^{th} interval and $\dot{e}_{zc_i}$ the increment of z creep strain during the $(i+1)^{th}$ interval where $e = \frac{E\varepsilon}{\sigma_o}$,

therefore $$e_{zc_{i+1}} = e_{zc_i} + \dot{e}_{zc_i} dT.$$

But $e'_z = 0$, therefore $$e_{zc_{i+1}} = -\left[S_{z_{i+1}} - \nu(S_{r_{i+1}} + S_{\vartheta_{i+1}})\right]$$

and $$\dot{e}_{zc_i} = (1-\nu)\bar{S}_i^{n-1}\left[S_{z_i} - \tfrac{1}{2}(S_{r_i} + S_{\vartheta_i})\right]$$

therefore $$S_{z_{i+1}} = \nu(S_{r_{i+1}} + S_{\vartheta_{i+1}}) - e_{zc_i} - (1-\nu)\bar{S}_i^{n-1}, \left[S_{z_i} - \tfrac{1}{2}(S_{r_i} + S_{\vartheta_i})\right] dT \qquad (11.18)$$

and $$e_{zc_{i+1}} = -\left[S_{z_{i+1}} - \nu(S_{r_{i+1}} + S_{\vartheta_{i+1}})\right]. \qquad (11.19)$$

When the solution for the $(i+1)^{th}$ time interval has been found, the total stresses $S_{r_{i+1}}$, $S_{\vartheta_{i+1}}$ are known and $S_{z_{i+1}}$ can be found from (11.18). This enables RHSN to be evaluated during the next time interval, after which S_z must again be calculated and this requires a value for e_{zc}. Thus $e_{zc_{i+1}}$ is found using (11.19). At the end of the first time interval, the values S_{r_i} etc. in (11.18)

are the initial elastic values and e_{zc_i} has the value zero.

11.2.3 Effective Strain

A value of effective strain can be found to give an indication of general straining. This is evaluated using the definition of ε^* in Finnie and Heller p.171[41]. In our notation and remembering that $e_z = 0 = e_{rz} = e_{\vartheta z}$ for plane strain, this gives

$$\bar{e} = \sqrt{\frac{4}{9}\left[e_\vartheta^2 + e_r^2 - e_r e_\vartheta\right] + \frac{1}{3}e_{r\vartheta}^2}$$

where e_ϑ etc. are total strains comprising elastic and creep parts.

11.3 Method of Solution

11.3.1 Introduction

Due to the similarity of the creep and elasto-plastic equations, many features of the method of solution are similar. The size of field is the same and once again fixed boundaries are employed. The discretization of the differential governing equations is the same, the variables for the creep problem being S'_ϑ, S'_r and $S'_{r\vartheta}$ instead of AS, BS and CS in the elasto-plastic problem dealt with in paragraph 7.3.3.

The method of solving for the three variables is identical with field equations being used for S'_r and $S'_{r\vartheta}$ and a circumferential integration being used for S'_ϑ, the boundary conditions for each variable are also identical. The main difference lies in the evaluation of RHSN — equation (11.16) where, unlike P in the elasto-plastic problem, the stress components are continuous over the field. RHSN is thus found by evaluation of the three stress expressions over the whole field and then by summing the various gradients and curvatures of these expressions.

In the elasto-plastic problem, for any load stage the solution of the field was carried out several times with the values of P being corrected each time. In the creep problem, the solution of the field represents the solution

of the stresses at the end of one time interval after which the various quantities are updated and the solution for the next time interval initiated.

11.3.2 Outline of Program

The following are the main steps of the program.

(i) The elastic stress values are fed in and, having selected an initial value of dT, RHSN – equation (11.16) – is evaluated with e_{zc} being initially zero.

(ii) The field equations for S'_r and $S'_{r\vartheta}$ are solved 10 times over the field and then S'_ϑ is found by circumferential integration. This step is executed 20 times, which is adequate to achieve convergence. The total stresses are then updated.

(iii) S_z is found using (11.18) and then $e_{zc_{i+1}}$ is found using (11.19). $\overline{S}$ is also evaluated along with quantities like $\overline{e}$ for reference.

(iv) The same or a different value of dT is selected and RHSN evaluated from (11.16).

(v) Return to step (ii) and resolve field for next time increment until either (i) a desired total time is reached or (ii) steady state conditions have been achieved or (iii) an instability initiates.

11.4 Results

11.4.1 Introduction

The main aims of this extension of the elliptical method into creep are –

1. to illustrate the feasibility and relative simplicity of extending the method using the hole in tension as an example.
2. to plot the relaxation of stress with time for several values of index n.

3. to show the effect of time and varying index n, on the ratio $\frac{\sigma_m}{\bar{\sigma}}$.

4. to plot the distribution of effective strain $\bar{e}$ along the $\measuredangle\ \vartheta = 0^\circ$ and the hole surface at various times and index values.

The field size and fixed boundary conditions were the same as those for the elasto-plastic solutions with the outer K boundary again being $\frac{r}{r_0} = 2.281$. Due to the time and money restrictions on computing†, the creep program was run for three index values $n = 2.5$, 3.0 and 3.5. It was intended to run the programs for 400 time steps dT, which varied between 0.0002 and 0.0032, up to a total time of $T = 0.57$. In the case of index values $n = 2.5$ and 3.0, this was achieved but for $n = 3.5$, a steady state condition was achieved at the point $K = 2$, $L = 2$ after time $T = 0.4$, after which an instability initiated and the program thus stopped.

A similar instability was also noticed by Byrne[43] when attempting numerical solutions with similar index values. He concluded that it was due to a cumulative error in the evaluation of creep strain from total strain and was not a function of the time interval dT taken; greater stability could be achieved by reducing grid size. The solution up to this instability can, however, be assumed to be acceptable.

11.4.2 Stress Results

Fig. 11.1 shows the relaxation with time of the effective stress at the two points $(K = 2, L = 2)$ and $(K = 6, L = 7)$ for various values of index n. The graphs for $n = 3.5$ terminate at a X, where the program was stopped; it will be noticed that the effective stress $\bar{\sigma}_{2,2}$ has reached steady state at this time.

---

†each program took 40 minutes to run on UNIVAC 1108, costing approximately £ 70.

Fig. 11.2 illustrates the variation of the distribution of the ratio $\frac{\sigma_m}{\bar{\sigma}}$ with time for the index $n = 3.0$. The very large increase at radius $\frac{r}{r_o} \doteq 1.6$ is most noticeable at $T = 0.57$. As a comparison with other index values, fig. 11.3 plots the $\frac{\sigma_m}{\bar{\sigma}}$ distributions for various n values at time $T = 0.25$.

11.4.3 Strain Results

To illustrate the development of strain with time, figs. 11.4(a) and (b) show the distribution of effective strain along the hole surface and along the $\measuredangle\, \vartheta = 0^o$ at various times using an index value $n = 3.0$. The shape similarity of these distributions with those of $\bar{\varepsilon}^p$ obtained from the elasto-plastic solutions is obvious and indeed to be expected since both creep and plasticity are shear deformation processes.

To show the effect of varying the index, similar effective strain distributions for $n = 2.5$, 3.0 and 3.5 are shown in figs. 11.5(a) and (b) at time $T = 0.25$.

11.4.4 Conclusions

The four aims of paragraph 11.4.1 have thus been achieved. The most important point is that the elliptical stress oriented approach developed for the elasto-plastic problem can be adapted without too much difficulty to creep problems and that the solutions obtained are convergent at each time interval and stable up to various times depending on the index n.

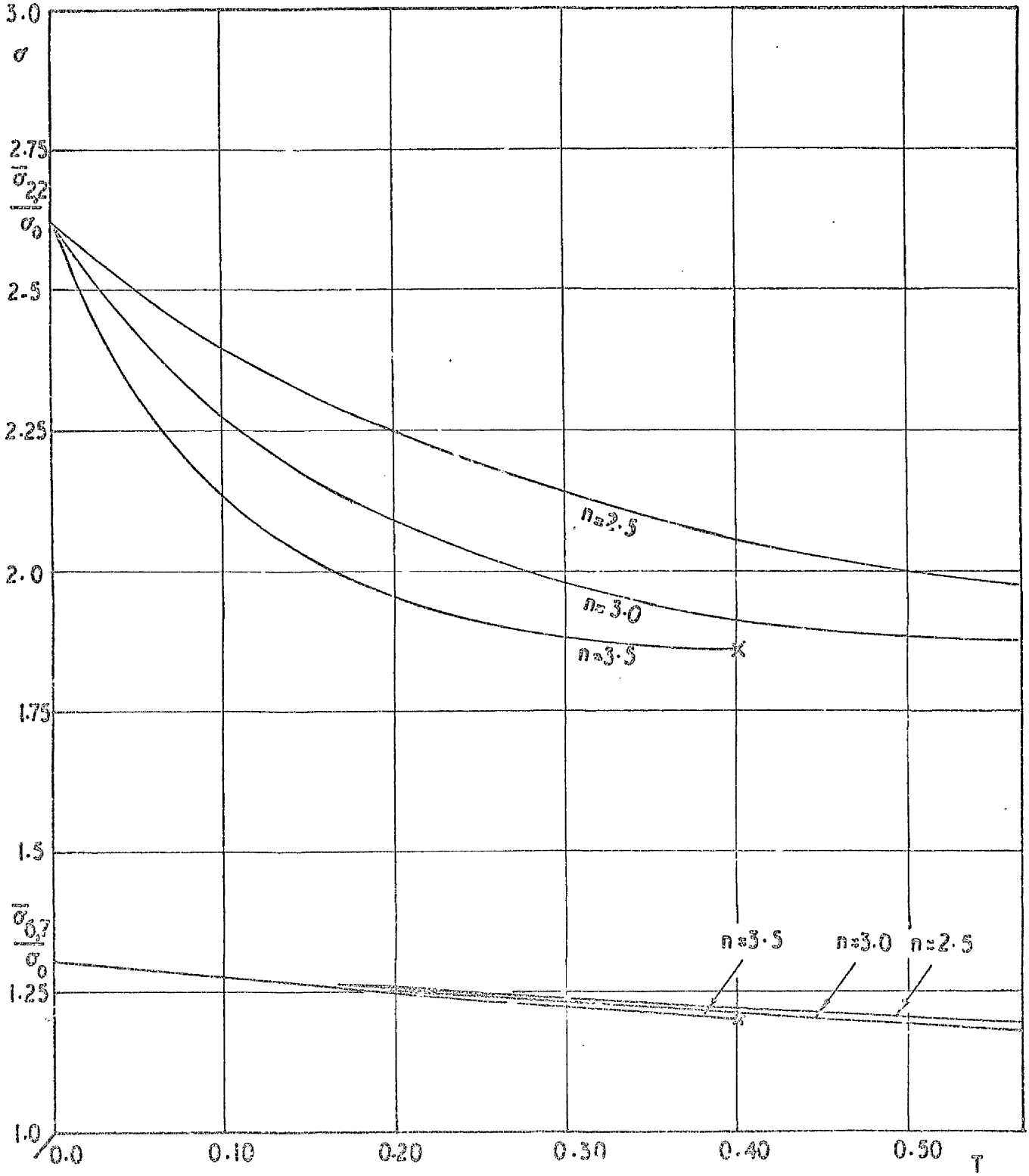

Fig III Relaxation of effective stress with time for various index values

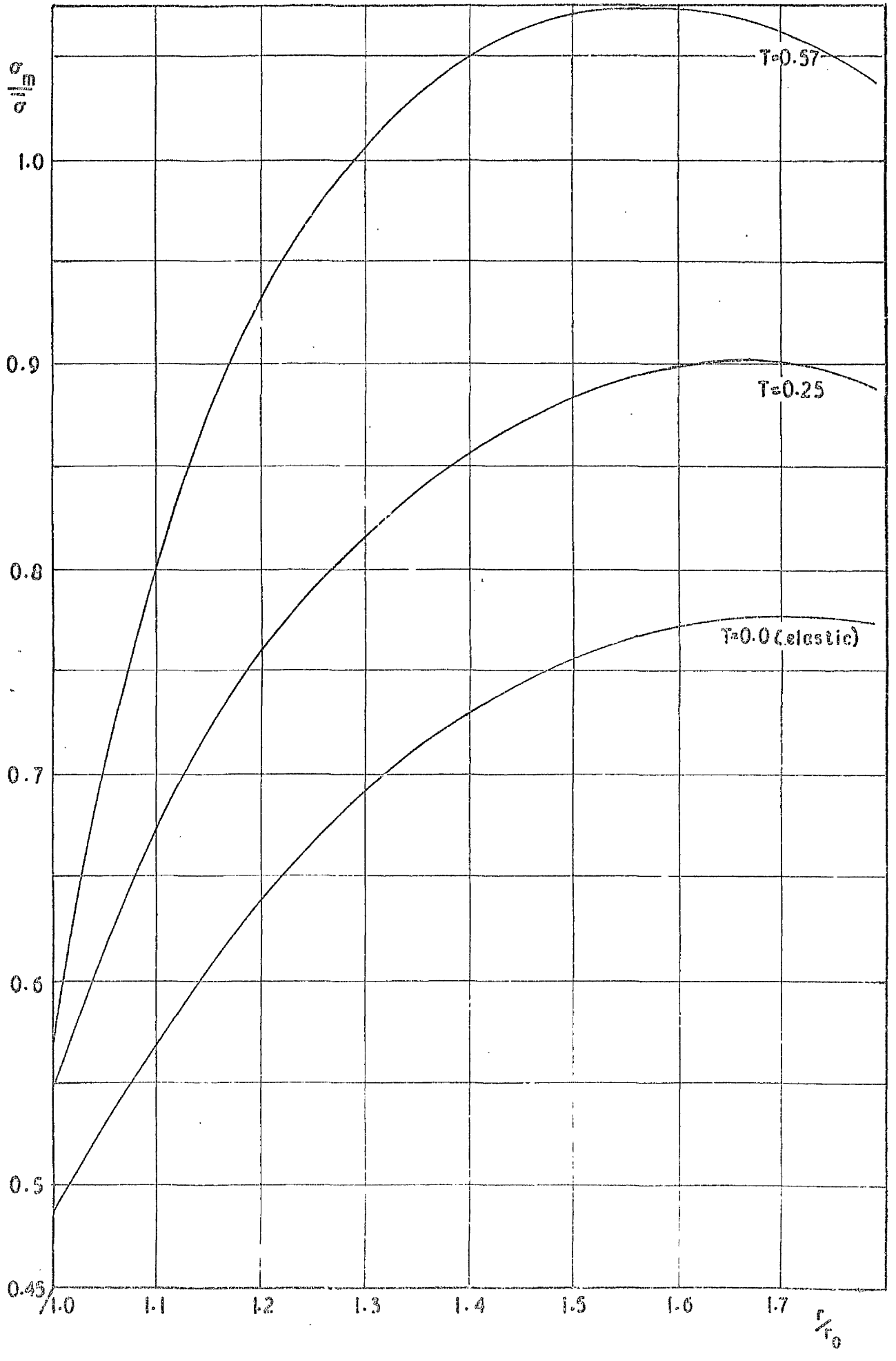

Fig 11.2 Variation of $\frac{\sigma_m}{\sigma}$ distribution

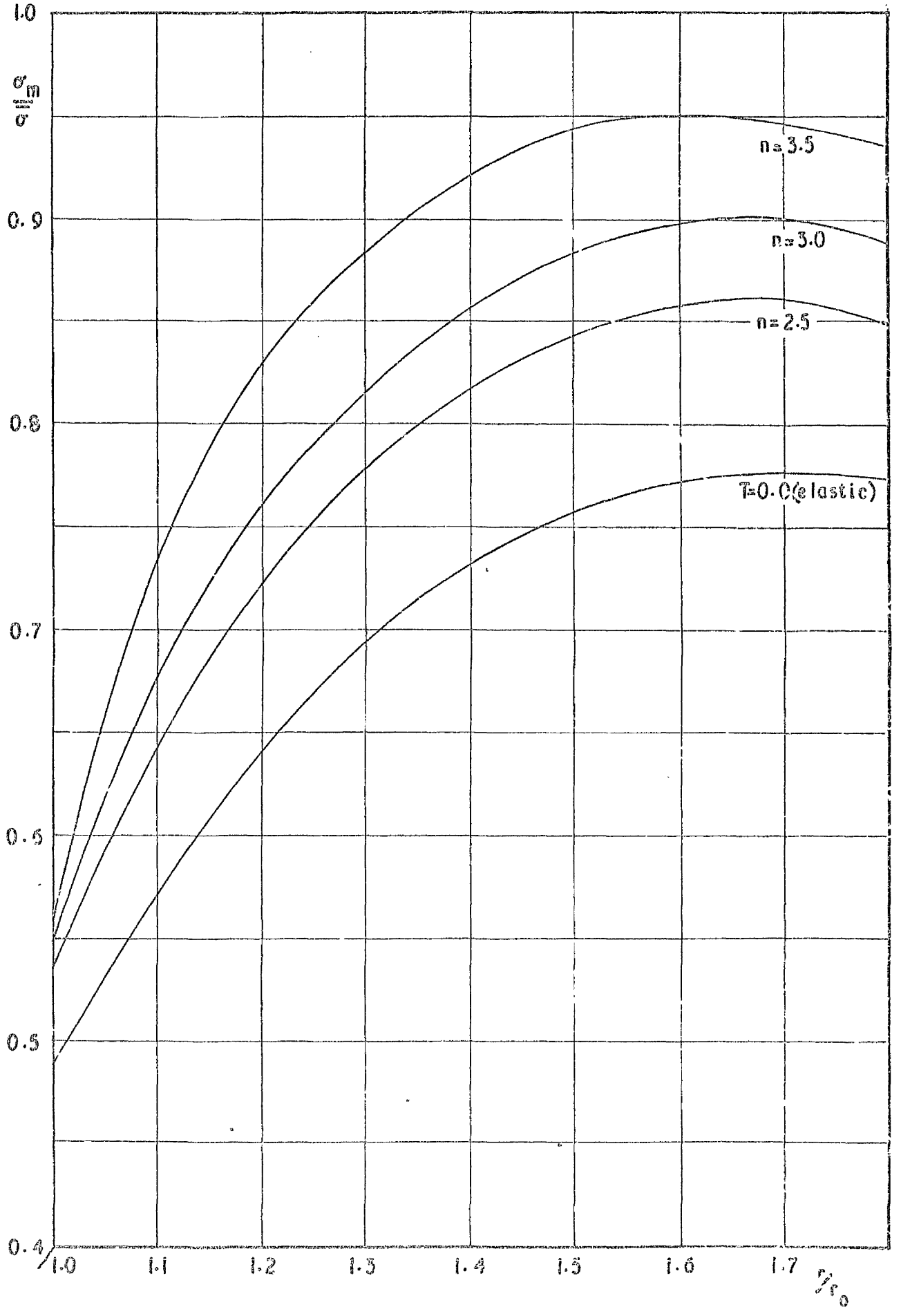

Fig II.3 Variation of $\frac{\sigma_m}{\sigma}$ distribution along ξ with index n - T=0.25

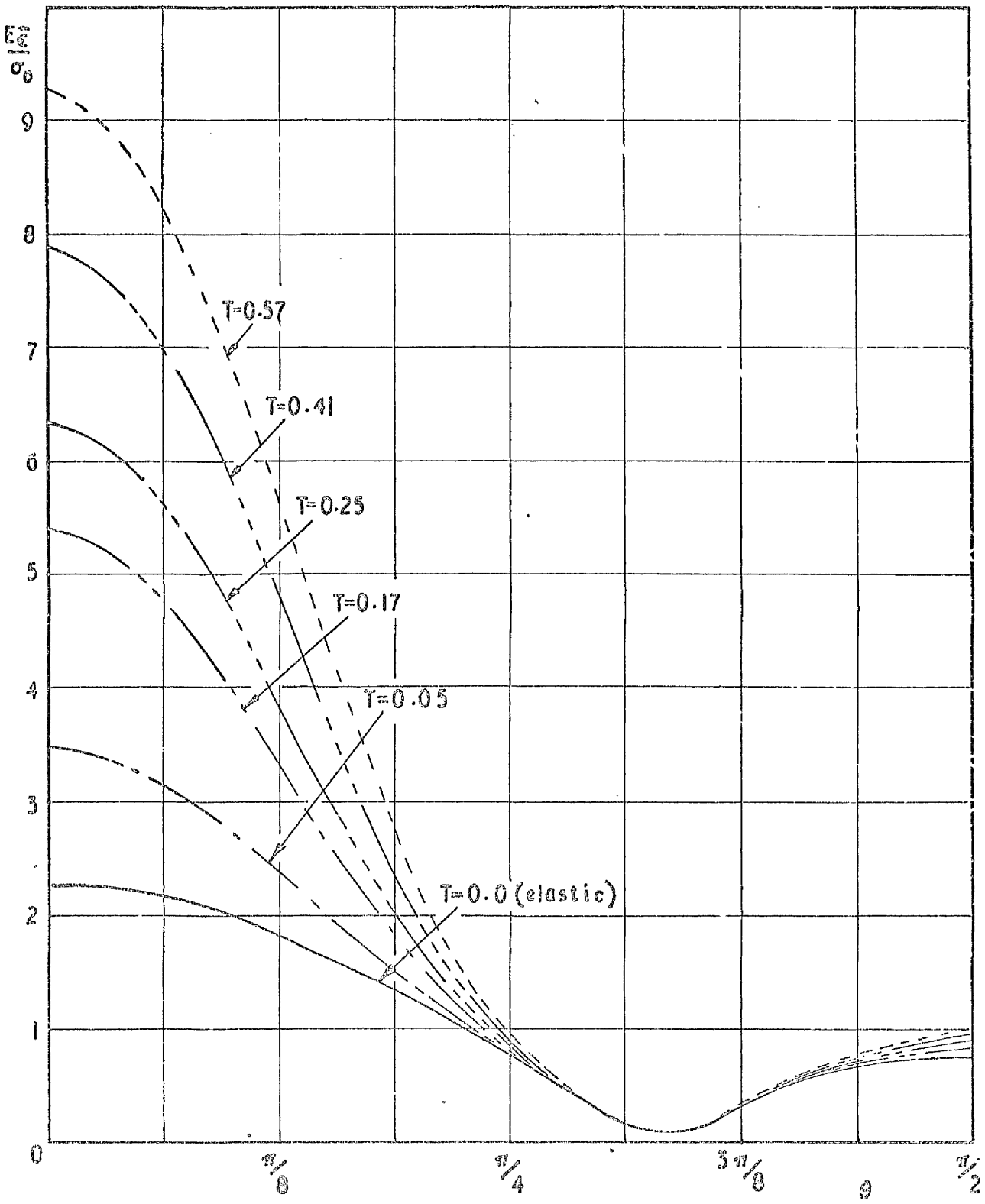

Fig 11.4(a) Distribution of effective strain along hole surface with time - n=3.0

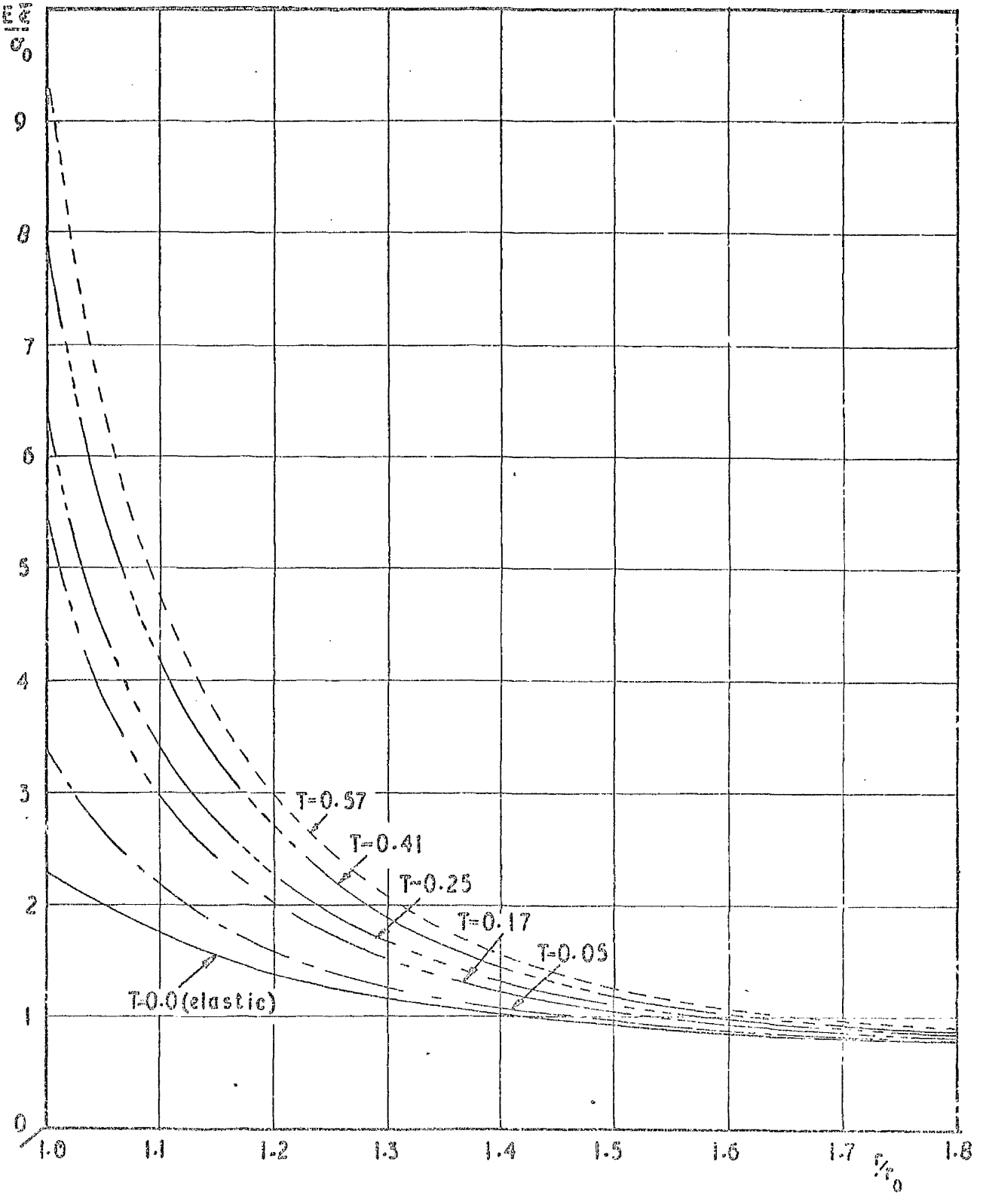

Fig 11.4(b) Distribution of effective strain along $\theta=0^\circ$ with time - n=3·0

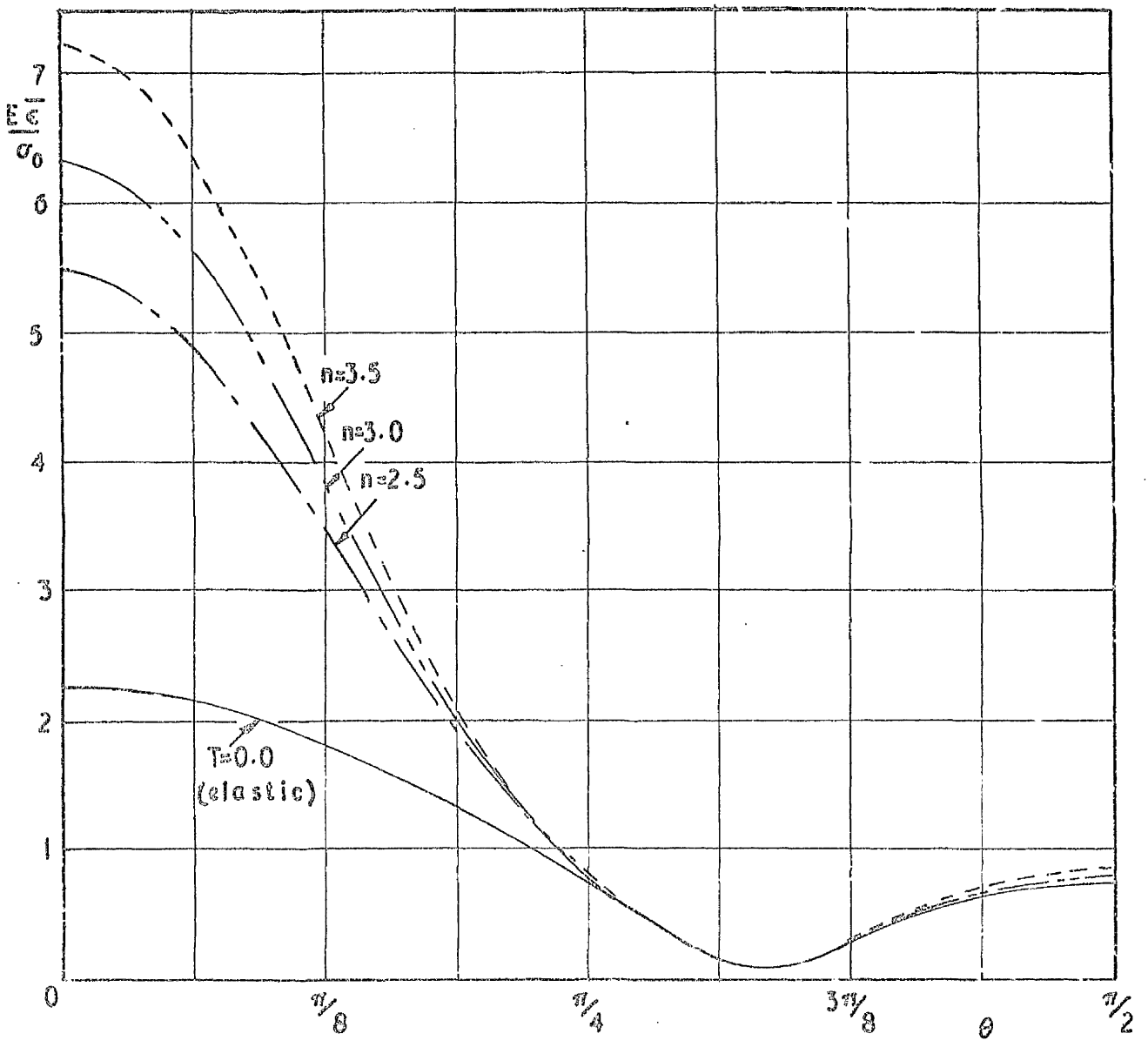

Fig 11.5(a) Variation of effective strain along hole surface with index n-T=0.25

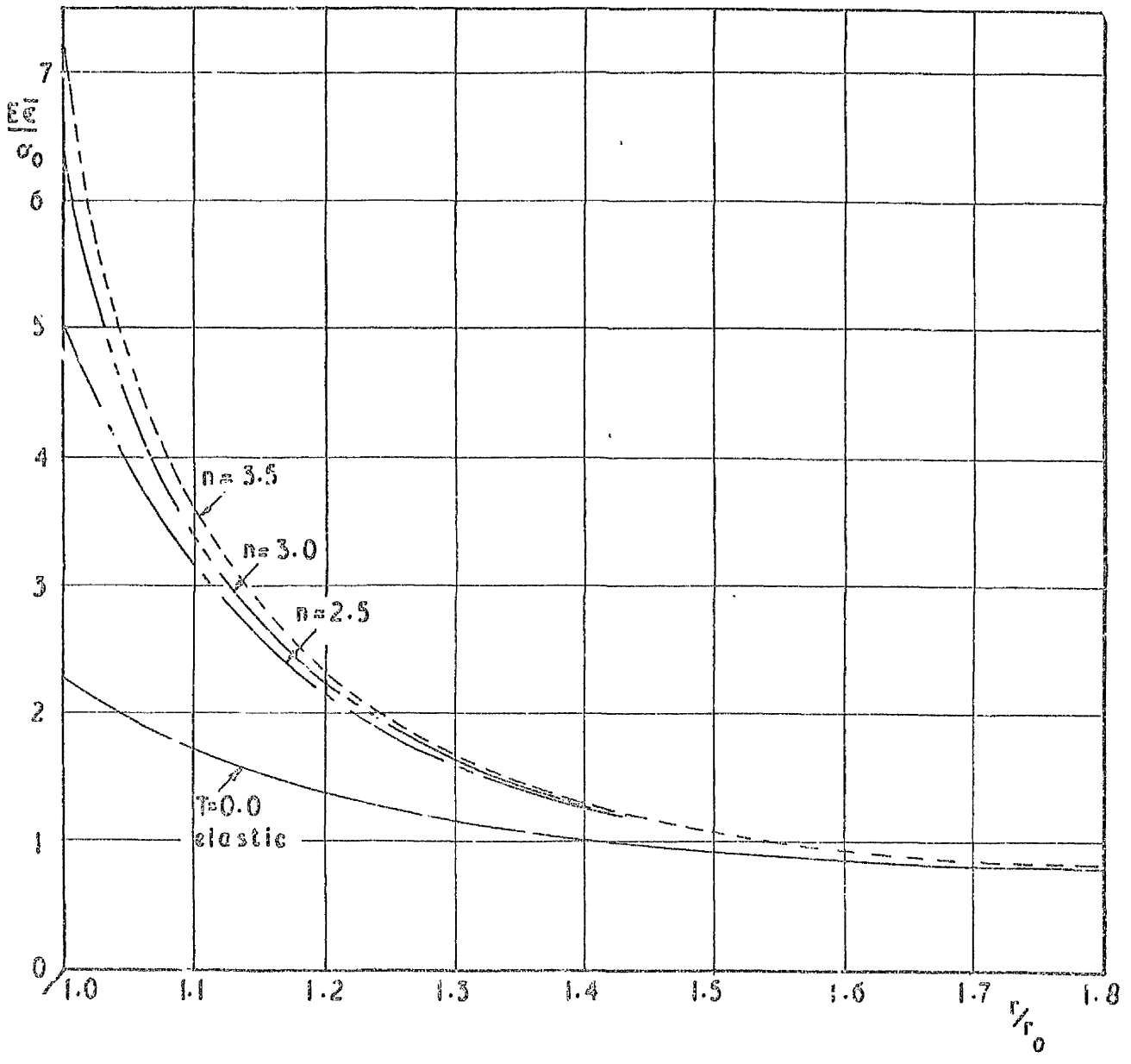

Fig 11.5(b) Variation of effective strain along ξ $\theta = 0^\circ$ with index n - T=0.25

CHAPTER 12

CONCLUSIONS AND FUTURE DEVELOPMENTS

CHAPTER 12

CONCLUSIONS AND FUTURE DEVELOPMENTS

12.1 Conclusions

The most important conclusion is that the method of using three first and second order partial differential equations in stresses or strains is practicable but must be of the boundary-value type. Although the grid used here was based on cylindrical coordinates due to the geometry of the keyhole (and the hole) the method could be equally well applied to a cartesian coordinate system with the equations reformulated. It must also be remembered that the equations could be formulated in terms of stresses or strains to match boundary specifications, with very little alteration to the method. Similarly, although the solutions produced were for plane strain, plane stress solutions using the same principles are possible.

The results for the hole in tension compare favourably where checks were made with other solutions.

Results for the keyhole show that the ratio $\frac{\sigma_m}{\bar{\sigma}}$ varies very little as plasticity developes and the slip line solution provides the limiting case. The development of plasticity is initially very slow with the main plastic deformation being concentrated around the notch surface although further recent results indicate that 'wings' will form at slightly greater loads, thus tending towards the slip line solution again.

The results show some peculiarities and these are explained by the use of linear work-hardening.

Chapter 11 shows that, with minor modifications, the method can be adapted to solve creep problems.

The method was developed to give solutions in the initial stages of plasticity up to 4--5% strain and this has been achieved. At the larger strains, convergence is, however, more difficult and consequently longer and more expensive computer runs are required. The method should not be extended too far, where cumulative errors will render the solution inaccurate anyway. In addition at larger strains, geometry changes become significant and, as the method exists at present, no account is taken of this; should such large strain solutions be required, it is suggested that finite element techniques be employed.

12.2 Future Developments

The work in this thesis describes chiefly a theoretical contribution to our fracture research group. In the continuing program of research in the fundamental studies of fracture, we have been examining two aspects –

(a) conditions for void growth from pre-existing voids
(b) conditions for void nucleation from inclusions and hard particles.

Hancock[44] has reviewed the current literature and makes the following comments. The mechanism by which holes are nucleated has been studied extensively for particles in an incompressible elastic material but the effect of an elasto-plastic surrounding matrix has been largely neglected. Only one paper has been written for this material, by Tuba, for a cylindrical rigid inclusion under plane stress conditions. He uses a deformation plasticity theory with a linear work-hardening index of $m = \frac{E}{10}$, and quotes concentrations of radial stress at the inclusion of 2 for the elastic phase and 1.5 for the plastic phase. It is instructive to note that McClintock, who based his analysis on a somewhat arbitrary slip line field for a rigid-plastic matrix, suggests that shear strain at a cylindrical inclusion, may become infinite at very low strain-hardening rates (perhaps $m = \frac{E}{100}$) and that this may be the true cause of decoherence.

It was thus proposed to conduct a plane strain analysis of inclusions in an elasto-plastic matrix obeying the incremental theory and with a low work-hardening index. It was thought that there would be two distinct problems here, both of which would use the methods described in Chapter 7 of this thesis – a finite difference solution on an elliptical boundary process. The finite difference method was preferred to finite elements because of its being able to handle the outer boundary condition more easily, where this is taken as a condition at infinity, and, in addition, probably giving a more accurate estimate of the stress and strain at the inclusion interface.

The first of these problems is <u>the effect of an inclusion in an infinite matrix under various states of stress, uniform at infinity.</u> It was proposed to study first a single cylindrical inclusion, then a row of inclusions at varying pitch/diameter ratios, and extend these to non-circular shapes. When the inclusion is assumed rigid the conditions at the inner boundary, suggest that the best field variables to use are the two components of displacement, since both are zero at the interface. The remarks in Chapter 7 apply here; there the stress components were chosen because, at the inner boundary, two of these variables were zero – here it is rather simpler. Except for the analysis being simpler there would be no real difference in the methods and the experience gained in the more difficult problem would be helpful.

In collaboration with Dr. J. Orr, some progress has in fact been made on the first of these analysis and some results are included here for interest. They are put forward rather tentatively, being the first (unchecked) results to hand, but they do support McClintock's estimate of high shear strains. The configuration is shown on fig. 12.1 and, figs. 12.2 and 12.3 show the development of radial stress at A and shear strain at B against effective plastic strain at infinity.

The second problem lies in the <u>effect of repeated straining at an inclusion.</u> Fig. 8.3 shows that there is

local yielding at the root of the notch in the bend specimen at a fairly small fraction of the load causing general yield; it emphasizes the point that local strains could be large even under working conditions. In the actual structure where the bulk of elastic material is much greater relative to the local area of stress concentration, it seems clear that this fraction could be less. Since design stresses are based on general yield it would be expected that local strains in a structure could be quite considerable under working conditions, perhaps of the order of 2–5% for a high tensile steel. It would be expected that for a typical structure the maximum working load would be repeated a number of times and that, for a thorough study, the effect of these repetitions of loading should be examined.

To provide a specification for the conditions of testing or type of test specimen, analyses would be attempted both for the inclusion studies described above and for a notched specimen. It is thought that the number of repetitions of loading would be limited, perhaps to about 10 to 50 in a test and much fewer in the analyses, where the trend might be sufficiently clear after two or three. It is necessary to solve the problem of the notched specimen in order to find the changing pattern of strains, which would be used for the boundary conditions at infinity in the inclusion problem. It is visualized that the critical area of inclusions would be at the root of the notch.

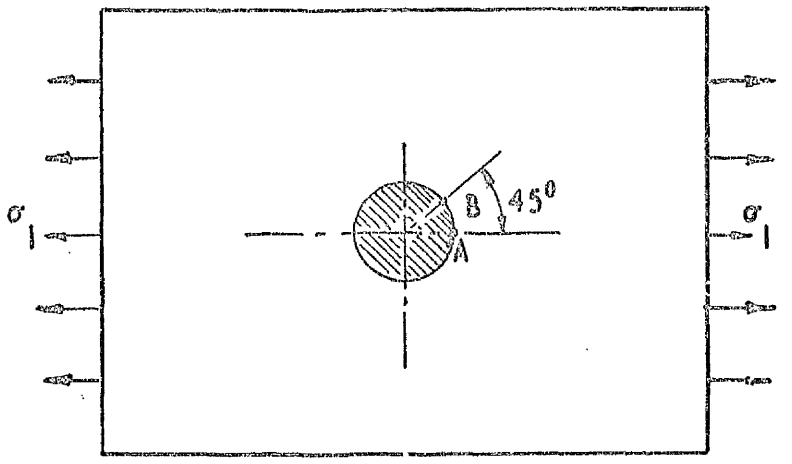

120 HY STEEL

strain at yield = 0.4%

uniaxial stressing and plane strain.
linear work-hardening matrix $E/40$; rigid inclusion.

Fig 12.1

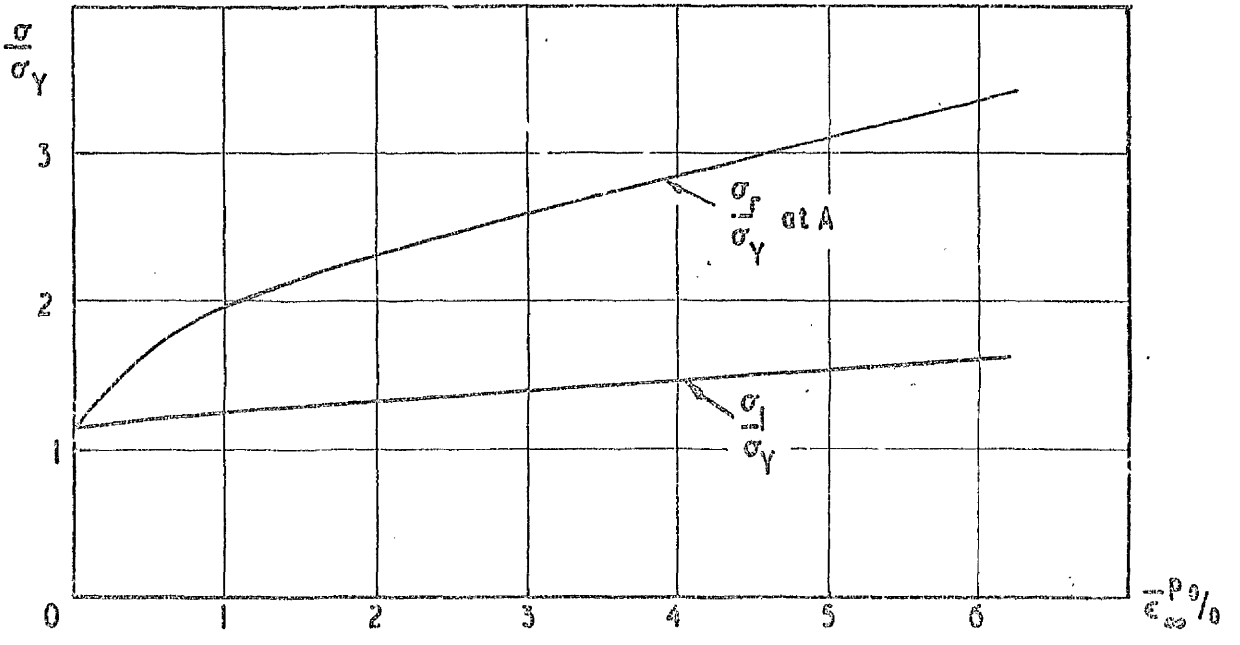

Fig 12.2 Maximum radial stress at inclusion plotted against effective plastic strain at infinity

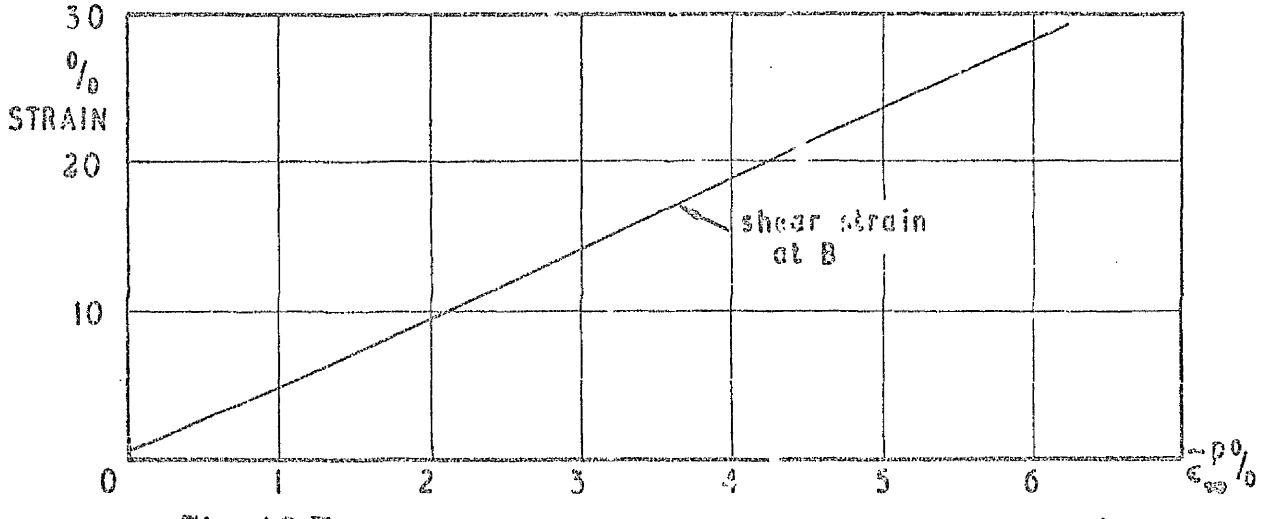

Fig 12.3 Maximum shear strain at inclusion plotted against effective plastic strain at infinity

List of References

1. BLAND, D.R. 'Elasto-plastic Thin-walled Tubes of Work-hardening Materials Subjected to Internal and External Pressures and Temperature Gradients'. J. Mech. Phys. Solids, Vol.4 (1956).

2. TUBA, I.S. 'Elastic Plastic Analysis of Hollow Spherical Media under Uniform Radial Loading'. J. Franklin Inst., Vol. 280, No. 4 (1965).

3. MENDELSON, A. 'Plasticity; Theory and Application' McMillan, London (1968).

4. ORR, J. Private Communication re. Closed Solution of Thick Sphere.

5. ALLEN, D.N.de G. and SOUTHWELL, R. 'Relaxation Methods Applied to Engineering Problems; XIV Plastic Straining in Two Dimensional Stress Systems'. Phil. Trans. Roy. Soc. (London) A242 (1950).

6. JACOBS, J.A. 'Relaxation Methods Applied to Problems of Plastic Flow. I Notched Bar under Tension'. Phil. Mag. 41 (1950).

7. GRIFFIN, D.S. and VARGA, R.S. 'Numerical Solution of Plane Elasticity Problems'. J. Soc. Ind. App. Math. 11(4) (1963).

8. SPENCER, A.J.M. 'The Solution of Plane Elastic/Plastic Problems by Relaxation Methods'. App. Sci. Research Sect. A, 12(4-5) (1962).

9. HILL, R. 'The Mathematical Theory of Plasticity'. Oxford Univ. Press, London (1950).

10. MENDELSON, A. and MANSON, S.S. 'Practical Solution of Plastic Deformation Problems in the Elastic-Plastic Range'. N.A.S.A., T.R. R-28 (1959).

11. MENDELSON, A. and SPERO, S.W. 'A General Solution for the Elasto-Plastic Thermal Stress in Strain Hardening Plate with Arbitrary Material Properties'. J. App. Mech. 29, Trans. A.S.M.E. 84 (Series E) (1962).

12. DAVIS, E.A. 'Extension of Iteration Method for Determining Strain Distributions to Uniformly Stressed Plate with a Hole'. J. App. Mech. 30, Trans. A.S.M.E. 85 (Series E) (1963).

13. ROBERTS, E. and MENDELSON, A. 'Analysis of the Plastic Thermal Stresses and Strains in Finite Thin Plate of Strain-Hardening Material'. N.A.S.A. T.N. -D- 2206 (1964).

14. TUBA, I.S. 'Elastic Plastic Stress and Strain Concentration Factors at a Circular Hole in a Uniformly Stressed Infinite Plate'. J. App. Mech. 3, Trans. A.S.M.E. 32 (Series E) (1965).

15. TUBA, I.S. 'A Method of Elastic-Plastic Plane Stress and Strain Analysis'. J. Strain Anal. Vol. 1, No. 2 (1966).

16. GRIFFIN, D.S. and VARGA, R.S. 'Numerical Solution of Plane Elasticity Problems'. J. Soc. Ind. App. Maths. 11(4) (1963).

17. TUBA, I.S. 'An Elastic-Plastic Analysis of Stresses and Strains at Hyperbolic Notches in Flat Plates'. Nuclear Struc. Engg. 2 (1965).

18. NEUBER, H. 'Theory of Notch Stresses'. English Trans. from a publication of Springer-Verlag, Berlin. J.W. Edwards, Ann. Arbor, Michigan (1945).

19. TUBA, I.S. 'An Analytic Method for Elastic Plastic Solutions'. Int. J. Solids Structures, Vol. 3, (1967).

20. TIMOSHENKO, S. and GOODIER, J.N. 'Theory of Elasticity'. McGraw-Hill, New York. Now in its 3rd Ed. (1971).

21. SNEDDON, I.N. Private Communication regarding the use of first order partial differential equations.

22. MITCHELL, A.R. 'Computational Methods in Partial Differential Equations'. John Wiley and Sons, London (1969).

23. ORR, J. 'Stress Analysis for Fracture', an Introductory Course'. Notes given at One-week Course at the University of Glasgow (1968).

24. FORSYTHE, G.E. and WASOW, W.R. 'Finite Difference Methods for Partial Differential Equations'. John Wiley and Sons Inc., New York (1960).

25. OTTER, J.R.H., CASSELL, A.C. and HOBBS, R.E. 'Dynamic Relaxation'. Trans. I.C.E. Paper No. 6986 (1967).

26. YOUNG, D.M. 'Ordvac Solutions of the Dirichlet Problem'. J. Assoc. Computing Machinery Vol. 2, No. 3 (1955).

27. CARRÉ, B.A. 'The Determination of the Optimum Accelerating Factor for Successive Over-Relaxation'. Computer Journal 4 (1961-62).

28. McCLINTOCK, F.A. 'Plasticity Aspects of Fracture'. Chapter 2 of 'Fracture: an Advanced Treatise Vol. III'. Academic Press, New York (1971).

29. COURANT, R. and HILBERT, D. 'Methods of Mathematical Physics Vol. II Partial Differential Equations'. John Wiley and Sons, New York (1962).

30. WILSHAW, T.R., RAU, C.A. and TETELMAN, A.S. 'A General Model to Predict the Elastic-Plastic Stress Distribution and Fracture Strength of Notched Bars in Plane Strain Bending'. Engg. Fracture Mech. Vol. 1 (1968).

31. GRIFFITHS, J.R. and OWEN, D.R.J. 'An Elastic-Plastic Stress Analysis for a Notched Bar in Plane Strain Bending'. J. Mech. Phys. Solids Vol. 19 (1971).

32. STOWELL, E.Z. 'Stress and Strain Concentration at a Circular Hole in an Infinite Plate'. N.A.S.A. TN 2073 (1950).

33. THEOCARIS, P.S. and MARKETOS, E. 'Elastic-Plastic Analysis of Perforated Thin Strips of a Strain-Hardening Material'. J. Mech. Phys. Solids Vol. 12 (1964).

34. GEIRINGER, H. 'Complete Solutions to the Plane Plasticity Problem'. Proc. 3rd Int. Cong. App. Mech. 2, 185 Stockholm (1930).

35. PRAGER, W. and HODGE, P.G. Jnr. 'Theory of Perfectly Plastic Solids'. John Wiley and Sons, New York (1951).

36. GREEN, A.P. 'Plastic Yielding of Notched Bars due to Bending'. Q.J. Mech. App. Math., 6, 223 (1953).

37. GREEN, A.P. and HUNDY, B.B. 'Initial Plastic Yielding in Notch Bend Tests'. J. Mech. Phys. Solids, 4, 128 (1956).

38. LIANIS, G. and FORD, H. 'Plastic Yielding of Single Notched Bars due to Bending'. J. Mech. Phys. Solids, 7, 1 (1958).

39. GREEN, A.P. 'On the Use of Hodographs in Problems of Plane Plastic Strain'. J. Mech. Phys. Solids, 2, 73 (1954).

40. MACKENZIE, A.C. Private Communication regarding strain measurement in notch bend specimens.

41. FINNIE, I. and HELLER, W.R. 'Creep of Engineering Materials'. McGraw-Hill, New York (1959).

42. Fracture Research Group, University of Glasgow. 2nd Report to N.C.R.E. 'Investigation into the Influence of State of Stress on the Ductility of High Strength Steels' (1972).

43. BYRNE, T.P. 'Creep of Cylindrical Shells Subject to Axisymmetric Loading'. Ph.D. Thesis (1967).

44. HANCOCK, J.W. 'Void Nucleation at Hard Particles'. Symposium on Void Growth and Ductile Fracture, Department of Mechanical Engineering, University of Glasgow (1971).